NOTICE

The quality of this microform is heavily dependent upon the quality of the original thesis submitted for microfilming. Every effort has been made to ensure the highest quality of reproduction possible.

If pages are missing, contact the university which granted the degree.

Some pages may have indistinct print especially if the original pages were typed with a poor typewriter ribbon or if the university sent us an inferior photocopy.

Reproduction in full or in part of this microform is governed by the Canadian Copyright Act, R.S.C. 1970, c. C-30, and subsequent amendments.

AVIS

La qualité de cette microforme dépend grandement de la qualité de la thèse soumise au microfilmage. Nous avons tout fait pour assurer une qualité supérieure de reproduction.

S'il manque des pages, veuillez communiquer avec l'université qui a conféré le grade.

La qualité d'impression de certaines pages peut laisser à désirer, surtout si les pages originales ont été dactylographiées à l'aide d'un ruban usé ou si l'université nous a fait parvenir une photocopie de qualité inférieure.

La reproduction, même partielle, de cette microforme est soumise à la Loi canadienne sur le droit d'auteur, SRC 1970, c. C-30, et ses amendements subséquents.

Enhancement of the Display and Diagnostic Capabilities of an Opto-Electronic Instrument for the Assessment of Injuries to the Cervical Spine.

Peter Roozmon

A Thesis

in

The Department

of

Mechanical Engineering

Presented in Partial Fulfilment of the Requirements for the Degree of Master of Applied Science at

Concordia University

Montreal, Quebec, Canada.

March 1992

ISBN 0 315-73694-1

ABSTRACT

Enhancement of the Display and Diagnostic Capabilities of an Opto-Electronic Instrument for the Assessment of Injuries to the Cervical Spine.

Peter Roozmon, M.A.Sc.

Injuries to the cervical spine may occur in the home, the workplace, and in accidents related to sports or automobiles. Physicians are aided in the identification of such injuries by instruments for objectively analyzing the motion of the cervical spine. This investigation examines the evaluation and subsequent improvement of a new opto-electronic device developed for this purpose.

To determine the market for this tool, relevant imaging systems and measurement techniques are reviewed. The particular system to be enhanced uses two cameras to track small infrared emitting diodes affixed to the subject's skin. Discrete motion samples are recorded and kinematic data is processed by a computer. Various parameters of interest are then displayed on a video screen.

These displays must, however, be related to the underlying injuries. The review thus includes biomechanical factors such as injury mechanisms, some analytical models used to quantify these, and normal range of motion studies. The movement of skin markers versus that of underlying vertebrae, as well as the importance of coupled joint motion, are also discussed.

An evaluation of the above instrument indicates that the precision of the displays does not permit sufficiently accurate diagnoses. Hence, the development of an enhanced display for characterizing cervical coupled joint motion is described. Direction angles are used to represent angular displacements of the spine in the principal planes.

These angles correspond to the movement of virtual vectors normal to the planes defined by markers on the head, neck, and shoulders. This treatment is found to increase the precision of the instrument in describing neck motion and thus to improve the accuracy of the resulting diagnoses.

Dedication

To my wife Mireille for her inspiration, as well as
to Serge Gracovetsky and Gerard Gouw for
their patient guidance.

Table of Contents

List of figures

List of tables

CHAPTER 1 - INTRODUCTION

1.1 GENERAL

Neck injuries frequently occur to people in the course of their daily activities at home, at play, or in their work environment. The effects are often entirely minor and temporary. In other cases, serious damage may occur to the vertebral column or spinal cord, with sometimes tragic and permanent results.

We are concerned here mostly with a device for the diagnosis of those types of injuries which fall in between these two categories. In particular, we will consider non-acute, soft tissue cervical injuries. At first these may go unnoticed or be misdiagnosed. However, they may eventually lead to longterm, chronic discomfort.

As in most areas of modern medicine, physicians depend upon instruments to help them identify such injuries, as well as to subsequently decide upon a course of treatment. Some of these devices involve the use of radiation or magnetic fields to provide contrast images of the tissues within the neck. Others are designed to describe the motion of the spine.

Instruments for measuring spinal mobility range from plumb lines and inclinometers to sophisticated opto-electronic systems.[25] The latter usually involve the attachment of reflective markers on the subject's skin.[26] Hence, mathematical techniques must be used to correlate skin motion to that of the underlying vertebrae.[27,28,29]

We will focus upon one such instrument in this investigation. It will be evaluated, in order to determine its effectiveness as a diagnostic device, and subsequently enhanced. In order to perform these tasks, it is necessary to be aware of the alternative tools available on the market. Hence, we will begin by reviewing the relevant imaging and measurement systems currently available.

In general, clinicians are not trained to analytically relate diagnostic displays with the underlying kinematics (ie. motion analysis). The engineer must therefore determine if the user is provided with all of the information required to perform a diagnosis, and then help him/her to analyze this information.

To do this, we need to understand the mechanics of neck injuries. This requires

an analysis of relevant human physiology and biomechanics. The latter is defined as the application of mechanics and material science theory to the behaviour of biological tissue.

In recent years numerous analytical models have been proposed to explain the dynamics of the cervical spine. These models allow the verification and quantification of the theories which are used to describe injury mechanisms. They are thus important for understanding how cervical motion analysis may be related to injury. We will examine a few of these models.

The ability to objectively differentiate normal from pathological (ie. injured) motion may facilitate the diagnosis of neck injuries. However, it is essential to have data upon which to which to base such comparisons. Hence, we will thus consider how the neck moves.

Then we will review studies undertaken elsewhere to document the range of motion for specific portions of the cervical spine. The required comprehensive tables were not previously available together in the literature. They were thus compiled exclusively for this investigation.

Since the instrument under consideration tracks the motion of skin markers, we will examine how this movement may be related to that of the underlying vertebrae. In particular, we will determine whether a linear relationship exists. Finally, we show that the description of coupled joint motion is an important factor in identifying normal versus pathological cervical movement.

In chapters 2 and 3 we will see how the evaluation of the instrument under consideration led to the development of enhanced displays to characterize such coupled motion. An outline of how this investigation proceeds is presented in section 1.4, where we summarize the literature review and consider the scope for the remainder of the thesis.

The purpose of the review is primarily to provide the background information required to understand the steps taken in this investigation. In order to maintain continuity, only a minimum of material is presented here - particularly with respect to biomechanics. However, this information was obtained from numerous sources and may not easily be reproduced. The details are therefore provided for interested readers in Appendix A.

1.2 IMAGING SYSTEMS AND MEASUREMENT TECHNIQUES FOR THE DIAGNOSIS OF SOFT TISSUE INJURIES IN THE CERVICAL SPINE

A few examples of existing imaging systems and measurement techniques were mentioned in the previous section. We will now look at some of these in detail. Our purpose is to determine whether these methods provide the information required to identify relevant injuries to the cervical spine.

The devices and methods being considered should be of practical use in a clinical setting, specifically for the diagnosis of non-acute, soft tissue injuries. Ideally, the results presented to the user should also be useful for verifying analytical models of the neck. Hence each method must be considered both from a clinical and an experimental point of view.

1.2.1 Radiographs and Cineradiography

Plain X-rays play a valuable but subsidiary role in diagnosis of soft tissue injuries to the cervical spine. The standard series may include three anterio-posterior (A-P) views (left/right bending and neutral), two lateral views (extension and flexion), both obliques and an open-mouth view.[21,59]

In the latter, the tongue must be depressed to avoid shadows, and the head positioned to avoid interference from the lower jaw or occiput.[31] The details of using radiographs in evaluating soft tissue injuries of the cervical spine are covered elsewhere (section 1.3).

Plain radiographs can be used to indirectly infer spinal canal size using Pavlov's ratio. The anterio-posterior diameter of the canal is about the same as that of the anterio-posterior diameter of the vertebral body at the same level. The result of the former divided by the latter is Pavlov's ratio. Normally it has a value of about 1.0. A value of 0.8 or less indicates an abnormally small canal.[59]

Cineradiography began with the use of motion picture photography together with roentgenography to record motion. Modern techniques involve filming or videotaping of an enhanced image produced by a radiographic image intensifier. This specialized type

of cathode ray tube permits clear images with minimal exposure to the subject (fig 1.2.1). Hence, cineradiography is an invaluable tool in studying osseous movement.[31]

1.2.2 Computer Tomography (CT) and Magnetic Resonance Imaging (MRI)

CT scans contribute a cross sectional view which is useful in complementing the standard views listed above. It diminishes the need for complex motion tomography, providing more information with less radiation exposure. Reconstructions are helpful in evaluating a variety of diseases.

However, soft tissues are not usually visible enough without the injection of a contrast agent, such as metrizamide. This effectively converts an otherwise non-invasive procedure into an invasive one.[32] Myelography is the use of this process to highlight the spinal cord. A lower concentration of contrast material is required for CT myelography than for conventional radiography.[59]

As in computer tomography, the contrast between tissues visible using MRI is enhanced by administering external agents. The most commonly used contrast agents are manganese and gaolinium. They have been used in differentiating between normal and ischaemic tissue. However, the lack of ability to specifically target them has hampered their usefulness.

Magnetic resonance has two unique advantages over other medical imaging techniques. Firstly, contrast can be manipulated between different parts of the image by adjustment of the MRI system alone. Secondly, an image 'slice' can be taken in any plane. Hence, coronal and sagittal sections are available, as well as the transaxial slices produced by CT scans.[36] In addition to spinal cord compression, MRI illustrates pathology within the cord.[59]

Range of motion studies do not appear to have been undertaken using MRI. However, this type of imaging has played an important role in evaluation of spinal cord damage. Models of spinal cord injury have been hampered by the inability to monitor changes as time passes.

MRI has a high sensitivity for differentiating edema and hemorrhage, which can help determine whether damage is potentially reversible. These considerations are

addressed elsewhere (section 1.3).[37]

Comparative studies using magnetic resonance and computer tomography images indicate them to be complementary. CT produces better osseous details while MRI provides superior soft tissue resolution. MRI offers the advantage of direct imaging in the sagittal plane, without need for reconstruction. However, the resolution is not as fine as in transaxial CT scans.[43,53,59]

There are no known hazards from the magnetic fields and radiofrequency pulse sequences used in MRI. The procedure can be performed on an outpatient basis. Conversely, CT scanning uses ionizing radiation and requires overnight hospitalization due to side effects of metrizamide. The comparison is summarized in table 1.2.1.[43]

1.2.3 Reconstruction and Automated Interpretation of Images

The images described above show areas of different intensities. They may be modified to make them more readily interpretable by computer. Early attempts at automatic interpretation focused on chest radiographs.

The advent of digital CT and MR images simplified the task of recognition. Systems which fully describe such images exist for aerial photographs. Interpretation of a medical image is more complex because the patterns being sought are less circumscribed. MRI is particularly difficult to interpret due to the many variations in the process.[52]

Sophisticated reconstruction algorithms permit near real-time display of 2 and 3D images. The resultant constructions can be used to view either bone, muscle, or a combination of these.[54] However, artificial intelligence may be required to clearly display bone and soft tissue in the same image.[53]

Such displays are particularly useful in orthopedics, where complex joints require many different planes and orientations to be fully understood. Fishman et al. (1989) found that use of their 3D image by orthopedic surgeons resulted in significantly altered surgical procedures in up to 30% of cases.[54]

Another application is in the construction of prostheses. Indeed, the output of 3D reconstruction programs may be fed directly to a digital milling machine.[53]

The imaging modalities that can be displayed in three dimensions are shown in table 1.2.2. Such images are actually pseudo 3D images, where a 2D projection of a 3D image is displayed. The illusion of 3D is provided through shading, perspective, and on-screen rotation of the object. A true 3D image may be obtained using holograms or vibrating mirrors, but these are not yet commercially available.[53]

1.2.4 Moiré Photography

Different numerical methods have been developed for rendering the evaluation of Moiré photographs more objective. The method of analyzing and presenting the data is what finally determines the value of a system. Measurement, analysis and presentation must be performed within a few minutes to be useful.

One such instrument is the Integrated Shape Imaging System (ISIS) developed in Oxford, England. The system combines digitization of Moiré photographs and a high speed computer-video link. It has been successfully in use since 1983.[39]

The ISIS system works by digitizing the lines produced by projecting horizontal planes of light on a surface. Polynomials up to fourth order are used to correlate the measurements with the surface. Accuracy is not considered as important as repeatability in measuring back shape.

Prior knowledge of human back shape is used to eliminate extraneous information (eg. arms). The camera for the ISIS system is not stationary, but moves with the plane of projected light.[40] The video interface is the Vicon system illustrated in figure 1.2.2 (see also section 1.2.5).[26]

Anatomical landmarks are identified by palpation and marked by black paper rectangles. This enables the coordinate system for surface shape data to be defined with respect to the body and gravity alone. Hence the position of the scanner and the patient are not important. [39]

The top landmark identified is near the hair line. Unambiguous identification requires a clear area of surrounding skin, making it necessary to hold the hair out of the way.[40]

Implementation of ISIS analysis has resulted in radiographic examination being

restricted to initial diagnosis. In the past it was common for all but the mildest cases to undergo such examination up to three times per year. Now further X-rays are taken only when ISIS analysis indicates significant deterioration.

Weaknesses include partial dependence of the analysis upon the patient's posture. In addition, manual identification of anatomical landmarks is subject to human error.[39]

1.2.5 Opto-electronic Scanners

Pearcy (1987) compared two opto-electronic devices.[26] The CODA-3 emits a fan shaped beam of light toward retro-reflective prisms attached to the subject. The reflected light is detected by light-sensitive monitors.

The VICON system consists of stroboscopic lights mounted on video cameras. Scanning of the image is synchronized with the lights. Markers covered with retro-reflective tape are attached to the subject. Each marker is required to be in the view of at least two cameras at all times.

CODA-3 was found to be more appropriate for gait analysis. The main advantage of CODA-3 was the convenience of real time data and infrequent need for calibration. The use of VICON was found to be limited if movements are large and the markers obscured. Pearcy (1987) pointed out that a multi camera system would alleviate this problem.[26] Goel et al. (1988) arrived at the same conclusion after using a two camera system to track LEDs attached to cadaveric spines.[72]

Using multiple cameras would allow a 360° view. However, analysis would be complicated since markers must be identified manually. Stokes (1977) and Towle (1986) have shown that surface markers move relative to underlying vertebrae.[91,92] The systems described here indicated ranges of motion larger than those recognized for the spine.

There is also a problem with identifying bony landmarks over which the markers are attached. Nevertheless, non-invasive measurement of physiologic movement appears to be currently possible only with this type of system.

These systems measure dynamic 3D body segment movements but not those of individual spine elements. They are thus suitable for measurement of 2D movements in 3D space but not for 3D movements. Their complex nature necessitates thorough training

to operate them. Pearcy (1986,1987) thus concluded that it may be unlikely that these particular systems will become clinical tools.[25,26]

Another opto-electronic device designed for analyzing the motion of skin markers is the Spinoscope. This particular instrument uses two cameras to track infrared emitting diodes placed on the lower back and has been available for several years. In the following chapters we will consider in detail a descendant of the Spinoscope, known as the Cerviscope, which was recently developed specifically for cervical motion analysis.

This kind of device appears well suited for performing routine, non-invasive examinations, to detect non-acute injuries to the cervical spine. Such a tool should complement the other methods described above by detecting motion anomalies. Then the CT, MRI and/or 3D reconstruction techniques may be used to investigate further.

1.2.6 Discussion

We have seen that CT and MRI techniques are difficult to use for clinical range of motion evaluations. CT range of motion studies are complicated affairs suitable mostly for research, while MRI images require subjects to be motionless for long periods. Cineradiography is excellent for motion analysis, but high radiation doses make it unsuitable for routine examinations. Hence, none of these techniques are applicable to the diagnosis of soft tissue injuries which are manifested by abnormal motion.

Moiré photography and related techniques may prove useful in evaluating cervical spine abnormalities. However, the systems described above do not appear suitable for motion analysis. Conversely, the available opto-electronic scanners are promising for dynamic thoracolumbar evaluations. Nevertheless, their applicability to the cervical spine is uncertain.

In chapter 2 we will consider a new device developed specifically for clinical cervical motion analysis. To evaluate such an instrument, we must understand the relevant biomechanics. It is incumbent upon the engineer to explain how this may be related to the information provided by the device to the user. We will thus examine next the numerous biomechanical factors involved in identifying possible causes of abnormal cervical motion.

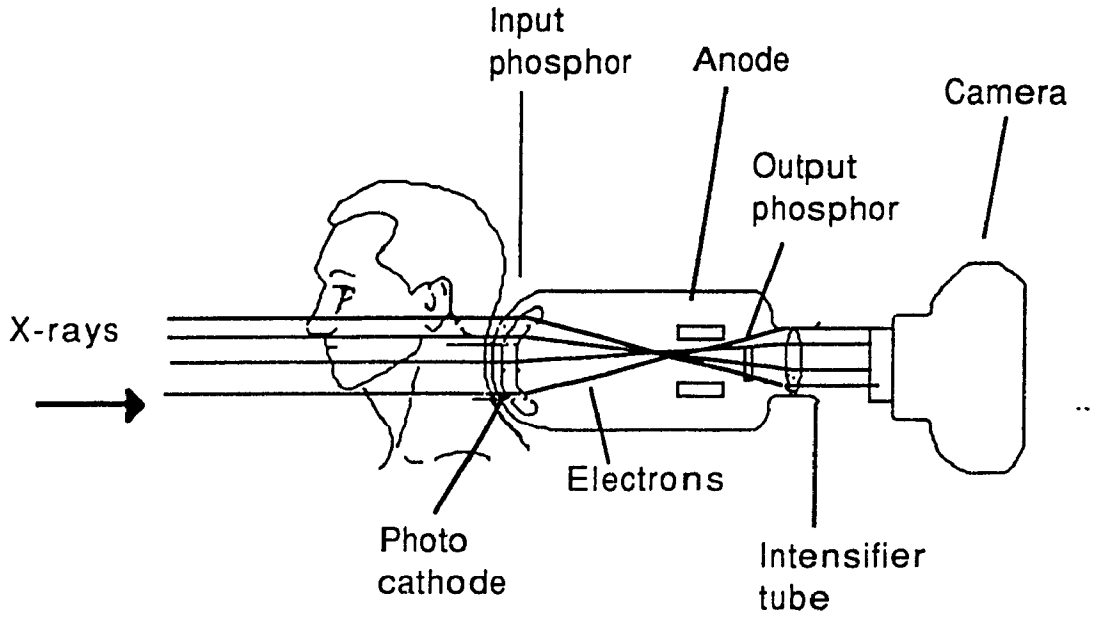

Fig 1.2.1: Indirect cineradiography with an image intensifier tube. Adapted from Fielding (1974). [31]

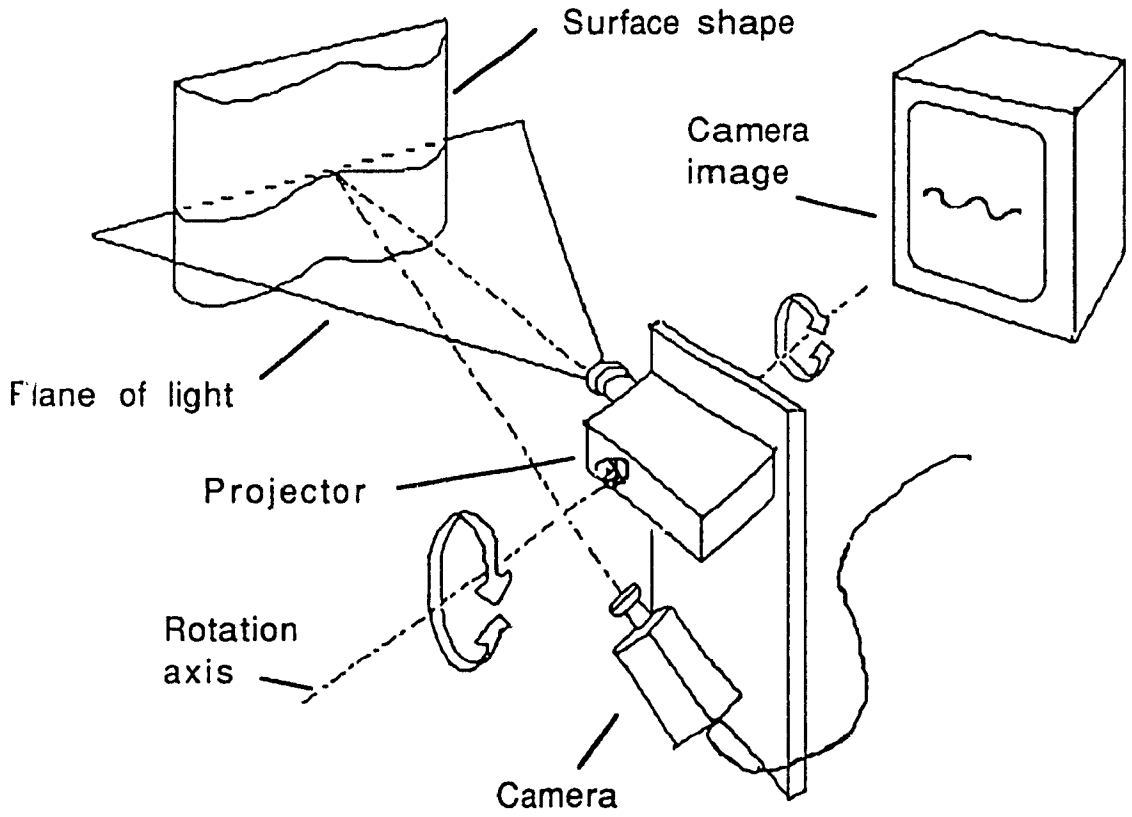

Fig 1.2.2: Principles of operation for the ISIS shape measuring system. Adapted from Turner-Smith (1988). [40]

Table 1.2.1: **Comparison of CT and MRI in cervical spine diagnosis**

Computer Tomography	Magnetic Resonance Imaging
Uses ionizing radiation.	No radiation or known hazards.
Requires puncture and insertion of contrast material.	No contrast agent required.
Computer reformatting of image required for sagittal and coronal views.	Direct sagittal, coronal, and oblique imaging.
Complete sequence of axial images needed for each change in position.	Allows for functional flexion/ extension cuts
1mm or better resolution.	2-3mm resolution.
Metrizamide side effects usually require overnight hospital stay.	Can be done on an out-patient basis.
Few contraindications (eg. allergy to metrizamide)	No cardiac pacemakers or ferromagnetic implants.
Imaging time on the order of seconds.	Each image requires 2-7 minutes.

Table 1.2.2: **Imaging modalities applicable to 3D displays**

Reconstructed 3D Imaging from Slices	Direct 3D Imaging
Computer tomography (CT)	Flashing tomosynthesis
Magnetics resonance imaging (MRI)	Compton scatter imaging
Positron emission tomography (PET)	
Single photon emission computed tomography (SECT)	
Ultrasound (UT)	

1.3 BIOMECHANICS OF THE CERVICAL SPINE: THE BASIS FOR INTERPRETATION OF DIAGNOSTIC DISPLAYS

In order to provide a useful instrument or display for performing motion analysis, it is essential to understand how the spine moves and how it may be injured. Clinicians are not generally familiar with the principals of mechanics and dynamics. Hence, the engineer developing the device must be able to explain the relationship between what the user sees on the screen and the possible injury mechanisms.

We will begin by briefly examining the components of the human spine and how neck injuries may occur. Following this, we look at how analytical models may be used to quantify these injury mechanisms.

Next, the way the cervical spine moves is examined, along with the results of studies performed to determine normal ranges of motion. We will then consider how the motion of skin markers can be related to that of the underlying vertebrae. Finally, we will study how coupled joint motion may be used to describe three dimensional motion in the spine.

These discussions involve a mixture of bioengineering and medical factors required to properly interpret diagnostics displays. In order to maintain continuity, emphasis is placed on subjects related to biomechanics and engineering. Only a minimum of clinical background information is presented here. Readers interested in a more thorough discussion of the topics presented in this chapter are referred to Appendix A.

1.3.1 Elements of the Spine and Relevant Injury Mechanisms

Consider figure 1.3.1, which shows the human spinal column in its entirety. This consists of a series of bony cylinders called "vertebrae", which are joined together by soft "intervertebral discs" of cartilaginous tissue. These discs allow the spine to be flexible.

The vertebrae are numbered from the top down. There are seven cervical (C1-C7), twelve thoracic (T1-T12), and five lumbar (L1-L5) vertebrae. Two adjacent vertebrae and their disc form what is known as a "motion segment". The movement of the spine is generally described clinically in terms of the coronal, mid-sagittal, and transverse planes

of the body (fig 1.3.2).

All the vertebrae, as well as the bony protrusions extending from their rear, are linked by elastic tissue called "ligaments". The ligaments of the neck generally act to control, limit and guide motion of the spinal segments. The discs tend to absorb shocks, while the muscles provide motor activity and dissipate energy. Ligamentous structures must be sufficiently relaxed to allow extensive motion, yet be able to check excessive movement.

Due to their resiliency, intervertebral discs also help to prevent excessive motion of the ligaments and capsular structures. Soft tissue injury may result from uncontrolled neck motion during trauma. Pain may then follow from any motion of the joints.[20,31]

According to Edwards et al. (1988), any study of mechanisms of injury (MOI) should include the following:

1) clinical observation
2) experimental investigation
3) analytical modelling [48]
4) validation
5) application.

They added that external conditions do not always reflect patterns of injuries. Severe injuries usually involve compression together with other loads. This may involve combinations of vertical forces, shear forces, and bending moments. These correspond to patterns of reproducible fractures and ligamentous injuries.

A detailed discussion of such injury mechanisms is beyond the scope of this introduction, but interested readers are referred to Appendix A. Let us now consider how these mechanisms may be described analytically.

1.3.2 Applicable Analytical Models

As we saw above, in order to verify the significance of curves describing cervical motion to a clinician, the engineer must understand the relevant injury mechanisms. To this end, it is helpful to be able to quantify the forces being applied to the physiological tissue considered above.

Extensive analytical models have been developed in order to describe the

behaviour of all parts of the human body, including the neck. Mathematical models incorporating biomechanical principles have the advantage of repeatability. They may thus eventually develop into injury-predictive models.[50,68]

In recent years the cervical spine has become the subject of numerous biomechanical studies. Several multi-disciplinary teams formerly associated with low back pain research have now turned their attention to the neck. As a result, the previous dearth of experimental data on the cervical spine has been somewhat alleviated.

The consequence of this is that analytical models may now be tested using realistic data for simulations. In Appendix A, we consider several models for various accelerations and loadings which have been proposed during the past decade.[1,2,3] Using the data available on the ultimate strengths of soft tissues and cervical vertebral bodies, these may now be verified.[4,5,6] This requires the use of motion analysis tools, since precise measurement of spinal motion is needed to perform these verifications.

However, the first step in modelling is to determine what questions are to be answered. Then it must be determined what methodologies are available to solve the problem.[63] Experimental studies are also required to provide pertinent physiological data.

Hence, a fundamental understanding of physiology is necessary to correlate these. Indeed, a comprehensive cervical spine model should include both neurophysiological and neuroanatomical considerations.

According to Sances et al. (1988), such a unified spinal injury model is not yet available.[68] We nevertheless need to consider some of the models that do exist, in order to understand how they may be used to relate motion to injury in the cervical spine. The details of this discussion may be found in Appendix A.

1.3.3 How the Cervical Spine Moves: Range of Motion Studies

The geometry of the articulating surfaces and the elastic properties of the ligaments tend to determine the relative motion of the vertebrae. Since these change as we move up the neck, the kinematics of the lower and upper cervical spine are quite different.

The top two vertebrae in the cervical spine are known as the "atlas" and "axis", respectively. The atlas meets the skull at the "occiput". The set of occipital/atlantal/axial articulations, which joins the head to the neck, is among the most complex in the body.[67] The cervical area is also the most flexible region of the spine. The degree of mobility generally corresponds to the age of the subject.

Motion between the atlas and axis allows flexion, extension, gliding and rotation to occur. The entire cervical spine normally has a forward projecting curvature, known as "lordosis". Conversely, the thoracic spine normally curves in the opposite direction, a condition called "kyphosis".

Like the neck, the lumbar spine also has a lordotic curvature. The principal movements associated with the cervical spine, as well as the progression of lordosis and kyphosis for the entire spine, are illustrated in figure 1.3.3.

The atlas and the skull were previously thought to move in rotation as a unit.[31,67] However, some rotation occurs at this level (see Appendix A). Nevertheless, the position of the skull may still be used to approximate the position of the atlas in rotation.

Forward "flexion" of the neck is defined as the act of bending forward. It begins at the atlanto-occipital joint. There is a bony protrusion, known as the "odontoid process" which extends from the axis and passes up through the atlas. It is held in place by the "transverse ligament". When the transverse ligament is injured, motion about the odontoid process may become asymmetrical.

The detection of abnormal motion may thus demonstrate the presence of soft tissue injury. However, the degree of mobility in individuals is highly variable. Furthermore, compensatory hypermobility (ie. excessive movement) is often seen above and below vertebrae which have been fused or blocked surgically.[31]

Range of motion measurements depend upon the collaboration of the patient, who may be in pain. Dvorak et al. (1988) showed that there is a significant difference in motion obtained by passive and active means (ie. with and without assistance from the examiner).[33] However, they emphatically recommend against passive examination if vertebral instability is suspected, since this may lead to further damage.

Motion in the neck is a complicated phenomena, which requires some knowledge

of cervical anatomy in order to be understood. A few more details on how the neck moves are provided in Appendix A, together with a review of several cervical range of motion studies.

These involve the use of various in-vivo and in-vitro techniques, resulting in a comprehensive description of motion in the cervical spine. Tables A.3.1 to A.3.4 summarize all of this data in a concise form, which may not be found elsewhere in the literature.

1.3.4 Correlating Motion of the Skin and the Underlying Vertebrae

Pearcy et al (1987) used the VICON systems described earlier (section 1.2) to examine the motion of skin markers.[27] They compared this with similar intervertebral movement previously recorded radiographically. The patterns of movement were consistent, suggesting a relation between spinal and back surface motion. A method developed from the work of Benatti permitted the definition of rotations in terms of the standard anatomical axes.

This was based on a concept from linear algebra concerning the relative orientations of two rigid bodies. They may be described by expressing the orthogonal base vector m_B of one in terms of the orthogonal base vector m_A of the other. This can be written as

$$[m_B] = [R][m_A],$$

where R relates the two (fig 1.2.4). We consider such transformations in detail in chapter 3.

According to Drerup and Hierholzer (1987), localization of anatomical landmarks must not depend on a fixed exterior coordinate system.[38] It should also be insensitive to moderate asymmetry of the back. Such a body-fixed coordinate system may be defined using anatomical landmarks, as shown in figure 1.3.4.

The above authors present a method for automatic determination of these landmarks using the process of segmentation. It involves successive isolation of regions

of interest, such as the vertebra prominens.[a] Anatomical lines of symmetry are used as references. A 2D second order polynomial is used to smooth asymmetrical curves. Isolated points not belonging to the central landmark area are deleted.

Plamondon and Gagnon (1990) evaluated displacement error in locating anatomical landmarks.[41] They employed the method of Euler's angles with a least squares treatment.[b] Their results indicated errors in identifying landmarks had greatest repercussions in determining axial rotation. However, results were sufficiently accurate for measuring rotations down to 1^{o}.

The Weierstrass Approximation Theorem states that any continuous function can be approximated by a polynomial. When the original function is only piecewise continuous, a piecewise polynomial approximation is used.[51]

Cubic polynomials are popular for this purpose as they have continuous first and second derivatives. Hence they are always 'smooth' at the subinterval endpoints. When the second derivatives of the end nodes are zero, the spline is called 'natural'.[51]

The profile of the spine in the sagittal plane can be approximated by a cubic spline. Bethune (1986) showed that a natural cubic spline could describe a back surface profile.[93] It follows that the normalized difference between these two curves would also be a spline function.

This was demonstrated by Bryant et al. (1989), and is illustrated in figure 1.3.6.[28] Note that the spine is naturally separated into three regions by the zero curvatures found at the C7-T1 and T12-L1 junctions. More details on how the motion of skin markers may be related to that of the spine are given in Appendix A.

---

[a] This is an easily identifiable anatomical landmark located at the junction of the cervical and thoracic spine.

[b] In the literature, Euler's angles are often used to describe the rotations of vertebrae in 3D space. An alternative is to use directional angles to define the orientaion of a vector normal to the vertebrae. This subject is discussed further in chapter 3 and Appendix C.

1.3.5 Describing Coupled Joint Motion in the Spine

There appears to be no clear consensus concerning the exact nature of coupled motion in the cervical spine. This disagreement may perhaps be attributed to the wide variety of different techniques being used, as well as to the complexity of the analysis.[112] Nevertheless, the ability to quantify and subsequently analyze such motion may be of use in the diagnosis of some neck injuries.

Both in-vivo and in-vitro techniques have been employed to quantify the movement of cervical motion segments. Computer tomography and biplanar radiographs have been used in live subjects to determine limits of rotation for each joint.[119,120,121] Motion segment testing machines have yielded extensive data on coupled motion in cervical spines from cadavers.[65,113]

According to Schultz (1987), the three dimensional nature of configurations such as bending and twisting of the spine make them difficult to describe.[65] Furthermore, attempts to correlate changes in motion ranges with various spinal abnormalities have met with mixed success. He noted:

" ... there still seems to be no completely satisfactory scheme to measure longitudinal axis rotations or other complex motions in a clinical setting, despite their possible diagnostic importance."

Frymoyer et al (1979) suggested that non-invasive methods be developed to analyze coupling motion.[119] They wrote:

"The most important attribute of ... spinal behaviour is the complex coupling which occurs. ... it is important that these motion characteristics be quantitatively analyzed as far as possible. "

Pearcy et al (1984) also examined the phenomenon of coupled motion in the spine.[121] They found that:

"The complex nature of the intervertebral joints results in coupling movements, such that when a joint flexes it also may exhibit lateral bending or axial rotation at the same time; a full three dimensional analysis is required to describe these movements."

In Appendix A, a more complete discussion of the unique nature of coupled motion in the cervical spine is provided, along with the results of several previous studies on this subject. These constitute important factors in the decision to develop the enhanced displays described in chapter 3.

1.3.6 Discussion

In order to identify pathological motion, it is necessary to understand how it manifests itself. The mechanisms of cervical soft-tissue injury, as well as the diagnostic methods used to detect them, have been reviewed briefly here and more thoroughly in Appendix A.

The condition resulting from hyperflexion and hyperextension, commonly known as whiplash, appears to be the major contributor to neck pain. The diagnosis of these conditions is, however, not standardized.

Nevertheless, the soft tissue injuries we have considered are representative of the type of pathology that might be detected through motion analysis. Since osseous (ie. bony) injuries are usually detected by radiographs, these were not considered in detail.

Delayed injury to the spinal cord may result even from non-acute trauma, particularly due to hemorrhaging (ie. internal bleeding). Pain and subsequent dysfunction, or even paralysis, can eventually occur. Hence it is essential to objectively identify possible indicators of injury.

The engineer must be capable of guiding the clinician in linking these factors with the information provided by the diagnostic device. We have examined some of the analytical models that have been developed to quantify cervical motion and injury mechanisms.

The models considered were all developed through analogous approaches. Points of insertion for muscles or ligaments were digitized and the resulting forces estimated. Approximations were used to render the systems of equations deterministic. The cerebrospinal fluid may be accounted for by considering flexible, liquid filled tubes. However, a biomechanical model for the spinal cord is not yet available.

Physical models are used primarily to test their analytical counterparts. It appears

that the physical models do not yet simulate head/neck motion adequately. Accurate predictive injury modelling is thus not possible at this time, though normal and pathological motion can be approximated.

Any cervical range of motion analysis should take these models into account. Algorithms executed by diagnostic equipment to treat motion data must be consistent with the analytical models. However, pathological motion can only be identified if it can be compared to known patterns of normal movement.

Hence, the range of normal cervical movement was considered next. By combining results of in-vitro and in-vivo studies, we were able to approximate the parameters for nor al cervical motion. However, it is apparent from the range of motion tables (see Appendix A) that there are large variations in the data.

Therefore, they cannot be used as an absolute reference for normal motion. It appears necessary to accumulate range of motion data specifically meant for use with a given diagnostic instrument to be used clinically. Nevertheless, such a database should be compared with the results of studies obtained using other instruments, in order to verify their credibility.

We also saw that it is possible to obtain a linear relationship between the motion of skin markers and the spine underneath. This has already been established for the lower back and may similarly be determined in the future for the neck. Thus, it is reasonable to make deductions about underlying injuries based on data from the tracking of skin markers.

Coupled joint motion was identified as an important factor in the analysis of cervical movement. Previous studies of coupled joint motion in the spine have tended to use complicated methods to deduce simultaneous motion in the three principal orthogonal planes. Hence, as we will see in chapters 2 and 3, the ability of a diagnostic tool to quantify this motion in a straightforward manner may potentially be very useful.

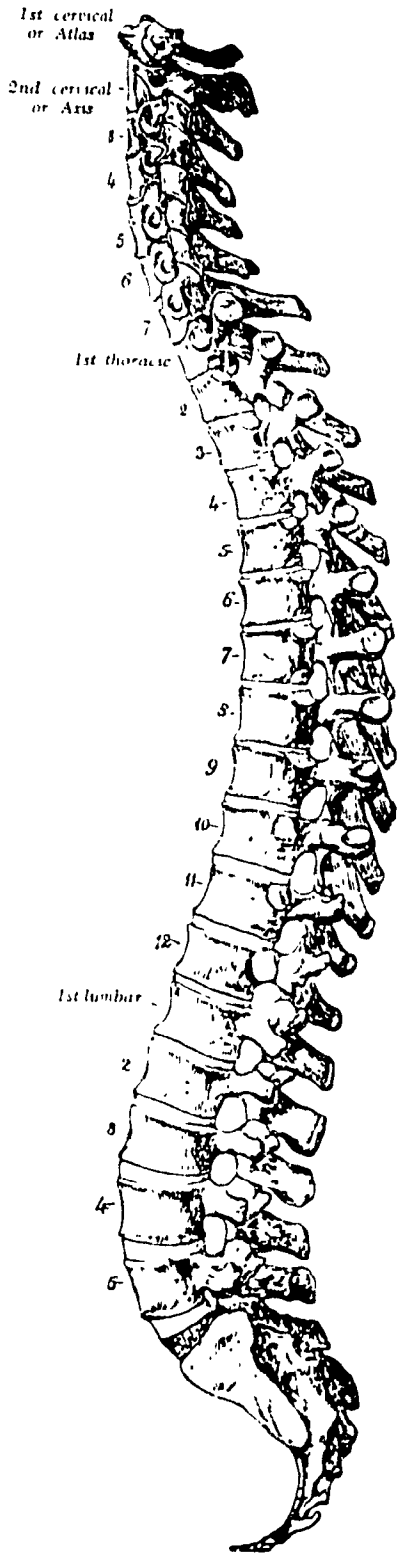

Fig 1.3.1:

Lateral view of the vertebral column (right).

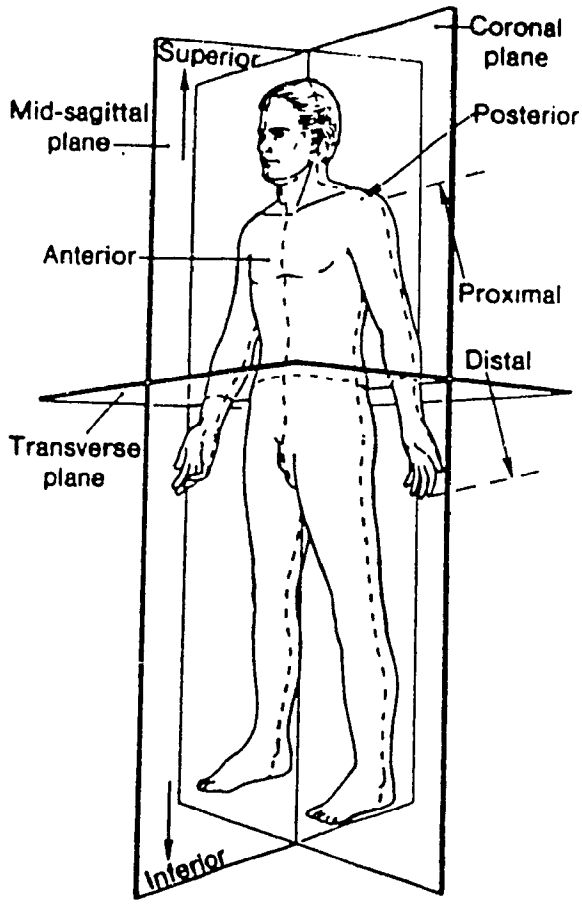

Fig 1.3.2:

Planes of the body (above).

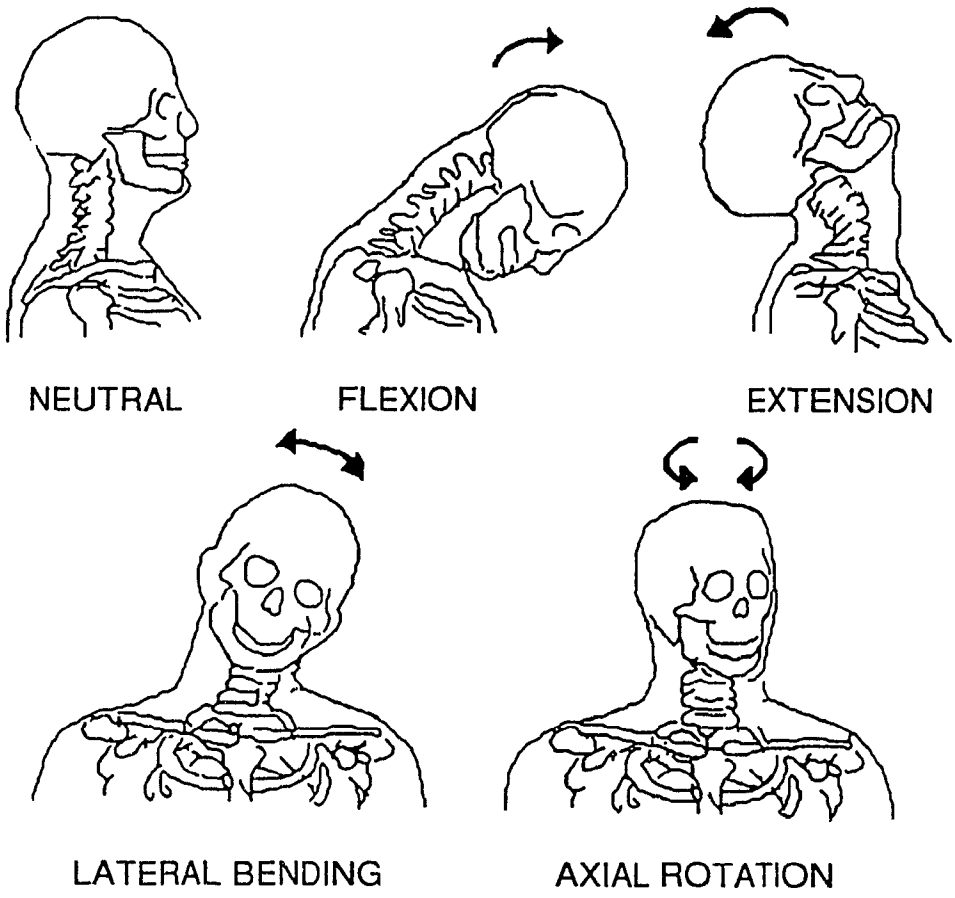

Fig 1.3.3 (a): Principal movements associated with motion of the cervical spine. Adapted from Sances et al. (1984).[30]

Fig 1.3.3 (b):

Simplified diagrammatic reresentation of extremes of motion for the entire human spine. Adapted from Sances et al. (1984). [30]

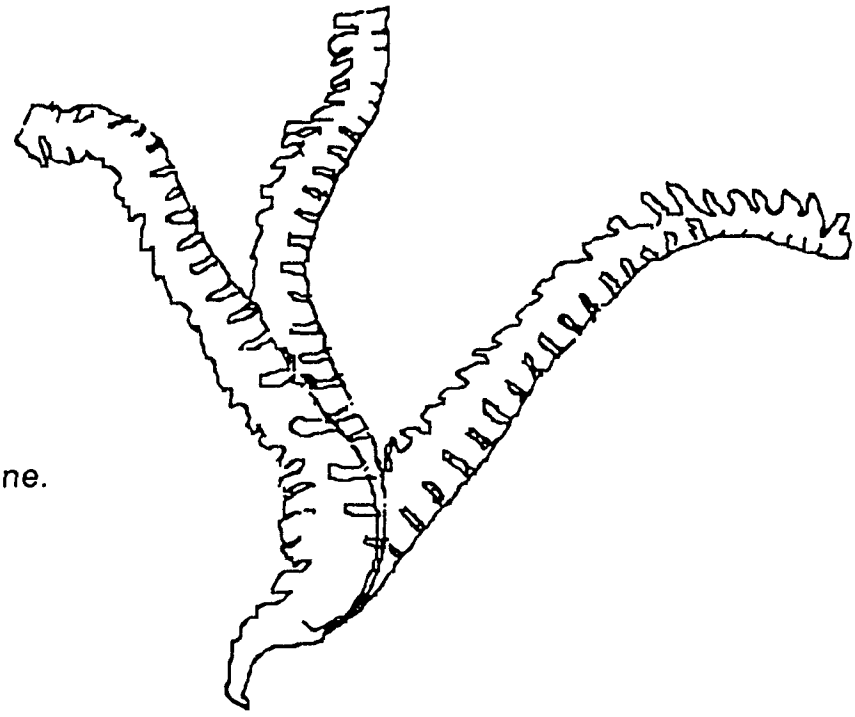

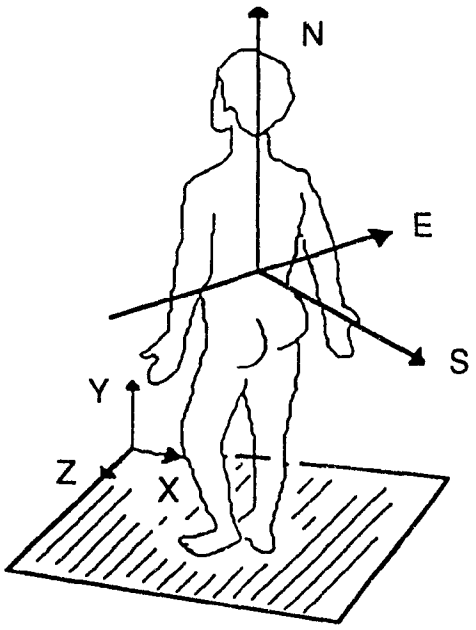

Fig 1.3.4: Laboratory fixed and body fixed coordinates systems. Adapted from Drerup and Hierholzer (1987). [38]

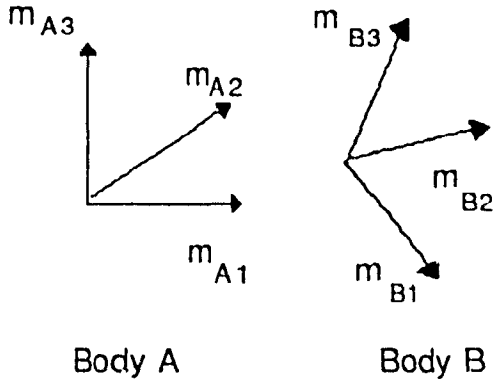

Fig 1.3.5: Orthogonal base vector system for two rotating bodies. Adapted from Pearcy et al. (1987). [27]

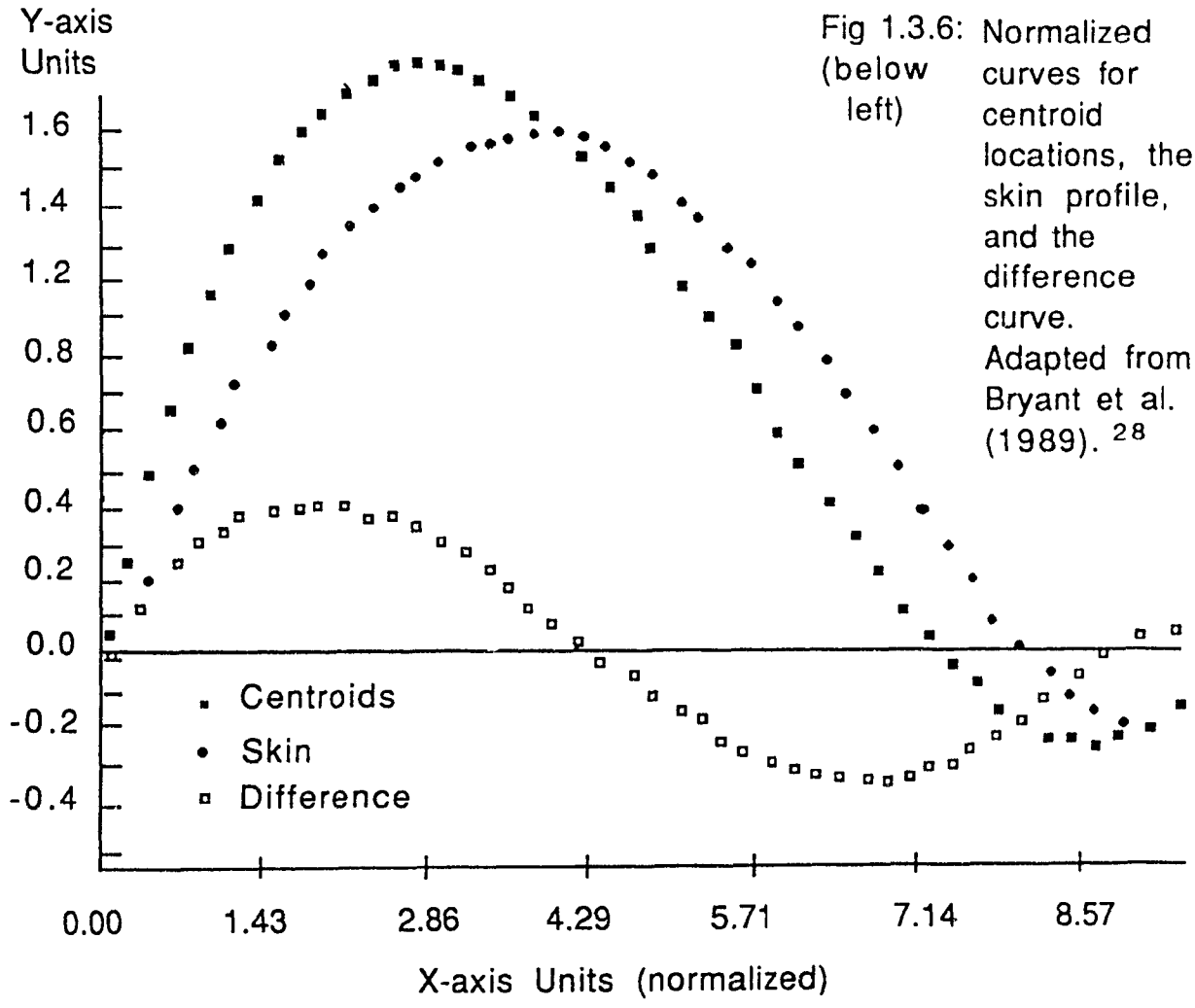

Fig 1.3.6: (below left) Normalized curves for centroid locations, the skin profile, and the difference curve. Adapted from Bryant et al. (1989). [28]

1.4 SCOPE OF THE THESIS

We have determined the need for an instrument to perform non-invasive analysis of cervical soft tissue injuries. We then considered the numerous biomechanical factors involved in relating the information provided by such an instrument to the injury.

Following a brief summary the review presented in this chapter, we will now establish the objectives of this investigation. In particular, we will consider the evaluation and subsequent enhancement of a device designed to meet the need identified above.

This is an on-going research area, which requires a long time to gather and properly interpret data. Hence, at the end of this section we will clearly define the bounds of this study, while identifying possible directions for future investigations.

1.4.1 Summary of the Review

This review included consideration of the following topics relevant to cervical motion analysis:

- current imaging and measurement techniques for relating range of motion to cervical soft tissue damage,
- the mechanics of relevant injury mechanisms,
- analytical models which may be used to quantify the above,
- a comprehensive summary of cervical range of motion results,
- the localization of anatomical landmarks and how to relate the movement of skin markers to that of the underlying vertebrae, as well as
- the importance of coupled joint motion in identifying cervical injuries through motion analysis.

We have thus summarized the many factors relevant to motion analysis in the cervical spine. First the tools currently available for this purpose were reviewed. It was determined that they are inappropriate for routine evaluation of soft tissue injuries to the cervical spine.

We then saw that improperly diagnosed injuries may result in chronic long-term

effects. In order to design or improve an applicable diagnostic instrument, the engineer must be able to explain how the clinician may relate the information provided to possible mechanical injury mechanisms.

Analytical head/neck models are useful in quantifying these. We saw that elements of these models should be considered in algorithms which perform range of motion analyses. To eventually be able to differentiate normal from pathological movement, we also considered results from other cervical range of motion studies.

However, these indicated large discrepancies in the data. Therefore, any comparison between normal and pathological data should primarily consider results acquired directly with the particular instrument being used.

Mathematical techniques may be used to establish a relationship between the motion of skin markers and the vertebrae underneath. Hence, it appears valid to identify injuries based on the tracking of skin markers. Coupled joint motion was found to be an important indicator of injury, but existing instrumentation does not provide a simple means for its analysis.

1.4.2 Objectives

Based on these considerations, it should now be possible to evaluate and, if necessary, to improve upon a given cervical diagnostic instrument. Hence, we may now turn our attention to the study of a specific device.

First, however, let us summarize the overall objectives of this study. These areas follows:

i) Determine the need for, as well as the subsequent requirements of, any new instrumentation designed to help identify injuries to the cervical spine. The information relevant to this objective was provided in chapter 1.

ii) Evaluate whether a particular new diagnostic instrument meets these requirements. If it does not, the necessary improvements will be identified. This will be the topic of chapter 2.

iii) The improvements described above will be carried out and explained in detail. These concerns are addressed in chapter 3.

iv) The results of this investigation will be examined and recommendations for further work outlined. This is the subject of chapter 4.

Thus the investigation consists of several distinct steps, as described above. Before proceeding with the second objective, we will briefly consider the extent of the investigation and the means which will be used to arrive at the stated goals.

1.4.3 Extent and Methodology of the Investigation

We will begin by describing the diagnostic instrument which is under consideration here. It is known as the Cerviscope and is manufactured by Spinex Medical Technologies of Montreal. This device is closely related to a similar instrument used for lower back diagnoses, called the Spinoscope.

The evaluation of the Cerviscope involves the analysis of some preliminary experimental data. We then compare this device for examining the cervical spine with the Spinoscope. The latter is employed for assessing disorders of the lower back. Since both devices make use of skin markers to analyze underlying spinal motion, we must consider the relationship between radiographic data and that obtained for the markers.

The above evaluation leads to the conclusion that the displays provided by the original Cerviscope lack the precision required to accurately identify cervical soft tissue injuries. This results in the development of a new set of diagnostic displays designed specifically to analyze three dimensional coupled joint motion.

The enhanced displays are meant to provide information complementary to the existing displays, as well as to help verify their results. This feature describes cervical motion in terms of direction angles, which characterize the angular displacement of the spine in both fixed and moving reference frames.

These angles are derived from the projections onto three orthogonal planes of vectors whose motion is directly proportional to that of the spine. The three planes correspond to those typically used to describe the human body (mid-sagittal, coronal, and transverse).

The software for such a display must be developed to work in conjunction with

the half a million lines of code already developed, over the course of several years, for the Cerviscope (and its ancestor, the Spinoscope). Once the motion data accumulated by the device is treated, it must also be converted into a format consistent with other displays being developed by the company.

In particular, the code should be compatible with graphics and mouse handling capabilities designed in-house, specifically for this machine. It will be written in Metaware High C, which is a professional quality development system being used for all software related to this product.

All code is divided into modules, which are sets of files containing routines preforming related tasks. Modules for the calculation engine, data handler, graphics, and mouse driver must be developed exclusively for this application. Commercial CAD packages are not applicable, since they involve the manipulation of data and subsequent display of lines in a format inconsistent with this product.

In addition, the above modules must be written using state of the art programming techniques (eg. data abstraction, object oriented design, etc), in order to be consistent with other code being developed concurrently by Spinex.

Finally, we consider further investigations that will be required. This involves the integration of both the original tool and the enhanced displays into the clinical diagnostic process. The accumulation of a large database over a long period of time will be necessary.

This will lead eventually to a matching of the biomechanical factors described above with the information provided by the diagnostic displays. The user should then be able to objectively differentiate between pathological and normal motion in the cervical spine.

CHAPTER 2 - EVALUATION OF A DEVICE FOR THE ANALYSIS OF MOTION IN THE CERVICAL SPINE USING KINEMATIC DATA FROM THE TRACKING OF SKIN MARKERS

2.1 GENERAL

In this chapter we will consider the evaluation of a specific device designed for the analysis of motion in the cervical spine. This involves a description of the instrument and the clinical protocol used, as well as some of the factors considered in determining the potential usefulness of this diagnostic tool. Much of the evaluation results from the gathering and analysis of data from twenty preliminary test subjects.

The user interface, analytical displays, and printed reports available to users of the Cerviscope are described in detail. Examples and sample interpretations of the displays are given. The analytical functions provided by the device are examined next. The capacity for curve fitting, correctly representing physiological movement, and quantifying coupled motion are evaluated.

A comparison is made between the methods used for examining the lumbar and cervical spine using the above device and another closely related instrument. In particular, we consider how the algorithms for the former were adapted from those developed for the latter.

Since the lumbar and cervical spine have both differences and similarities, these must be considered. Finally, we examine the applicability of the device under consideration to the traditional clinical diagnostic process.

As in chapter 1, the minimum information required to describe and evaluate the instrument is given here. However, this assessment involves additional factors which are relevant to the development of the enhanced displays presented in chapter 3. The interested reader is referred to Appendix B for this information.

2.2 OVERVIEW OF THE DIAGNOSTIC TOOL UNDER CONSIDERATION: THE USER INTERFACE AND DISPLAY SCREENS

In this section we will examine those aspects of the device under consideration which are visible to the user. The configuration of the instrument, the user interface, and the display screens are all related to the ease with which diagnostic information may be interpreted. We will begin with a description of the hardware configuration involved.

2.2.1 Description

The diagnostic tool being evaluated here is known as the 'Cerviscope'. It is a modified version of the previously developed 'Spinoscope', which has been used as an aid to lumbar spine diagnoses for several years. Both instruments are manufactured by Spinex Medical Technologies of Montreal.

The Cerviscope and Spinoscope function on the same basic principles: infrared emitting diodes (IREDs) are attached to the subject's skin and motion is recorded by two cameras.[a] Discrete data is accumulated at the rate of 180 frames per second, using a customized version of the University of Waterloo's WATSMART motion analysis system. The overall layout for these devices is shown in figure 2.2.1.

In the Cerviscope, seven markers are located between vertebrae C2 and T3. Two more are placed at T4 and T7, as well as four above the iliac crests and the scapulae, respectively. In addition, two EMG surface electrodes are positioned bilaterally above the sternocleidomastoid muscles. The configuration of diodes and EMG electrodes for the Cerviscope is illustrated in figure 2.1.2.

The kinematic data from the motion of the markers is processed to reduce noise, such that the spatial coordinates of each marker are defined with an accuracy of one part in 500. A polynomial is fitted to the best estimate of marker coordinates, from which the

---

[a] Note that the latest versions of these devices will incorporate a three camera system. This new system, known as the 'Optotrak', will replace Northern Digital's previous 'Watsmart' system. The Optotrak is expected to reduce noise related to data acquisition from infrared emitting diodes.

location of the projection of the vertebrae is calculated using anthropomorphic tables. From these it is possible to deduce the various parameters of interest. [74]

The original overall analysis provided by the Cerviscope included assessment of cervical lordosis, thoracic kyphosis, and intersegmental mobility. In addition to these, a three-dimensional characterization of coupled motion has also been developed as a result of the present study.

Note that since the IREDs are mounted on the skin surface, the underlying vertebral motion may only be inferred indirectly. This problem was introduced in chapter 1 (section 1.3.4). The performance of the original Cerviscope software will be deduced indirectly from its overall capacity to help identify cervical injuries.

2.2.2 The User Interface

Many aspects of the interface originally developed for the Spinoscope were carried over into the Cerviscope displays. The user interface is entirely mouse driven. Upon power up of the system, a simple menu is displayed, which allows the user to select the following functions:

i)	Record	v)	Archive
ii)	Playback	vi)	Utilities
iii)	Report	vii)	Exit
iv)	Database		

The first of these is used for recording patient data and the second for reviewing the recorded motion. The 'report' screens show groups of parameters, such as gross motion, intersegmental mobility, etc, derived from the data by the software.

The 'database' option allows selection of any patient whose data is currently loaded on the computer's hard disk drive. This may be either lumbar or cervical data, and the appropriate report screen will be displayed based on flags saved in the data base.

The 'archive' feature is used to transfer patient data to or from floppy disks for portability and storage and the 'exit' option returns to the operating system. The 'utilities' consist of the following installation and maintenance functions:

i)	Data base maintenance	v)	Real time display
ii)	Graphics board diagnostics	vi)	Super user mode
iii)	Camera setup	vii)	Spinex hot line
iv)	Camera calibration	viii)	Exit

The first four of these are self explanatory. The fifth item shows the diodes and EMGs on screen to verify that they are all functioning properly. The 'super user mode' is enabled from here to allow access to extra features not normally available to users (eg. untreated raw data). The Spinex hot line is used for connecting by modem with consultants from the manufacturer, in order to perform trouble-shooting.

2.2.3 The Report Screens and Standard Report

In Appendix B a printout of the various pages of the original Cerviscope report is illustrated. They are shown in a condensed format known as the "standard report". A guide exists which explains how the Spinoscope report, which is analogous to the Cerviscope, may be interpreted.[74]

This format condenses most of the information available from the Cerviscope 'report' screens into four printed pages. The interpretation of the screens themselves is similar to that for the standard report, which is also described in Appendix B. The latter format is designed for convenient analysis of a patient's Cerviscope examination in hard copy format. Examples of the report displays as they appear on screen are given below (section 2.2.5).

The first page of the standard report contains general information on the subject, followed by an overview from several perspectives. The remaining pages repeat the subject identification and then present details of specific views. Each of these is described in detail in Appendix B, along with a discussion of their physiological significance.

2.2.4 The Playback Screen

The Cerviscope includes a feature known as 'playback' which allows the user to view the motion of the IREDs in real time. Thus stick figures representing the position

of markers for subsequent frames are displayed in sequence.

This feature provides an intuitively simple way to observe the subject's motion. The successive frames may be viewed continuously or one at a time. In Appendix C, a sequence of several frames from the playback screen is used to illustrate a given lateral bending motion. In this case, an interval of ten frames was chosen between the printed pages.

Note that the user may zoom in on a particular view (ie. back, top, or side) and automatically display the distances between specified IREDs for each frame. In Appendix C the back view is enlarged in order to examine the lateral bending motion. For considering flexion extension or axial rotation motion, the respective side and top views might be enlarged instead.

2.2.5 Examples From the Original Cerviscope Displays

Figure 2.2.1 (a) shows the original menu which appears upon startup of bath Spinoscope and Cerviscope. As explained earlier (section 2.2.2), this menu allows access to various functions common to the two instruments. In figure 2.2.1 (b) we see the new report selection menu which appears when the user chooses 'report' in the original menu.

From here the cervical coupled motion display (ie. the enhancement described in chapter 3 may be selected, along with several other options. The 'regular report' is just the original report format, the 'thoracic report' is another new program developed concurrently with the cervical software, and the 'gait analysis' display is an offshoot of the latter which is not yet available. 'Exit to shell' simply returns to the original menu.

In figure 2.2.2 the original Cerviscope report screens are shown. These pages correspond to the standard report printout described in section 2.2.3 and Appendix B. The overview page [fig 2.2.1(a)] shows stick figures of the subject from various points of view. This is helpful in giving the user an intuitive picture of the subject's position, but provides no quantitative information.

The two flexion extension pages [figs 2.2.2(b)-(c)] describe the forward bending movement. The curves shown indicate mobility between vertebrae, as well as curvature and angular displacement for different portions of the spine. The mobility curves are

difficult to interpret objectively and sensitive to errors in treatment of the data by the original software (see section 2.3). The latter, conversely, tend to be very noisy and have limited value.

Similarly, the lateral bend page [fig 2.2.2(d)] describes the side to side motion in terms of the mobility and orientation of the various vertebrae. Both the inter-segment mobility and the segmental orientation are prone to the same difficulties as the mobility box for flexion extension.

Finally, in figure 2.2.3 we see the 'playback' screen, which is used to illustrate continuous or stop action motion for any frame. The inset box in the side view for figure 2.2.3 (b) gives a running count of the distances between selected IREDs (referred to as LEDs here).

As we will see later (section 2.3.3), deducing coupled motion in orthogonal planes is very tedious using this information. Nevertheless, this display is very useful in observing the progression of the subject's motion.

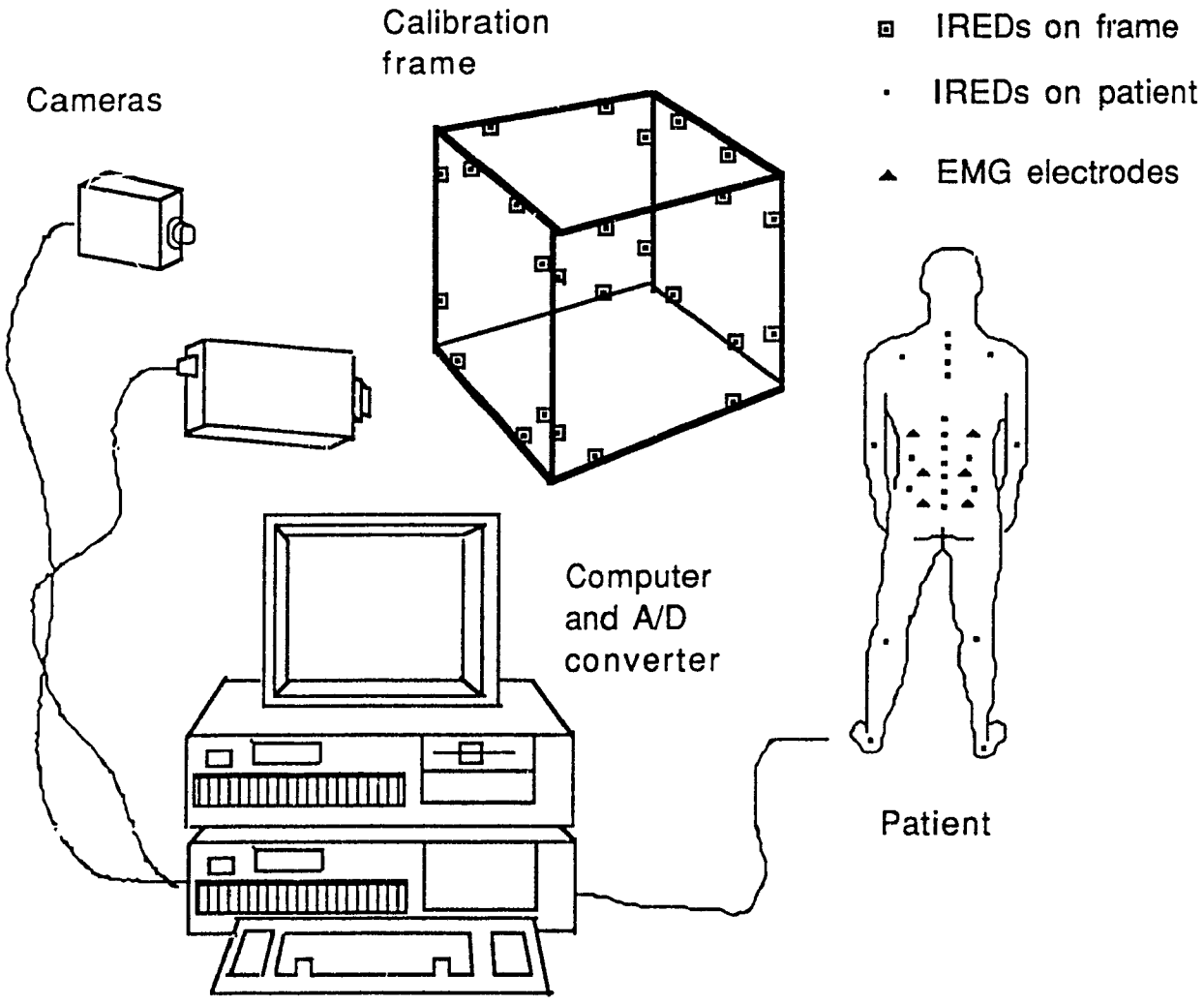

Fig 2.2.1: Overview of the Spinoscope system from which the Cerviscope was adapted. Redrawn from Gracovetsky et al. (1989). [74]

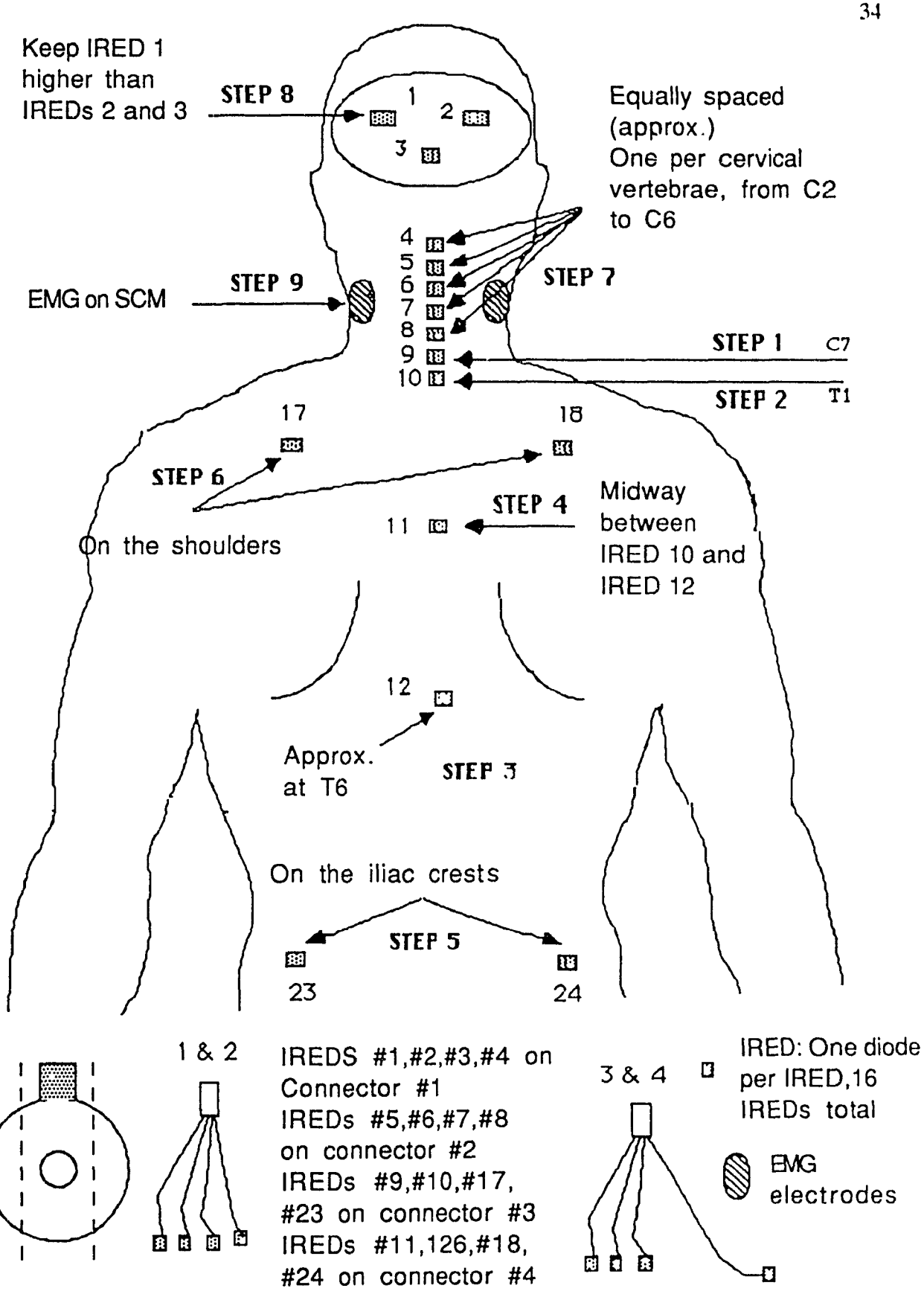

Fig 2.2.2: Cerviscope IRED and EMG placement. Adapted from Papagiannis et al. (1990). [88]

Fig 2.2.3: Menus for selecting the old and new Cerviscope displays.

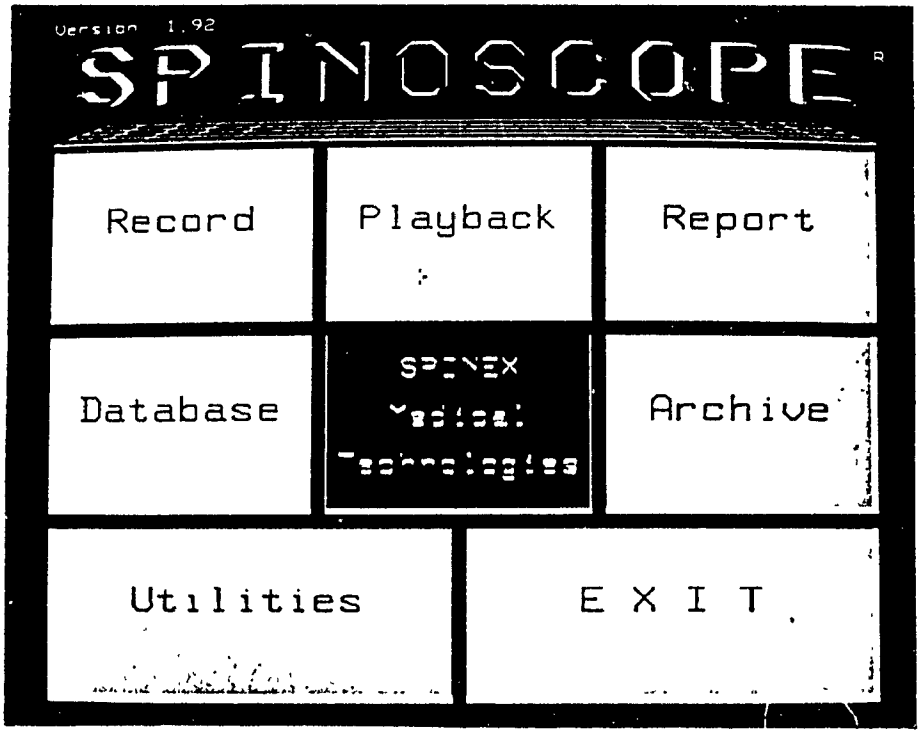

a) Main menu for selecting Spinoscope and Cerviscope functions.

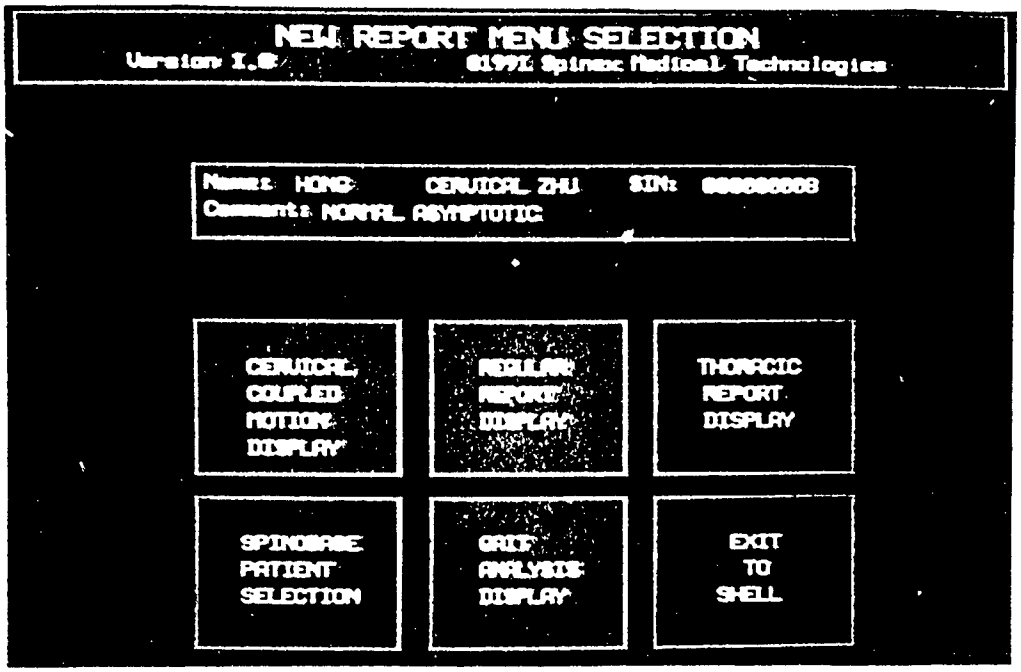

b) Selection menu for accessing the new versions of the report, including the new cervical coupled motion display.

Fig 2.2.4: The original Cerviscope report displays.

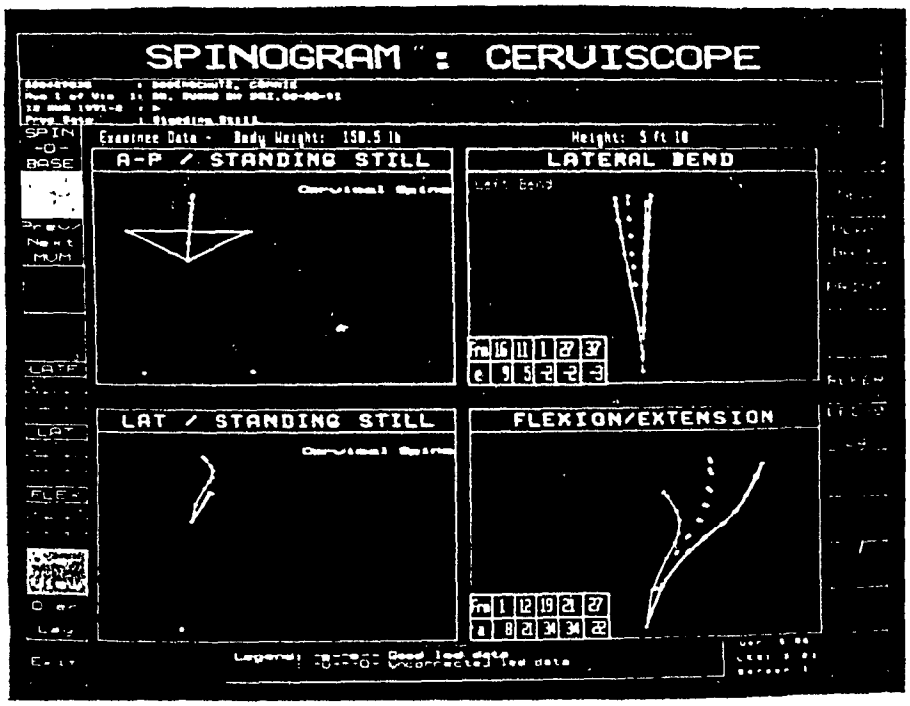

a) Overview page.

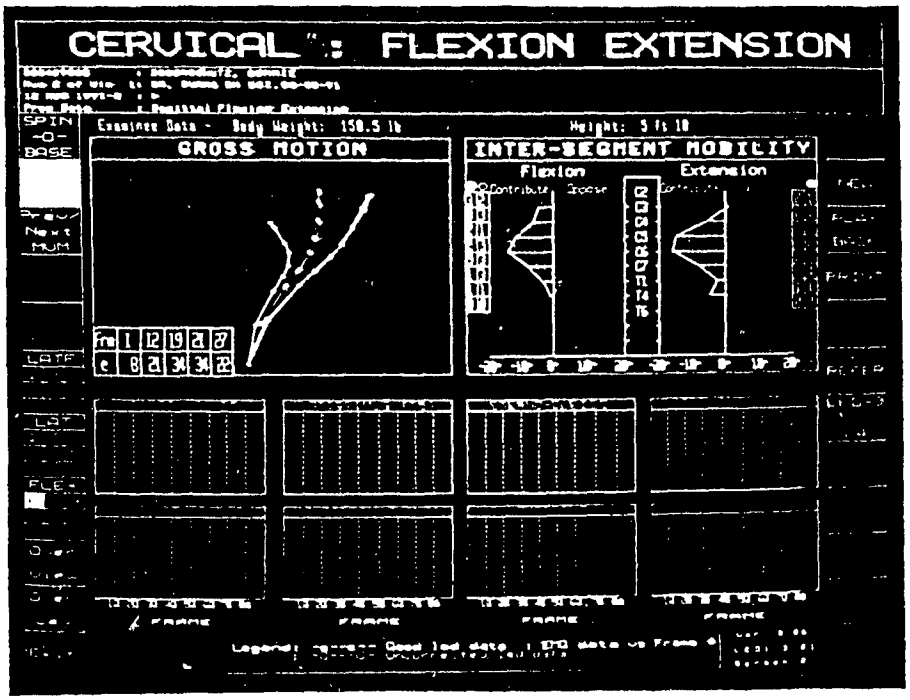

b) Report of flexion/extension gross motion and intersegmental mobility, as well as EMG (not active for this subject).

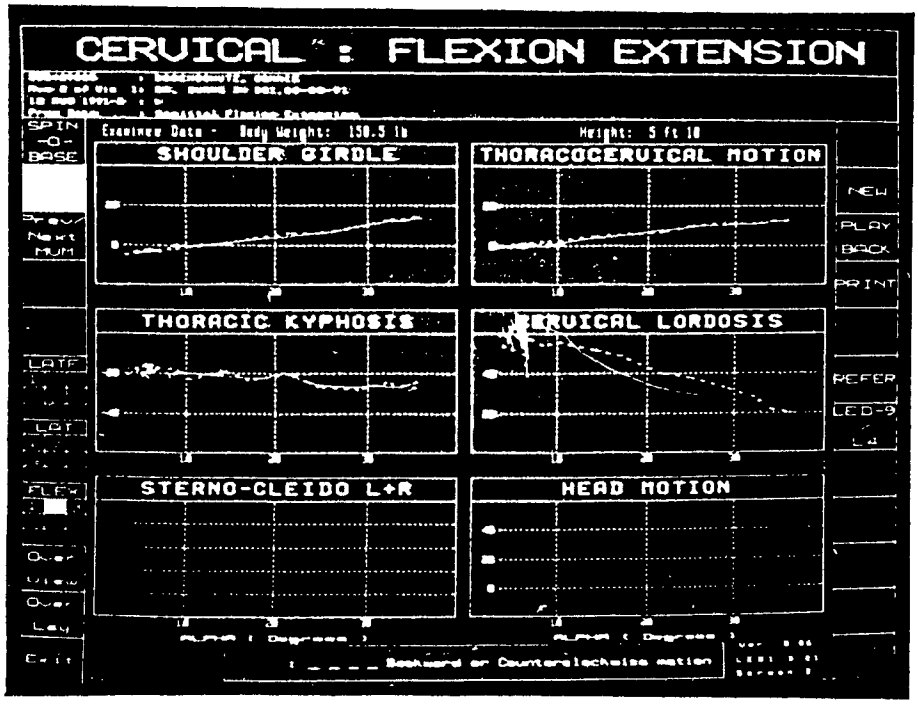

c) Derived results for original cervical flexion extension motion. The high noise level shown is typical of this display.

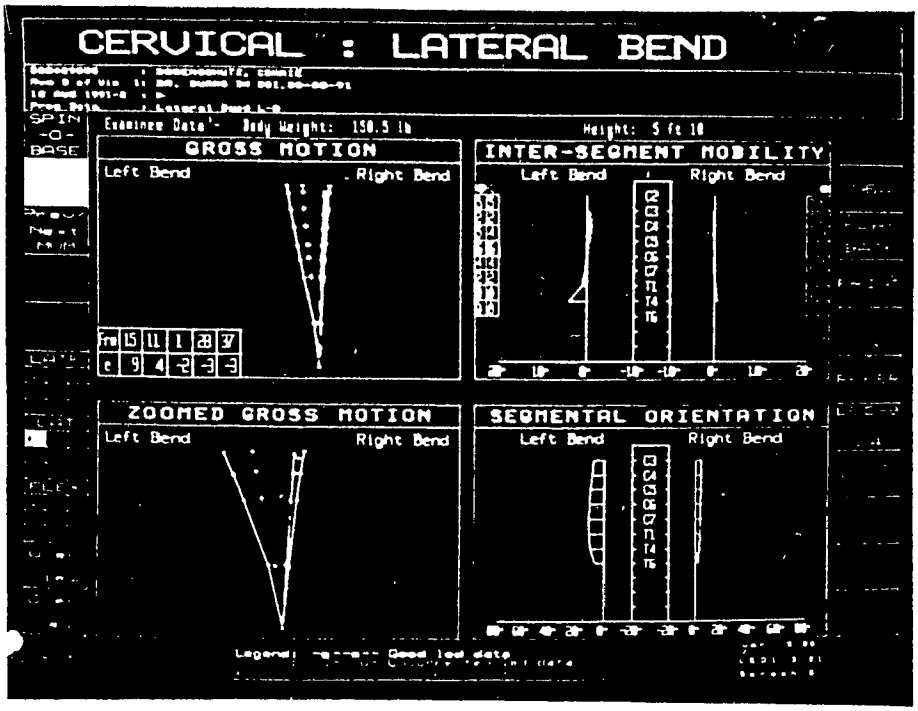

d) Gross motion, intersegmental mobility , and segmental orientation for lateral bend movement.

Fig 2.2.5: Original Cerviscope playback display.

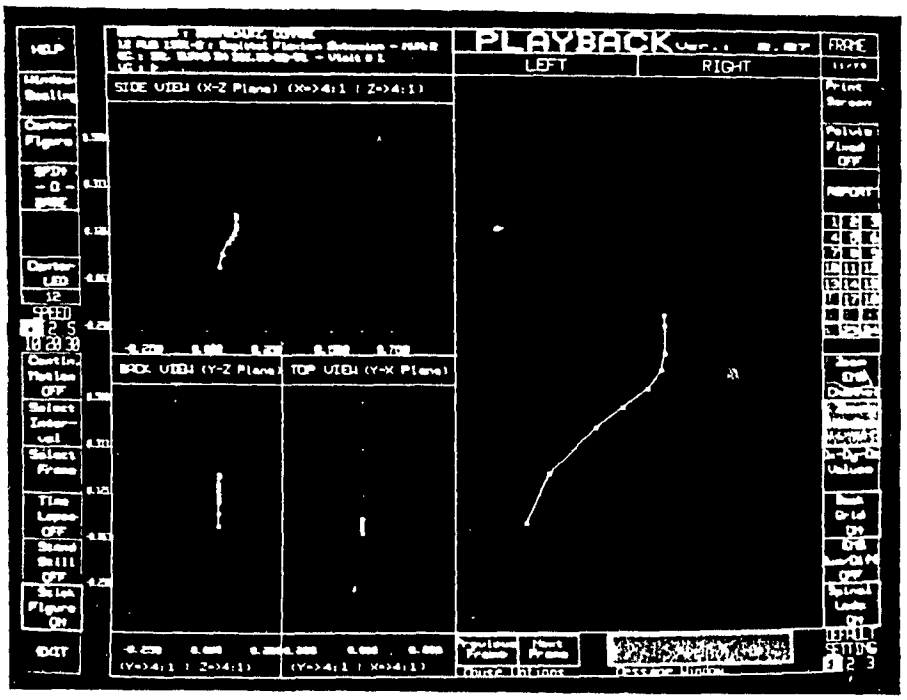

a) Playback view of flexion/extension movement, midway through flexion.

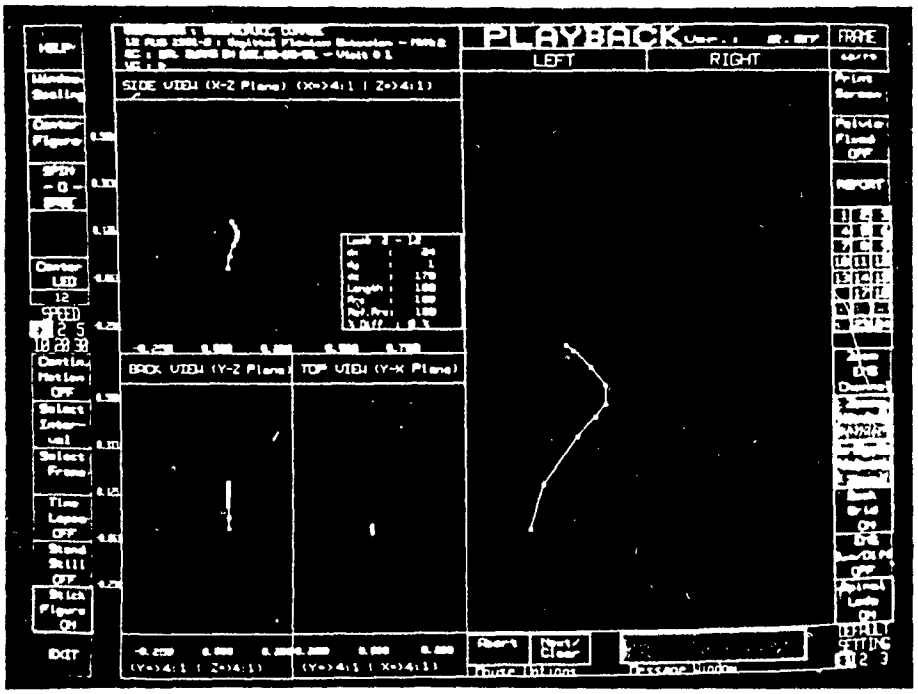

b) The same movement as in (a), midway in the extension phase. Inset shows distances between top and bottom IREDs, which may be used to indirectly calculate coupled motion.

2.3 ANALYTICAL FUNCTIONS OF THE DIAGNOSTIC INSTRUMENT

Now that we have seen the aspects of the Cerviscope which are visible to the user, let us now consider how the data from the skin markers is treated internally. We will want to consider how the instrument filters the data and whether the resulting curves represent a true physiological picture of the subject's motion.

We also need to determine if the Cerviscope has the capacity for adequately describing coupled motion. We will consider how the algorithms used for treating data in the Cerviscope were adapted from those developed for its ancestor, the Spinoscope. Finally, we will consider situations where examinations with the Cerviscope may be inappropriate.

2.3.1 Curve Fitting for the Upper Spine

In figure 1.3.3(b) we saw how the progression of lordosis vs kyphosis occurs in the entire spine. Polynomial curves are used to approximate this curvature for the lower back in the Spinoscope software. Cubic splines are used to represent different portions of the lower spine, with interpolation at the thoraco-lumbar junction.

The concept of curve fitting for the spine was considered previously (section 1.3.4). However, this was in the context of correlating the motion of skin markers and vertebrae. Here we are concerned with goodness of fit between the actual curve and that used in the software.

Recall that the profile of the spine in the sagittal plane can be approximated by a cubic spline.[28] The spine is naturally separated into three regions by the points of inflexion found at C7-T1 and T12-L1.

The cubic spline representation appears to be incorrect for lateral bending in the upper spine. This may be due to the smaller radii of curvature in this area. The use of a single second order spline (ie. parabola) was proposed as an alternative in lateral flexion.

Now let us consider the actual curve fitting that occurs to smooth the representation of the spine that is displayed. Figure 2.3.1(a) shows an unfiltered A-P view

of a subject in the neutral position. The three IREDs on the back of the head are included. Note again the asymmetry due to uneven placement of the cervical IREDs by the examiner.

In figure 2.3.1(b), the filtered view is shown without the IREDs for the head, as it would appear on a typical Cerviscope display. Note that the asymmetry has been smoothed out. Figure 2.3.1(c) shows the same filtered view with the horizontal axis magnified eight times. This results in an exaggerated point of inflexion and cervical curvature.

Without the curve fitting, and with the three head IREDs included, the view would appear as in figure 2.3.1(d). The magnified filtered and unfiltered views are superimposed in figure 2.3.1(e). Hence, when we consider again the filtered, unmagnified view of figure 2.3.1(b), it appears to be correctly derived from the raw data.

A different configuration than that shown in figure 1.6.1 may be required for the Cerviscope IREDs. This would be a response to the problems described above. In fact, the preliminary examinations described here required a slight modification to the original configuration.

In particular, the cervical IREDs had to be spaced further apart than originally anticipated. Indeed, this change may have been partly responsible for the incorrect curve fitting described earlier. However, it appears unlikely, as the software allows enough latitude for the cervical IREDs to go as low as T2.

We also saw earlier (section 1.3.3) that the position of the skull may be used to approximate that of the atlas in rotation.[31,67] Hence the placement of three IREDs on the back of the head will track the occipital motion. Unfortunately, these IREDs are not normally shown on the Cerviscope displays. We'll consider this further in chapter 3.

Another problem is that the point of inflexion between the cervical and thoracic curves actually moves. Hence, it is necessary for the software to constantly track this point. This procedure is also required if a parabola is used to fit the lateral bending curve of the upper spine. Note that the actual vertebral motion can only be determined with certainty from radiographs. This question will be examined again in chapter 4.

2.3.2 Capacity for Representing Physiological Motion

At this point it is possible to speculate upon whether the Cerviscope represents physiological motion in a realistic manner. In figure 2.3.2 we see time lapse images of lateral bending and flexion extension. These have been reproduced from numerous individual frames displayed in the playback mode.

The result is similar to the motion illustrated in the standard reports for forward and lateral bending. Note, however, that there is one major difference. The standard reports do not show the three IREDS placed on the back of the head.

In the motion shown here, views including the head IREDs have been compared with the usual 'truncated' ones. Furthermore, the former views represent raw, unfiltered data. The latter, conversely, represents the data after filtering (ie. curve fitting) by the software.

Figure 2.3.2(a) corresponds to the latter type of display, normally seen in Cerviscope reports for lateral bending. As we can see in figure 2.3.2(b) for frame 59, sometimes the curve fitting results in exaggerated smoothing.

It appears from figure 2.3.2(c) that the unfiltered views, with the head IREDs included, convey no more useful information than figure 2.3.2(a). Hence, the curve smoothing and truncation for lateral bending result in an esthetically acceptable image with no loss of clarity.

The situation is different for sagittal flexion/extension. Figure 2.3.3 shows time lapse views of two separate flexion/ extension movements performed by the same subject. In figure 2.3.3(a) the curves are unfiltered and the head IREDs are shown. There is clearly more forward motion in the movement illustrated on the right.

When the IREDs from the head are eliminated and the curves are smoothed, much of the information appears to be lost. Even in a magnified view, as shown in figure 2.3.3(b), very little motion can be discerned.

The distinct frames have not been superimposed in figure 2.3.3 as they were in figure 2.3.2. That would have resulted in too much of the curves being obscured. This in itself indicates that little change occurs between the successive frames.

However, the sagittal flexion-extension views shown in figures 2.3.1 and 2.3.2

do indicate clear motion. Perhaps the subject chosen for figure 2.3.3 had an abnormally low range. Nevertheless, the time lapse views of lateral bending appear to be much more explicit.

In Appendix A we saw the comprehensive cervical range of motion data from several in-vivo and in-vitro studies. An analysis of coupled motion in the preliminary Cerviscope test subjects showed some agreement with these results.

Yet, some subjects are unable or unwilling to perform the full range of movements prescribed for a Cerviscope examination. It is therefore essential that deductions can be made about one type of motion from another. This was one of the factors which led us to the development of the enhanced displays for analyzing coupled motion, which are described in chapter 3.

Recall that assessments of cervical lordosis, thoracic kyphosis, and intersegmental mobility may be made with the Cerviscope. The standard report page for axial rotation consists only of separate lateral and flexion/ extension views. Hence, if the conclusions reached from our characterization of coupled motion are consistent with these, it should provide an additional means of verifying their validity.

All of the four standard views described in Appendix B were obtained for the first eight Diagnospine subjects. These did not provide sufficient information for an analysis of coupled motion. This led to the development of displays designed specifically to characterize coupled motion.

The data collected for the remaining Diagnospine and AST subjects does not correspond to the standard protocol. Few rotational views were taken, and some lateral bending views only included one side. Nevertheless, the standard reports were similar, and this is where the printouts for the initial observations of Appendix B were derived.

2.3.3 Indirect Analysis of Coupled Motion

Deductions inferred from coupled motion may be the only way to diagnose patients unwilling or unable to perform the standard movements. Until an enhanced set of displays designed specifically to illustrate coupled motion became available, indirect analysis had been used.

In chapter 3 we will see how coupled motion may be deduced from flexion/extension, lateral bending, and rotation movements. Such inferences may be made from the report and playback screens alone, but this requires tedious manual tabulation of motion in the respective planes. The enhanced displays make this process automatic.

2.3.4 Comparison of Two Closely Related Instruments

In this chapter we have often considered how the software for the Cerviscope was adapted from that for the Spinoscope. In many cases this was quite acceptable, since the functions being illustrated were similar.

In other cases, however, the displays developed for the lower back were found to be inappropriate for the neck. In fact, the entire Spinoscope report format will eventually be replaced by a new, more flexible one which is currently under development.

Many of the features to be used in the new Spinoscope displays were incorporated into the cervical coupled motion display described in the next chapter. However, before considering the latter further, we may wish to examine some factors which differentiate motion analysis in the lower back and in the neck.

This would be helpful in distinguishing between features of the Spinoscope which are compatible with the Cerviscope and those which are not. A detailed discussion of this comparison is given in Appendix B.

2.3.5 Applicability of the Cerviscope to Clinical Situations

Figure 2.3.4 shows several algorithms for the diagnostic evaluation of injury to the cervical spine. They are differentiated by the perceived possibility of neurologic deficit. It must be emphasized that the Cerviscope was not conceived as a tool to be used when neurologic dysfunction is suspected.

However, according to Herkowitz and Rothman (1984), neurologic deficit may occur after several weeks, when none was present initially.[78] Indeed, initial radiographs may show no bony or soft tissue abnormality. Although this eventuality is rare, it should be considered when determining the role of the Cerviscope in diagnoses.

Fig 2.3.1: Curve fitting by the Cerviscope software. Adapted from playback screen of Diagnospine preliminary data (L-R lateral bending, frame 2, subject RM).

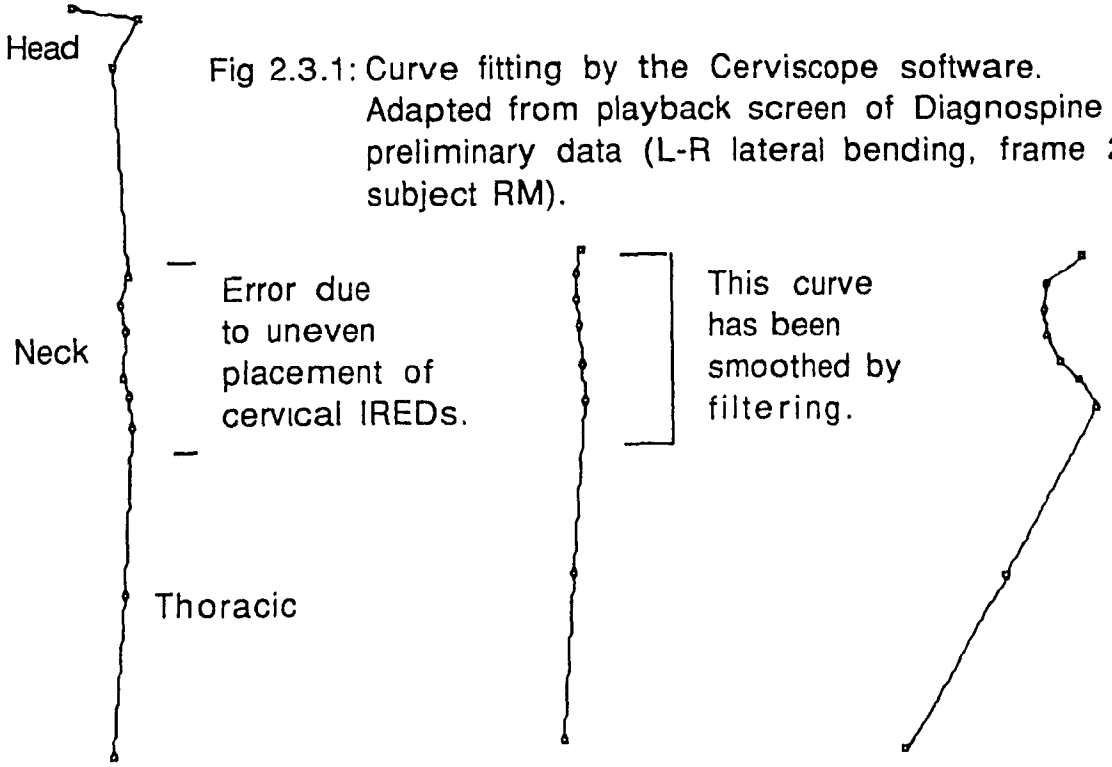

Fig 2.3.1(a): Unfiltered A-P view in neutral position, with three IREDS on (above left) back of head, six on neck, and two on the thoracic spine.

Fig 2.31(b): Filtered version of the same view, without the (above center) IREDs from the head.

Fig 2.31(c): Filtered version with the horizontal axis magnified (above right) eight times.

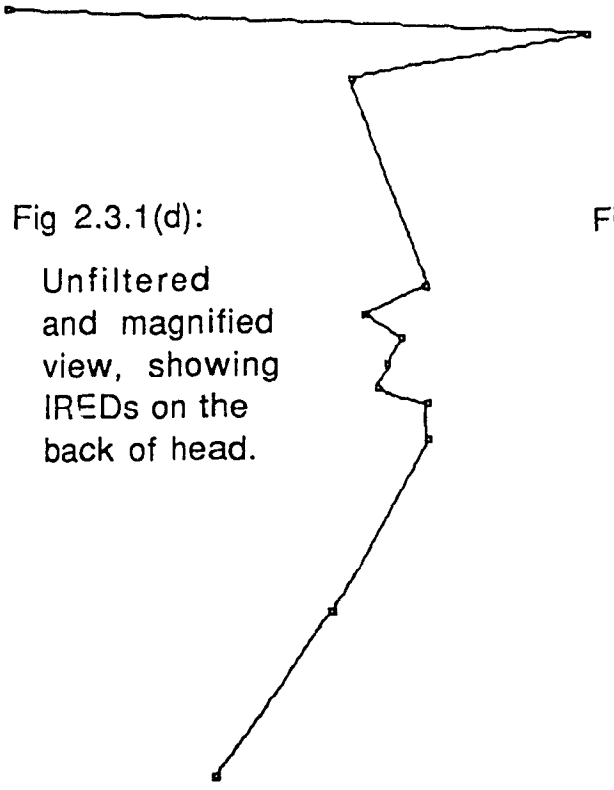

Fig 2.3.1(d): Unfiltered and magnified view, showing IREDs on the back of head.

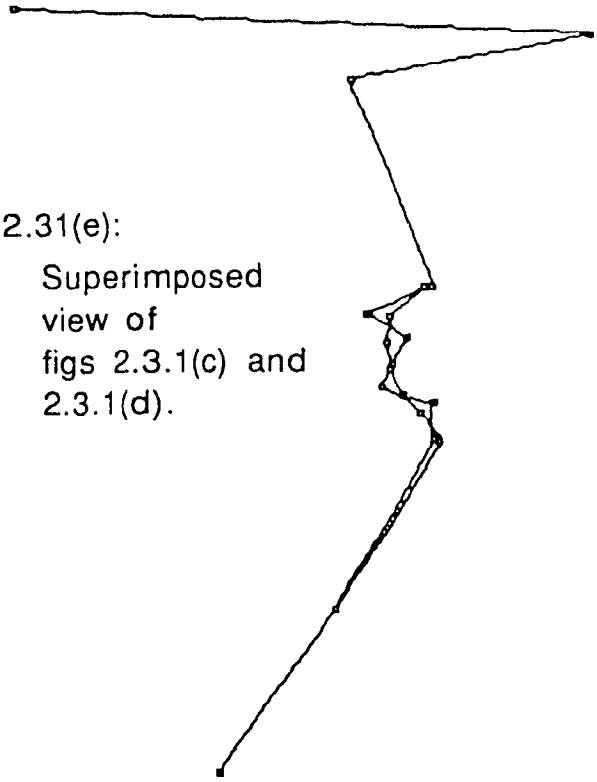

Fig 2.31(e): Superimposed view of figs 2.3.1(c) and 2.3.1(d).

Fig 2.3.2: Superimposed views of lateral bending from successive frames, simulating time lapse display. Adapted from playback screen of Diagnospine preliminary data (L-R lateral bend, subject RM, frames 1-59).

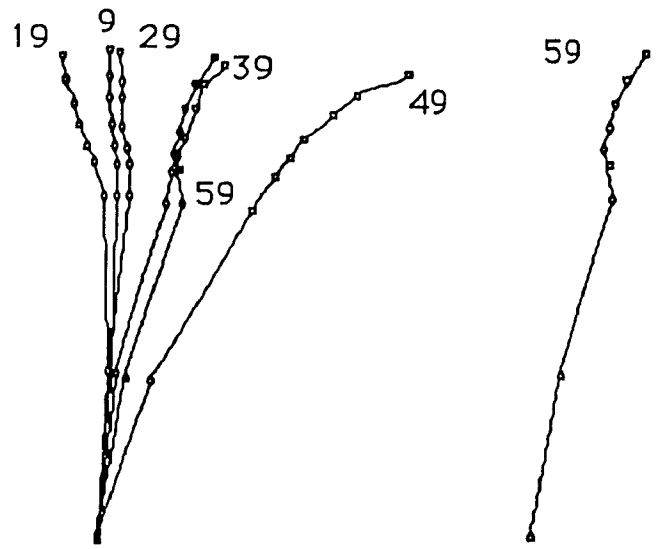

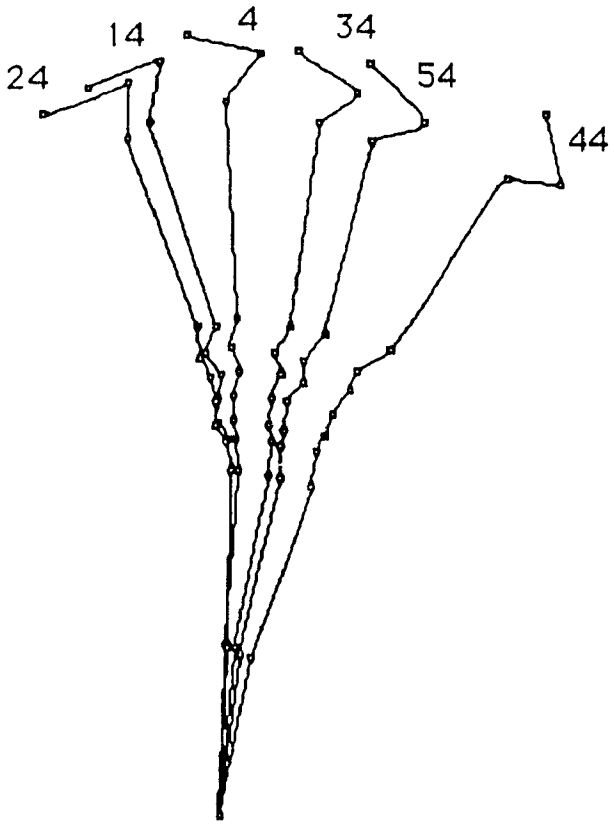

Fig 2.3.2(a): (top left)

Superimposed filtered views, without the IREDs from the head. This is how the Cerviscope time lapse display would appear.

Fig 2.3.2(b): (top right)

Isolated view of frame 59 from fig 2.4.2(a). Note how the cervical curve is exagerated. This may be due to incorrect curve fitting at the thoracocervical point of inflection .

Fig 2.3.2(c): (bottom)

Superimposed, unfiltered views showing IREDs on back of head. Note the crooked curves in the cervical area, due to assymetrical placement of the IREDs. These curves are smoothed out prior to display, as shown in fig 2.3.2(a).

Fig 2.3.3: Views from successsive frames of sagittal flexion extension. The movement has been performed twice by the same subject. Adapted from playback screen of Diagnospine preliminary data (subject RF, flexion-extension movements 2 and 4, frames 1-44).

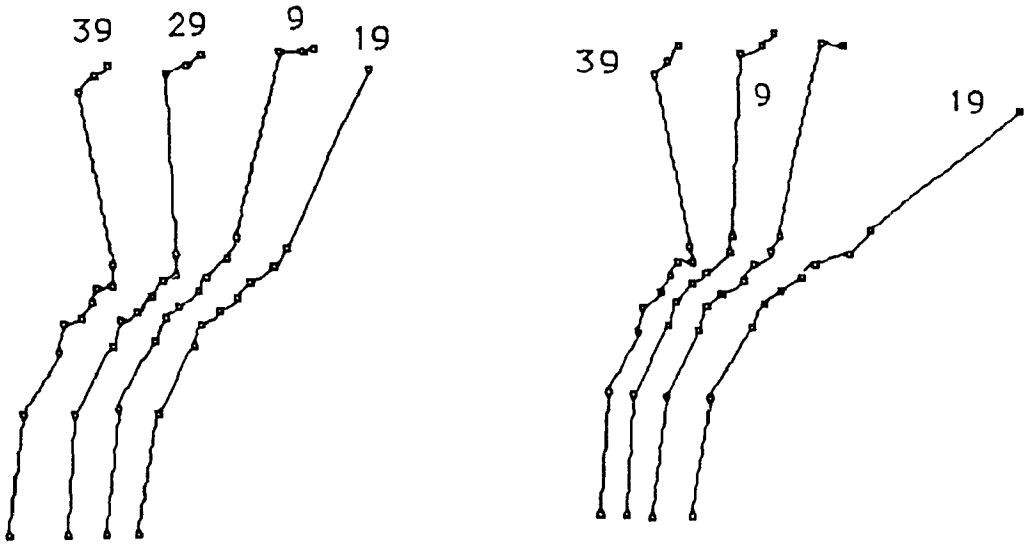

Fig 2.3.3(a): Successive unfiltered views for the two flexion extension movements, showing the IREDs on the head. Notice that in some frames not all of these are in the view of the cameras.

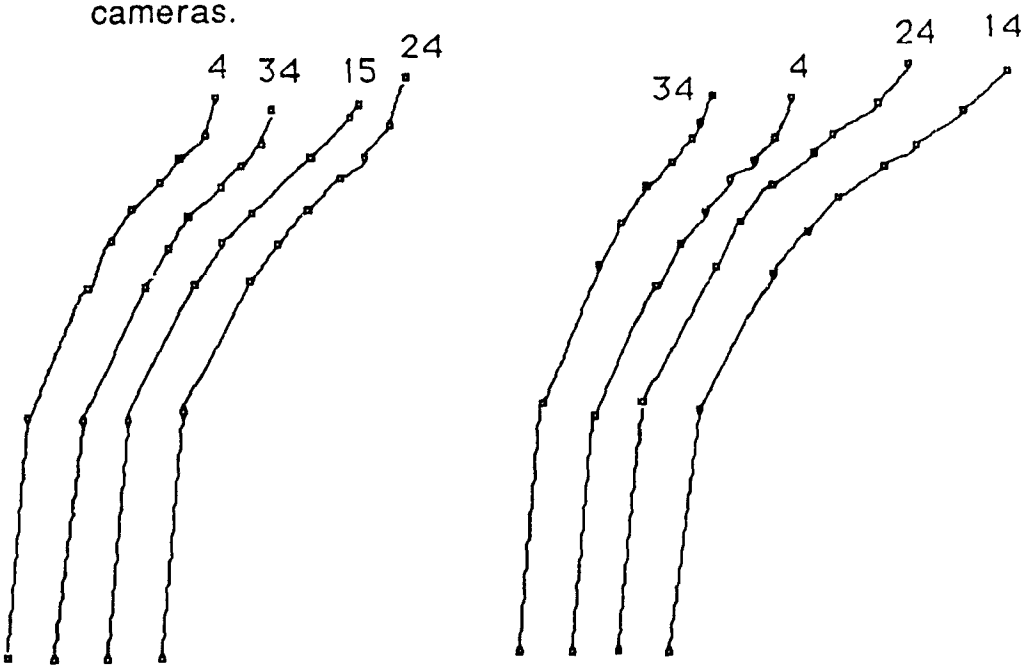

Fig 2.3.3(b): Filtered views of frames from the same movements, without the head IREDs and with the vertical axis magnified 100 %.

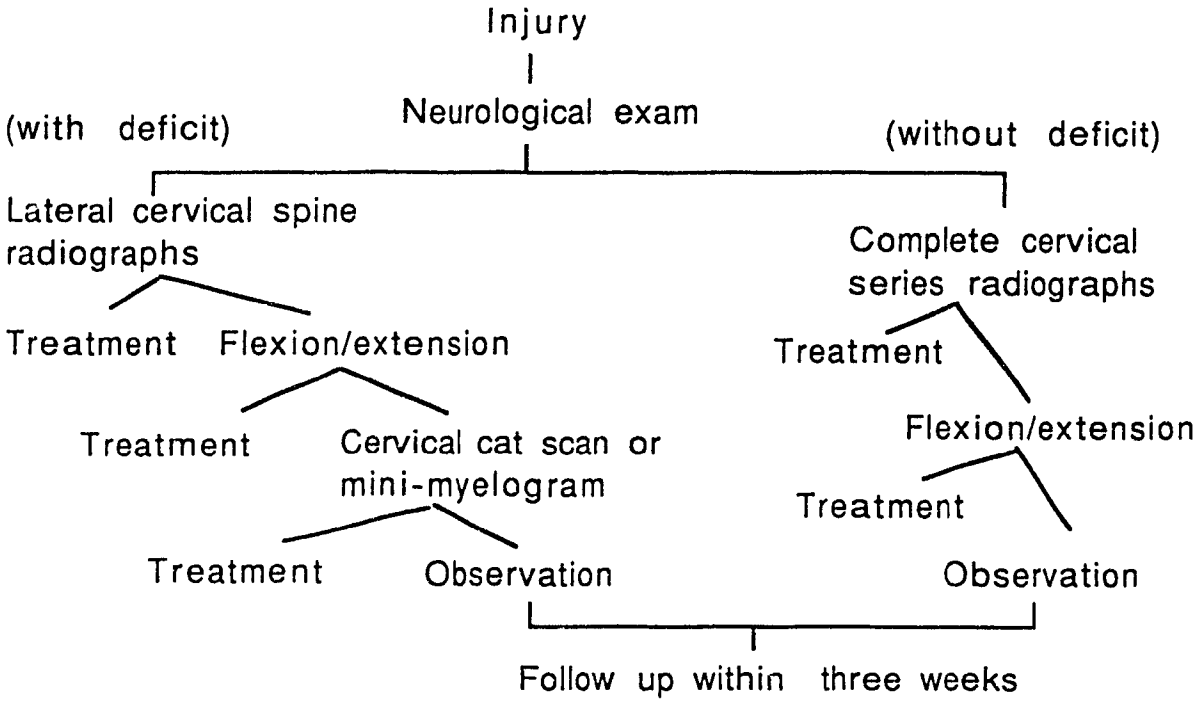

Fig 2.3.4: An algorithm for the diagnostic evaluation of injury to the cervical spine, with and without suspected neurological deficit. Adapted from Herkowitz and Rothman (1984).[78]

2.4 DISCUSSION

In this chapter we began by considering the methodology for the present study. The Cerviscope, the cervical diagnostic instrument being considered, was described. This device is the descendant of a similar instrument used for lower back diagnoses, called the Spinoscope.

We proceeded to evaluate the capacity of the Cerviscope to meet the requirements specified in chapter 1. The user interface, display screens, and some aspects of automatic data analysis were explained. This was followed by an examination of the data for some of the twenty preliminary test subjects of this study.

The purpose of this preliminary study was primarily to identify general trends from the data and to simulate the diagnostic process. It was not meant to represent an expert or a comprehensive analysis. However, it did illustrate that interpretation of the original Cerviscope displays may be somewhat subjective.

We have examined here some aspects of inter-subject variability. However, subsequent testing should also involve re-examination of individuals. This would help to determine intra-subject variability as well (see chapter 4).

It was also useful to compare how the Cerviscope and Spinoscope operate and the requirements of their respective roles. Both of these instruments use skin markers to characterize underlying motion of the spine. We therefore must consider how the data from radiographs on movement of the vertebrae may be related to that of the skin markers.

Our evaluation of the Cerviscope indicated that there are some significant shortcomings in the original diagnostic displays. In particular, characterization of coupled motion could only be performed manually.

Since this constitutes an important indicator of spinal function, it was decided that a display automatically calculating coupled motion should be developed. In order for this to be useful, the interpretation of this new representation of cervical motion must be more objective than the original Cerviscope displays. The implementation of this enhancement is the subject of the next chapter.

CHAPTER 3 - ENHANCEMENT OF THE DIAGNOSTIC DEVICE: THE DEVELOPMENT OF DISPLAYS TO CHARACTERIZE THREE DIMENSIONAL COUPLED JOINT MOTION

3.1 GENERAL

The evaluation of the Cerviscope presented in chapter 2 illustrated that there were some shortcomings in its ability to meet the requirements described in chapter 1. A software development project was undertaken to enhance the device by adding a display describing coupled motion in the cervical spine. We saw earlier (section 1.3.5) that the quantification of coupled joint motion is an important factor in analyzing spinal movement.

This project coincided with work being done to revamp the entire format of displays available on the Cerviscope and its low back counterpart, the Spinoscope. Thus the coupled motion project resulted in several pages of displays illustrating general, as well as coupled, motion in the cervical spine.

In this chapter we will examine how these enhancements were implemented. We begin with a summary of the methodology involved in the development of the new displays. Definitions of the relevant parameters and description of the required calculations are provided. Then we examine the implementation of these ideas into a working software package.

In lieu of commercial CAD packages, program modules are developed for specific tasks. The role of contemporary programming techniques, the development environment, the various files within the modules, and the integration of old and new software are described. We will also consider how some corrections were made to resolve errors in the original program design.

Finally, we will examine in detail the pages of the new displays. The user menu and parameter selection functions are described. Some examples are then given to illustrate how the user may obtain the maximum amount of information from these displays. Additional details on how the user may interact with these displays are provided in Appendix D.

3.2 METHODOLOGY

The results of experiments with the Cerviscope also required the application of analytical methods for reducing experimental error. However, the critical factor in obtaining precision with this software turned out to be correcting the subject's orientation in space.

Characterization of coupled motion ultimately involves a series of plots illustrating principal vs secondary motion. Principal movements include flexion-extension, lateral bending, and axial rotation (see figure 1.3.3). However, both absolute motion and that of the markers relative to one another must be considered. Mobility may be represented in terms of direction angles which correspond to the orientation of vectors calculated from the positions of the markers.[a] In particular, vectors normal to triangles defined by IREDs placed on the head, neck, and shoulders may be determined.

Motion of one such vector may be displayed relative to that of another. Since translation is automatically neutralized by considering vector motion, only rotational motion need be examined (ie. vectors have a common origin by definition). We will thus concentrate here on how the spatial coordinates of the moving IREDs may be treated to obtain the normal vectors and then the characteristic direction angles.

A thorough understanding of how transformation matrices and direction angles may be used to relate two moving reference frames is essential to this analysis. This subject is reviewed in detail in Appendix C. General linear transformations are also considered (along with an introduction to tensor algebra, which is relevant to the discussion of the control of head movement given in Appendix B).

3.2.1 Development of the Coupled Motion Display

The coupled motion software is based on the motion of vectors calculated from

---

[a] In this discussion we will refer to 'directional' angles, rather than the Euler angles typically used in the literature. This nomenclature is explained in section 3.4.3 and Appendix C.

the 3D spatial coordinates of IREDs placed on the head, neck, and shoulders. In particular, the direction angles described by vectors normal to the planes of these markers are used to characterize this motion.

These angles are first calculated with respect to the absolute reference frame defined when the Cerviscope is calibrated. Then the relative motion of one of the vectors is shown in the moving reference frame of the other. A total of three algorithms were developed to deduce the relative direction angles between the vectors normal to the head, neck and upper back.

The first method involved transformation matrices describing the rotational motion of each vector relative to the absolute coordinate system.[21] Relative motion between the two vectors was then obtained by multiplying these two matrices and deducing the direction angles from the resulting matrix for each frame.

The second algorithm bypassed the calculations involving transformation matrices, by algebraically summing the absolute angles determined for each vector. In both of these methods, the absolute direction angles of each of the vectors were first calculated for each frame recorded.

These angles were determined trigonometrically, relative to the calibration frame shown in figure 2.2.1. In the third algorithm, the relative angles were deduced directly from the dot (ie. scalar) products of the two vectors.

Cervical motion data for the twenty test subjects considered in chapter 2 was treated using each of the above three algorithms. It was found that the algebraic summation of angles was the simplest and most reliable method for deducing the relative angles. The calculations for each algorithm are examined again later in this chapter.

Tables indicating principal versus coupled motion in the mid-sagittal, transverse, and coronal planes were thus obtained for each subject. This corresponds to views from the side, top, and back, respectively. A single page was sufficient to show the six permutations of these coupled angles on the display screen.

The results were mostly as expected. Flexion-extension was accompanied by slight lateral bending. Lateral bending resulted in coupled motion in flexion-extension. Axial rotation was seen to consist of a combination of the other two movements. Ranges of

motion were comparable to those reviewed in chapter 1 (see section 1.3.3).

However, for many of the patients, the results displayed were entirely erratic. In order to determine the cause of this behaviour, extra pages were gradually added to the display. These included pages illustrating the motion of the vectors, as well as that of the IREDs themselves, for each frame recorded.

Other added pages showed the absolute direction angles made by the vectors, as well as their positions in space, for each frame. Note that since frames were recorded with a constant sampling frequency, this was equivalent to plotting the angles and positions versus time.

Some progress was made in obtaining consistent results, particularly through the addition of various digital filtering algorithms. Then cervical data for a new group of patients from an affiliated clinic in Denver was treated with the new software. Unfortunately, erratic curves still resulted for some subjects.

It was eventually discovered that the source of the problem lay in the perspective from which the IREDs are viewed prior to calculation of the direction angles. Recall that all calculations are based on projections of vectors onto planes representing the side, top, and back views.

However, if the test subject or IRED placement results in a skewed orientation relative to the absolute reference frame, then the projections on the principal planes will also be skewed. In addition, some vectors may be viewed head-on at some phases of their motion, resulting in projections with disproportionate magnitudes. This will be considered further below (section 3.4).

The solution to this problem was simply to rotate the vectors in the various planes prior to calculating the direction angles. The purpose of this was to always view the vectors on a line perpendicular to their actual orientation in space.

This resulted in the determination of direction angles with a surprisingly high precision. The calculated angles corresponding to motion of the vectors in the three principal planes appear to have an error of less than one degree. This estimate is based on the relatively small range of the various direction angles which result after the vectors are rotated.

3.2.2 Determination of the Vectors Defining Absolute Motion

If the motion of the IREDs themselves were plotted, it would be difficult to eliminate noise resulting from movement of portions of the body other than the neck. Hence, the motion of vectors normal to planes on the head and neck is plotted instead. As we saw earlier, such vectors may be easily rotated in space to focus specifically upon the movement of interest.

We will begin our analysis by considering the spatial coordinates of the three IREDs placed on the head, as shown in figure 3.2.1 (see also figure 2.2.2 for the overall IRED placement). Each of these IREDs corresponds to a position vector with its origin defined by the calibration frame shown in figure 2.5.2. These 'absolute' coordinates are calculated automatically for each IRED and each frame recorded.

In figure 3.2.2 we see how an imaginary vector may be defined normal to the plane determined by the position vectors of these three IREDs. This normal is just the cross product of two vectors between the IREDs. Note that, by definition, the base of these deduced vectors is the origin. This negates the effects of translation in the absolute reference frame, so that we may now consider only rotation.

The same procedure is used for calculating vectors normal to the cervical and thoracic spine. While the IRED chosen for the apex of the head triangle is fixed, that for the others is variable. Thus the motion of any two IREDs on the spine may be compared. When the IREDs are adjacent to one another, this comparison corresponds roughly to intervertebral mobility (ie. relative motion of two adjoining vertebrae).

Alternatively, we may compare the motion of the vector normal to the head with that of the normal to the cervical or the thoracic spine. In general, the absolute motion of the latter two will be much more closely related than they would be with the head vector.

3.2.3 Calculation of the Absolute and Relative Direction Angles

Once the vectors normal to the head, neck, and thoracic spine have been determined, the direction angles of these vectors may be determined with respect to the absolute reference frame. This is a simple calculation based on the spatial coordinates of

the normal vectors.

In particular, the angles may defined as follows:

α = arctan(y/z) [corresponds to flexion/extension movement or side view]

Θ = arctan(x/y) [" " axial rotation " " top view]

ϵ = arctan(x/z) [" " lateral bending " " back view]

This calculation is illustrated in figure 3.2.3. The orientation of these angles in space is shown in figure 3.2.4. The perspectives for the side, top, and back views (as well as the definitions of the coordinate system) are as shown in figure 3.2.1.

As explained earlier in this chapter, three methods were developed for deriving the relative angles between the two dimensional projections of the normal vectors. They involve algebraic summation of the absolute angles, derivation of the relative angles from the scalar product of the two vectors, or the use of transformation matrices.

In the first two methods, the absolute direction angles of each of the vectors are first calculated for each frame recorded. These angles are determined trigonometrically relative to the calibration frame shown in figure 2.2.1.

A transformation matrix describing the rotational motion of each vector relative to the absolute coordinate system may also be determined. Relative motion between the two vectors is then obtained by multiplying these two matrices and deducing the direction angles from the resulting matrix for each frame.

The first algorithm makes use of the above method. The second algorithm bypasses the calculations involving transformation matrices, by algebraically summing the absolute angles determined for each vector. In the third algorithm, the relative angles are deduced directly from the scaler products of the two vectors.

In the first algorithm, the motion of the head vector with respect to the shoulders, is calculated as follows:

i) Find the direction angles of the two vectors, with respect to the absolute coordinate system, for each frame recorded.

ii) Determine the transformation matrices to relate the rotating coordinate systems of the two vectors to the absolute reference

frame.

iii) Perform matrix algebra on these two transformation matrices to obtain a third transformation matrix relating the two rotating coordinate systems.

iv) Deduce the direction angles relating the two coordinate systems from the definition of the third transformation matrix.

For the second algorithm, steps ii) and iii) above are bypassed. Instead the relative direction angles in step iv) are determined by algebraically summing the absolute angles for the two vectors. This requires consideration of the quadrant of each angle in order to determine its correct sign. The third algorithm deduces the angles between the two vectors directly from their scalar product. This follows from the formula

$$\mathbf{a} \cdot \mathbf{b} = \|\mathbf{a}\| \, \|\mathbf{b}\| \cos \sigma \, ,$$

for the angle σ between two vectors **a** and **b**. Note that this is in effect the 'triple product', since the normals to the head and shoulder planes were obtained from the cross products of vectors in these planes.

In practice it was found that the first method (ie. algebraic summation) was the simplest and most reliable. However, it was nevertheless necessary to rotate the vectors prior to calculating the absolute angles. This requires the use of transformation matrices, as we will see later in this chapter.

3.2.4 Sample Code from the Calculation Engine

Figure 3.2.5 illustrates some sample code from the file CCE_ABS.C of the calculation engine module. In particular, the subroutine in figure 3.2.5(a) initiates calculating the absolute angles for each valid movement. Figure 3.2.5 (b) shows the calling sequence for the subroutines which derive the vectors from the IREDs and then calculate the appropriate direction angles from their projections.

Finally, in figure 3.2.5 (b) we see how the vectors are derived from the spatial coordinates of the head IREDs. The code shown here comprises only a small fraction of the several thousand lines which constitute the coupled motion software. Next we will see how this code and that from all the other files fit into the overall picture (figure 3.3.2).

Fig 3.2.1:

Vectors normal to the triangles formed by groups of IREDs on the head, neck, and shoulders. The normal vectors originate from IREDs at the apexes of these triangles (on the head, cervical and thoracic spine). Direction angles are derived from projections of these vectors onto the principal planes. Inset shows two normal vectors with their base at the origin, and the angle between them.

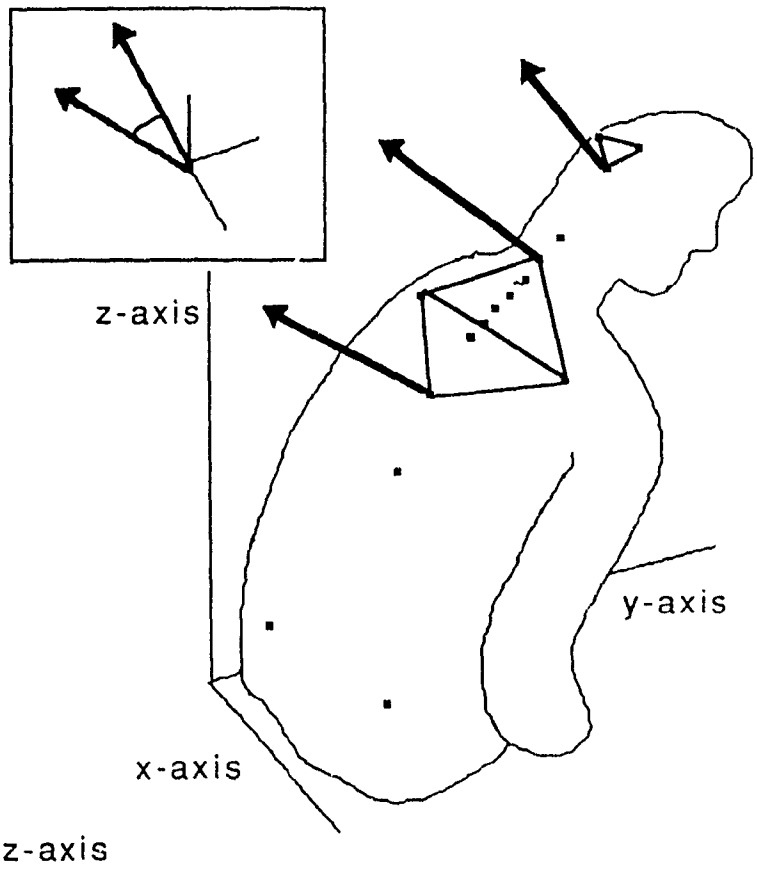

Fig 3.2.2:

Position vectors r1 to r3 are shown for three diodes. The vector n is normal to the plane defined by the vectors v1 and v2 between the diodes.

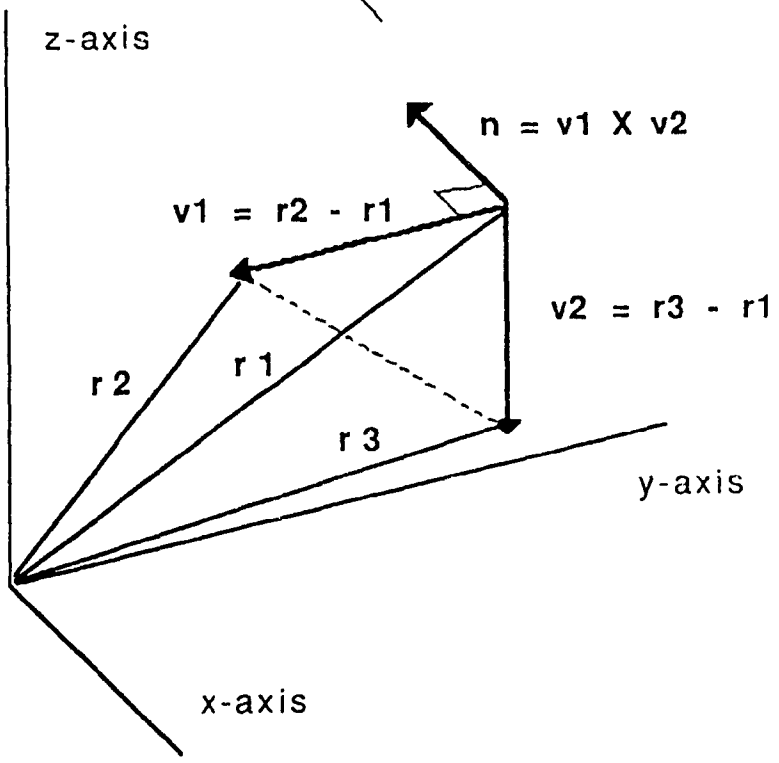

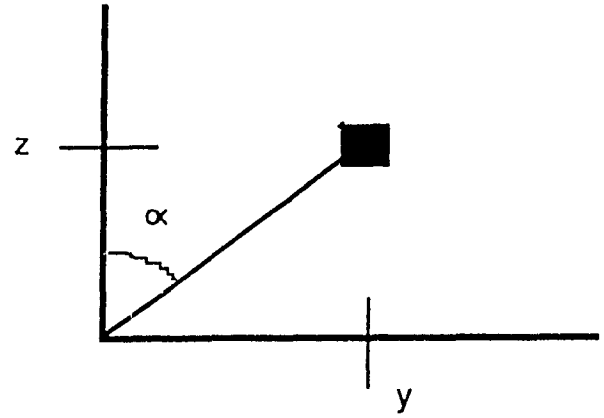

$\tan(\alpha) = y/z$

Mid- sagittal plane (ie. side view: corresponds to flexion extension movement)

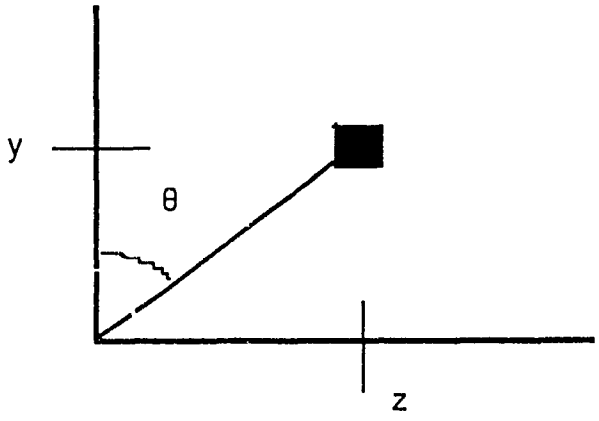

$\tan(\theta) = x/y$

Horizontal or coronal plane (ie. top view: corresponds to axial rotation movement)

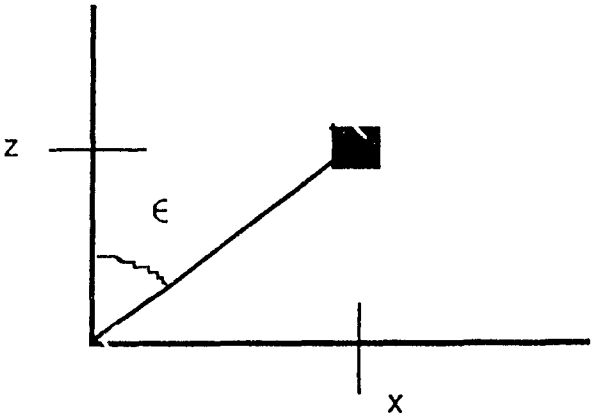

$\tan(\epsilon) = x/z$

Transverse plane (ie. back view: corresponds to lateral bending movement)

Fig 3.2.3: Calculation of direction angles obtained from the projections onto the three principal planes

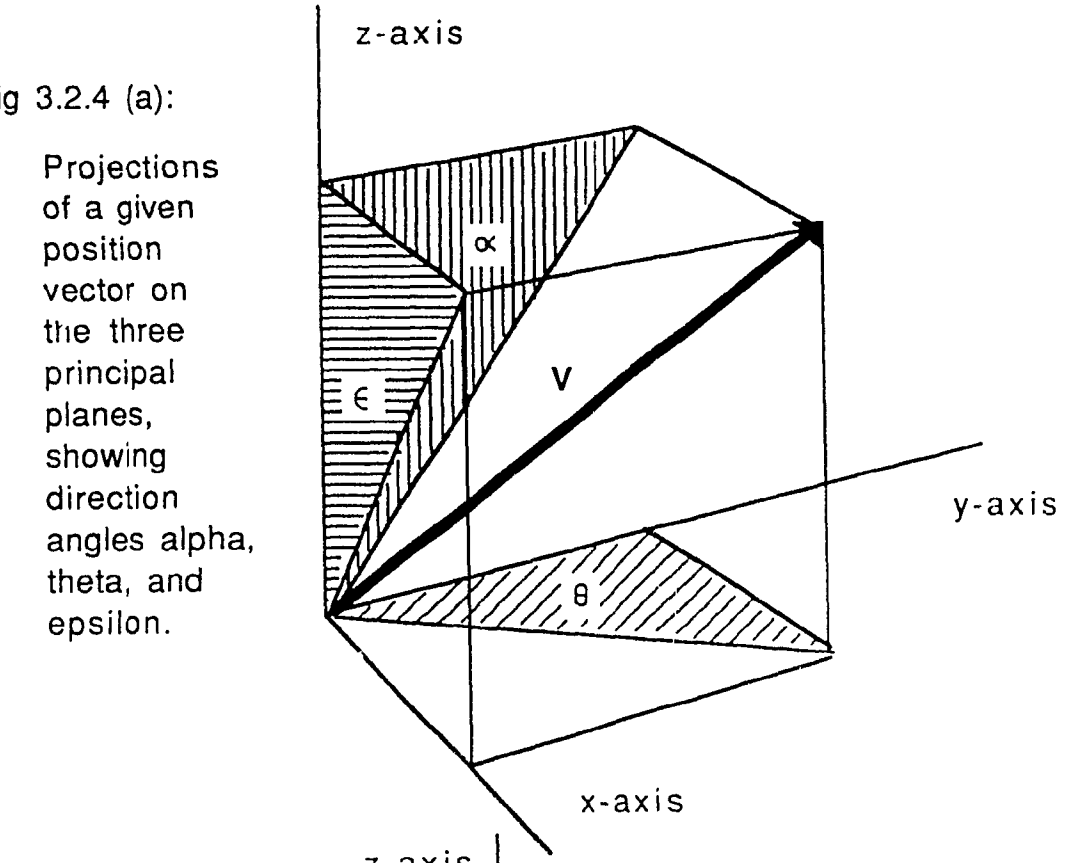

Fig 3.2.4 (a):

Projections of a given position vector on the three principal planes, showing direction angles alpha, theta, and epsilon.

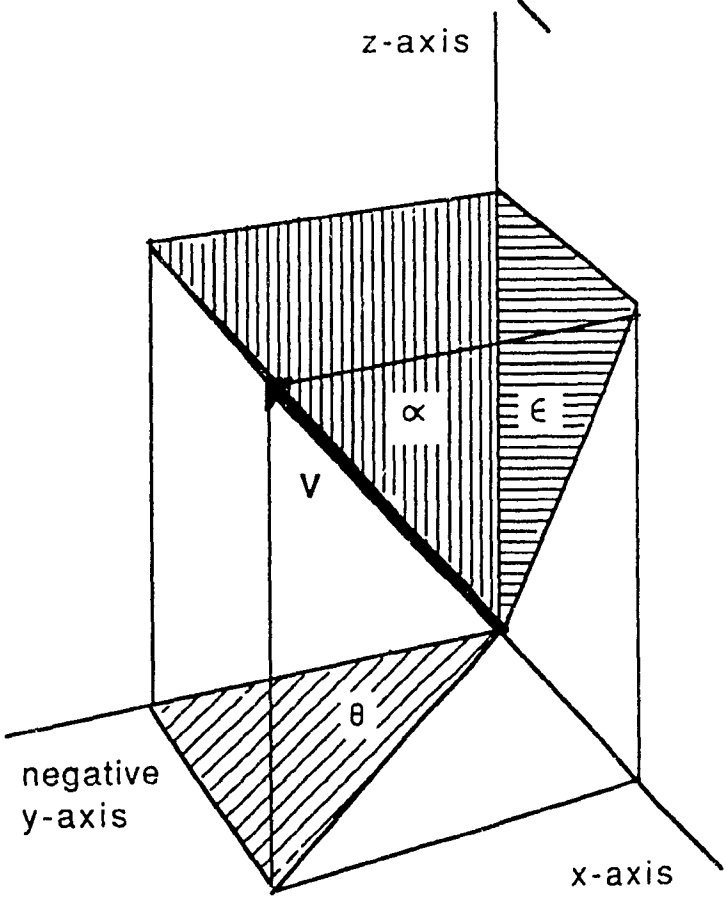

Fig 3.2.4 (b):

Projections of a vector normal to head, neck, or thoracic spine. Although the y coordinates are negative, this will not affect the magnitudes of the direction angles.

Fig 3.2.5: Sample program code from 'CCE_ABS.C' file of the calculation engine module.

Fig 3.2.5 (a): Subroutine which initiates calculations of the absolute angles for each valid movement (ie. Flexion/Extension, Lateral Bend, and axial rotation - which is called Other Movement in the software). This routine is called from CCE_MAIN.C, the main drived for the calculation engine.

```
// Create tables of data corresponding to absolute motion of IREDs
int abs_tables(
        int nk_ired, int th_ired, // selected neck and thoracic IREDs
        Method_Type method)       // calculation algorithm
{

 // Calculate absolute angles and transformation matrices
 // for each valid principal movement
   if ( dbcm_valid_movement(FE) )
        abs_frames(FE,nk_ired,th_ired,method);
   if ( dbcm_valid_movement(LB) )
        abs_frames(LB,nk_ired,th_ired,method);
   if ( dbcm_valid_movement(OM) )
        abs_frames(OM,nk_ired,th_ired,method);

   return 0;

} // end of absolute_tables procedure
```

Fig 3.2.5 (b): Calling sequence for the subroutines which derive the vectors from the IREDs and then calculate the appropriate Euler angles from their projections. This routine is called from the 'abs_tables' routine above.

```
// For each frame determine Euler angle corresponding to vectors normal
// to groups of head, neck, and thoracic IREDS
static int abs_frames(
        Movement_Type movement,          // current principal movement,
        int nk_ired,int th_ired,         // neck and thoracic IRED numbers
        Method_Type method)              // calculation method
{
 int frame;                  // current frame
 int total_frames;   // number of frames for current movement
 int err = 0;                // error flag

 // Get number of frames for current movement
     err = dbcm_get_frames(movement,&total_frames);

 // STEP 1: Get coordinates of IREDs for each frame and determine
 //       vectors normal to head, thoracic and neck planes
 for (frame = 0; frame < total_frames; frame ++) {
     err = abs_vectors(movement,HD_GR,frame,0);
     err = abs_vectors(movement,NK_GR,frame,nk_ired) || err;
     err = abs_vectors(movement,TH_GR,frame,th_ired) || err;
        if (err) {
                MESSAGE(Fatal, "abs_frames()-- could not determine vectors.");
         goto clean_up;
                }
    }

 // STEP 2: Filter vector normal to head, thoracic and neck planes
     err = filter_normal(movement,HD_GR);
     err = filter_normal(movement,NK_GR) || err;      // neck group
     err = filter_normal(movement,TH_GR) || err;      // thoracic group
        if (err) {
                MESSAGE(Fatal, "abs_frames()-- could not filter vectors.");
```

```
        goto clean_up;
                }

// STEP 3: Calculate alpha angles for above normal vectors
for (frame = 0; frame < total_frames; frame + +) {
    err = abs_alpha_angles(movement,HD_GR,frame,method);
    err = abs_alpha_angles(movement,NK_GR,frame,method) || err;
    err = abs_alpha_angles(movement,TH_GR,frame,method) || err;
        if (err) {
                MESSAGE(Fatal, "abs_frames()-- could not calculate alpha.");
         goto clean_up;
                }
    }

// STEP 4: Based on above results determine rotation angles required to
//          correct normal vector in alpha plane
    err = alpha_rotation_angles(movement,HD_GR,total_frames);
    err = alpha_rotation_angles(movement,NK_GR,total_frames) || err;
    err = alpha_rotation_angles(movement,TH_GR,total_frames) || err;
        if (err) {
                MESSAGE(Fatal, "abs_frames()-- could not determine alpha rotations.");
         goto clean_up;
                }

// STEP 5: Calculate theta angles for normal vectors
for (frame = 0; frame < total_frames; frame + +) {
    err = abs_theta_angles(movement,HD_GR,frame,method);
    err = abs_theta_angles(movement,NK_GR,frame,method) || err;
    err = abs_theta_angles(movement,TH_GR,frame,method) || err;
        if (err) {
                MESSAGE(Fatal, "abs_frames()-- could not calculate theta angles ");
         goto clean_up;
                }
    }

// STEP 6: Based on above results determine rotation angles required to
//          correct normal vector in theta plane
    err = theta_rotation_angles(movement,HD_GR,total_frames);
    err = theta_rotation_angles(movement,NK_GR,total_frames) || err;
    err = theta_rotation_angles(movement,TH_GR,total_frames) || err;
        if (err) {
                MESSAGE(Fatal, "abs_frames() - could not determine theta rotation ");
         goto clean_up;
                }

// STEP 7: Calculate epsilon angles (and transformation matrices)
for (frame = 0; frame < total_frames; frame + +) {
    err = abs_epsilon_angles(movement,HD_GR,frame,method);
    err = abs_epsilon_angles(movement,NK_GR,frame,method) || err;
    err = abs_epsilon_angles(movement,TH_GR,frame,method) || err;
        if (err) {
                MESSAGE(Fatal, "abs_frames()-- could not calculate epsilon angles.");
         goto clean_up;
                }
    }

// STEP 8: Normalize the Euler angles with respect to first frame
    err = abs_normalize_angles(movement,HD_GR,total_frames);
    err = abs_normalize_angles(movement,NK_GR,total_frames) || err;
    err = abs_normalize_angles(movement,TH_GR,total_frames) || err;
        if (err) {
                MESSAGE(Fatal, "abs_frames()-- could not normalize angles ");
         goto clean_up;
                }
```

```
 // STEP 9: Filter the above angles
     err = filter_absolute_angles(movement,HD_GR);
     err = filter_absolute_angles(movement,NK_GR) || err;
     err = filter_absolute_angles(movement,TH_GR) || err;
         if (err) {
                  MESSAGE(Fatal, "abs_frames()-- could not filter angles.");
          goto clean_up;
                  }

clean_up:

   return err;

} // end of 'abs_frames' procedure
```

Fig 3.2.5 (c): **Excerpt from the 'abs_vectors' routine called from 'abs_frames' above. Here we see how the vectors for the head are determined from the psotions of the three head IREDs. The procedure for the neck and thoracic vectors is similar.**

```
// Calculate vectors between specified group of IREDs
static int abs_vectors(
         int movement,int group,      // current movement, group, frame
         int frame,int ired)          // and selected LED
{

 // Temporary variables to be used for calculations
 Point r1,r2,r3;
 Point v1,v2,*nrm,
 double magn;
 double magn_xy, magn_xz, magn_yz;

         ...

 // Get coordinates of 3 head IREDs for current frame
 // and movement
         dbcm_get_point(&r1,movement,IRED_1,frame);
         dbcm_get_point(&r2,movement,IRED_2,frame);
         dbcm_get_point(&r3,movement,IRED_3,frame);

 // Calculate two vectors between these three points
         v1.x = r1.x - r3.x; v1.y = r1.y - r3.y; v1.z = r1.z - r3.z;
         v2.x = r2.x - r3.x; v2.y = r2.y - r3.y; v2.z = r2.z - r3.z;

 // Normalize the vectors
     magn = sqrt(v1.x*v1.x + v1.y*v1.y + v1.z*v1.z);
     v1.x = v1.x/magn; v1.y = v1.y/magn; v1.z = v1.z/magn;

     magn = sqrt(v2.x*v2.x + v2.y*v2.y + v2.z*v2.z);
     v2.x = v2.x/magn; v2.y = v2.y/magn; v2.z = v2.z/magn;

 // Determine end point of the normal vector as the cross product of
 // these two (see also 'ml_norm' in 'mathlib.h')
         nrm->x = (v1.y * v2.z) - (v2.y * v1.z);
         nrm->y = (v1.z * v2.x) - (v2.z * v1.x);
         nrm->z = (v1.x * v2.y) - (v2.x * v1.y);

 // Save the results in a table of vectors for the current
 // movement, group of IREDs and frame
           dbcm_set_vectors(v1,v2,nrm,movement,group,frame);

         ...

}        // end 'abs_vector' procedure
```

3.3 SOFTWARE IMPLEMENTATION: OBTAINING A WORKING PRODUCT

Any new software written for the Spinoscope or Cerviscope must be compatible with the other programs developed by Spinex. Over the past ten years, roughly 500,000 lines of code have been written for these machines by various engineers and programmers. In comparison, the new software modules which were written specifically for the enhanced cervical display consist of about 10,000 lines of code. All programs are written in Metaware High C, which is a professional grade compiler. They are run from MSDOS (Microsoft Disc Operating System) on INTEL 80386 compatible processors.

As we saw in the previous section, the implementation of the enhanced display to characterize coupled motion was not just a simple application of the biomechanics theory. The original version of this enhancement consisted only of a new calculation engine module and a means for interfacing with the old Cerviscope software (ie. the old report and graphics). However, the latter was difficult to use and nearly impossible to modify.

Meanwhile, a new set of utility programs for lowlevel graphics and mouse capabilities was being developed in-house by Spinex. These were designed to be compatible with the high resolution Matrox graphics boards and Metaware High C. As a result, when the interface between the enhanced cervical display and the old report did not immediately work properly, it was considered simplest to implement this display by making use of the new lowlevel graphics and mouse utility routines instead.

3.3.1 Applicability of Available CAD Packages

Commercially available CAD packages were not deemed appropriate for the lowlevel graphics and mouse handlers described above. They are generally slow, require too much memory, and have limited programming capacity (eg. no arrays or nested loops). There is also limited capacity for report generation and curve fitting.

These packages tend to be run through interpreters, rather than be compiled. In addition, the data input and user interfaces do not correspond to the formats required for Spinex products. Perhaps more important, however, is that CAD packages are not compatible with Matrox boards and High C. Hence, all software for Spinex products is currently written in-house, although this may change if the Matrox card is no longer used.

3.3.2 Programming Techniques and the Classification of Modules

Modern software engineering techniques require adherence to the principles of data abstraction and object oriented programming. The former involves the division of software packages into distinct modules dealing with specific tasks. These modules are in turn divided into traditional subroutines, with information passed back and forth through particular parameters.

Data abstraction requires that calling programs in distinct modules not be aware of the definition of data structures in other modules. Parameters are passed back and forth with globally defined structures, with the calling routine expecting specific results.

How the called routine accomplishes these results, however, need not (and should not) be known. Thus internal changes within the various modules need not affect other modules, as long as the calling conventions for subroutines remain unchanged.

Conversely, in the case of object oriented programming, the called routine is unaware of the origins of the parameters which are passed to it. The calling program defines pointers to objects (ie. data structures) and passes these to subroutines. There could be one or many versions of this object, all with the same format.

The calling programs decide which one(s) to pass to the subroutines. The subroutines, in turn, know only that they are receiving pointers to a specific type of object, but not which one. Hence the operations preformed are generic in nature.

In the new cervical software being considered here, separate modules were implemented for the calculation engine, the main driver, data handling, and graphics. Names of files within these modules all start with 'C' for cervical, followed, by the prefixes CE, DR, DH, or GR, respectively. Each file has a suffix identifying its particular role (file names must be under eight characters in MSDOS). These modules are shown in figure 3.3.1.

The coupled motion display eventually grew from a single page to a comprehensive set of screens describing cervical motion in detail. The modules described above consisted of files which contained sets of routines designed for specific tasks. These files are shown in figure 3.3.2.

In particular, the main driver module consists of a main program (located in the

file CDR_MAIN), a mouse command file (CDR_MSE), and an initialization file (CDR_INIT). The main program first calls the initialization routines (within CDR_INIT) to set up the screen and mouse. Then the spatial coordinates of the IREDs and any other pertinent data is obtained from the original Cerviscope data base for the current patient.

This data is entered into a new database specifically for the coupled motion display through the data handler. All subsequent data extraction or entry is accomplished by passing parameters to and from subroutines within the data handler.

In accordance with the principals of data abstraction only the data handler "knows" in what format this data is stored. By the same token, only the calling routines know which specific objects they are asking the data handler to modify (eg. the data structure corresponding to a specific patient).

The calculation engine is then called to treat this data and save it (through the data handler module) to a format suitable for the new display. The initial page of the display is then put on the screen by the graphics module. After this, control is relinquished to the mouse driver, which waits for input from the user and reacts to this appropriately.

3.3.3 The Role of Various Files Within the Modules

We saw above how the main module is divided into files. Similarly, the other modules each include files with specialized roles, within which are sets of subroutines that correspond to specific related tasks. For example, the calculation engine contains the files CCE_MAIN, CCE_ABS, CCE_REL, CCE_FILT, and CCE_PLOT.

These correspond, respectively, to the main driver for the calculation engine, files which handle absolute and relative data, one which preforms filtering operations, and one which tabulates data to be plotted. The first of these calls the others in turn to perform their specific tasks.

The second, CCE_ABS, treats the raw data corresponding to spatial coordinates of the IREDs in the absolute reference frame to obtain direction angles for each frame. Then CCE_REL converts these to relative angles corresponding to the moving reference frames associated with each IRED. Routines from the file CCE_FILT are called at various times to smooth the resulting curves. Finally, CCE_PLOT tabulates the relative

angles of the specific IREDs selected by the user in a format compatible with the display.

In the data handler module there are only two files: CDH_DBCM and CDH_LEDS. The first suffix stems from 'data base for coupled motion'. It is a relatively large file containing the definitions for the data structures of the cervical coupled motion database, as well as numerous routines for interacting with it. Only these routines are aware of the format of the database and may access this data directly.

All other modules access the data by passing parameter to and from the modules within this file. The file CDH_LEDS contains a single routine, which is called during the main programs initialization phase, to get the patient data and store it in the new database.

In the graphics module there are files corresponding to the drawing of each page of the display (CGR_PG01 to CGR_PG06). Another file (CGR_AUX) contains auxiliary output routines for tasks such as printouts, on-screen messages, and so on. There is a single file (CGR_HELP) to display the help screens corresponding to each page and another for the screen describing how parameters may be modified by the user (CGR_PARM).

All information is shown on the screen by being added to particular types of boxes (ie. containing text, data points, etc), which are int turn added to various display areas. Three files include routines specifically for creating boxes containing the title (CGR_TITLE), remarks (CGR_RMRK), and the menu (CGR_MENU) areas, which are appear on the various pages. The file CGR_DRAW contains routines common to the others (eg. add a series of points to a data box, add text to a text box, add a specific type of box to an area, etc).

Finally, let us consider again the main driver module. We saw above how the main program in CDR_MAIN calls the initialization routines, the calculation engine, the graphics module, and the mouse handler in turn. The mouse handler, like the main data handler CDH_DBCM, is a relatively large program.

It contains a short routine which waits for the input from the mouse, as well as a much longer routine for taking action when any of the twenty three menu boxes are activated. Each of these boxes is a sub-area of the mouse area, and is sensitive to either or both of the mouse buttons being depressed.

The code segments which handle each specific box receive a pointer to the box itself, so that it may refresh the box when it is activated, and an object called 'report'. The report contains data describing the current status of the display and the parameters selected by the user (or chosen by default). Even the various areas to be displayed (titles, remarks, data boxes, etc) are defined here.

Since the report object is the only contact that the mouse handler has with the rest of the program, it must provide access to any parameters that are to be altered or areas to be re-displayed. However, there is no reason why two or more reports cannot exist simultaneously (eg. to be displayed on separate screens or overlaid). Similarly, the data base described above is an object which need not be unique. In this way, the results calculated for two or more one patients may be simultaneously displayed and compared.

3.3.4 Integration of the Old and the New Cerviscope Software

Although the coupled motion display eventually became distinct from the old Cerviscope displays, a common data base was required for accessing patient information. The flow of data is illustrated in figure 3.3.3. Note, however, that once the IRED coordinates were accessed, the new display makes use of its own independent data handler for subsequent storage and retrieval.

Originally the new display was meant to be compatible with the old Cerviscope software. However, it eventually became part of the new line of products which were meant to entirely replace the old Spinoscope and Cerviscope displays.

This left the problem of how this new display could be distributed to customers immediately, since the remaining new report displays were not yet available. The solution was to implement an interface between the old and the new software, as shown in figure 3.3.4.

This consists of a secondary menu accessed by selecting the 'report' option in the original 'Spinoscope/Cerviscope' menu. From here the user chooses which version of the report software to run. The result is a smooth transfer between the old and new displays. The selected programs are actually run directly from the operating system, rather than as subroutines, but this is transparent to the user.

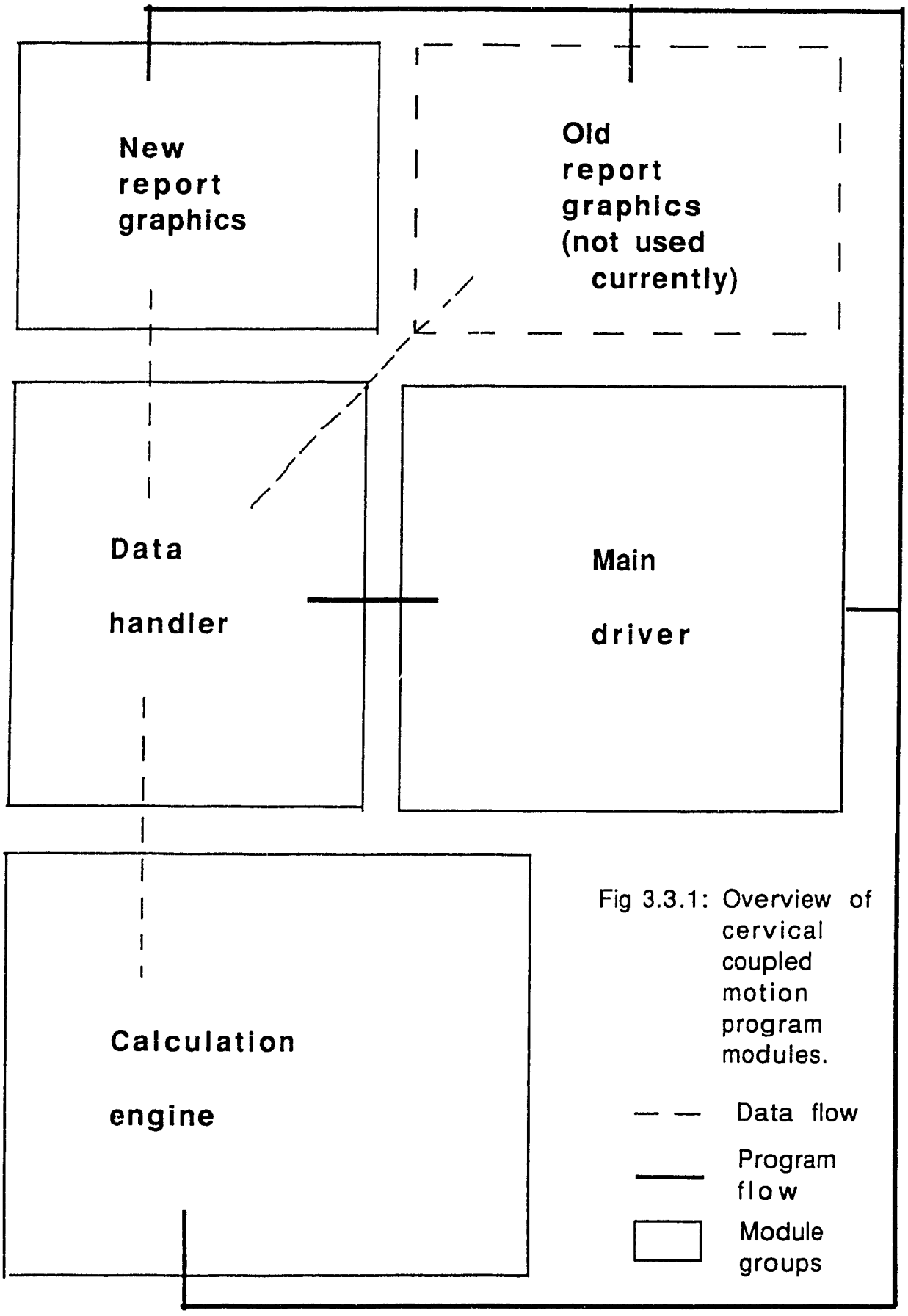

Fig 3.3.1: Overview of cervical coupled motion program modules.

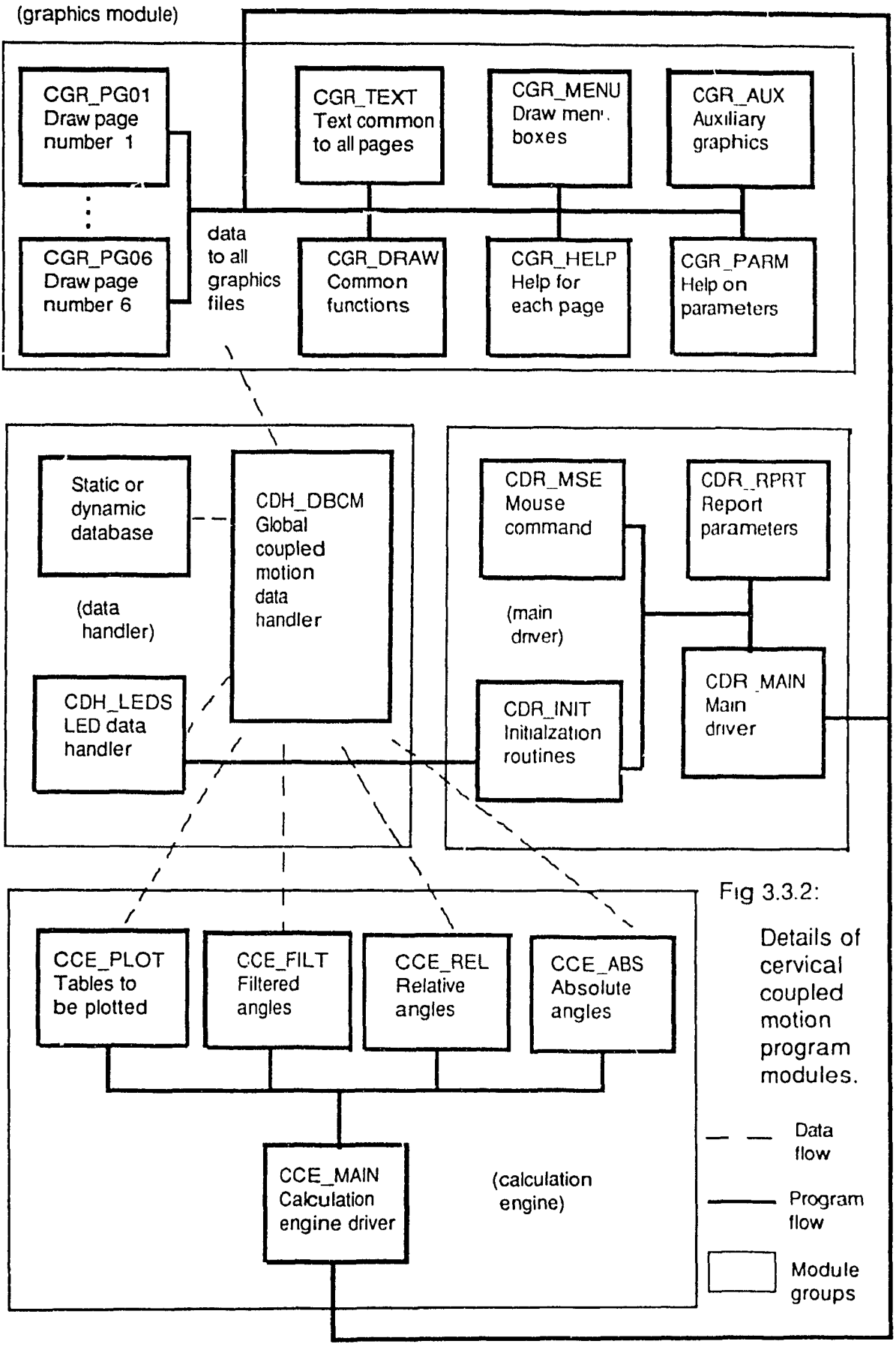

Fig 3.3.2:

Details of cervical coupled motion program modules.

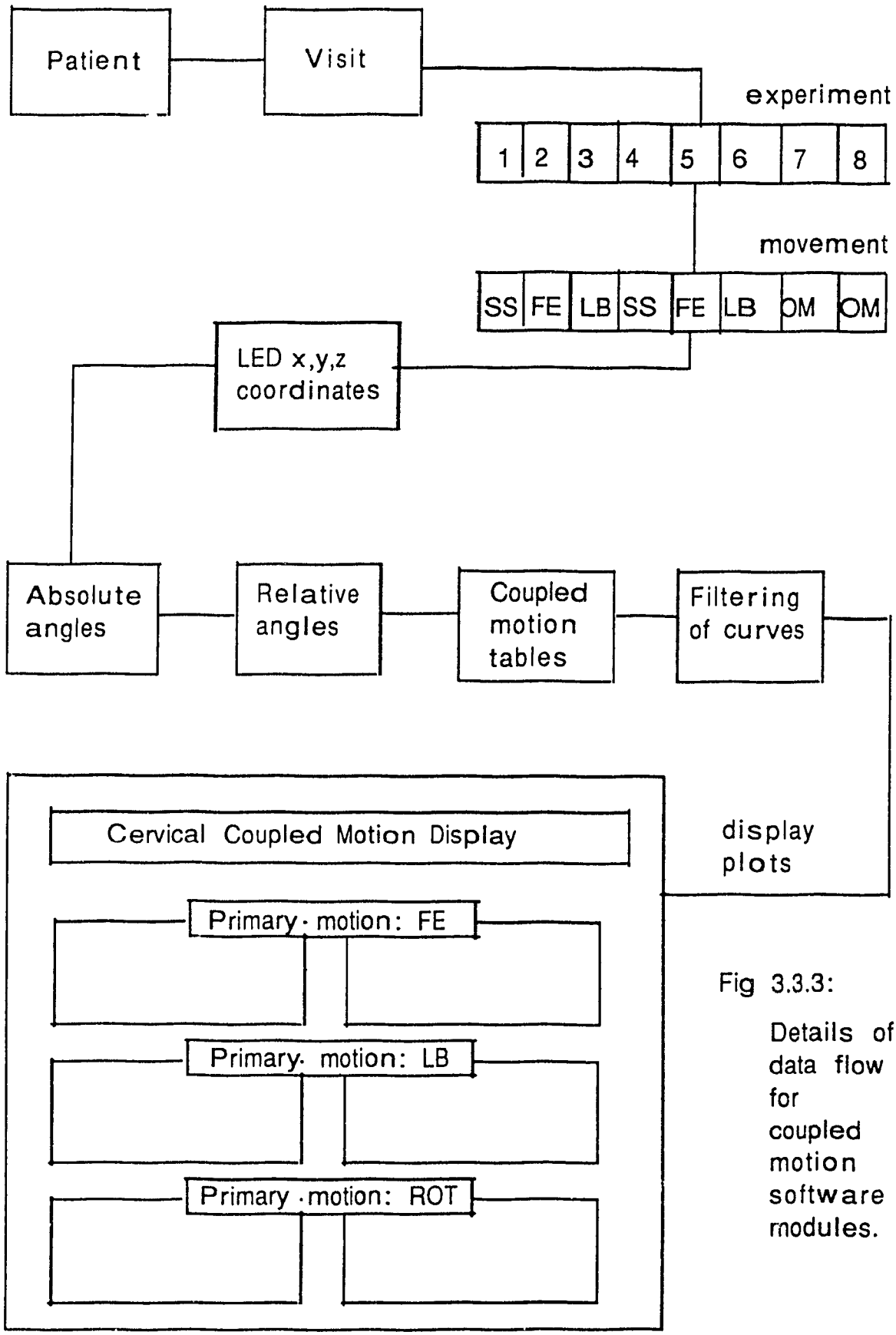

Fig 3.3.3:

Details of data flow for coupled motion software modules.

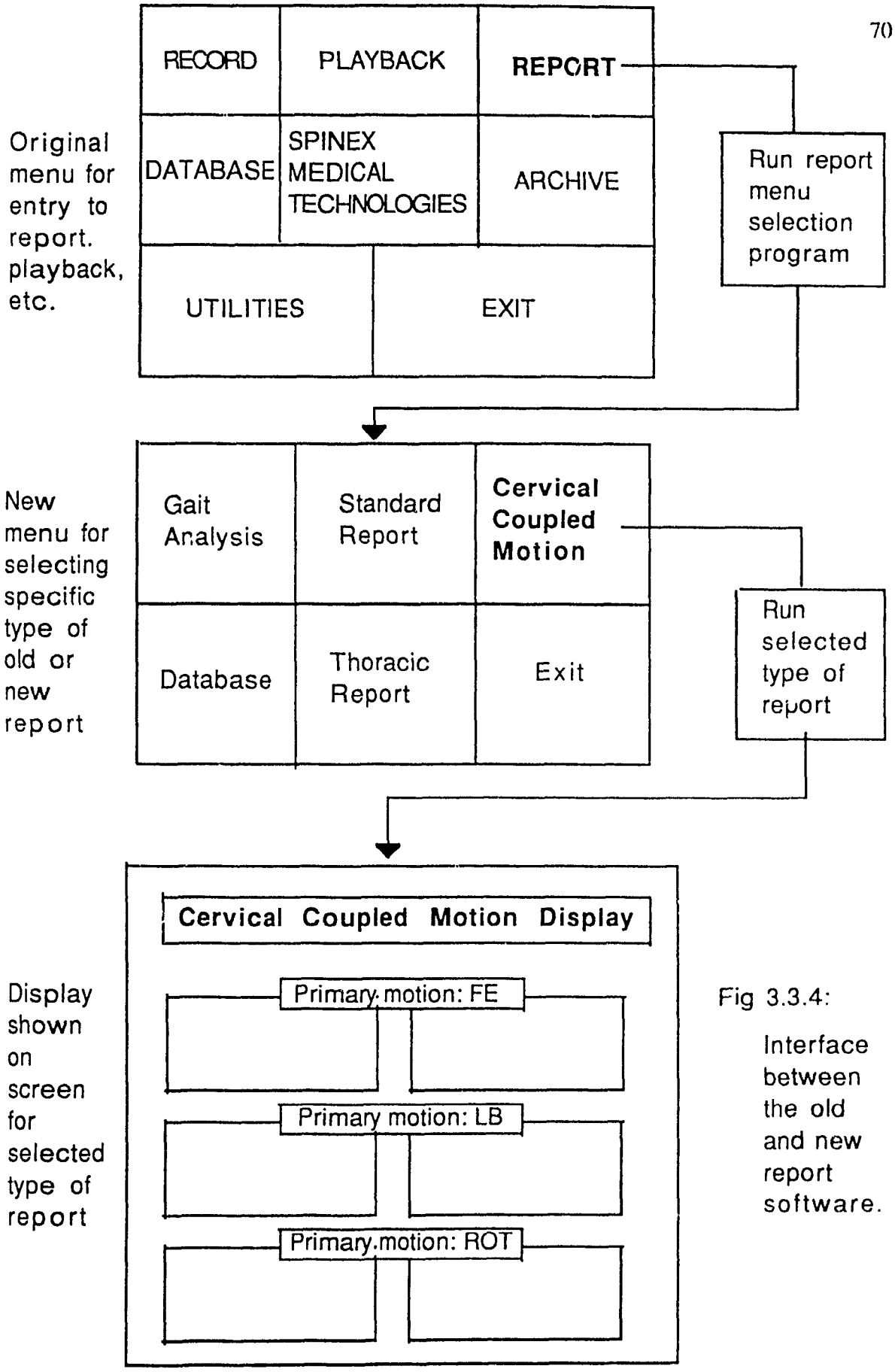

Fig 3.3.4:

Interface between the old and new report software.

3.4 REFINEMENTS AND CORRECTIONS

So far in this chapter we have seen how the new cervical coupled motion software was implemented. We also saw, however, that this implementation did not always have the desired results. In particular, for some time the curves displayed did not appear as expected. We will consider here how this problem was eventually resolved.

3.4.1 Curve Smoothing

Various forms of curve smoothing were implemented during development of the coupled motion display. Originally, the smoothing was required simply to eliminate noise inherent in the data acquisition process of tracking skin markers.

For this purpose a variable order polynomial curve fitting algorithm was first used. This achieved the desired results, but was too slow. It was thus replaced by a third order cubic spline fitting algorithm which was very effective.

However, it was eventually discovered that vectors viewed head-on caused spikes to occur in the curves for the affected frames. This later led to implementation of the vector rotations described below. An interim solution was to try to remove the spikes using a digital filter with a variable window size.

The idea behind this was to predict when the spikes would occur, label the frames which were at risk, and then increase the window size for these frames only during filtering.

The cubic spline filter mentioned earlier was too inflexible to allow this procedure. Hence, a simple, but highly variable moving average filter was developed to implement the above scheme. In particular, the window size varied from 5 to 25 frames, depending upon the weighted risk factor attached to a given frame (fig 3.4.1).

As it turned out, once the vector rotations were added, the spikes disappeared. The filter window size was then fixed at five frames, which was suitable for curve smoothing related to data acquisition noise. The variable size option was maintained, though, in case a future problem is discovered which requires this type of 'smart' filter.

Another problem was that some IREDs, particularly on the head, were periodically

lost from view to one or both of the cameras. This resulted in an interpolation algorithm being automatically enabled by the data acquisition software.

Unfortunately, the resulting interpolation was not precise enough for the type of calculations made by the coupled motion software. Hence, such data had to be recognised and labelled as erroneous on the display screen.

This problem was partially resolved by modifying the Cerviscope head harness in order to make these IREDs more visible to the camera. Nevertheless, IREDs might still sometimes be lost from view and the resulting data should be identified.

Fortunately, the vector rotation scheme resulted in angle calculations of sufficient precision that the interpolated angles could easily be differentiated from the true ones. In particular, specific ranges for the various angles were determined (eg. the axial rotation angle Θ was always in the range (-15, 15) degrees for a flexion extension movement). Angles resulting from interpolated data were thus easily recognisable as being well outside these ranges.

3.4.2 Rotation of Normal Vectors

Despite all efforts to smooth curves, recognize interpolated data from invisible IREDs, etc, there remained some unexplained erratic curves. It was finally discovered that the main culprit was the perspective from which the normal vectors were viewed prior to calculating the absolute direction angles.

As we can see from figure 3.4.2, the angle from which we view a given vector will affect the magnitude of its projection onto a plane. Hence, vectors viewed head-on will have very small magnitudes in comparison to those seen from a viewpoint perpendicular to the vector.

When calculating angles described by these vectors (particularly using the arctan function), the results will jump whenever the magnitude of the vector approaches zero. Indeed, in the variable window size filter described above, this was the test used to determine if a vector had a high risk of producing a spike for a given frame.

In order to have smooth curves describing the angle made by the vectors for each frame, it is necessary to rotate the vectors prior to calculating the direction angles. Since

the direction angles are always calculated from only two out of three of its 3D coordinates, a rotation about the third axis will not affect the values of the angles.

It will, however, result in consistent magnitudes for the vector itself, as its moves through space. These magnitudes never come close to zero, and the spikes in the angle curves are thus eliminated. The required rotations are indicated in figure 3.4.3 .

3.4.3 Direction Angles Versus Euler Angles

We saw in chapter 1 (section 1.3.5) and in Appendix A that the literature tends to discuss coupled joint motion in the spine in terms of Euler angles. However, the correct use of Euler angles should refer specifically to the series of rotations required to translate from one coordinate system to another. These are known as the angles of nutation, precession, and proper rotation.

Another way to define the 3D motion of a vertebra is to consider the orientation of a vector defined to be normal to its anterior surface. In particular, we may refer to the direction angles between the vector and the three orthogonal coordinate axes. These angles are often defined by the direction cosines of the vector's 2D projections. As we saw earlier (section 3.2), however, they may also be defined using the tangent function.

Since we often discuss transformations between rotating coordinate systems in this chapter, reference to Euler angles would be appropriate. Nevertheless, the definitions of the angles alpha, epsilon and theta given in section 3.2 correspond more closely to direction angles. Hence, strictly speaking, it is incorrect to call them Euler angles. More complete definitions of Euler and direction angles, as well as a discussion on linear transformations, are given in Appendix C.

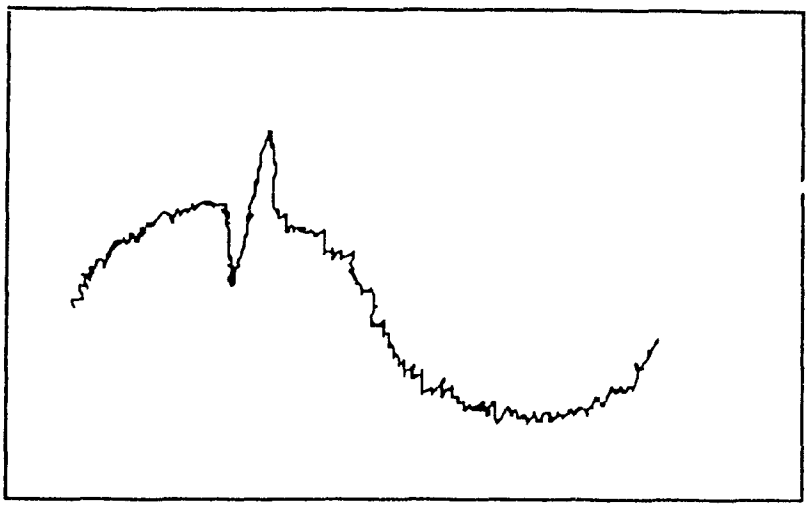

Fig 3.4.1 (a):

Original unfiltered curve, showing noise due to the data acquisition process.

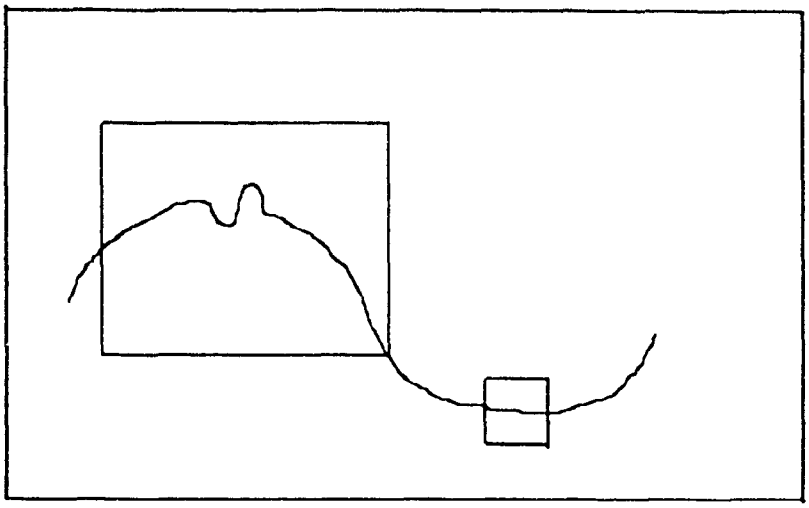

Fig 3.4.1 (b):

Curve after first pass of the moving average filter, showing variable window sizes .

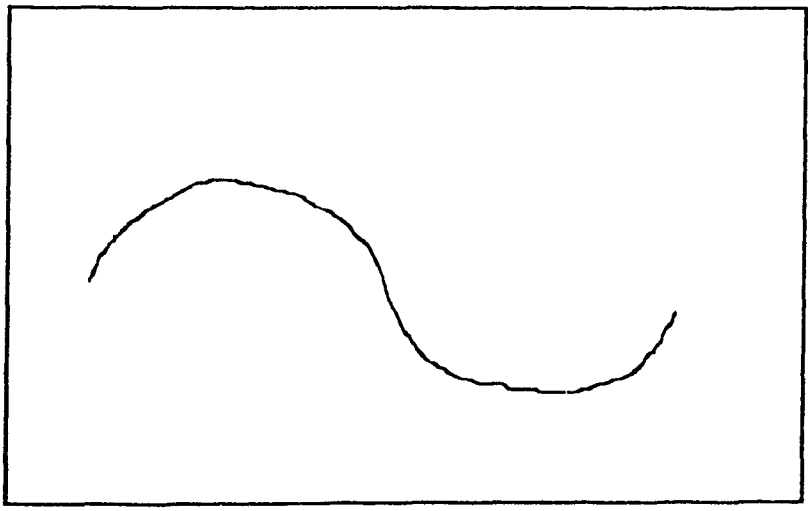

Fig 3.4.1 (c):

Curve after third pass of filter. For less severe spikes, only two passes are required.

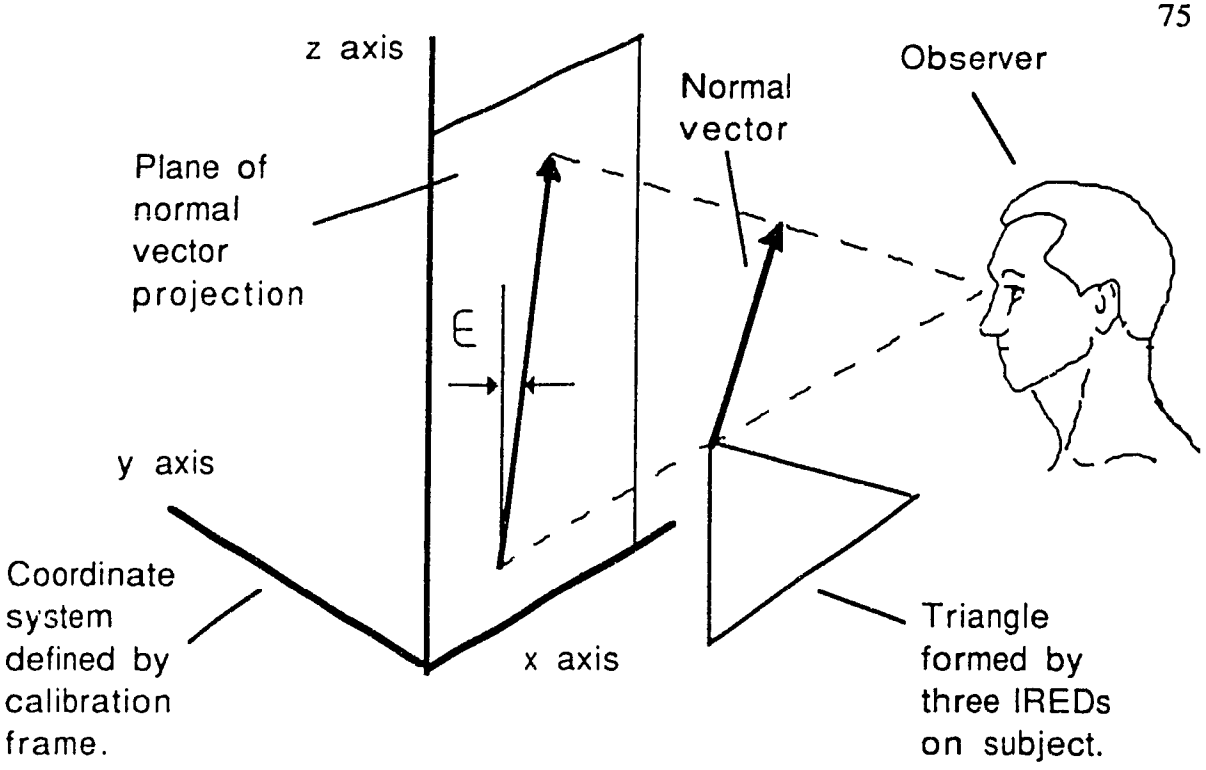

Fig 3.4.2 (a): A vector normal to the plane formed by three IREDs on the head, or on the neck and shoulders. Here the normal vector is viewed from the back at an an angle more or less perpendicular to its direction in space. The projection of the vector has a large magnitude and the angle epsilon is easily determined.

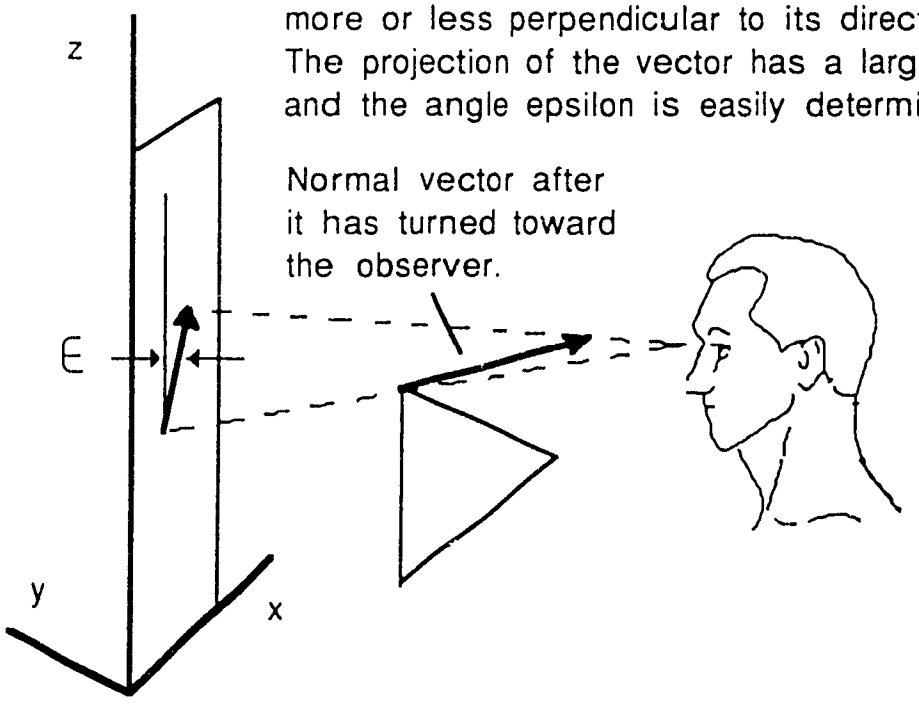

Fig 3.4.2 (b): As the vector moves, at some points it may be viewed almost head on. The resulting projection has a small magnitude and the angle epsilon is more difficult to calculate.

Fig 3.4.3 (a): (right)

From the side the projection of the normal vector has a nearly constant magnitude. Hence, no rotations are required prior to calculating angle alpha.

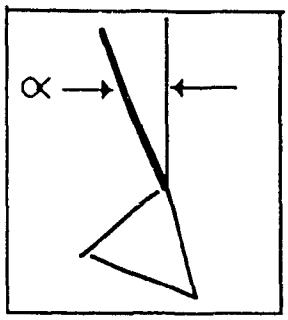

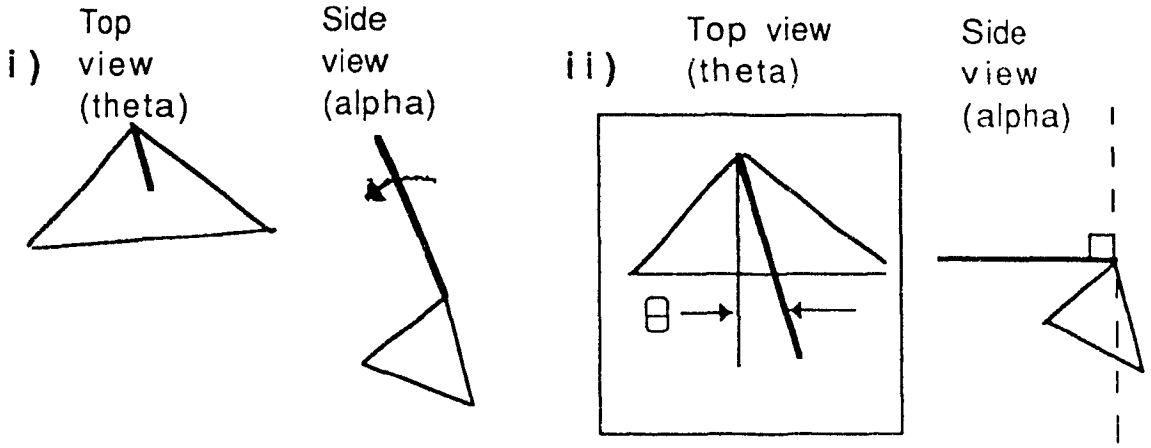

Fig 3.4.3 (b): i) Here the unrotated normal vector is too small when projected onto the theta plane. ii) Rotation in the alpha plane results in clear view of vector in the theta plane (box).

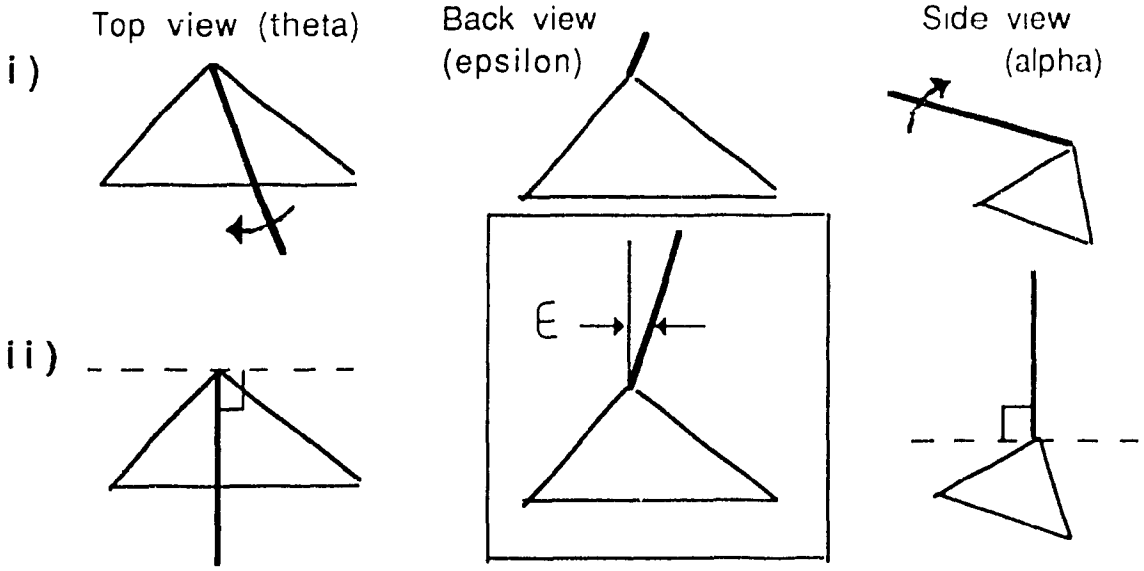

Fig 3.4.3 (c): i) In this case, the unrotated normal vector's magnitude is too small when projected on the epsilon plane.
ii) Rotations in theta and alpha planes result in clear view of normal vector in epsilon plane (box).

3.5 RESULTS: THE SIGNIFICANCE OF THE ENHANCED DISPLAYS

At the conclusion of chapter 2 we saw how that it was mainly the inability of the original displays to characterize coupled motion which led to development of the enhancements. However, as it turned out the new software also provided more precise curves describing the projected motion of the IREDs in the various planes.

In addition, it is fully compatible with the other new report software being developed concurrently by other programmers to replace the old report completely. This reflects an improvement in programming style, esthetic presentation, and maintainability, as well as precision of the curves (and hence accuracy of the resulting interpretations) displayed on the screen.

The implementation of the various steps described in this chapter led to a working product with consistent results. Recall that both the data from the preliminary study of chapter 2, as well as for patients from an affiliated clinic in Denver, originally showed erratic curves for the coupled motion software.

Incorporation of the vector rotation scheme resulted in smooth curves and ranges of angles within clear limits for these subjects. One set of data even included interpolated results for IREDs lost from view. The situation was successfully recognised by the coupled motion software and labelled as such on the display screen (this can be verified using the old Cerviscope playback mode).

Hence the coupled motion software eventually resulted in a new set of working displays which had conveyed the desired information to the user. In this section we will examine photographs from both the original and enhanced Cerviscope displays, as well as compare the two.

Then we will look at some specific aspects of the new display and how the user interface operates. In particular, we consider examples of how some parameters may be varied by the user, as well as the vector rotations described earlier. The use and interpretation of the new display is described fully in Appendix D, which is a guide produced for distribution to Spinex customers.

3.5.1 The Pages of the Enhanced Display

Let us now briefly examine the six pages of the enhanced Cerviscope display. Figure 3.5.4 shows each of these, along with the help screens which accompanies them. The latter provide descriptions of what the user sees for each page Note that it is not possible to combine pages from the original and enhanced Cerviscope reports.

Hence, the new display must provide a complete and self contained picture of the subject's motion. This results in a certain degree of redundancy, since the new display must provide some information contained in the original, as well as new details previously unavailable.

The mouse driven menu is on the left. On the top of this area are seven green boxes for selecting pages 0 to 6 (page 0 has not yet been implemented, but will probably consist of an overview of the others). A single small yellow box is used to illustrate the vector rotations described in section 3.4.2.

The larger yellow box bellow is used to vary parameters for each page, and is described in the next section. The red boxes on the bottom left are used to select the printout, exit, and help screen functions. An overlay function, allowing comparison of curves for different patients, will be added later.

Patient and page identification are on the top, and a box providing comments or instructions to the user is on the bottom of the screen. For detailed descriptions of each page and the relevant parameters, please see the user's guide in Appendix D.

The motion of the vectors between the IREDs on the head, neck, and shoulders (which were defined in section 3.2), is illustrated on page 1 [fig 3.5.1 (a)]. The red and yellow lines represent the vectors which are in the plane of the subject's skin. The white lines are virtual normal vectors perpendicular to these and extending straight out from IREDs on the head, neck, or thoracic spine (see figure 3.2.1).

By examining the white lines, the user may determine the exact orientation of these for any frame(s). In particular, with some practice, he/she can recognise immediately if the subject had an exaggerated (or unusually small) motion in any given direction. Note that the vectors are scaled to have magnitudes between -1 and +1 non-dimensional units. This is thus mostly qualitative information, analogous to the overview

page of the original display (see also page 5 below).

On page 2, however, we see a quantitative description of the angles described by the normal (ie. white) vectors shown on page 1, for each frame [fig 3.5.1(b)]. These angles correspond directly to the forward/backward, side to side, or axial rotation motion of the subject's spine. Hence, even though it is actually the motion of the normal vectors which is shown, these curves may be used to interpret the motion of the spine.

Alpha, epsilon, and theta represent the angular displacement in forward flexion, lateral bending, and axial rotation movements, respectively. The latter is not currently included in the standard Cerviscope examination protocol (Appendix B). Please see section 3.2 for more exact definitions of these angles.

On this page the red and yellow lines represent the angles made by any two of the normal vectors emanating from the head, neck, or thoracic spine (see message on bottom of the screen). These are still 'absolute' angles, rather than relative, since they are calculated with respect to the fixed coordinate system of the calibration frame (see section 3.2.2).

On the next page, however, we see the same angles combined into a single relative angle between the two selected normal vectors [fig 3.5.1(c)]. In the next section we will see how the IREDs from which the normal vectors emanate may be varied. The result is that the user may display the relative mobility between any two IREDs on the head, neck, or thoracic spine.

This is directly proportional to the intervertebral mobility of the underlying vertebral column. Hence page 3 is analogous to the mobility boxes shown for flexion and lateral bend in the original Cerviscope report - but much more precise. At this point, however, we have not yet considered coupled motion (ie. simultaneous motion in orthogonal planes).

For that purpose we consider page 4 in figure 3.5.1 (d). Recall that the relative angles of page 3 represented the combination of the absolute angles of page 2, for each frame. On page 4 we see how these angles vary with respect to each other, rather than with respect to time.

Hence, for example, the subject may be seen to unintentionally bend five degrees

to the left while bending thirty degrees forward. Similarly, a lateral bend movement of fifteen degrees is accompanied by an axial rotation of the same amount (ie. there is a one to one correspondence between these two movements).

This type of 'coupled' motion is typical, since (as we saw in sections 3.1 and 1.3) the arrangement of the vertebrae relative to one another normally makes motion in a single direction impossible. By studying the degree of coupled motion present in both normal and pathological populations, it should be possible to quickly match this motion with type of injury (or lack of it) which produces it. We will consider the implications of such a database further in the next chapter.

Finally, pages 5 and 6 [fig 3.5.1(e)-(f)] of the new display are meant mainly to complement the previous pages. In particular, page 5 illustrates the position of the normal vectors (ie. the white lines of page 1) versus time. Since clinicians are primarily considered with the angular displacements of the spine, this page serves only to clarify and quantify the linear displacements shown on page 1.

As for page 6, these stick figure views were added only to provide an intuitive description of the movement of the IREDs themselves, as opposed to the vectors joining them. Recall that the qualitative information of page 1 is directly quantified by the curves shown on pages 2 and 5 (ie. showing angular and linear displacements, respectively, of the normal vectors). Page 6 is purely qualitative, however, and may be described as a simplified version of the original 'playback' display.

Fig 3.7.1: The enhanced Cerviscope displays for characterizing cervical coupled motion. The on-line help screens, which describe each page, are also shown.

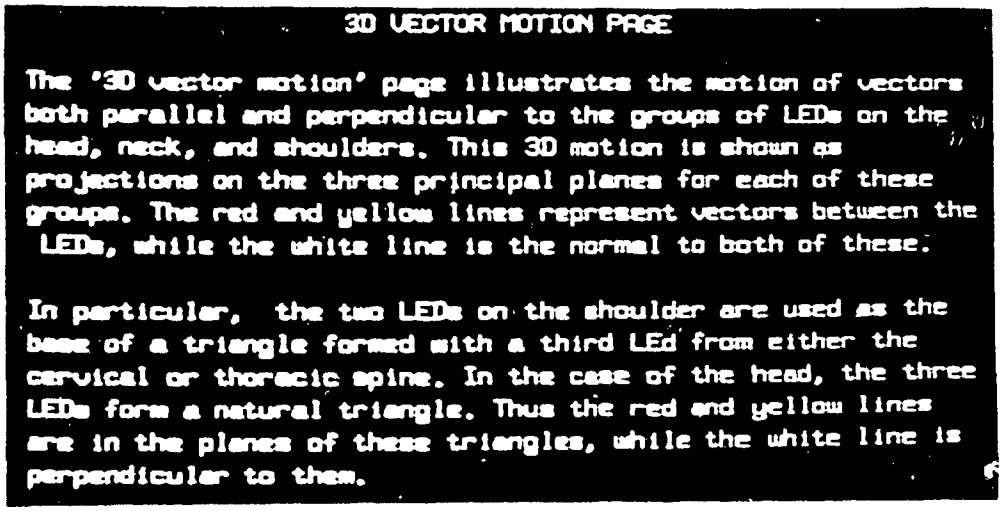

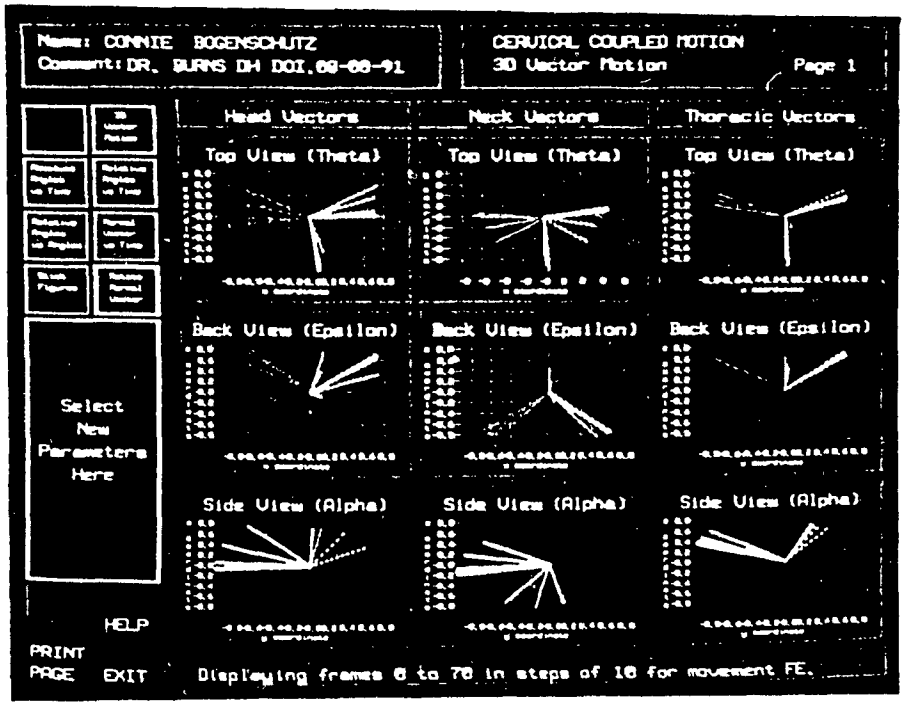

a) Page 1: 3D vector motion.

ABSOLUTE ANGLES VS TIME

The 'absolute angles vs time' page illustrates the absolute angles between the vectors perpendicular to the head, neck, and shoulders. On the 'relative vectors vs time' page these angles are shown combined. In the absolute case, they are seperate. For example, the angle 'alpha' boxes show the relative motion between the head and neck in the mid-sagittal plane. These angles will vary, depending on whether the primary motion is flexion/extension, lateral bending, or axial rotation.

Similarly, the epsilon and theta boxes show the absolute angles in the transverse and horizontal planes, respectively. Note that the relative motion between the neck and shoulders, or the head and neck may also be selected. Indeed, this may even be extended to the relative motion between two adjacent LEDs, which corresponds roughly to inter-segmental mobility.

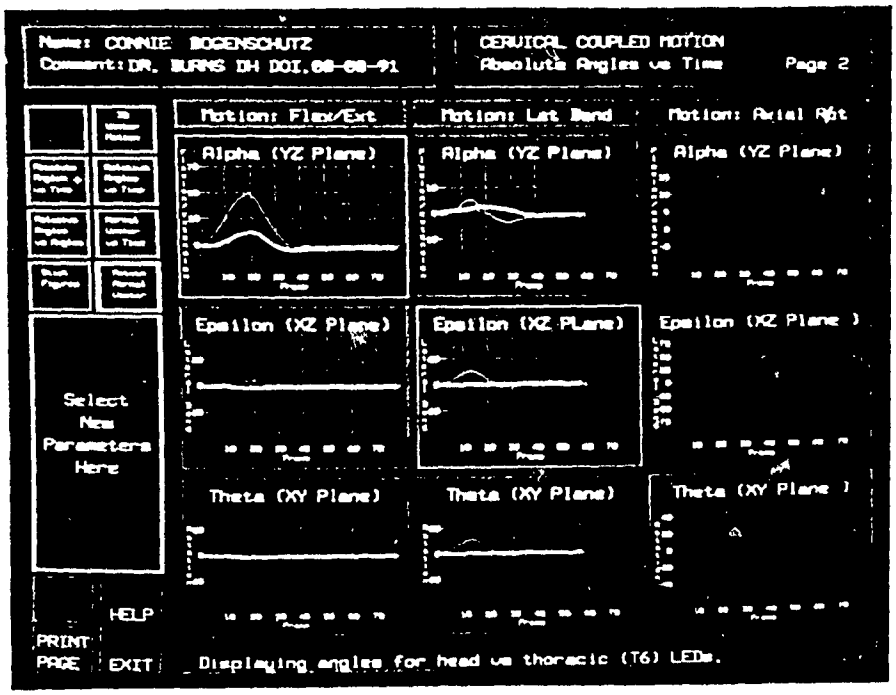

b) Page 2: Absolute angles versus time.

RELATIVE ANGLES VS TIME

The 'relative angles vs time' page illustrates the relative angles between the vectors perpendicular to the head, neck, and shoulders. On the 'absolute vectors vs time' page these angles are shown separately. In the relative case, they are combined. For example, the 'angle alpha' boxes show the relative motion between the head and neck in the mid-sagittal plane. This angle will vary, depending on whether the primary motion is flexion/extension, lateral bending, or axial rotation.

Similarly, the epsilon and theta boxes show the relative angles in the transverse and horizontal planes, respectively. Note that the relative motion between the neck and shoulders, or the head and neck may also be selected. Indeed, this may even be extended to the relative motion between two adjacent LEDs, which corresponds roughly to inter-segmental mobility.

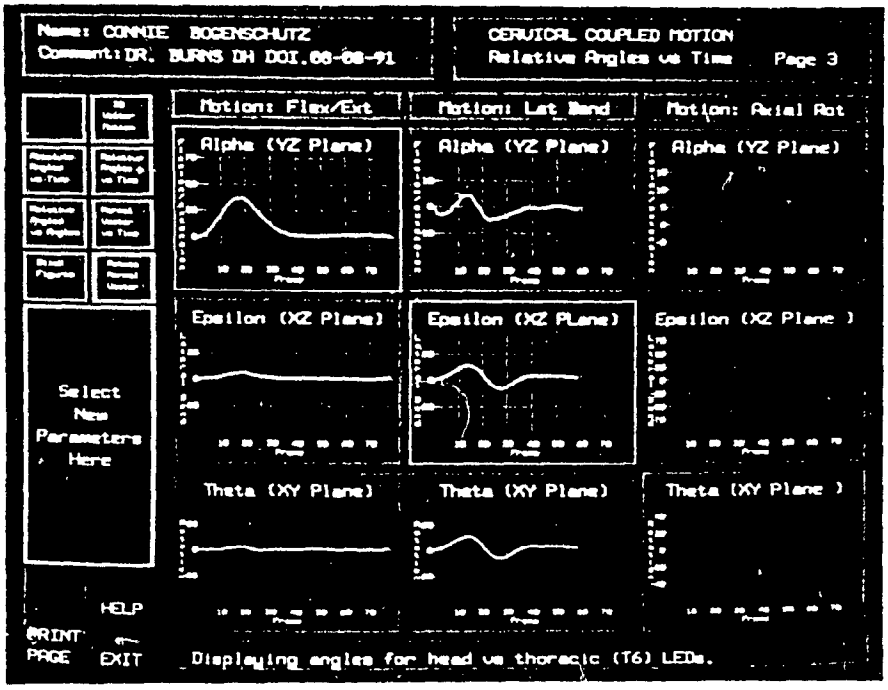

c) Page 3: Relative angles versus time.

RELATIVE ANGLES VS ANGLES

The 'relative angles vs angles' page combines the curves shown in separate boxes on the 'relative angles vs time' page. This results in a total of six combinations (ie.two for each of the three principal movements of flexion/extension, lateral bending, and axial rotation. For example, the 'FE vs LB' box for flexion/extension illustrates the lateral coupled motion which occurs when bending in the mid-sagittal plane. Similarly the 'FE vs ROT' box shows the rotational coupled motion linked with the same principal movement.

The 'LB vs FE' box illustrates the coupled forward or backward motion that occurs when bending laterally. The 'LB vs ROT' box shows the rotational coupled motion accompanying lateral bending. Finally, the 'ROT vs FE' and 'ROT vs LB' boxes show the coupled flexion/extension and lateral bending which accompanies axial rotation.

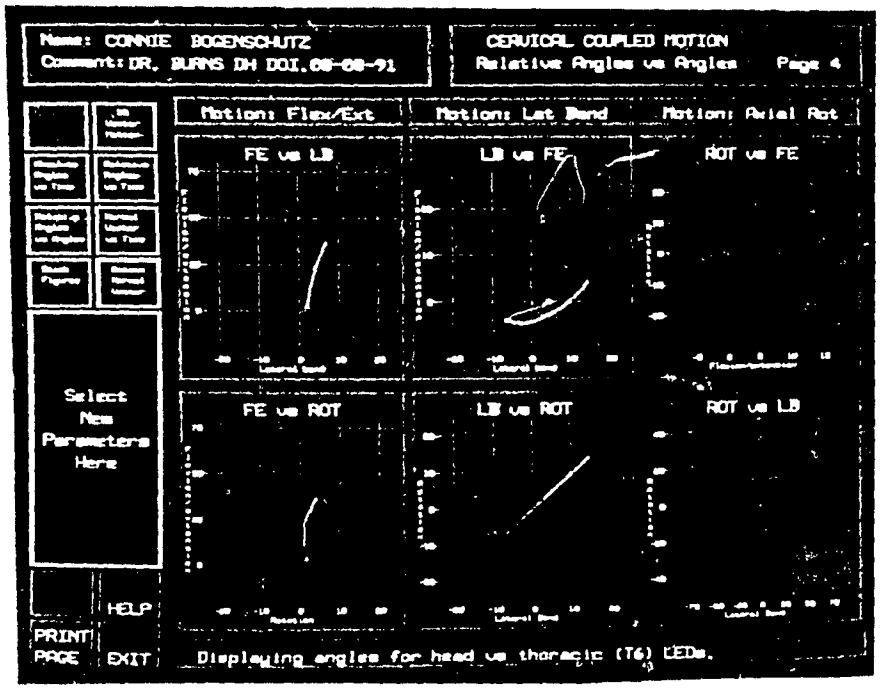

d) Page 4: Relative angles versus angles.

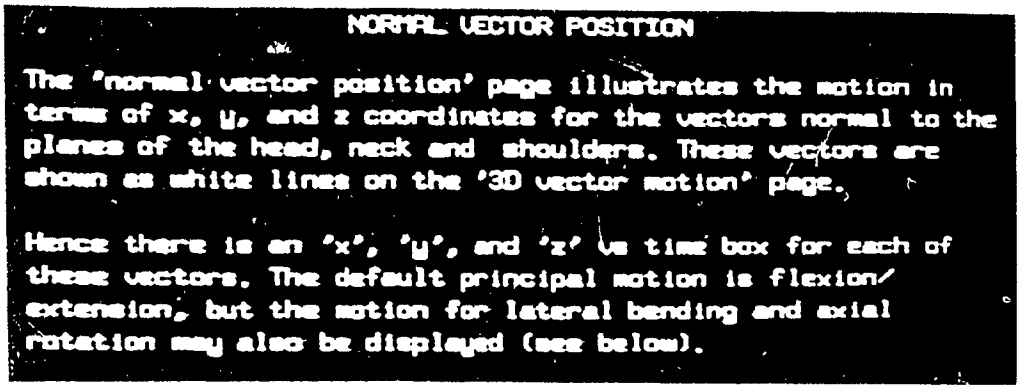

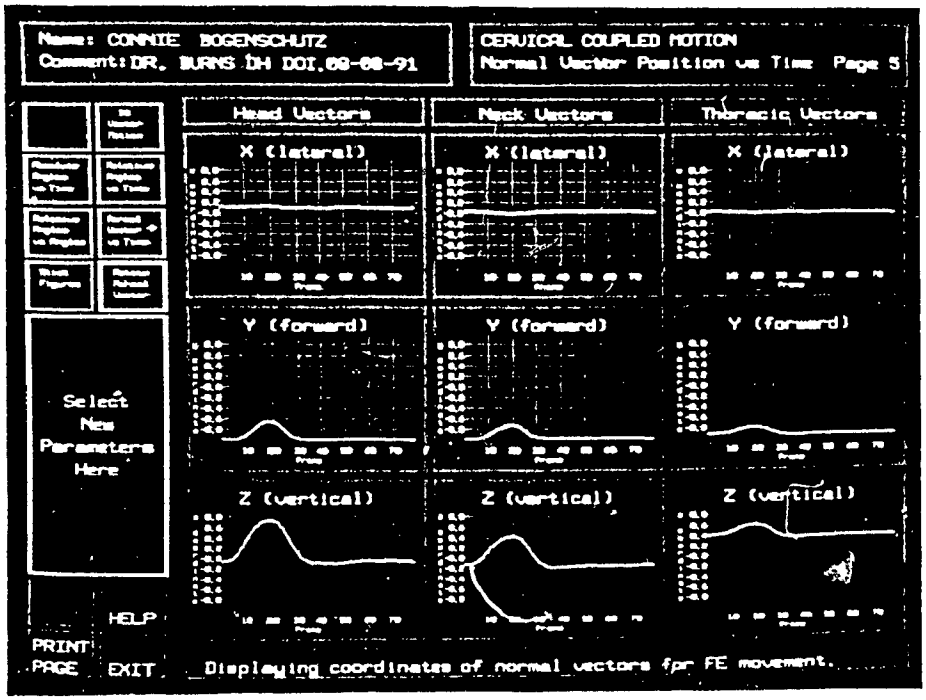

e) Page 5: Normal vector position versus time.

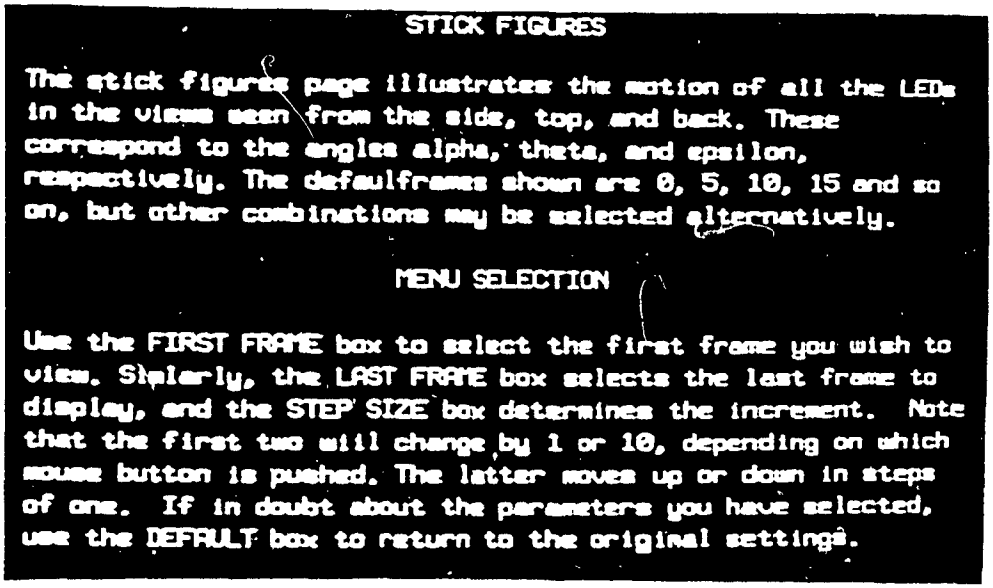

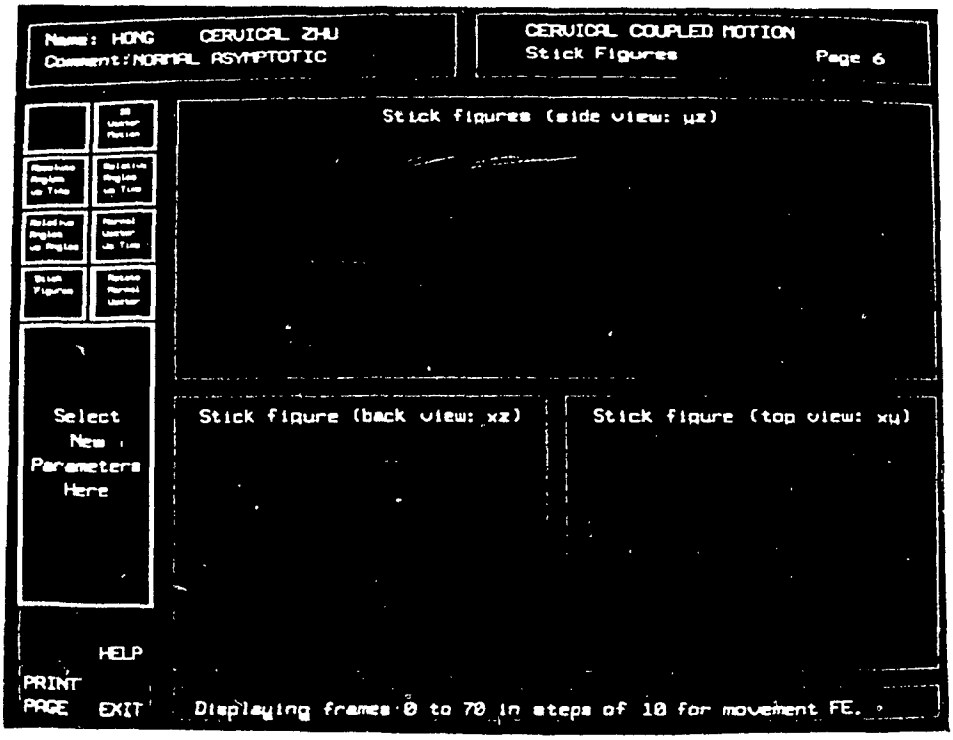

f) Page 6: Stick figures.

3.5.2 The Menu Area and Selection of Parameters

We will now consider how the user may vary the parameters that determine what he/she sees on the screen for any given page. There is considerable flexibility here, to the extent that the uninitiated user may easily become confused. It is for this reason that the parameter selection boxes of the menu are originally locked. They must thus be unlocked by the user before the default parameters may be changed.

In figure 3.5.1 we saw that upon entry to new displays the menu area contains several green and red boxes, a single small yellow box, and a single large yellow box. As explained above, the green boxes are used to select a page and the red boxes to select functions. The small yellow box shows the user how the normal vectors of page 1 may be rotated to correct their perspective.

Note that these rotations are always performed automatically in the background prior to calculating the angles shown on page 2. However, page 1 is normally shown with the vectors in their natural (ie. unrotated) state to illustrate the subject's uncorrected position. This may be useful in interpreting the motion, since he/she may be leaning, the IREDs may be positioned crookedly, and so on.

In figure 3.5.2 (a) we see how the menu looks after the user chooses the large yellow box labelled 'Select New Parameters here'. After confirming whether the user wishes to unlock the parameters, the single large yellow box is replaced by eight smaller ones. The original small yellow box is unaffected.

The main area of the display is also replaced by a special help screen, which describes how the parameters in the new yellow boxes may be varied. Note that the regular help function is specific to the page being displayed when it is invoked. The parameter selection help screen, conversely, is displayed whenever the parameter boxes are unlocked, regardless of the page.

Figure 3.5.2 (b) shows an expanded view of the menu are boxes. The green page selection boxes are identified by the page description shown within each of them. The red function boxes are also clearly identified by simple labels. The yellow parameter selection boxes, however, are more complicated to understand and use. We shall thus look at these more closely.

Consider the box labelled 'LED SETS'. This box is used to select the two sets of IREDs (ie. LEDs), and therefore the origins of the normal vectors, corresponding to the angles displayed on page 2. The user may thus choose to display the angles for the head and neck, the head and thorax, or the neck and thorax. This will also affect the relative angles displayed on pages 3 and 4.

The 'HIGH LED' and 'LOW LED' parameters determine which IREDs will form the apexes of the triangles shown on page 1 for the neck and thoracic spine. We saw in section 3.2 that the normal vectors, whose motion is described in the subsequent pages, are defined by the two IREDs selected along the spine. The other corners of the triangles are given by the two IREDs on the shoulders (see fig 3.2.2).

The 'FILT DATA' parameter allows the user to see how the curves of pages 2 to 4 appear before and after they are filtered (ie. smoothed) by the software. The 'RESET ALL' parameter is used to return all the parameters to their default values and lock them again. The 'FIRST FRAME', 'LAST FRAME', and 'STEP SIZE' boxes permit the user to specify exactly which frames he/she wishes to display, as well as the interval between them.

The 'MOVEMENT' parameter is used for pages 1,5, and 6 to determine which principal movement (ie. flexion/extension, lateral bending, or axial rotation) is being displayed. For pages 2 to 4, all the principal movements are shown at once. Finally, the 'ALARM OFF' button is used to disable the alarm message which covers part of the screen when some IREDs are recognised by the software as being obscured (see section 3.4).

This section has been a brief description of how the user may vary the parameters for the enhanced Cerviscope displays. The number of ways in which the parameters described above may be varied is virtually limitless. We will now consider a few illustrative examples. For more details on how to interact with these display, please see the user's guide in Appendix D.

Fig 3.5.2: Parameters which may be varied by the user in the coupled motion display.

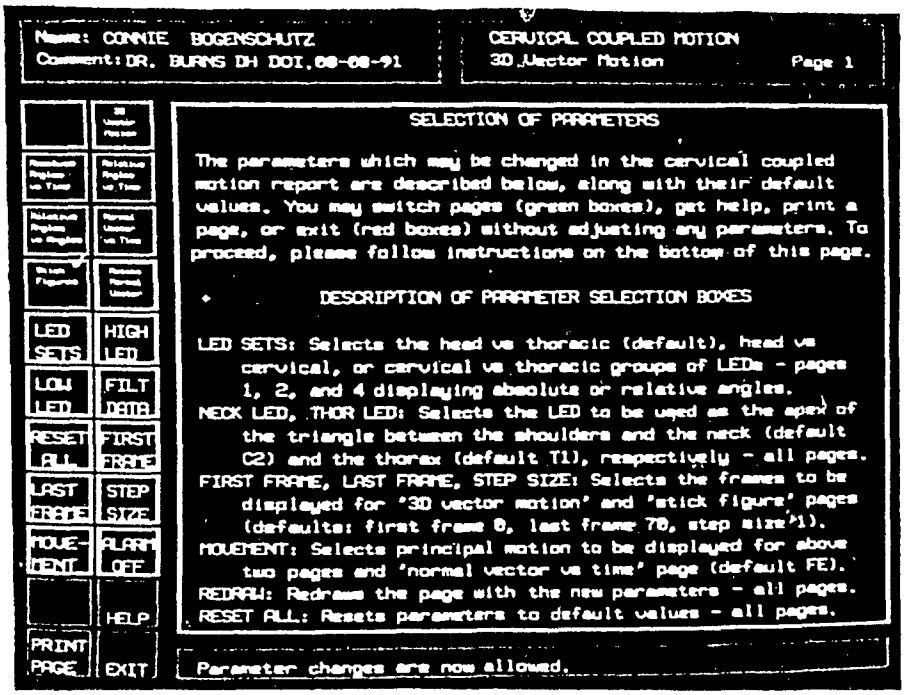

a) Selection and description of parameters (yellow boxes). To overide the default values the user must enable access to the these boxes.

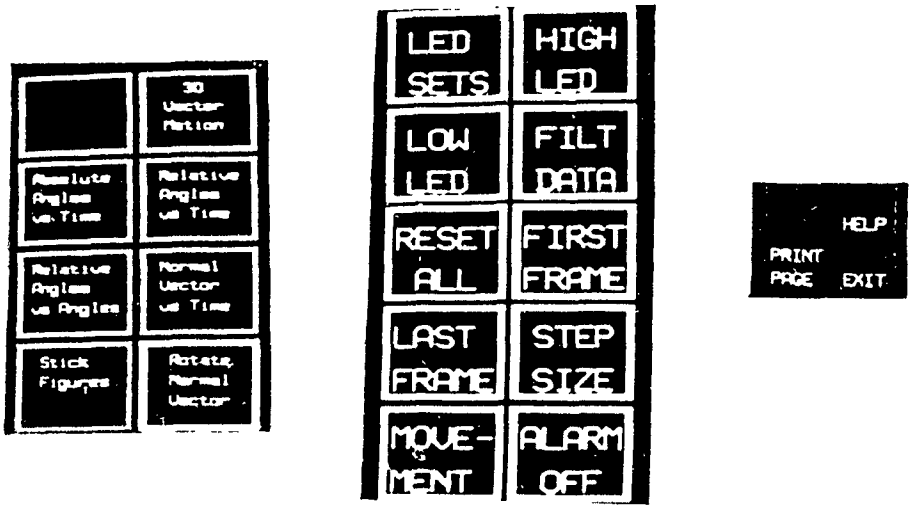

b) Menu boxes for page selection (green), parameter changes (yellow), and miscellaneous functions (red)

3.5.3 Some Parameter Variations

Let us consider how the display will change upon variation of the 'LED SETS', 'HIGH LED', and 'LOW LED' parameters. Recall that these will determine which IREDs are being used to determine the origins of the vectors normal to the head, neck, and thoracic spine shown on page 1. They will also determine which of these are being compared on pages 2, 3, and 4.

Figure 3.5.3 (a) shows the angles made by the vectors normal to the plane of the IREDs on the head and to the triangle formed by the IREDs at the top of the neck and on the shoulders. Hence, this describes the motion of the head versus the top of the cervical spine.

Similarly, figure 3.5.3 (b) shows the corresponding angles for the vectors normal to the head and the triangle formed by the IREDs at the mid thoracic spine and the shoulders. This corresponds, in turn, to the movement of the head versus the middle of the thoracic spine (which usually remains almost motionless when bending the neck).

The locations shown for the IREDs in figures 3.5.3 (a) and (b) are the default values for the vectors normal to the cervical and thoracic spine, respectively. In figure 3.5.3 (c), we see how the angles vary for the cervical versus the thoracic spine, with these IREDs selected.

Finally, figure 3.5.3 (d) shows how the 'high' and 'low' IREDs may be adjusted to describe the motion between any two IREDs along the spine. In particular, in this case the IREDs at C6 and T1 are the 'high' and 'low' values, respectively. This corresponds roughly to the mobility (ie. intervertebral mobility) between the vertebrae at C6 and T1.

Of course, even though the motion of the normal vectors is shown precisely, it is still only an approximation of the underlying vertebral motion, due to skin motion (see section 1.3.4). Nevertheless, this still represents an extremely useful and popular parameter for quantifying spinal motion.

Fig 3.5.3: Some variations in the selection of normal vector locations and the resulting absolute angles vs time.

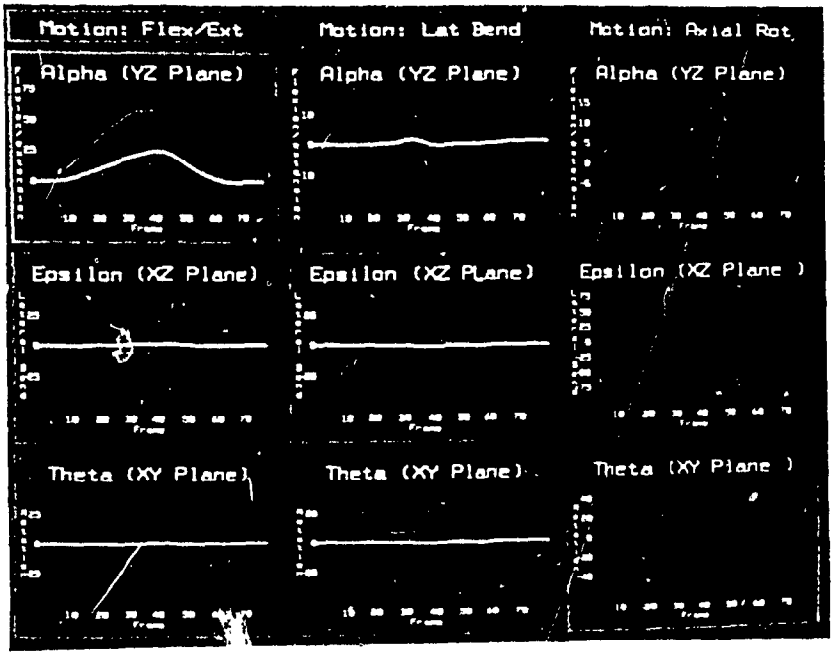

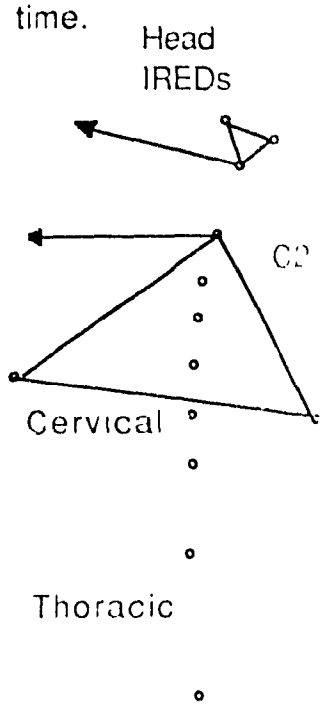

a) Head versus cervical (C2).

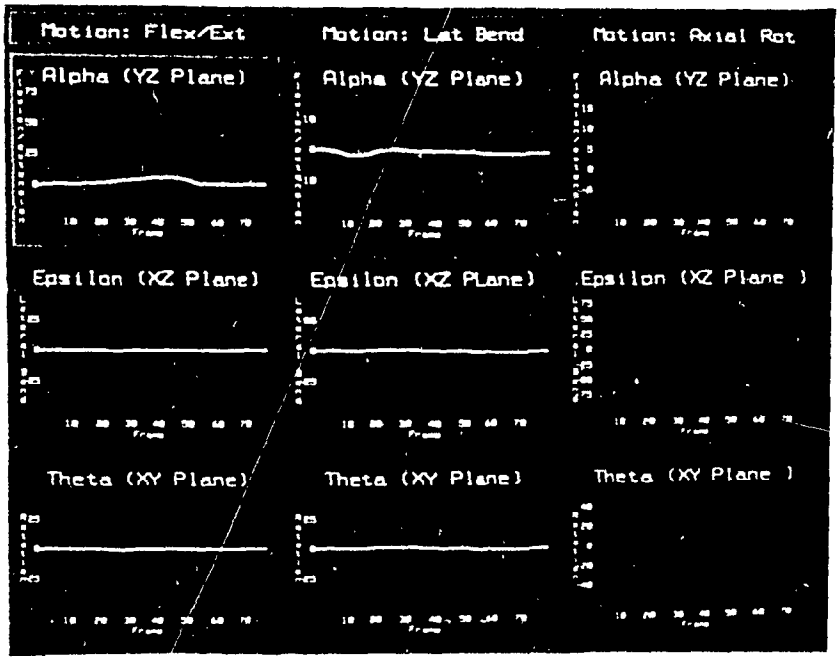

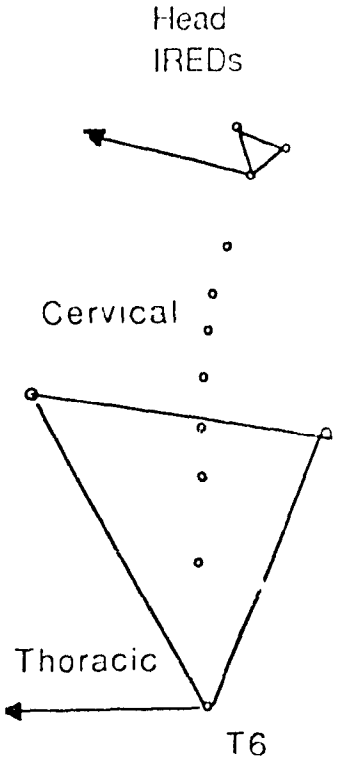

b) Head versus thoracic (T6).

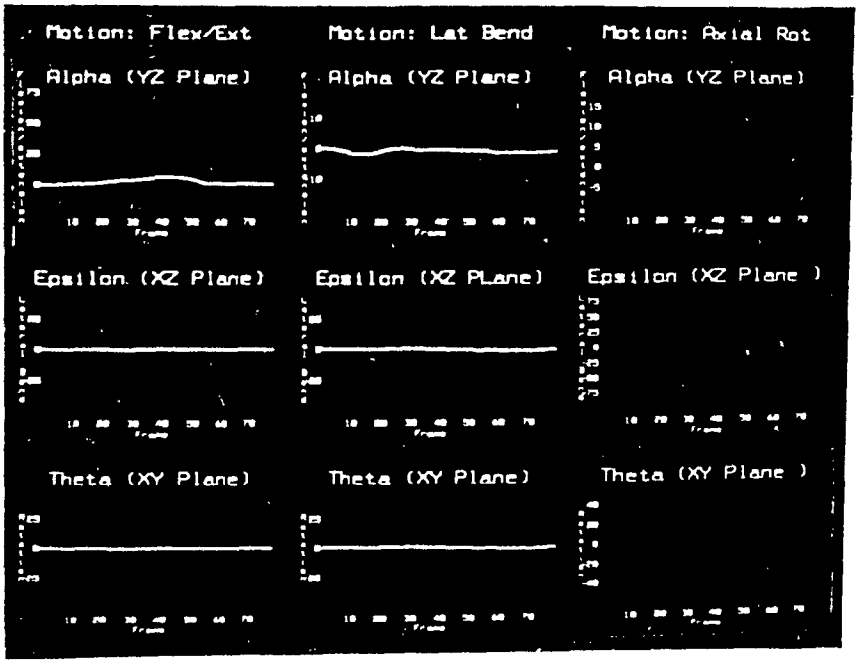

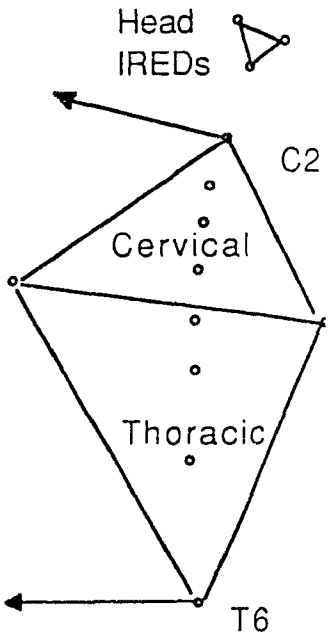

c) Cervical (C2) versus thoracic (T6).

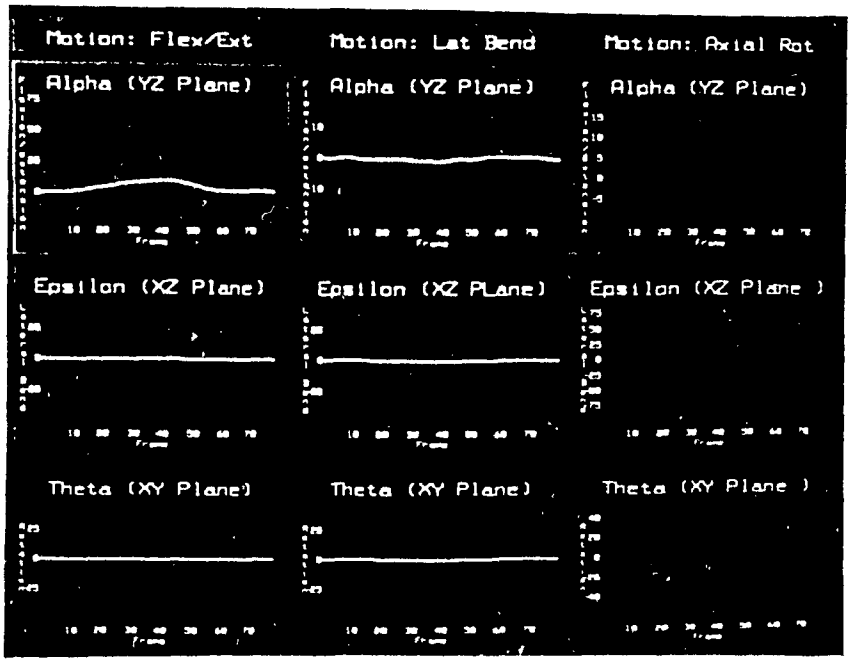

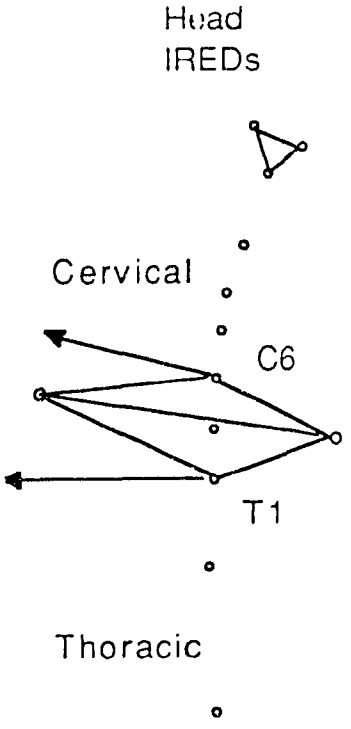

d) Cervical (C6) versus thoracic (T1).

3.5.4 Examples of Vector Rotations

To illustrate the vector rotations described in section 3.4, let us examine a few examples. Recall that these rotations are meant to correct for errors in perspective, due to the subject's position at any given time, when the projections of the normal vectors are used to calculate the corresponding angular displacements.

The rotations are performed automatically prior to calculating these angles, and the user may see them by using the 'Rotate Normal Vector' box in the menu. Note that only the normal (ie. white vector) is rotated, since the others are not used directly in the angle calculations).

Figure 3.5.4 shows the normal vector rotations in the Alpha plane, which corresponds to forward bending (see section 3.2). The unrotated position [fig 3.5.4(a)] is fine for determining the angular displacement alpha of the normal vector from the side view. However, from the top the perspective is distorted and the angle theta may be incorrect.

Hence, a counterclockwise rotation is performed [fig 3.5.4(b)] to insure that the top view is indeed perpendicular to the longest dimension of the normal vector. Similarly, a clockwise rotation is done to make sure that the back view is undistorted and epsilon is calculated correctly.

In figure 3.5.5 we see how one of these rotations affects the perspective in the Theta plane. At first the uncorrected vector points slightly to the right, indicating the person or the IREDs were positioned crookedly [fig 3.5.5(a)]. Then the first rotation in the alpha plane, described in figure 3.5.4(b), is performed.

We can see that this results in a more precise projection of the normal vector onto the Theta plane, with constant magnitude for all frames [fig 3.5.5(b)]. Remember, we are not concerned with the actual magnitudes of these projections, but rather with the angles that these projections describe.

The second alpha rotation is not shown in the Theta plane, since it is used in the calculation angle epsilon, rather than theta. The next rotation [fig 3.5.5(c)] is performed in the Theta plane, and is also required to correct the perspective in the Epsilon plane (ie. back view). This clockwise rotation in the Theta plane results in the projections onto the

epsilon plane sticking backwards, rather than to one side or the other.

Figure 3.5.6 shows how the previous rotations affect the projection in the Epsilon plane. This plane is most sensitive to uncorrected projections of the normal vector, as can be seen from the first picture [fig 3.5.6(a)]. Note that here the subject is oriented to the left, so the normal vector points to the right.

The clockwise rotation in the Theta plane, shown previously in figure 3.5.5 (c), results in a significant improvement in the back view [fig 3.5.6(b)]. Now the normal vector is being viewed directly from the back, rather than from one side. Finally, the (clockwise) second rotation in the Alpha plane, shown previously in figure 3.5.4 (c), completes the correction.

Fig 3.5.4: Rotations in the alpha plane to correct the viewing perspectives of normal vectors in epsilon and theta planes

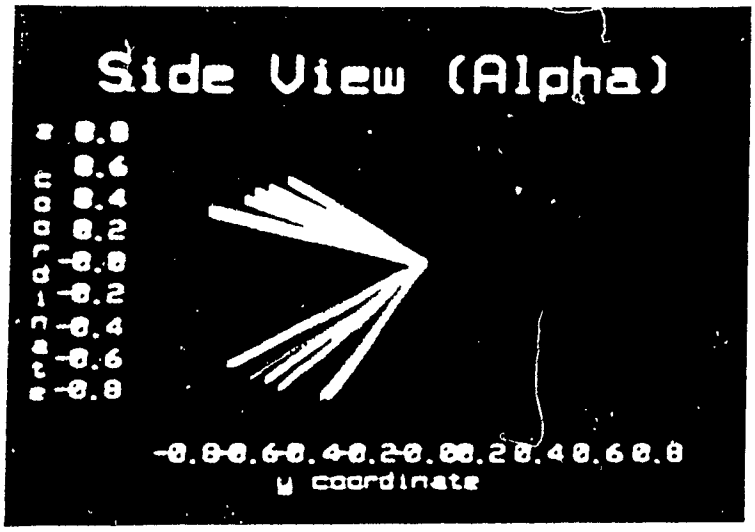

a) Original (unrotated) side view of normal vector for head in flexion/extension movement. No correction is needed for this angle.

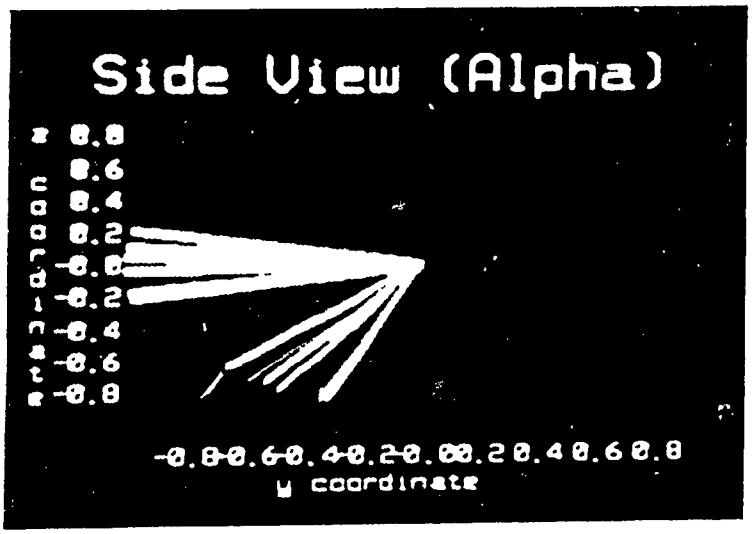

b) Normal vector rotated toward 9 o'clock position in the alpha plane. This will correct the perspective for determining angle theta (top view)

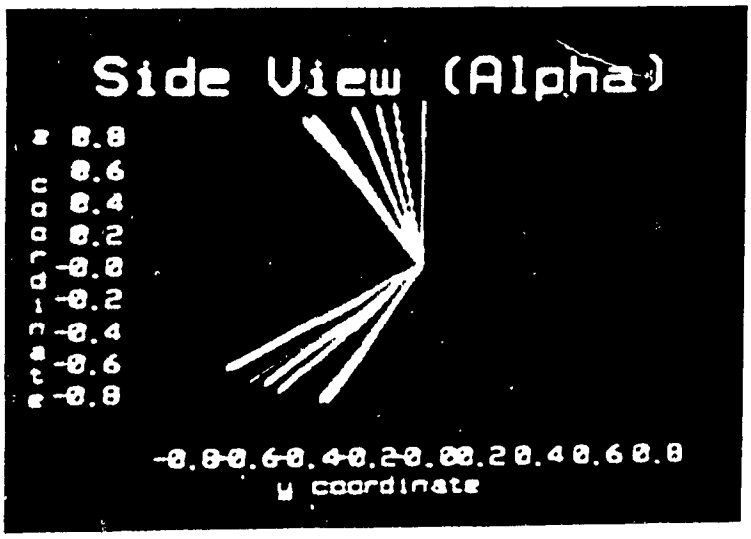

c) Same vector rotated toward the 12 o'clock position. This is the first of two rotations required to correct for angle epsilon (back view).

Fig. 4.5: Original and corrected views of normal vector in the theta plane.

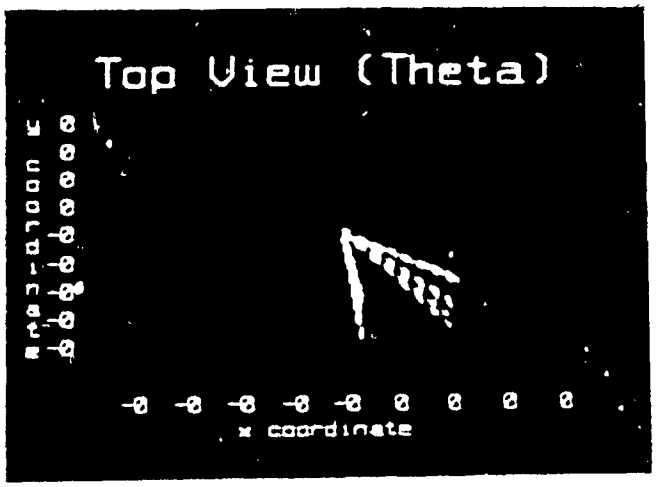

a) Original (uncorrected) top view of normal vector. Note how the projections of this vector (white lines) have varying lengths.

b) Corrected top view of normal vector after rotation in the alpha plane. Now all the projections of this vector have similar lengths.

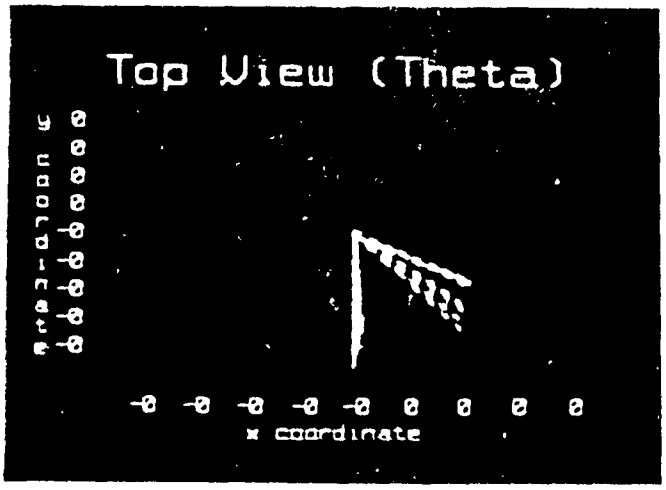

c) Rotation of normal vector towards 6 o'clock in theta plane to complete correction for angle epsilon.

Fig 3.5.6: Original and corrected views of normal vector in the epsilon plane.

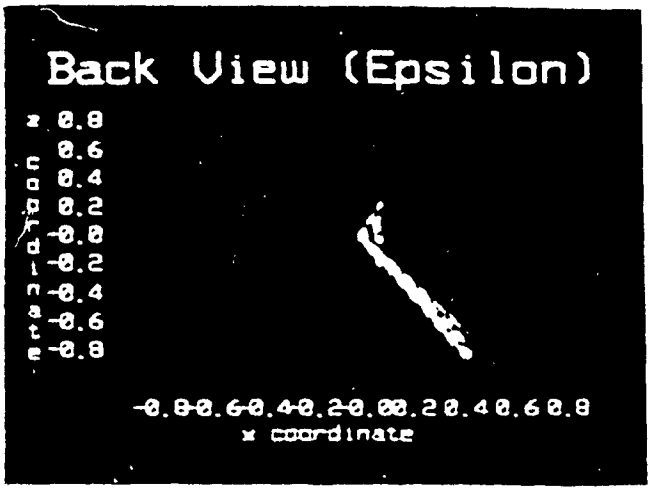

a) Original (uncorrected) back view of normal vector. The subject is actually oriented slightly toward the left, so that the normal vector appears to project toward the right

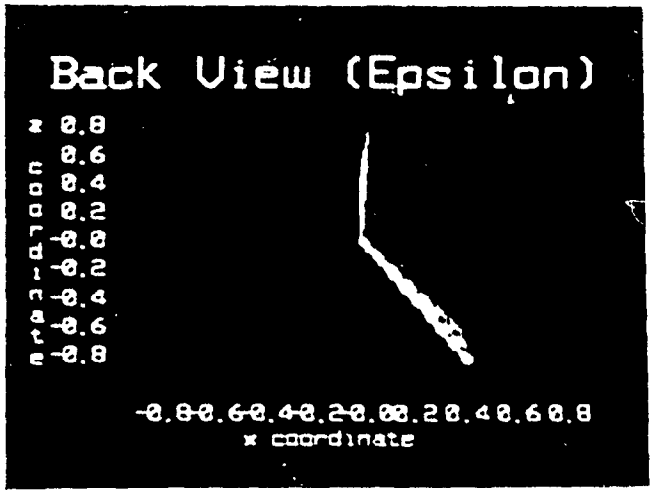

b) After rotating in the theta plane, the back view of the normal vector is now partially corrected (note how the white lines are still of varying lengths).

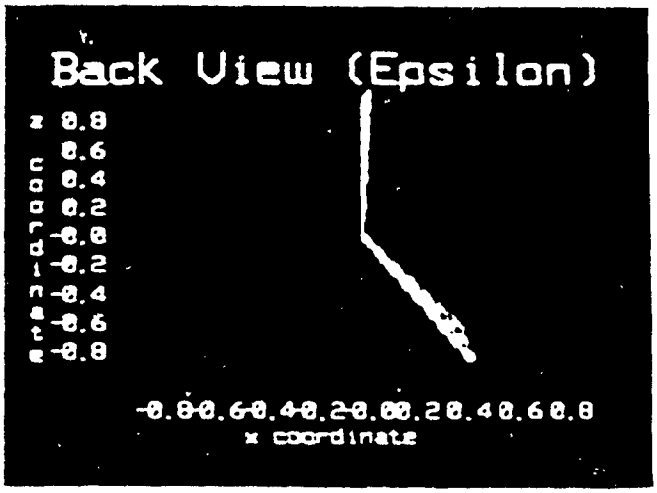

c) Adding a rotation in the alpha plane completes the correction for the back view.

3.5.5 Applications of the New Displays

In this chapter we have examined the implementation of an enhancement to the Cerviscope which will permit the effective analysis of coupled motion in the upper spine. This added feature is expected to allow users to establish quantitative relationships between simultaneous movements of the neck in various directions.

The coupled motion display for the Cerviscope appears to provide a new, non-invasive, method for measuring relative motion in the cervical spine. By plotting the direction angles for coupled versus principal motion, an intuitive representation of the intervertebral mobility is obtained.

Once a data base representing motion typical of normal subjects has been accumulated, it will be used for comparison with the curves for new patients. Evaluation of cervical lordosis, thoracic kyphosis, and inter-segmental mobility may be also made from previously existing displays, which were described in chapter 2.

Thus the results from the coupled motion display will be used in conjunction with these, or analogous updated versions. Future testing should include further inter and intra-subjects validation of the information deduced from each display. This analysis of mobility is expected to be valuable in differentiating between normal and pathological movement in the cervical spine.

However, the algorithms and displays implemented for this enhancement are equally applicable to other parts of the spine. Hence, coupled motion in the lower and middle portions of the spine may eventually be characterized in an analogous manner.

For example, it may be possible to similarly study the relationship between the shoulders and the pelvis in human gait. Thus the role of the spine in locomotion may also be verified using a modified form of this technique.

3.6 DISCUSSION

The complex nature of three dimensional coupled motion in the spine makes it difficult to characterize objectively. Although the attributes of this motion remains subject to discussion, it appears that there may be some diagnostic value in its analysis. In order for this to occur, however, the results must allow for a consistent interpretation.

In this chapter we have considered how a set of enhanced displays were added to the original Cerviscope, in order to quantify coupled motion. We first examined how the new displays were conceived, as well as the analytical calculations involved.

Then we saw how design requirements favoured the development of a new set of program modules instead of using available CAD packages. These modules had to incorporate modern programming techniques and be consistent with other software developed by the manufacturer of the Cerviscope.

Some refinements were required to obtain consistent results with the new displays. Digital filters were employed for curve smoothing and coordinate transformations were performed to correct errors in perspective of the vectors being observed. Nevertheless, a working product was obtained, with several pages of displays containing a variety of new information.

These pages were described, along with the user interface for accessing the new displays. Examples were given of how information may be extracted for various levels of the neck and for different portions of the movements being executed.

The coupled motion displays appear to provide an effective way to analyze simultaneous motion in the principal orthogonal planes. They are thus expected to be helpful in differentiating normal and pathological motion.

CHAPTER 4 - CONCLUSIONS AND RECOMMENDATIONS FOR FURTHER WORK

4.1 GENERAL

It has been established that there is a need for objective, non-invasive instruments for aiding in the diagnosis of non-acute cervical spine injuries. We saw how the mechanics of biological tissue must be understood in order to develop this type of equipment.

With some improvements, the Cerviscope was found to be effective in inferring the motion of the cervical spine through the tracking of skin markers. Although some limitations must be respected, such as the in-applicability of this device to neurological injuries, it should be possible to integrate it into traditional clinical diagnoses.

Following a summary of the highlights of this investigation, some suggestions for further study are given below. Correlation of skin markers with the underlying vertebrae must be determined using radiographic studies. Establishment of normal and pathological data bases will be undertaken through the collection of data from patients in some of the various clinics which use the Cerviscope.

Refinements in the user interface, the addition of the enhancement to characterize 3D coupled motion, and the eventual implementation of an expert system are all expected to improve the performance of this product. It is expected that the latter will help to quantify this process, thereby rendering it as objective as possible.

In the conclusion, we will consider how the areas of biomechanics, software development, and clinical diagnoses have been joined in this study. By relating the first two areas, the engineer is able to develop precise tools which will help the physician to increase the accuracy of the latter.

4.2 MAJOR HIGHLIGHTS OF THE INVESTIGATION

In this section we will briefly summarize the three major aspects of this study. In chapter 1 we considered existing applicable diagnostic tools and the biomechanics of cervical spine injuries. In chapter 2 we looked at a particular device designed for analyzing motion in the neck. Finally, in chapter 3, we explored the development of some new displays to improve the diagnostic capacity of this device.

4.2.1 Biomechanics

To properly assess the function of the cervical spine, objective diagnostic tools are required. Following a review of existing instrumentation, the mechanisms of injury and analytical models used to quantify these were examined.

The role of previous cervical range of motion investigations were considered next. A comprehensive set of normal range of motion data was tabulated for use in the identification of injuries through motion analysis.

Many devices for analyzing motion use cameras which track skin markers, in order to deduce underlying movement. The correlation between skin markers on the neck and the vertebrae underneath was thus investigated. It was determined that a linear relationship may be established.

Coupled joint motion in the spine was also identified as an important indicator of normal or pathological movement. Several techniques for quantifying such motion were examined. It was found that currently existing techniques are not adequate for characterizing the complex and unique coupled motion of the neck in a simple manner.

4.2.2 Evaluation of the Original Cerviscope

The performance of a new instrument for the diagnosis of neck injuries was evaluated. This new opto-electronic device, known as the Cerviscope, was designed specifically for the non-invasive assessment of soft tissue injuries in the cervical spine.

The instrument uses kinematic data from the motion of infrared light emitting diodes affixed to the subjects' skin. The instrument was described here in detail, with an

emphasis on the analytical techniques employed and the presentation of the results to users.

A preliminary analysis was undertaken using the Cerviscope. Following a comparison of motion analysis in the upper and lower spine it was determined that this instrument had the potential to be a useful diagnostic tool. However, some important shortcomings were identified, such as the somewhat subjective interpretation of the display screens.

Another problem was the inability to efficiently analyze simultaneous motion of the cervical spine in different directions. The relevance of this subject was then examined. As a result, an enhancement to the Cerviscope which would characterize coupled motion was implemented.

4.2.3 Development of the Enhanced Displays

The development of this enhancement involved the use of both analytical methods and contemporary programming techniques. Implementation of this new product occurred in stages and involved several refinements.

Software modules were defined for specific tasks, including calculations, graphics, the mouse interface, and data handling. Commercial CAD packages were considered inappropriate for these programs, which had to be consistent with other software developed by the manufacturer. The new displays were integrated with previously existing programs, as well as other products being developed concurrently.

Corrections were made to resolve analytical errors in interpreting the kinematic data. These included digital filtering and the rotation of vectors using three dimensional coordinate transformations.

It appears that this enhancement to the Cerviscope may provide a unique ability to objectively analyze coupled motion in the neck. The coupled motion analysis may be modified for application to the study of the lower and middle portions of the spine as well.

4.3 FURTHER WORK: ESTABLISHING AND INTERPRETING THE DATABASE

In chapter 2 we saw that in evaluating the Cerviscope, the following simple question must be answered: "Does the system satisfy its intended purpose ?". However, since the users are mostly clinicians, they must be able to use and understand this diagnostic tool. It can therefore also be asked whether the presentation of data from the tool and its interpretation by the users correspond.

Indeed, it is conceivable that the tool may be more accurate than the user in providing diagnoses. For example, expert clinical diagnoses may be provided together with the subject data. It will be necessary to consider the reliability of these, regardless of the credentials of their source.

An important consideration not addressed in the present study is that of intra-subject consistency. In chapter 2 we considered the results for treatments of the data from preliminary test subjects using the original Cerviscope software. In chapter 3 we looked at the same data, as well as that for another set of subjects, using the new coupled motion software. However, we did not re-test the same people to determine the variation in their responses. Thus we examined inter-subject, but not intra-subject, variability.

Finally, there is the question of the degree of usefulness of this diagnostic tool. This will only be determined after it has been on the market long enough to provide extensive feedback from the field. We can, nevertheless, already provide suggestions for improvements, as well as recommendations for further study.

4.3.1 Experimental Procedure for Data Acquisition

A protocol has been established for experimental studies in collaboration with clinics already using the Spinoscope and Cerviscope. The purpose of these studies would be to establish a data base for normal and pathological cases examined using the latter instrument. This protocol is basically a synopsis of the procedures outlined in chapter 2, and is presented in Appendix B. [88]

The need for the normative database stems from the inapplicability of range of motion information found in the literature. Because of its unique nature, the Cerviscope

requires a devoted set of data (see section 1.3.3). In particular, the available data in the literature is highly variable. It is thus not yet possible to establish a direct correspondence with the readings obtained from the Cerviscope.

This research will serve the following purposes:

- correlation between radio-opaque skin markers and vertebral motion. This is the first step in correlating traditional range of motion studies with Cerviscope data,
- establishing ranges of motion for cerviscope examinations of normal cases. This will provide a basis for comparison with pathological subjects. It should then be possible to clearly differentiate normal from pathological cases.

The data from the pathological cases may then be used for identification of pathologies. Abnormality may be established by comparison with normal patterns. The data base for previously identified pathologies will then provide the means for labelling subsequent ones.

Two types of subjects will be examined using the Cerviscope. The first constitutes a sample of people from the so-called normal population. These subjects will be chosen for their conformity with accepted standards of non-pathological spines. Each normal subject will undergo a series of standard cervical radiographs (as described in Appendix A), followed by a Cerviscope examination. The latter involves antero-posterior flexion and extension, lateral flexion, and rotation of the cervical spine.

Radio-opaque markers will be attached to the subject's skin in order to correlate surface and vertebral motion. Small metallic chains will be hung from one corner of all radiographs to ensure identification of the vertical direction.

The second group will include patients suffering from various non-acute cervical ailments, who will be referred by affiliated clinics for Cerviscope examinations. These subjects will be divided into subgroups according to their symptoms. Thus it should be possible to ascertain the effectiveness of the Cerviscope in detecting specific pathologies. This will ostensibly be accomplished by comparison of pathological motion with the established normal range of movement.

Hence the results from normal subjects will be used to define non-pathological range of motion. This will become the standard for comparison during subsequent diagnosis of pathological cases. For purposes of the study, each of these should be evaluated solely on the basis of the Cerviscope examination. Independent diagnoses will then be performed by certified medical practitioners, using traditional methods and instruments. These will be compared with those resulting from the Cerviscope data, in order to determine whether the Cerviscope is a reliable diagnostic device.

4.3.2 Interpreting the Database

A consensus must be reached upon how the above data will be interpreted. It is proposed that the methods based on the arguments of Bryant et al. (1989), Dvorak et al. (1988), Gracovetsky et al. (1989), and Reich et al. (1986) be used as a guide.[28,60,74,75]

Ideally, a common vector space should be obtained for all of the means used to accumulate data. Using a transformation function it should be possible to map each of these to the common space. Only then are entirely objective conclusions possible. This process is illustrated in figure 4.3.1.

Such a transformation is analogous to the transformation of measurements between skin markers and the vertebrae by Gracovetsky et al. (1990).[29] It may not always be practical in a clinical setting, but it should be considered when establishing empirical relationships.

In figure 4.3.2, a possible decision making process is illustrated for incorporating the Cerviscope into the diagnostic process. From this figure it can be seen that both transfer functions and relational transformations are involved. The former are provided by the Cerviscope and other imaging systems used to aid the diagnosis.

The human examiner corresponds to the qualitative transformation of information into a common space. However, a quantitative relational transformation between Cerviscope readings and data from other means is not yet available. Currently, only qualitative comparison between these databases is possible. A knowledge based expert system is currently being developed for the Spinoscope and Cerviscope, which should help in quantifying this analysis.

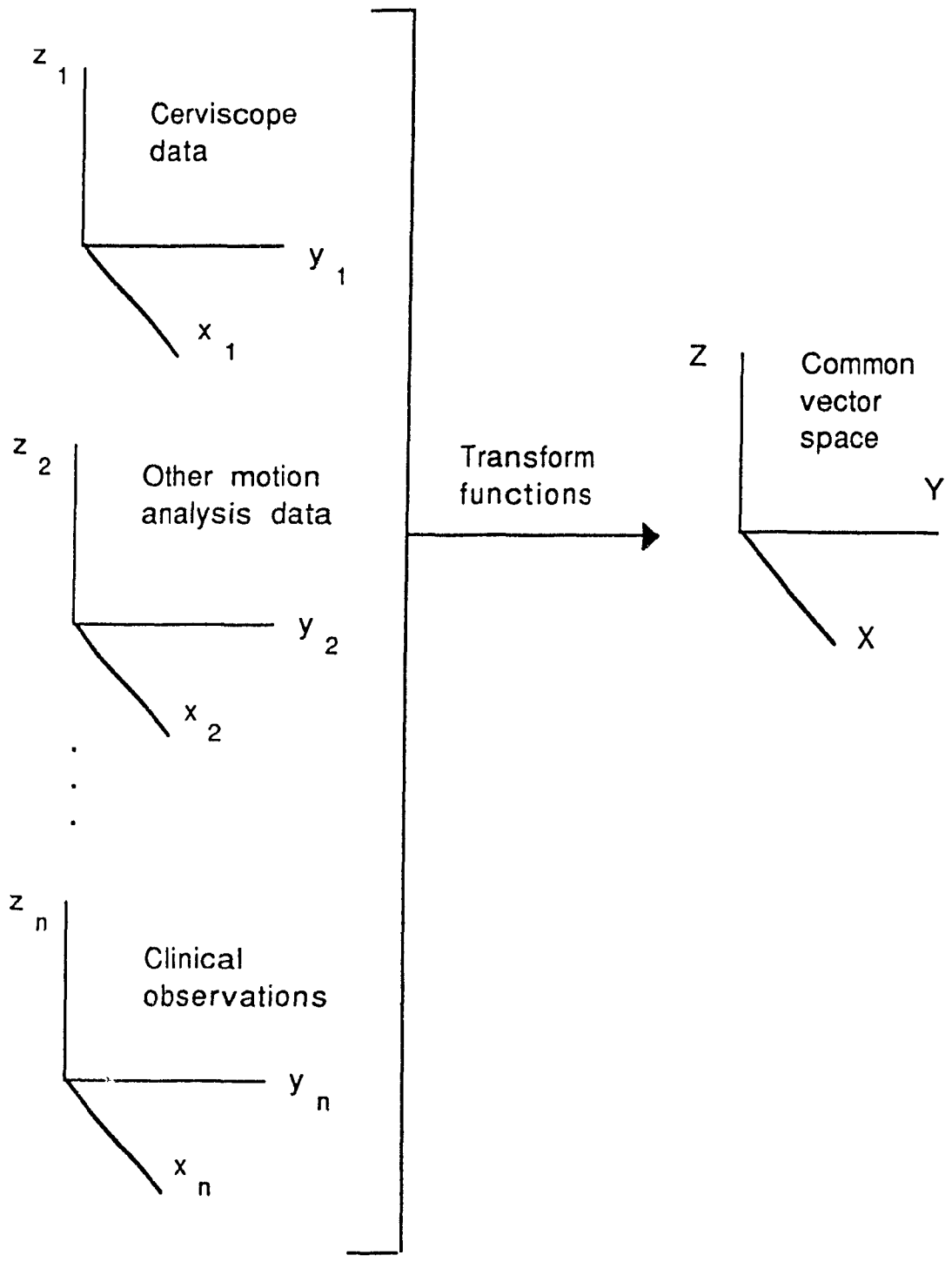

Fig 4.1.1: Transformation and normalization of data to common space where information from various sources can be compared.

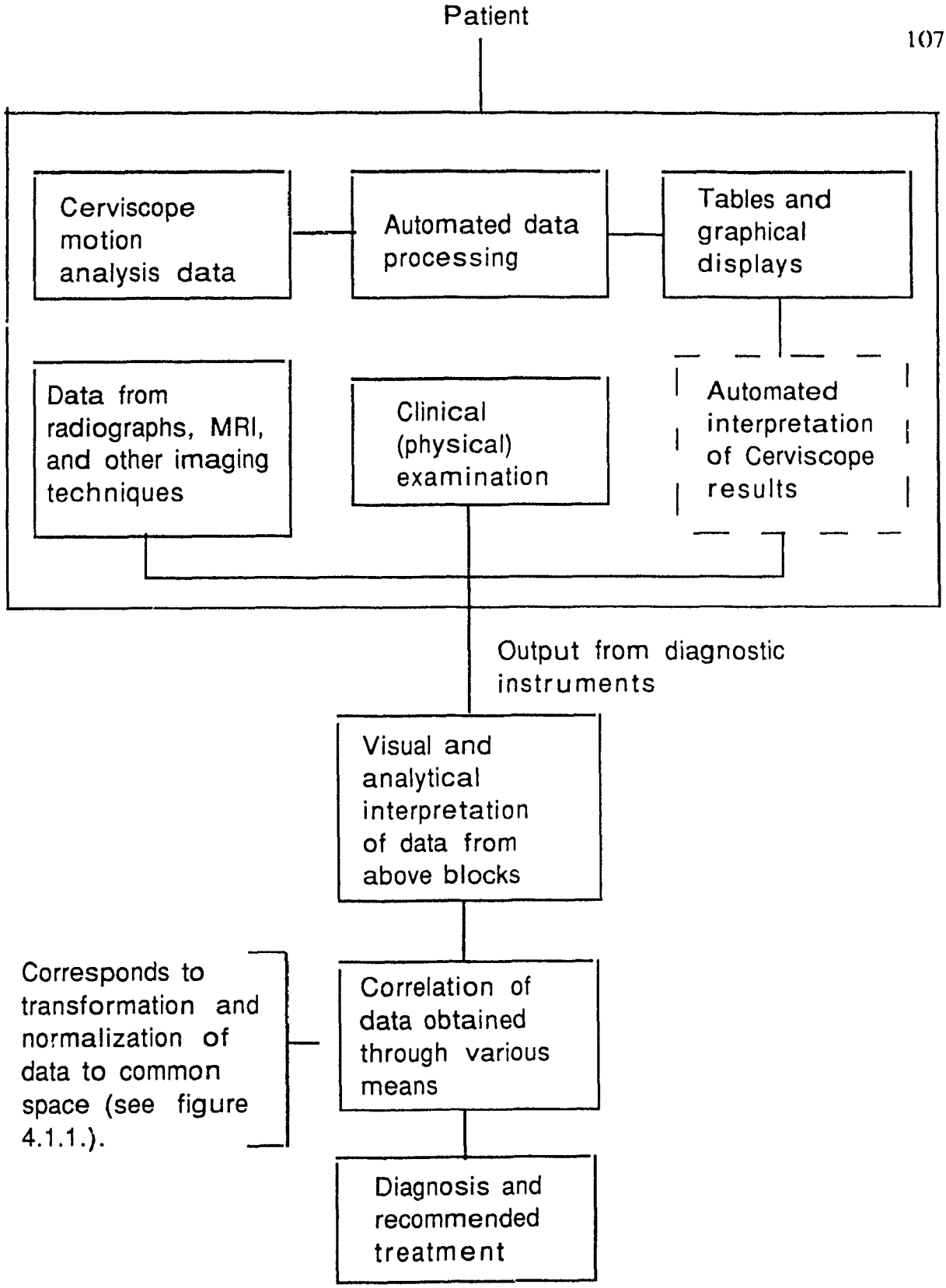

Fig 4.1.2: Incorporation of the Cerviscope into the diagnostic process.

4.4 CONCLUSIONS: CONSOLIDATING BIOMECHANICS, SOFTWARE DEVELOPMENT, AND CLINICAL DIAGNOSES

The three following basic questions were addressed in this study:

- is there a need for a new tool to aid in the diagnosis of soft tissue injuries to the cervical spine?
- if so, what are the requirements for this device, and does the prospective instrument meet these requirements ?
- if not, then how may it be improved ?

The literature review presented in chapter 1 was meant to provide the background needed for addressing the first two questions. Both the biomechanical and technical perspectives were considered, since the clinician relies upon the engineer to relate the two. Chapter 2 dealt with the latter part of the second question. As it turned out, the last question was also pertinent and it was covered extensively in chapter 3.

As we saw earlier (section 1.3.2), the first step in analytical problem solving is to determine what questions are to be answered. Having defined these in the chapter 1, the next step was to determine whether the device under consideration is effective in meeting them.

Following the literature review, the following steps were thus undertaken:

- preliminary experimental evaluation of the Cerviscope,
- evaluation of specific capabilities for motion analysis using the Cerviscope, and comparison with its predecessor (the Spinoscope),
- development of an enhancement to characterize three dimensional coupled motion in the cervical spine, and
- consideration of further avenues of investigation for verification of this instrument.

Chapter 2 covered the description and evaluation of a specific diagnostic instrument. The result of this evaluation was that the displays provided by the original

device do not provide information precise enough to allow an accurate diagnosis.

In chapter 3 we therefore examined the development of an enhanced set of displays designed specifically to characterize three dimensional coupled joint motion. As it turned out, the precision and scope of these new displays surpassed expectations. They are thus expected to form part of another, separate development package. The latter is designed to entirely replace the existing displays for the line of diagnostic instruments produced by this company.

Finally, in chapter 4 we considered how this product may eventually be integrated into the clinical diagnostic process. This will involve the accumulation of a large data base of normal and pathological cases. By combining this data with the information on bimechanics described in chapter 1, engineers and clinicians may work together to accurately identify injuries to the cervical spine.

We have seen that this investigation required a combination of biomechanics, software engineering, and clinical diagnosis. The use of biomechanics allows the engineer to quantify the mechanical behaviour of biological tissue. Sophisticated software engineering techniques are then required to efficiently and accurately present the required information to the users of a diagnostic device.

Ultimately the user (ie. clinician) will perform the diagnosis of injury and prescribe treatment. However, the clinician sometimes has only a rudimentary understanding of biomechanics and often none whatsoever of software development. During product development it is thus incumbent upon the engineer to understand how the user may interpret the diagnostic displays.

In particular, the engineer must verify whether the information displayed represents true motion and whether that motion may be linked to the underlying biomechanics. Once the product is on the market this may be explained to the user through a third party, such as a salesman or a specialist in user training.

After receiving training in the use of the instrument and acquiring some practice the clinician can use the device to objectively evaluate a patient's condition. By increasingly quantifying the diagnostic process, it should be possible to decrease the incidence of improperly diagnosed injuries and the resulting discomfort to patients.

REFERENCES

1. Helleur C, Gracovetsky S, Farfan H: Tolerance of the Cervical Spine to High Acceleration: A Modelling Approach. Av. Space & Env. Medicine 55: 903-909, 1984.
2. Helleur C, Gracovetsky S, Farfan H, Wingrowicz E: Modelling of the Muscular Response of the Cervical Spine. Mathem. Modelling 6: 443-462, 1985.
3. Deng YC, Goldsmith: Response of a Human Head/Neck/Upper-Torso Replica to Dynamic Loading - II. Analytical/Numerical Model. J. Biomechanics 20: 487-497, 1987b.
4. Yoganandan N, Pintar F, Butler J, Reinartz J, Sances Jr. A, Larson SJ: Dynamic Response of Human Cervical Spine Ligaments. Spine 14: 1102-1110, 1989.
5. Myklebust JB, Pintar F, Yoganandan N, Cusick JF, Maiman D, Myers TJ, Sances Jr. A: Tensile Strength of Spinal Ligaments. Spine 13: 526-531, 1988.
6. Yoganandan N, Pintar F, Wilson CR, Sances Jr. A: In Vitro Biomechanical Study of Female Geriatric Cervical Vertebral Bodies. J. Biomed. Eng. 12: 97-101, 1990.
7. Penning L, Wilmink JT: Rotation of the Cervical Spine: A CT Study in Normal Subjects. Spine 12: 732-738, 1987.
8. Dvorak J, Hayek J, Zehnder R: CT-Functional Diagnostics of the Rotary Instability of the Upper Cervical Spine; Part 2. An Evaluation on Healthy Adults and Patients With Suspected Instability. Spine, 12: 726-731, 1987.
9. Mimura M, Moriya H, Watanabe T, Takahashi K, Yamagata M, Tamaki T: Three-Dimensional Motion Analysis of the Cervical Spine with Special Reference to the Axial Rotation. Spine 14: 1135-1139, 1989.
10. Panjabi MM, Summers DJ, Pelker RR, Videman T, Friedlaender GE, Southwick W: Three-Dimensional Load-Displacement Curves Due to Forces on the Cervical Spine. J. Orthop. Res. 4: 152-161, 1986.
11. Moroney SP, Schultz AB, Miller JAA, Andersson GBJ: Load-Displacement Properties of Lower Cervical Spine Motion Segments. J. Biomechanics 21:

769-779, 1988.

12. Schuldt K, Harms-Ringdahl K: E.m.g./Moment Relationships in Neck Muscles During Isometric Cervical Spine Extension. Clin. Biomechanics, 3:58-65, 1988a.
13. Schuldt K, Harms-Ringdahl K: Cervical Spine Position vs. EMG Activity in Neck Muscles During Maximum Isometric Neck Extension. Clin. Biomechanics 3: 129-136, 1988b.
14. Deng YC, Goldsmith W: Response of a Human Head/Neck/Upper-Torso Replica to Dynamic Loading - I. Physical Model. J. Biomechanics 20: 471-486, 1987a.
15. Liu YK: Problems in the Mathematical and Physical Modelling of Head and Neck Injury. Proceedings of Head and Neck Injury Criteria: A Consensus Workshop, Washington D.C., March 1981. U.S. Department of Transportation, National Highway Traffic Safety Administration, 1981, pp 125-132.
16 Panjabi MM, White AA: Biomechanics of Nonacute Cervical Spinal Cord Trauma. Spine 13: 838-842, 1988.
17. Dvorak J, Grob D, Baumgartner H, Gschwend N, Grauer W, Larsson S: Functional Evaluation of Spinal Cord by MRI in Upper Cervical Spine. Spine 14: 1057-1064, 1989.
18. Clark CR: Cervical Spondylotic Myelopathy: History and Physical Findings. Spine 13: 847-849, 1988.
19. Bohlman HH, Emery SE: The Pathophysiology of Cervical Spondylosis and Myelopathy. Spine 13: 843-846, 1988.
20. Frankel VH: Comments on Soft Tissue Injuries of the Neck. Proceedings of Head and Neck Injury Criteria: A Consensus Workshop. Washington D.C., March 1981. U.S. Department of Transportation, National Highway Traffic Safety Administration, 1981, pp 121-122.
21. Caillet R: Subluxations of the Cervical Spine Including the "Whiplash" Syndrome. Chapter 5. Neck and Arm Pain. F.A. Davis Company, 1981.
22. MacNab I: Acceleration Extension Injuries of the Cervical Spine. Chapter 10. The Spine, Second Edition. Edited by RH Rothman, FA Simeone. W.B.

Saunders Company, 1982.

23. Bogduk N: The Anatomy and Pathophysiology of Whiplash. Clin. Biomechanics 1: 92-101, 1986.
24. Bailey RW: Soft Tissue Injuries of the Cervical Spine: Including the So-Called Whiplash Phenomenon. Chapter 5. The Cervical Spine. Lea & Febiger, 1974.
25. Pearcy M: Measurement of Back and Spinal Mobility. Clin. Biomechanics 1: 44-51, 1986.
26. Pearcy MJ: Measurement of Human Back Movements in Three Dimensions by Opto-Electronic Devices. Clin. Biomechanics 2: 199-204, 1987.
27. Pearcy MJ, Gill JM, Whittle MW, Johnson GR: Dynamic Back Movement Measured Using a 3D Televison System. J. Biomechanics 20: 943-949, 1987.
28. Bryant JT, Reid JG, Smith BL, Stevenson JM: Method for Markers. Spine 14: 258-265, 1989.
29. Gracovetsky S, Newman N, Ferron S, Lewis J: Preliminary Report Effects of Skin Markers on Measurements of Spinal Kinematics Made With External Markers, Diagnospine Research Inc., Montreal, Quebec, (Unpublished data).
30. Sances Jr. A, Myklebust JB, Maiman DJ, Larson SJ, Cusick JF, Jodat RW: The Biomechanics of Spinal Injuries. CRC Critical Reviews in Biomedical Engineering 11: 1-76, 1984.
31. Fielding JW: Dynamic Anatomy and Cineradiography of the Cervical Spine. Chapter 3. The Cervical Spine. Edited by RW Bailey. Lea and Febiger, 1974.
32. Alker Jr. GJ: Roentgenographic Evaluation: Computed Tomography. Chapter 3. The Cervical Spine. Edited by The Cervical Spine Research Society. J.B. Lippincott Co., 1983.
33. Dvorak J: Letter on "Investigation of Cervical Rotation Using CT". Spine 13: 595-597, 1988.
34. Lysell E: Motion in the Cervical Spine. An Experimental Study on Autopsy Specimens. Acta Orthop. Scand. Supp. No.123, 1969, pp 1-61.
35. Penning L: Differences in Anatomy, Motion, Development and Aging of the Upper and Lower Cervical Spine. Clin. Biomechanics 3: 37-47, 1988.

36. Foster MA, Hutchison JMS: NMR Imaging - Method and Applications. J. Biomed. Eng. 7: 171-182, 1985.

37. Bondurant FJ, Cotler HB, Kulkarni MV, McArdle CB, Harris Jr. JH: Acute Spinal Cord Injury: A Study Using Physical Examination and MRI. Spine 15: 161-168, 1990.

38. Drerup B, Hierholzer: Automatic Localization of Anatomical Landmarks on the Back Surface and Construction of a Body-Fixed Coordinate System. J. Biomechanics 20: 961-970, 1987.

39. Turner-Smith AR, Harris JD, Houghton GR, Jefferson R: A Method for Analysis of Back Shape in Scoliosis. J. Biomechanics 21: 497-509, 1988.

40. Turner-Smith A.R: A Televison/Computer 3D Surface Shape Measurement System. J. Biomechanics 21: 515-529, 1988.

41. Plamondon A, Gagnon M: Evaluation of Euler's Angles With a Least Squares Method for the Study of Lumbar Spine Motion. J. Biomed. Eng. 12: 143-149, 1990.

42. Eismont FJ, Clifford S, Goldberg M, Green B: Cervical Sagittal Spinal Canal Size in Spine Injury. Spine 9: 663-666, 1984.

43. McAfee PC, Bohlman HH, Han JS, Salvagno RT: Comparison of MRI and CT in the Diagnosis of Upper Cervical Spinal Cord Compression. Spine 11: 295-304, 1986.

44. Apuzzo MJ, Watkins RG, Dobkin WR: Biomechanics of the Neural Axis. Chapter 2. The Unstable Spine. Edited by SB Dunsker. W.B. Saunders Company, 1986.

45. Doppman JL: The Mechanism of Ischemia in Anteroposterior Compression of the Spinal Cord. Invest Radiol 10: 543, 1975.

46. Northrup BE: Neurologic Evaluation. Electrophysiologic Evaluation of Spinal Cord Lesions. Chapter 4. The Cervical Spine. Edited by The Cervical Spine Research Society. J.B. Lippincott Company, 1983, pp 140-146.

47. Yashon D: Evoked Potentials in the Assessment of Spinal Injury. Chapter 29. Spinal Injury, Second Edition. Appleton-Century-Crofts, Norwalk, Connecticut,

1986.

48. Edwards WT, Crowell RR, Coffee MS, White AA: Mechanisms of Injury in the Cervical Spine. Proceedings of IEEE Special Symposium on Maturing Technologies & Emerging Horizons, Biomechanics of Trauma & Vibration, 1988, pp 123-129.

49. Yoganadan N, Maiman DJ, Pintar FA, Sances Jr. A: Cervical Spine Injuries from Motor Vehicle Accidents. Proceedings of IEEE Eng. Med. & Biol. Soc. 11th Conference. Biomechanics of Trauma & Vibration, 1989, pp 808.

50. Viano DC, King AI, Melvin JW, Weber K: Injury Biomechanics Research: An Essential Element in the Prevention Of Trauma. J. Biomechanics 22: 403-417, 1989.

51. Burden RL: Interpolation and Polynomial Approximation. Chapter 3. Numerical Analysis, Second Edition. PWS Publishers, Boston, 1981.

52. Newell JA: Medical Images and Automated Interpretation. J. Biomed. Eng., 10: 555-561, 1988.

53. Strong A.B, Lobregt S., Zonneveld F.W: Applications of 3D Display Techniques in Medical Imaging. J.Biomed. Eng. 12: 233-238, 1990.

54. Fishman E.K, Ney D.R, Magid D: Interactive 2 & 3D Display of CT and MRI Data. Proceedings of IEEE Eng. in Med. & Biol. 11th Ann. Conf., 1989. Workstations for 3D Images, pp 528-529.

55. Raynor RB, Koplik B: Cervical Cord trauma: The relationship Between Clinical Syndromes and Force of Injury. Spine 10: 193-197, 1985.

56. Frankel VH: Whiplash Injuries to the Neck. Proceedings of the International Symposium on Cervical Pain. Wenner-Gren Center, Stockholm, January 1971. Edited by C Hirsch, Y Zotterman. Pergamon Press, 1971.

57. Yashon D: Whiplash, Soft Tissue Injuries and Functional Disorders. Chapter 31. Spinal Injury, Second edition. Appleton-Century-Crofts, Norwalk, Connecticut, 1986.

58. Liu YK, Chandran KB, Heath RG, Unterharcheidt F: Subcortical EEG Changes in Rhesus Monkeys Following Experimental Hyperextension-Hyperflexion

(Whiplash). Spine 9: 329-338, 1984.

59. Alker G: Neuroradiology of Cervical Spondylotic Myelopathy. Spine 13: 850-853,1988.

60. Dvorak J, Froehlich D, Penning L, Baumgartner H, Panjabi MM: Functional Radiographic Diagnosis of the Cervical Spine - Flexion Extension. Spine 13: 748-755, 1988.

61. Merrill T, Goldsmith W, Deng YC: 3D Response of a Lumped Parameter Head-Neck Model Due to Impact and Impulsive Loading. J. Biomechanics 17: 81-95, 1984.

62. Williams JL: comment on Response of a Human Head/Neck/Upper-Torso Replica to Dynamic Loading - II. Analytical/Numerical Model. J. Biomechanics 21: 687-692,1988.

63. Ibid 15.

64. Goldsmith W: Some Aspects of the Physical and Mathematical Modelling of Loading to Head/Neck Systems and Implications of Current DOT Injury Criteria. Proceedings of Head and Neck Injury Criteria: A Consensus Workshop, Washington D.C., March 1981. U.S. Department of Transportation, National Highway Traffic Safety Administration, 1981, pp 133.

65. Schultz AB: Biomechanics of the Human Spine and Trunk. Chapter 41. Handbook of Bioengineering. Edited by R Skalak, S Chien. McGraw-Hill, 1987.

66. McSwaine Jr. NE: Kinematics of Trauma. Chapter 3. Cervical Spine Trauma, Evaluation and Acute Management. Thieme Medical Publishers Inc. N.Y., 1989.

67. Jofe MH, White AA, Panjabi MM: Kinematics. Chapter 2. The Cervical Spine. J.B. Lippincott Company, Philadelphia, 1983, pp 23-34.

68. Sances Jr. A, Yoganandan N: The Societal Impact of Biomechanics. Proceedings of IEEE Special Symposium on Maturing Technologies & Emerging Horizons, 1988. Biomechanics of Trauma, pp 115-122.

69. Noyes DH: Electromechanical Impactor for Producing Experimental Spinal Cord Injury in Animals. Med. & Biol. Eng. & Computing 25: 335-340, 1987.

70. Goel VJ, Weinstein JN: Biomechanics of Intact Ligamentous Spine. Chapter 6. Biomechanics of the Spine: Clinical and Surgical Perspective. Edited by VJ Goel, JN Weinstein. CRC Press, 1990.

71. Panjabi MM, Dvorak J, Duranceau J, Yamamoto I, Gerber M, Rauschning W, Bueff HU: Three-Dimensional Movements of the Upper Cervical Spine. Spine, 13: 726-730, 1988.

72. Goel V', Clark CR, Gallaes K, Liu YK: Moment-Rotation Relationships of the Ligamentous Occipito-Atlanto-Axial Complex. J. Biomechanics 21: 673-680, 1988.

73. Gracovetsky S: The Spinal Engine. Springer-Verlag, 1988.

74. Gracovetsky S, Newman N, Asselin S: The Problem of Non-Invasive Assessment of Spinal Function. Monograph, Diagnospine Research Inc, 1989.

75. Reich C, Dvorak J: The Functional Evaluation of Craniocervical Ligaments in Sidebending Using X-Rays. Manual Medicine 2:108-113, 1986.

76. The Spinoscope- From the Clinician's Perspective. Promotional Information. Spinex Inc., Montreal, Quebec,1990.

77. Gracovetsky S, Kary M: The Spinoscope: A Tool Allowing the Physician to Objectively Assess Impairment, Disability and Capacity of the Spine. Diagnospine Research Inc., Montreal, Quebec, (Unpublished data).

78. Herkowitz HN, Rothman RH: Subacute Instability of the Cervical Spine. Spine 9: 348-357, 1984.

79. Weitz EM: The Lateral Bending Sign. Spine 6: 388-397, 1981.

80. Gracovetsky S: Elongation of Posterior Ligaments During Flexion-Extension: Non-Invasive Measurements and Validation. Diagnospine Research Inc., Montreal, Quebec (Unpublished data).

81. Gracovetsky S, Farfan H: The Optimum Spine. Spine 11: 543-573, 1986.

82. Helleur C: Modelling of the Muscular Response of the Human Cervical Spine Subjected to Acceleration. PhD thesis, Concordia University, Montreal, 1983.

83. Pope MH, Panjabi M: Biomechanical Definitions of Spinal Instability. Spine 10: 255-256, 1985.

84. Adams MA: letter on ' The Optimum Spine'. Spine 12: 1067-1068, 1987.

85. Gracovetsky SA: The Need to Change: Part I (response to A Critique of 'The Optimum Spine'). Spine 12: 1068-1074, 1987.

86. Stokes IAF, Krag MH, Wider DG: A Critique of 'The Optimum Spine'. Spine 12: 511-512, 1987.

87. Yahia H, Newman N: A Light and Electron Microscopic Study of Spinal Ligament Innervation. ISSN 0044-3107. Z. mikrosk.-anat. Forsch, Leipzig 103: 664-674, 1989.

88. Papagiannis G, Asselin S, Roozmon P: Cervical Spine Diagnosis, Research Proposal. Communication to affiliated clinics, Diagnospine Research Inc, Montreal, Quebec, 1990.

89. Troup JDG: Biomechanics of the Lumbar Spinal Canal. Clin. Biomechanics 1:31-43, 1986.

90. Penning L, Wilmink JT: letter on 'Biomechanics of the Lumbar Spinal Canal' by JDG Troup. Clin Biomechanics 1:228-232, 1986.

91. Stokes IAF: Relationships Between Movements of Vertebrae and Adjacent Skin Markers and Sections of the Back. Annual Report No. 4, Oxford Orthopaedic Engineering Centre, Headington, Oxford, UK, 1977, pp 41-43.

92. Towle JA: The Precise Measurement of Knee Joint Kinematics as an Aid in Clinical Assessment. Clin. Biomechanics 1: 214-215, 1986.

93. Bethune DD, Brookhoven LH, Kunh E, Snewing DG: Statistical Method forr Evaluating Human Thoracolumbar Spinal Curves in the Sgaittal Plane, A Preliminary Report. Arch Phys. Med. Rehabil. 67: 590-594, 1986.

94. Ducker TB, Salerman M, Perot PL, Ballatine D: Experimental Spinal Cord Trauma I, Correlation of Blood Flow Tissue Oxygen and Neurologic Status in the Dog. Surg Neurol 10: 60, 1978.

95. Kobrine AI, Evans DE, Rizzoli HV: Correlation of Spinal Cord Blood Flow, Sensory Evoked Response and Spinal Cord Function in Subacute Experimental Spinal Cord Compression. Adv Neurol 20: 389, 1978.

96. Singer PA, Prockop LD, Anderson DK: Somatosensory Cortical-Evoked

Responses After Female Experimental Spinal Cord Injury. Paraplegia 15: 160, 1977-1978.

97. Alem NM, Nusholz GS, Melvin JW: Head and Neck Response to Axial Impacts. Proc of the 28th STAPP Car Crash Conference, Soc of Automotive Engineers, Warrendale, PA, 1984, pp. 275.

98. MacNab I: Acceleration Injuries of the Cervical Spine. J Bone and Join Surg 46A: 1797-1799, 1964.

99. Ommaya AK, Hirsch AE, Martinez JL: the Role of Whiplash in the Cerebral Concussion. Proceedings of the 10th STAPP Car Crash Conference, 1966, pp. 314-324.

100. Breig A: Biomechanics of the central Nervous System. Stockholm, Almquist & Wicksell, 1960.

101. Breig A: Adverse Mechanical Tension in the Central Nervous System. New York, John Wiley & Sons, 1978.

102. Hukuda S, Wilson C: Experimental Cervical Myelopathy, Effects of Compression and Ischemia on the Canine Cervical Cord. J Neurosurg 37: 631-652, 1972.

103. Ewing C, Thomas D: Human Head and Neck Response to Impact Acceleration. National Aerospace Medical Research Laboratory, Pensacola, Florida. Monograph 21, 1972.

104. Hosey RR, Liu YK: A Homeomorphic Finite Element Model of the Human Head and Neck. Chapter 18. Finite Elements in Biomechanics. Edited by RH Gallagher, BR Simon, TC Johnson, JF Gross. John Wiley and Sons Ltd, 1982.

105. Yoganandan N, Sances A, Maiman D, Myklebust JB, Pech P, Larson SJ: Experimental Spinal Injuries with Vertical Impact. Spine 11: 855-860, 1986.

106. Werne S: Studies in Spontaneous Atlas Dislocation. Acta Orthop Scand 23, 1957.

107. Jirout J: the Rotational Component in the Dynamics of the C2-C3 Spinal Segment. Neuroradiology 17: 177-181, 1979.

108. Selecki BR: The Effects of Rotation of the Atlas on the Axis, Experimental

Work. Med J Aust 1: 1012, 1969.

109. Hall MC: Luschka's Joint. Charles C. Thomas Publishers, Springfield, Illinois, 1965.

110. Penning L: Normal Movements of the Cervical Spine. Am J Roentgenol 30: 317-326, 1978.

111. Henke W: Handbuch der Anatomie und Mechanik der Gelenke. Leipzig und Heidelberg, 1863.

112. White AA, Panjabi MM: Kinematics of the Spine. Chapter 2. Clinical Biomechanics of the Spine. J.B. Lippincott Company, Philadelphia, 1978.

113. Chisholm JSR: Transformations of Vectors. Chapter 4. Vectors in Three-Dimensional Space. Cambridge University Press, Cambridge, 1978.

114. Robinson L: Spinoscope User's Manual. Monograph, Spinex Medical Technologies, 1991.

115. Lamb DA: Software Engineering: Planning for Change. Chapter 1. Introduction. Prentice Hall, New Jersey, 1988.

116. Bowen RM, Wang CC: Reciprocal Basis and Change of Basis. Section 14. Vector Spaces. Chapter 3. Introduction to Vectors and Tensors, Volume I. Plenum Press, 1975.

117. Winters J: Biomechanical Modelling of the Human Head and Neck. Chapter 2. Control of Head Movement. Edited by BW Peterson, FJ Richmond. Oxford University Press, 1988.

118. Nashner LM, Shupert CL, Horak FB: Head-Trunk Movement Coordination in the Standing Posture. Chapter 21. Prog Brain Res 76: 243-251, 1988.

119. Frymoyer JW, Frymoyer WW, Wilder DG, Pope MH: The Mechanical and Kinematic Analysis of the Lumbar Spine in Normal Living Human Subjects in Vivo. J Biomechanics 12:165-172, 1979.

120. Panjabi MM: Experimental Determination of Spinal Motion Segment Behaviour. Orth Clin N Am 8:169-180, 1977.

121. Pearcy M, Portek I, Shepherd J: Three-Dimensional X-Ray Analysis of Normal Movement in the Lumbar Spine. Spine 9: 294-297, 1984.

122. Pearcy MJ, Tibrewal SB: Axial Rotation and Lateral Bending in the Normal Lumbar Spine Measured by Three-Dimensional Radiography. Spine 9: 582-587, 1984.

123. Panjabi M, White AA: A Mathematical Approach for Three-Dimensional Analysis of the Mechanics of the Spine. J Biomechanics 4:203-211, 1971.

124. Richmond FJR, Vidal PP: The Motor System: Joints and Muscles of the Neck. Chapter 1. Control of Head Movement. Edited by BW Peterson, FJ Richmond. Oxford University Press, 1988.

125. Suh CH: The Fundamentals of Computer Aided X-Ray Analysis of the Spine. J Biomechanics 7: 161-169, 1974.

126. Brown RH, Burstein AH, Nashi CL, Schock CC: Spinal Analysis Using a Three-Dimensional Radiographic Technique. J Biomechanics 9: 355-365, 1976.

127. Pearcy MJ, Tibrewal SB: Axial Rotation and Lateral Bending in the Normal Lumbar Spine Measured by Three-Dimensional Radiography. Spine 9: 582-587, 1984.

128. Penning L: Functioneel Rontgenonderzoek Bij Degenerative en Traumatische Afwijkingen der Laag-Cervical Bewegingssegmenten. Thesis, University of Groningen, the Netherlands, 1960.

129. Buetti-Bäuml C: Funktionelle Röntgendiendiagnostik der Halswirbelsäule. Thieme, Stuttgart, Fortschritte auf dem Gebiete der Roentgenstrahlen vereinigt mit Roentgenpraxis. Ergäzungsband 70, 1954.

130. Graf W, Wilson VJ: Afferents and Efferents of the Vestibular Nuclei: The Necessity of Context-Specific Interpretation. Chapter 13. Prog Brain Res 80: 149-157, 1989.

131. Albert A : Regression and the Moore-Penrose Pseudoinverse. Academic Press, New York, 1972.

132. Pellionisz A: Coordination: A Vector-Matrix Description of Transformations of Overcomplete CNS Coordinates and a Tensorial Solution Using the Moore-Penrose Generalized Inverse. J Theoret Biol 110: 353-375, 1984.

133. Pellionisz A: Tensorial Aspects of the Multidimensional Massively Parallel

Sensorimotor Function of Neuronal Networks. Chapter 30. Prog Brain Res 76: 341-354, 1988.

134. Pellionisz AJ, Peterson BW: A Tensorial Model of Neck Motor Activation. Chapter 14. Control of Head Movement. Edited by BW Peterson, FJ Richmond. Oxford University Press, 1988.

135. Gray H, Van Dyke Carter H: Gray's Anatomy. Lea and Febiger, Philadelphia, 1973.

136. Roozmon P, Robinson L, Lazlo V: New Crrtvical Report Software, Notes for the User. Monograph. Diagnospine Research Inc, Montreal, Quebec, 1991.

137. Salas SL, Hille E: Calculus, One and Several Variables. Chapter 2. Vectors, Second edition. John Wiley and Sons, 1974.

138. Fowles GR: Analytical Mechanics. Chapter 8. Motion of Rigid Bodies in Three Dimensions, Third edition. Holt, Rinehart and Winston, 1977.

139. Bronstein IN, Semendyayev KA: Aide Mémoire de Mathematiques. Géométrie dans l'Espace, Notions Fondamentales et Formules. Editions Eyrolles, Paris, 1963.

APPENDIX A: DETAILS FROM THE LITERATURE REVIEW ON BIOMECHANICS OF THE CERVICAL SPINE

A.1 INJURY MECHANISMS

A.1.1 Kinematics and General Mechanisms of Injury

The straightened cervical spine (ie. with mild forward flexion) can withstand the highest axial loads of all positions studied (fig A.1.1). There appear to be three patterns of response to impact:

- bending of the curved spine under axial load
- buckling of the straightened spine under axial load
- deflection of the spine out of the load path.

Following cadaver weight drop experiments, Alem et al. (1984) concluded that force was a poor predictor of injury.[97] The impulse (ie. integral of force over time) was found to be a more useful predictor.[48] In whiplash injuries, Ommaya (1966) stressed the importance of angular acceleration versus linear acceleration.[56,99]

The spinal column may be compared to a stack of 24 building blocks with an 8 pound bowling ball on top. When landing head first from a fall, the cervical spine at C1-C2 and C5-C6 appears to be at greatest risk. If a person lands feet first the head may continue its motion, resulting in hyperflexion or hyperextension injuries (fig A.1.2).

When the head impacts a windshield or other body, the momentum of the thorax continues. Its energy must be absorbed eventually, usually by bending or crushing of the cervical spine. Injury to the victim's head or face can indicate that this has occurred.

In lateral impact the anteriorly located center of gravity of the head results in rotation toward the impact point (fig A.1.3). The resultant position of the spine is a combination of rotation and flexion. If disruption of the ligaments then occurs this may result in compromise of the cervical canal and thus spinal cord injury (fig. A.1.4).[66]

A.1.2 Definition of Whiplash

The ambiguous term 'whiplash' was introduced by Crowe in 1928.[22] It refers to a sudden backward snapping of the head and neck followed by forward recoil.[24] A more precise description might be cervical sprain due to hyperextension, resulting from sudden deceleration.[21] Although often associate with automobile accidents, similar trauma may result from falling, diving, a blow to the head, convulsions, or contact sports.[24]

Bogduk (1986) pointed out that whiplash is frequently associated with litigation.[23] Hence there is always the suspicion that complaints are exaggerated. Victims have been neglected, mistreated, and accused of deception, while malingerers were unjustly rewarded. This situation has resulted in confusion regarding the relevant mechanisms, symptoms, and diagnoses for whiplash injuries.

A.1.3 Mechanism of Injury in Rear End Collisions

The most common cause of whiplash injuries is rear end collisions. Low velocities under 15 km/hr are often involved. Adults of all ages and both sexes are affected, but car seat backs are believed to protect the heads of small children.[56]

Previously it was believed that upon impact the head was suddenly jerked backward.[24] The current view is that movement of the body, rather than the head, causes injury. This results in compression-avulsion rather than flexion-extension injuries.[21]

Computer models indicate a brief flexion immediately following impact.[23,61] Then the shoulders move forward and pull the neck from under the head, imparting a backward and upward rotation to it. The head eventually begins to accelerate and is catapulted into flexion (see also Appendix A.2).[23]

In flexion the movement is limited by the chin hitting the chest. Similarly, in lateral bending, the ear hits the shoulder. Hence, physiological limits are not exceeded. However, in extension there is no such natural block. When the occiput reaches the back of the neck, normal limits have already been exceeded.[22,23]

Seatbelts are thought to place a person in an erect position and thus minimize damage.[21] The three-point system standard on modern cars is considered almost as effective as the five or six-point systems employed in race cars.[66]

Prior to the introduction of head rests, it was thought that these would decrease the number and severity of whiplash injuries.[24] However, the head also rises above the horizontal plane in an arc, due to torque.[21] The vertical component of this force pushes the victim upwards. The head may thus fall back over the top of the head rest. High speed impact may also break the back of the seat. Ironically, the occupant is thus less likely to sustain neck injury (fig A.1.5).[22]

According to Liu (1981), air bags protect the chest and head but dangerously increase the load on the neck by prolonging the impact.[63] During this additional time the head may undergo repeated hyperflexion and hyperextension while the chest is held in place.

Caillet (1981) explained that as joints exceed their physiological limits, periarticular damage of subluxation results.[21] This involves incomplete luxation accompanying sprain, whereby tendons, ligaments and articular capsules are overstretched. An acute stretch reflex of the neck flexors occurs.

Normal contraction is accompanied by relaxation of the antagonist muscles. Hence there is no stretch reflex in the contracting muscles. However, an abrupt stretch reflex may result in muscle fibril injury. Initially this involves intrafusal fibers, but extrafusal fibers may also be damaged if the force is severe.

The extent of damage depends on the force of impact, the exact position of the head, and awareness of impending injury. This is because muscle contraction minimizes the pendular action of the head on the neck.

However, the physiologically permitted range of extension is much less when the neck is rotated. In cadavers, rupture of the anterior longitudinal ligament is much more readily produced when the head is rotated prior to extension (fig A.1.6).

A.1.4 Diagnosis of Hyperextension and Hyperflexion Injuries

Many cervical injuries may be overlooked for prolonged periods if the dynamics are not understood. The examiner must mentally reconstruct the accident. This leads to the determination of what parts of the body were traumatized to cause the injury.[66]

Hence, the first stage in examination is a careful case history.[22] The prognosis may be adversely affected by such factors as preexisting degenerative spondylosis and osteoporosis.[57,50]

The spine may be perceived to behave like the frame of an automobile in a collision. This can lead to muscle, ligament or tendon rupture, without fracture.[66] Conventional plain radiographs may not reveal abnormalities shown by specialized techniques.[23] Radiographs will usually show only loss of lordosis. Later X-rays may

reveal degenerative changes.[23] Thus some investigators consider conventional radiographs inadequate in assessing conditions such as soft tissue hypertrophy, superimposed upon bony changes.[96,97]

Straightening of the cervical lordosis is thought by some to relieve pain (anatalgic position).[21] However, some cases of reversal of physiological lordosis have been reported in apparently normal individuals.[31] This effect may also simply be due to the patient's position during filming.[21,22]

A reversed segmental curve in the neck is perhaps more significant. This may indicate subluxation, ligament tear or disc herniation. [21] Physical examination may indicate only guarded motion of the head and neck.[24] The range of neck motion must be evaluated by comparison with what is normal.[21] Nevertheless, changes in patterns of movement may reflect pain rather than specific tissue damage.[22]

Abnormal radiographs may be unrelated to symptoms, while injury may exist even with 'negative' X-rays.[21] For example, in experiments with primates, MacNab (1964) found that disc injuries were often undetected on radiographs.[98]

Like Ommaya (1966), he discovered that some animals became stunned or dazed, as if they had suffered concussions. Cerebral spinal fluid changes were also noted.[22,23,56,99] Similar experiments by Liu et al. (1984) showed a connection between symptoms of neck injury and electro-encephalographic (EEG) disturbances in the brain.[57,58]

Yet, severe neurological deficit may occur with minimal change in vertebral alignment. A possible cause is transient insufficiency of the vertebral artery. When cord damage results in hemorrhage, symptoms may progress cephalad or caudad and death may result.[21]

Hemorrhagic damage expands radially with time, ultimately disrupting axonal tracts and permanently altering function. However, the mechanism of functional damage to central nervous tissue is not yet entirely understood.[50]

According to Bogduk (1986), the most likely soft tissue lesions in the literature were found to be:

- strain of anterior longitudinal ligament, disc herniation,

vertebral end-plate avulsion,

- strain or rupture of sternocleidomastoid and longus colli muscles, and
- zygapophyseal joint fractures or capsular damage (fig A.1.7).[23]

He added that diagnoses in clinical literature are infrequently correlated to specific structural pathology. For example, cervical zygapophyseal joints are liable to whiplash injury but are rarely considered.

MacNab (1982) stated that significant soft tissue damage may result from acceleration extension injuries. [22] He noted that lateral hyperflexion does not usually result in injury. Hence it is questionable why anterioposterior injuries would be singled out for neurotic origins. Indeed, it appears possible that physicians may actually contribute to litigation neurosis by improper treatment.[22,56]

Injection of fluid under pressure into posterior neck muscles produces pain radiating to the head, shoulders, and arms. Hence the development of edema in soft tissue may explain headaches associated with whiplash. Such pain can not be used to localize lesions. Persisting suboccipital pain may be referred from damaged cervical ligaments, rather than being local to the C1-C2 region.[22,24]

The most confusing symptoms in whiplash injuries may be attributable to the sympathetic nervous system. These are most frequently aural (tinnitus, postural dizziness) or ocular (blurred vision, pain behind eyeballs). Most sympathetic symptoms are subjective. There may also may be symptoms of cerebral concussion with momentary loss of consciousness.[21,22]

The lower cervical nerve roots supplying the arm are easily identifiable clinically. Yet the nerves originating from the cervical plexus may also be damaged and overlooked. If major nerves are not initially involved, there may be no immediate abnormal sensation or paresis. Referred pain and confusing symptoms attributable to the sympathetic nervous system complicate matters further.[20,21]

Thus Bogduk (1986) concluded that in case of doubt all possible lesions should be considered.[23] To paraphrase him:

"Patients should be accorded the dignity of organic diagnosis, rather than being dispatched to psychiatrists out of hand. Such consistent symptoms would seem to have at least some organic basis.

Yet, the medical literature fluctuates between complete denial and absolute acceptance of whiplash injury. The mere persistence of symptoms indicates a consistency in their cause. Hence, it appears that undiagnosed organic lesions must be considered at least as likely as psychological factors. "

A.1.5 Spinal Cord Impingement

The size of the spinal canal in relationship to the cord has been considered carefully in recent years. It is an important factor in determining whether an injury will result in damage to the spinal cord.[42]

The significance of intrusions into the canal is assessed relative to their size.[59] In normal cervical rotation, the spinal canal at the atlanto-axial joint is narrowed by about one third.[31] Mimura et al. (1989) suggested that osteophytes may develop where rotational motion bears flexion-extension loads.[9] This is consistent with Alker's (1988) description of bone spur formation.[59]

Patients with small canals will have less space available for the spinal cord. Hence an injury or osteophyte is more apt to result in neurological damage (fig A.1.8). This knowledge is useful in counselling patients regarding return to activities with a high risk of cervical injury.[42,59]

Dvorak et al. (1989) used MRI to evaluate the neurologic deficit in relation to the width of the spinal canal and diameter of the cord.[17] Patients were positioned with their necks in the neutral position, followed by maximal extension and flexion. They all suffered from cervical rheumatoid arthritis.

The spinal canal diameter was found to decrease significantly in the flexed position.[17] According to Bohlman and Emery (1988), this may occur with hyperextension as well.[19] The majority of Dvorak's patients with spinal cord diameters less than 6mm in flexion exhibited myelopathy.

Values below this were thus considered pathologic, as shown in figure A.1.9.

Compression was due to a combination of atlanto-axio subluxation and inflammation of the tissue behind the odontoid process.[17]

Penning and Wilmink (1987) used CT scans in similar experiments.[7] They found that symptoms of spondylitic myelopathy appear after the spinal cord has been reduced in size by 30%. According to Alker (1988), the low limit for normal function in the lower cervical spine is 12mm.[59] Jofe et al.(1983) considered the upper limit of relative horizontal displacement to be 3.5mm.[67]

Dvorak et al (1989) recommended that in pathologic cases anterior decompression should be performed.[17] This is in agreement with Panjabi and White (1988).[16] According to them, posterior decompression will not decrease anterior pressure on the cord. Doppman (1975) pointed out that the common factor with anterior and posterior compression is flattening of the spinal cord.[19,45]

Panjabi and White (1988) found that anterior impingement does not significantly affect the posterior wall of the dura.[16] The resulting forces on the spinal cord are shown in figure A.1.10. These loads were offered as explanation for the predominance of posterior spinal cord dysfunction in cervical spondylitic myelopathy.

Breig (1960) showed that changes in the length of the spinal canal do not normally produce significant stresses in the spinal cord.[100] According to him, the cord effectively folds and unfolds like an accordion. In pathological situations, however, abnormal stresses and strains in the spinal cord may lead to myelopathy.[16]

Breig (1978) listed four critical actions: external unilateral thrust, internal multilateral thrust, pinching or clamping, and concentration of tension around an intramedullary fissure.[44,101]

Bohlman and Emery (1988) attributed stress related myelopathy to ischemia of the anterior two thirds of the spinal cord, including most of the grey matter.[19] They suggested that direct spinal cord compression results in interruption of the sulcal and terminal vessels of the anterior vertebral artery. In canine experiments, Hukuda and Wilson (1972) found the effects of vascular insufficiency and compression on the cord to be additive.[19,102]

Thus an understanding of how the spinal cord reacts to stress requires analysis of

its blood supply. Within the cord the radicular branches of the pia mater consist of a peripheral and a central portion. The former supplies the superficial structures and the white matter.

The central area, grey matter and innermost aspects of the white matter are vascularized by the central system. The condition of the vessels will influence their tolerance to stress. For example, an arteriosclerotic vessel may rupture following only minima. compression.[44]

A.1.6 Evoked Potentials

The evoked potential across a given set of nerves measures the degree of electrical activity present. This constitutes a sensitive and easily disturbed indicator of spinal cord injury. They are most useful for intraoperative monitoring of sensory function. Improvement of spinal cord function due to surgical intervention can be demonstrated this way. However, they are not commonly used for clinical evaluation of spinal cord injury.[44,46,47]

Ducker et al. (1978) examined evoked potentials in dogs using the weight drop technique.[94] They found that spinal cord blood flow was not uniform for intermediate grades of injury. This supported findings by Kobrine et al. (1978) indicating that ischemia may only be partially responsible for spinal cord trauma.[95]

Singer et al. (1970) linked loss of evoked potentials with the onset of spinal cord hemorrhage and edema.[96] This etiology is relevant to the consequences of cervical soft tissue injury.

Fig A.1.1: Loading vs initial position for the cervical spine. Adapted from Edwards et al. (1988).[48]

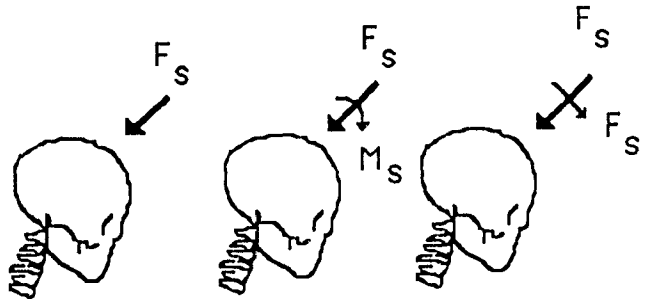

Fig A.1.1 (a): Variations in external loading for the straightened cervical spine.

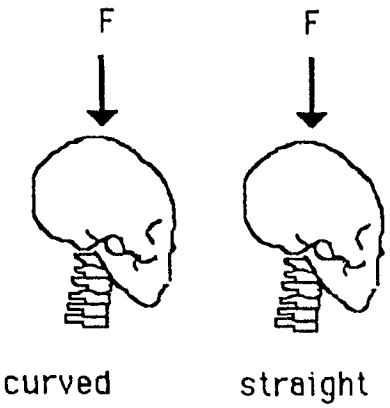

Fig A.1.1 (b): Initially curved spine leads to bending failure. Initially straight spine fails after buckling.

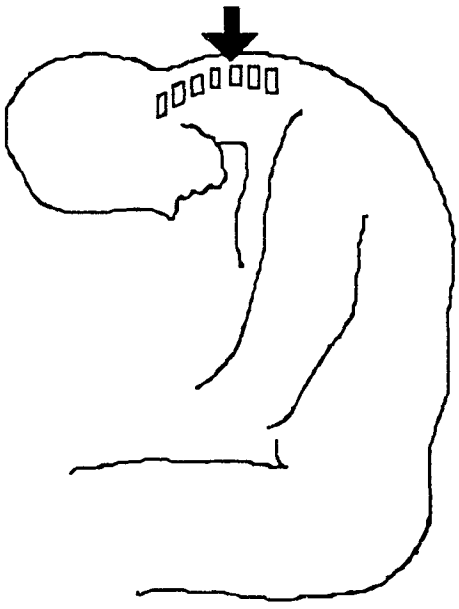

Fig A.1.2: Momentum of the head continues after a fall, leading to hyperflexion and hyperextension. Adapted from McSwaine Jr. (1989). [66]

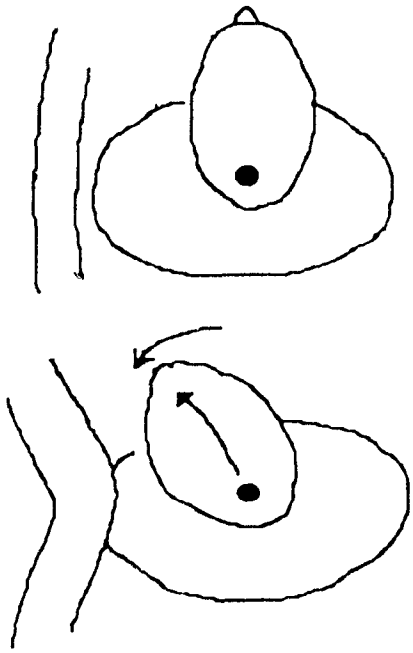

Fig A.1.3: Rotation of head toward the impact point due to anterior location of the center of gravity. Adapted from McSwaine Jr. (1989).[66]

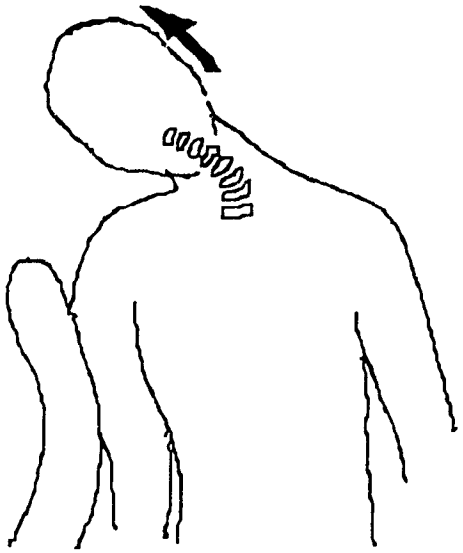

Fig A.1.4: Position of the cervical spine in lateral hyperflexion. Adapted from Mcswaine Jr. (1989).[66]

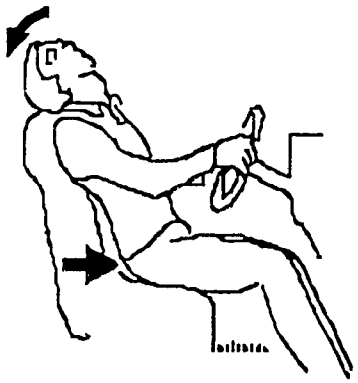

Fig A.1.5 (a): Resultant forces on the driver from the steering wheel and seat.

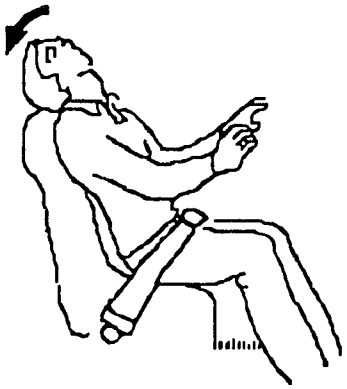

Fig A.1.5 (b): Resultant force on passenger from a lap belt

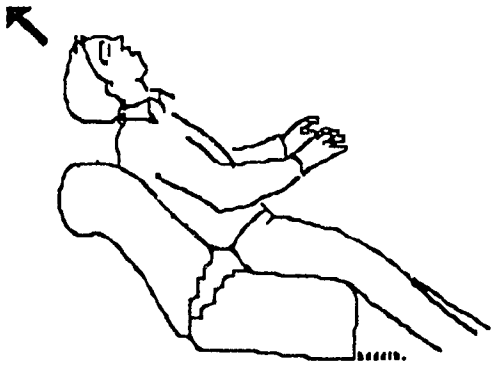

Fig A.1.5 (c): Resultant force oxccuring when back of seat breaks.

Fig A.1.5 : Forces on driver and passenger resulting from rear-end collision (see above and top right). Adapted from MacNab (1982). [22]

Fig A.1.6:

Effect of a deceleration injury to the neck with the head turned. Adapted from Caillet (1981). [21]

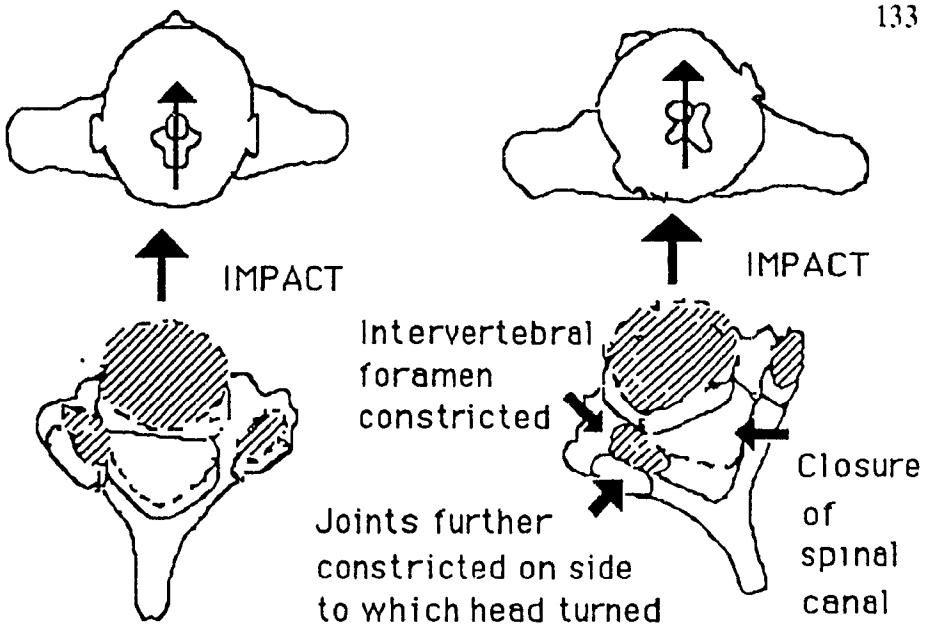

Fig A.1.7 (below):

Most likely locations for cervical soft tissue injuries from hyperflexion and hyperextension. Adapted from Bogduk (1986). [23]

ALL: anterior longitudinal ligament
IVD: intervertebral disc
OES: oesophagus
OP: odontoid process
ZJ: zygapophysial joints
TMJ: temporomandibular joint

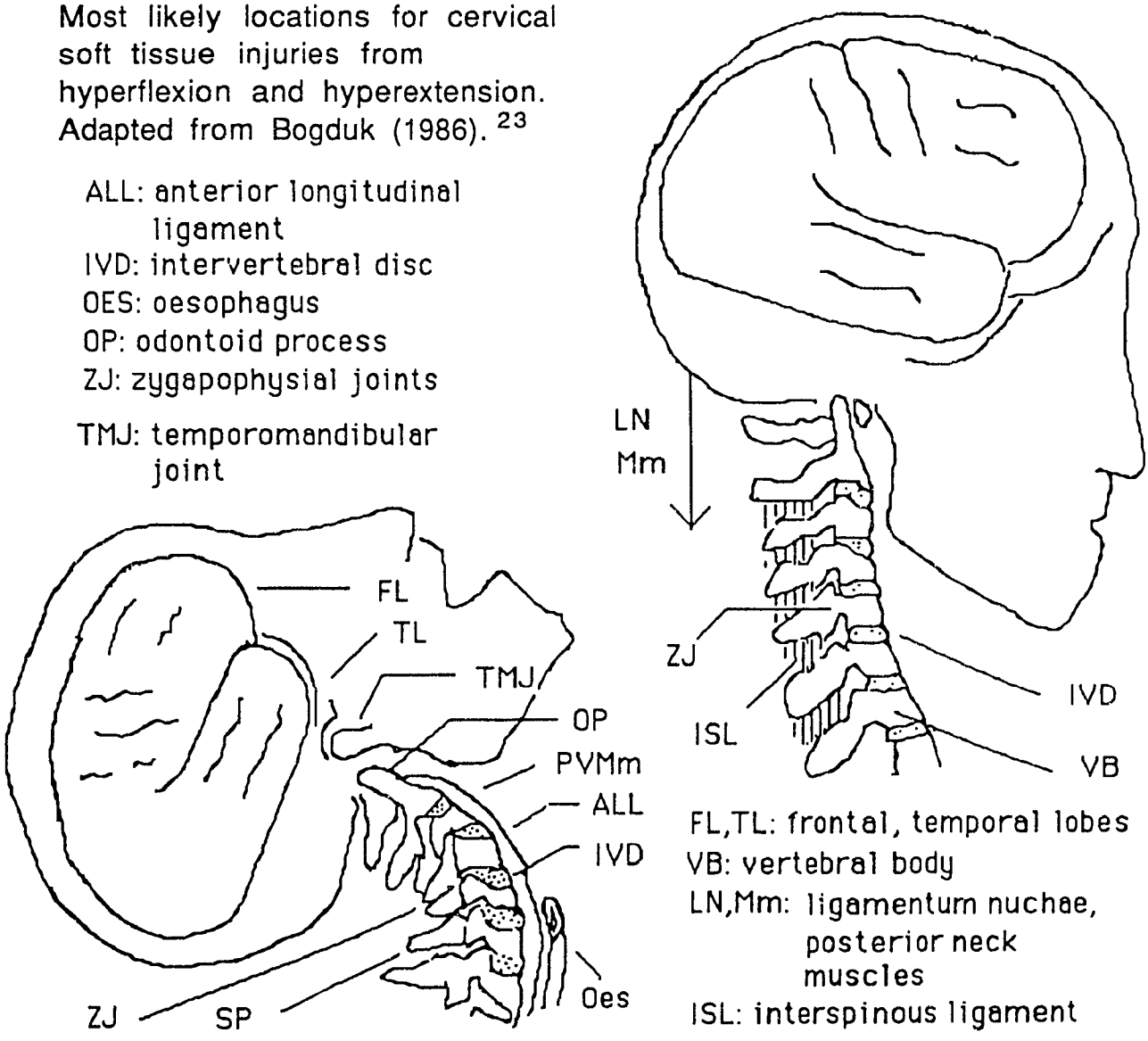

FL,TL: frontal, temporal lobes
VB: vertebral body
LN,Mm: ligamentum nuchae, posterior neck muscles
ISL: interspinous ligament

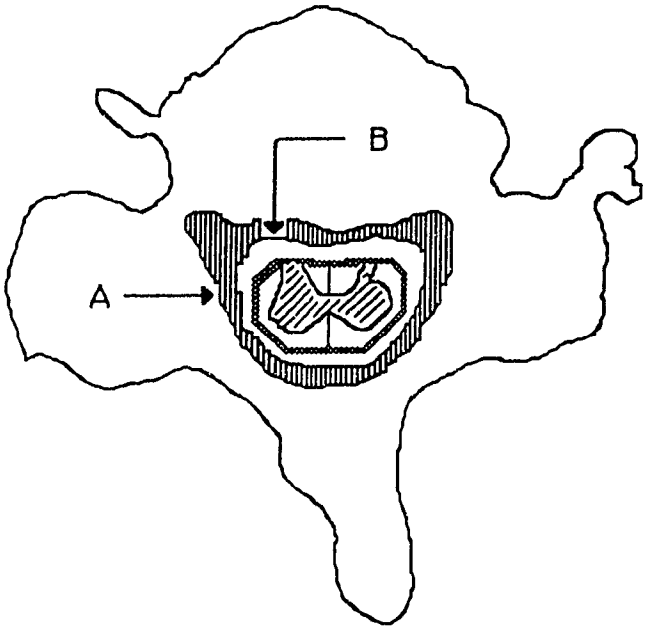

Fig A.1.8:

Comparison of the space available for the spinal cord with a large canal (A) and a small canal (B). Adapted from Eismont et al. (1984). [42]

Fig A.1.9 (below):

Comparison of the spinal cord diameter in the neutral and flexed positions showing the pathologic limit of 6 mm. Adapted from Dvorak et al. (1989). [17]

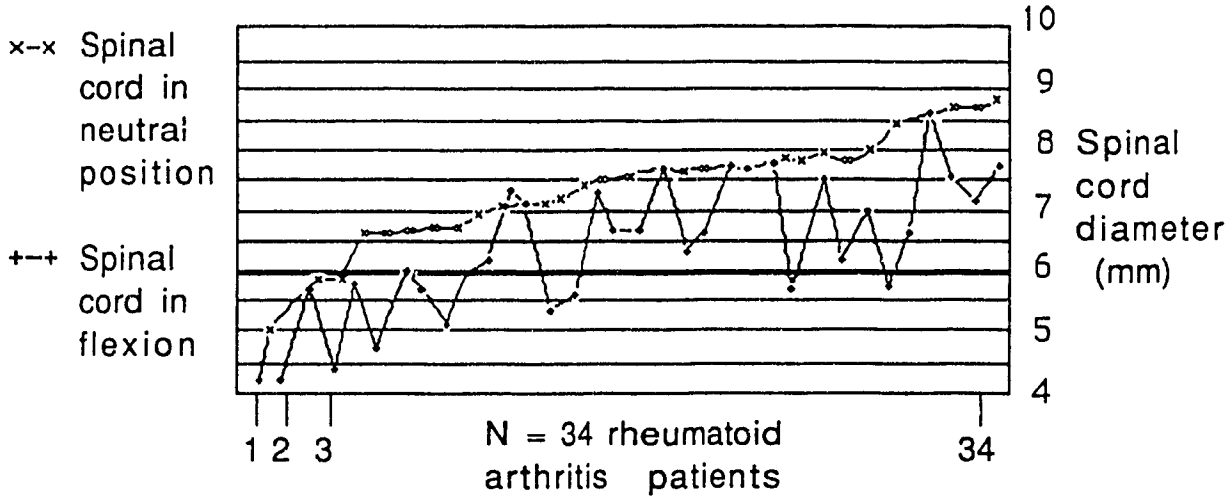

Fig A.1.10:

Impingement on the spinal cord causing bending, tension, and compression forces. Adapted from Panjabi and White (1988). [16]

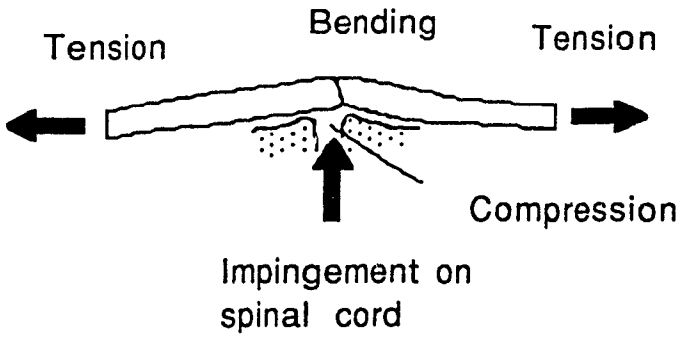

A.2 APPLICABLE ANALYTICAL MODELS

A.2.1 The Role of Analytical Models in Studying the Spine

The bulk of what is known regarding the mechanics of the spine pertains to the lower back region. Comprehensive data on biomechanical properties of individual spinal components have been gathered, mostly from cadaver measurements.

The basic mechanical unit of the spinal column is the "motion segment". This includes any two adjacent vertebrae as well as the disk and ligamentous tissue joining them. The mechanical properties of motion segments vary significantly from segment to segment.

Schultz (1987) provided a comprehensive review of current low back models. [65] Let us carefully examine Schultz's findings. According to him, mathematical models for the lumbar/thoracic region fall into three categories:

i) rigid body models,

ii) lumped parameter deformable element models, and

iii) distributed parameter deformable element models, often using finite element methods.

He pointed out that rigid body analyses are usually indeterminate. In dynamic problems the number of unknowns exceeds the number of equations. In static problems it is the equations of equilibrium which are exceeded.

Assumptions are used to render the problems determinate in order to obtain internal force estimates. He noted that this concept works in mechanically simple situations, but that complex situations require more sophisticated schemes.

The objective function is the quantity to be optimized in such models. Schultz found that a scheme which works well in a wide range of situations is to minimize approximately the largest muscle contraction intensity needed to perform a task.

The internal loads imposed on the spine are determined more by the moments of external forces about the spine than by the forces themselves. Measurements of intradiskal pressures and myoelectric activities determine internal forces directly. These techniques

are used to validate the various spinal load calculation models. According to Schultz, dynamic considerations are considered important only when a motion involves significant linear or angular accelerations.

Deformable element models are required for predictions of what deformations occur in response to loads. Models of this kind have been used to study the progression of idiopathic scoliosis and injuries that result from accidents. Each mobile vertebra is idealized as a rigid body.

If there are N bodies so modeled, 6N degrees of freedom result in a set of 6N simultaneous equations. The internal forces in every deformable segment can be computed by solving the equations. Data on the cross sectional areas of the muscles in different regions of the trunk is used to determine the generated forces.

Schultz noted that finite element methods have been used to analyze several components of the trunk. Structural analysis is combined with experimental measurements in order to explain motion segment displacements and rotations. These are then related to parameters such as disk bulge, intradiskal pressure, and stresses in the annulus fibrosis or vertebral body.[65]

However, models describing the upper portion of the spine are far less numerous than those for the lower back. They usually represent the head, neck and upper torso as a deformable collection of rigid bodies. For example, Merrill (1981) developed a three dimensional model for impact loading that involves ten lumped parameter masses, from the head to T2, connected by springs.[61]

The sagittal plane model developed by Helleur et al. (1984, 1985) describes the neck's response for both static loading and high acceleration.[1,2] Applications such as the design of ejection seats have become increasingly dependant on such models.

Analytical modelling enhances the fundamental understanding of spinal biomechanics. The development of information for strength, stiffness, and dynamic characteristics must be undertaken in parallel with this.[5,72] Increased communication among researchers from varied disciplines will accelerate progress in understanding of cervical spine injuries. However, quantitative descriptions of vertebral loads and displacements are required to investigate them.[48]

A.2.2 Experimental Methods

During extreme compression the entire cervical spine may bend or buckle in a manner inconsistent with normal physiologic motion. Edwards (1988) defined buckling as displacement from initial curvature, rather than the usual buckling of a column.[48] The initial position of head, neck and thorax are crucial in determining the response to a load combination (see Appendix A.1.1).

Alem et al. (1984) performed cadaver weight drop and pendulum impact studies.[97] These experiments showed that buckling occurred with axial loading when the neck was in natural sitting or standing positions. No buckling occurred when the spine was aligned along the line of action of the impact force.[48]

The severity of injury depends on external loading and the initial position. Experimental data suggests that patterns of injury are best described by considering three cervical regions: CO-C2, C2-C5, and C5-T1. The craniocervical junction is the most frequent site of fatal injuries. The most common mechanism of injury among survivors is compression-flexion at C5 or C6, with and without rotation.[48,49]

In laboratory experiments, the investigator is provided with immediate knowledge of the magnitude of the mechanical impact. By inference, he or she can predict the extent of neurological damage. A voltage waveform represents the desired characteristics of the impact. The negative feedback signal from the controller represents the actual impact.[69]

The gelatinous contents of the intervertebral disk nuclei exhibit hydrostatic behaviour. Disk pressure measurements have been used extensively to estimate compressive loads on the spine.[65] Electromyographic (EMG) measurements are also used to quantify cervical muscular responses. Suggested placement for the EMG electrodes is shown in figure A.2.1.

However, large discrepancies exist in the experimental mechanical properties of connective tissues. Differences in experimental techniques between studies may account for this.[11]

A.2.3 Selected Cervical Muscle and Ligament Models

We will consider here four comprehensive models for cervical motion. Each

combines theory and data from several related previous studies. The intent here is to illustrate some methods used in analytical modelling, rather than to evaluate or compare any of these.

We begin by examining a two dimensional lumped parameter analytical model presented by Raynor and Goldsmith (1979).[3] This involved 10 lumped masses: the head(1), vertebral bodies C1-T1(2-9), and T2 combined with rigid torso(10), as shown in figure A.2.2. Merrill et al (1984) extended this model to three dimensions.[3,61]

Deng and Goldsmith (1987) modified Merrill's model slightly in developing a physical and analytical model pair to predict motion for any initial conditions.[14] The numerical model was found to compare favourably with human motion test results.

The position and orientation of the skull and vertebrae were originally digitized from textbook radiographs. Due to lack of data on individual cervical joints, their stiffness was assumed proportional to cross-sectional area.

In Merrill's model, seven pairs of muscles were represented by non-linear springs connecting two points. Deng and Goldsmith used a 'three point piecewise' representation to account for muscles passing around bones and other tissue.

They also included more muscle elements in their model, resulting in more realistic force magnitudes and directions. The spring constants were obtained from cadaver test results, also leading to more realistic mathematical modelling.

Six simulation runs were designed for comparison with the physical model and human subjects. Runs 1 and 2 corresponded to the tests by Ewing and Thomas (1972) on the response to impact acceleration, using volunteers.[103] Runs 3 to 5 correspond to tests on the physical model for impact in frontal, rear and side directions. Run 6 was used to simulate impact to the head with initial velocity in the anterior direction.

In flexion whiplash there was little rebound of the volunteer's head. The analytical model indicated a return to the neutral position after 300ms. This discrepancy was attributed to voluntary muscle contraction by the volunteer.

For lateral whiplash the human subject rebound was faster than in flexion whiplash. This was associated with the smaller number of muscles controlling lateral motion and to the shorter sled acceleration time (fig A.2.3).

The physical model was found to have excessive flexibility. Two parameters were incorporated in the numerical model as multipliers for joint stiffness and muscle spring constants. Reducing these to 1/5 of their original values resulted in responses matching the physical model.

A possible explanation for the excessive flexibility is that the muscles were essentially massless and did not have in vivo dimensions. For the extension whiplash case it was found that the T1/T2 joint had much greater deformation than other joints due to low stiffness (fig A.2.4). Comparisons between the numerical and physical models were consistent. Hence improved muscle modelling for the latter in the future is expected to give better results.[3]

The William s and Belytschko (1983) model was meant to mimic the stretch reflex response with no consideration of contractions following the initial response.[62] The muscle elements in the Deng and Goldsmith model considered contraction effects by incorporating a magnification factor in the passive stress-strain relationship.[62]

Hosey and Liu (1982) optimized the mass distribution with respect to known experimental masses, making theirs an "anthropo-dynamic" model.[104] Simulations with head impacts showed that if skull fracture did not occur then most of the load was transferred to the cervical spine. Liu (1981) also stated that so called 'stress wave' propagation effects are not relevant.[15]

Helleur et al. (1985) attempted to determine the muscle firing combination which would balance the applied load while minimizing the stress distribution among supporting structures.[2] Shear, compression and ligament moments at each joint were to be minimized while imposing the quality constraints required to match the load.

Their model incorporated principles developed by Gracovetsky and Farfan (1986) in their study of the lumbar spine.[81] The muscles were considered to be a collection of two ended strands represented by vectors. The cross-sectional area of each strand was multiplied by the corresponding stress to determine shear, compression and moments at each joint.

The static forces acting on the cervical joint were divided into the following four groups (fig A.2.5):

1. The weight of the head and neck, together with external loads.
2. The reaction forces of the joint.
3. The resulting muscle tensions.
4. The ligament tensions.

In order to make the equilibrium equations determinate, additional constraints were imposed. Determining the minimum number of independent muscle groups resulted in a reduction in the computational burden. The model was used to simulate five tasks which volunteers performed in experiments.

These tasks involved pushing and pulling of the head in various positions against a harness connected to a force transducer. Muscle responses were monitored using EMG probes applied to the volunteer's necks. Following tuning of the model response using weighting coefficients, the degree of correlation to experimental results was considered to be good.[2]

The dynamic model assumed that the nervous system will not allow the stress in any component of the cervical spine to exceed two thirds of its ultimate limit. It was found that a high acceleration load can be supported if the resulting moments are small.

A neutral neck posture, along with combined action by the muscles and ligaments, resulted in supportable accelerations up to 50 g. However, deviation from the optimum orientation led to lower supportable accelerations. This is consistent with the mechanisms of injury for the cervical spine presented in Appendix A.3.1. Stress equalization and minimization were used by Helleur et al. (1984) to explain this result.[1]

A.2.4 Models of the Spinal Cord

Animal experiments are required to measure the magnitude of cord compression versus quantitative functional output. Such data may be used, in conjunction with a model correlating bony pathology to cord stresses, to predict neurological dysfunction.[16]

Engineering theory predicts that a well defined stress pattern results from a shear tforce applied to a long structure with elliptical cross-section. Raynor and Koplik (1985) showed that such stresses adequately explain neurological dysfunction due to preferential

central spinal cord damage (fig A.2.6).[55]

When producing spinal cord lesions in experimental animals, predictability is an important requirement. Researchers at Ohio State University have developed an electromechanical impactor with this idea in mind. It incorporates two levels of feedback control to allow reproducible results. This work is similar in principal to vertical impact experiments performed by Yoganandan et al (1986).[105] The latter dropped cadavers vertically, head down, and studied the resulting cervical injuries.

According to Panjabi and White (1988), however, there are currently no mathematical models that relate external loads to the internal stresses within the spinal cord.[16] This is apparently an area that will require considerable investigation before it can be incorporated into existing cervical spine models.

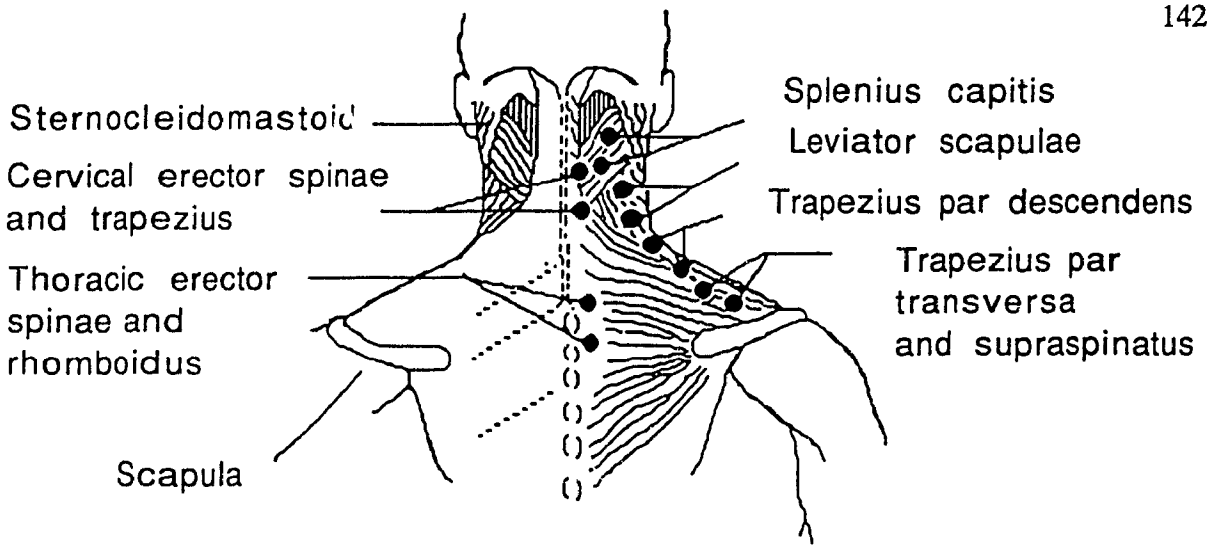

Fig A.2.1: Suggested locations of EMG electrodes for measuring cervical muscle activity. Adapted from Schuldt and Harms-Ringdahl (1988a). [12]

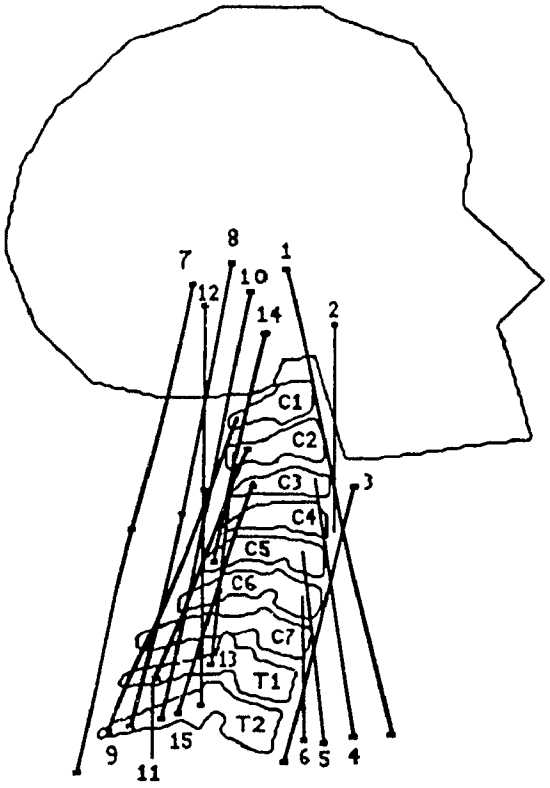

1 Sternocleidomastoid
2 Longus capitis
3 Longus colli
4 Scalenius anterior
5 Scalenus medius
6 Scalenus posterior
7 Trapezius
8 Splenius capitis
9 Splenius cervicis
10 Spinalis capitis
11 Spinalis cervicis
12 Semispinalis capitis
13 Semispanalis cervicis
14 Longissimus capitis
15 Longissimus cervicis

Fig A.2.2: Three point muscle insertions for the head/neck model of Merrill, Deng, and Goldsmith. Adapted from Deng and Goldsmith (1987). [3]

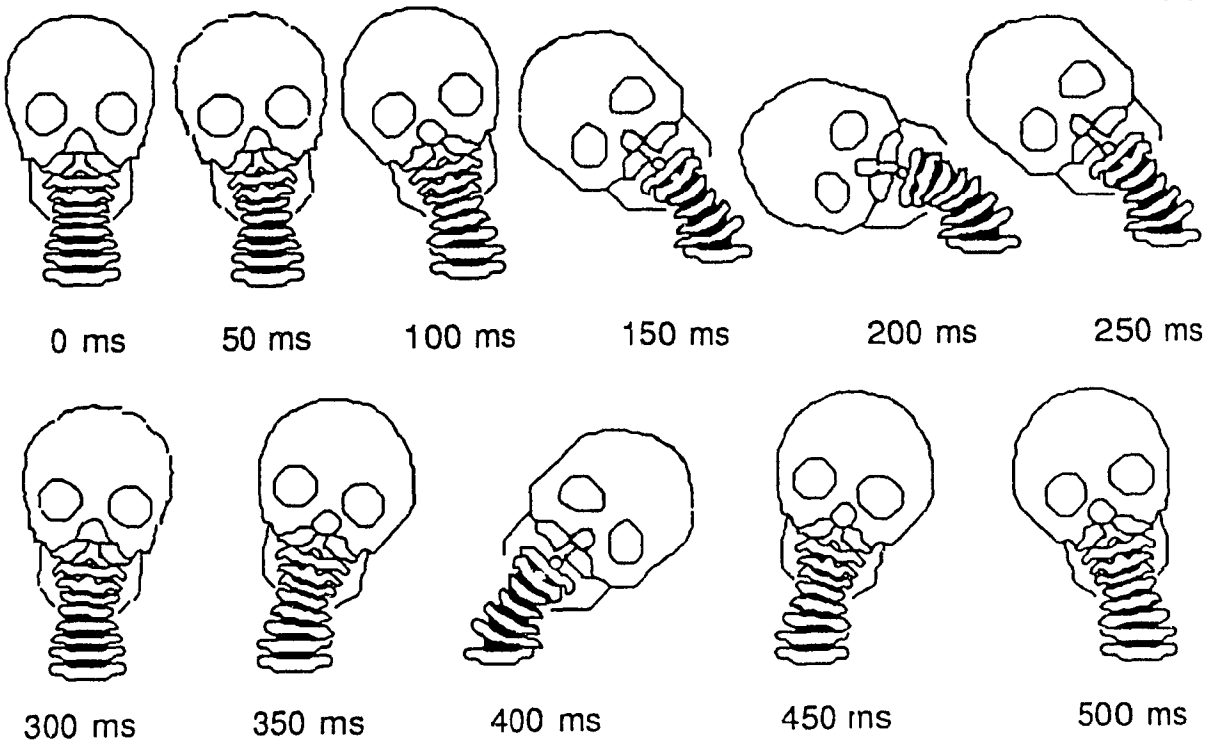

Fig A.2.3: Lateral whiplash simulation for Merrill's analytical model. Adapted from Deng and Goldsmith (1987). [3]

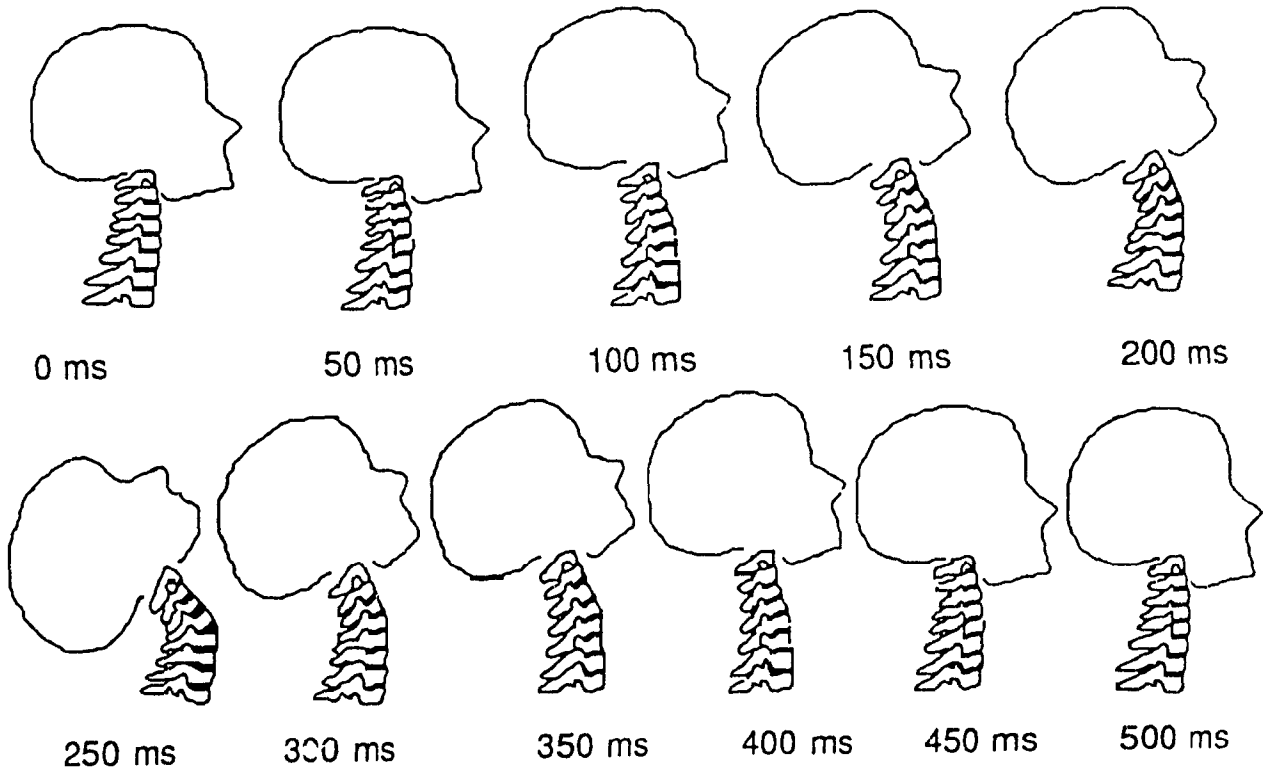

Fig A.2.4: Hyperextension simulation for Merrill's analytical model. Adapted from Deng and Goldsmith (1987). [3]

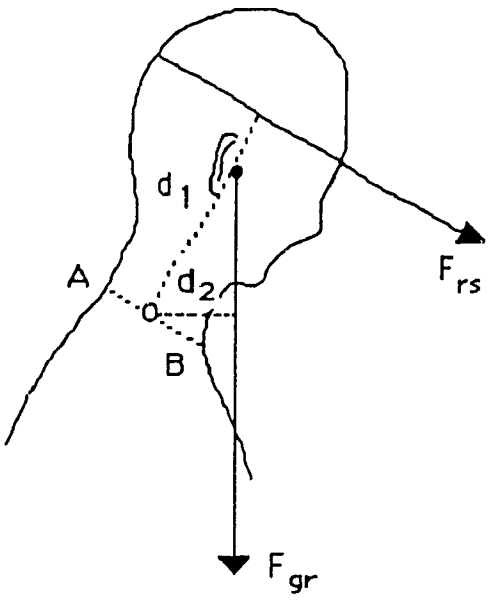

Fig A.2.5(a): Moment calculations for the cervical spine.

F_{rs} = resistance force
F_{gr} = gravitational force
d_1, d_2 = moment arms
M_m = muscle moment

$$\therefore M_m = d_1 F_{rs} + d_2 F_{gr}$$

Adapted from Schuldt and Harms-Ringdahl (1988a). [12]

Fig A.2.5:

Examples of muscle moment calculations and determination of load distributions for the cervical spine.

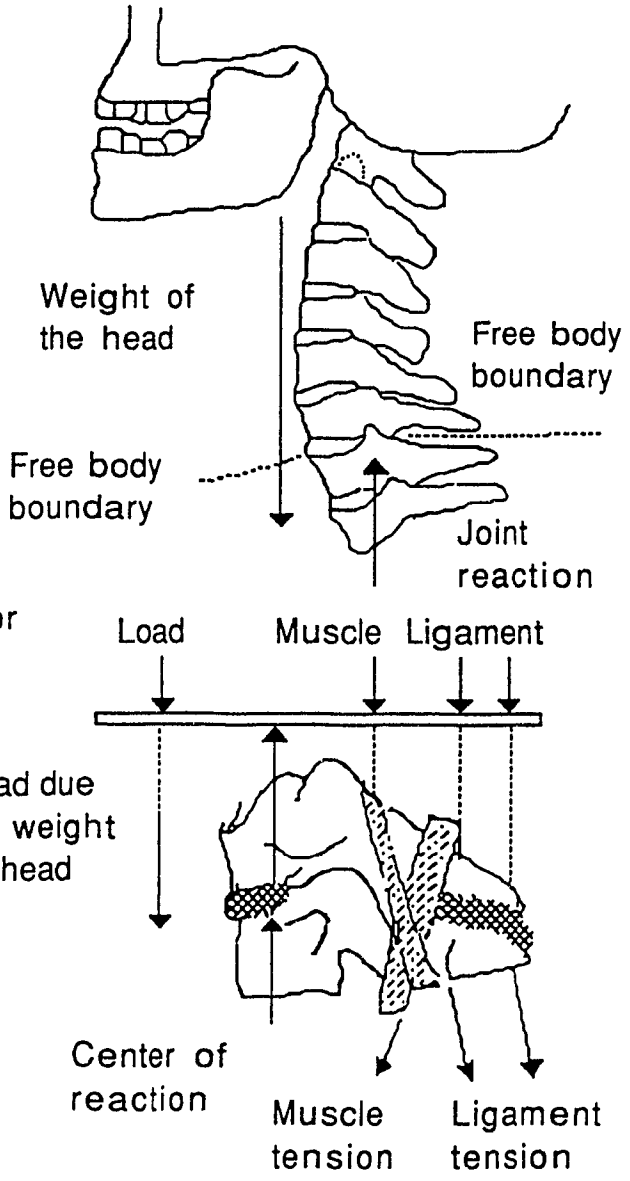

Fig A.2.5(b):

Free body analysis of an intervertebral joint in the lower cervical spine, showing load distribution. Adapted from Helleur et al. (1985). [2]

Fig A.2.6: Stress patterns for the spinal cord under various loading conditions. Adapted from Panjabi and White (1988). [16]

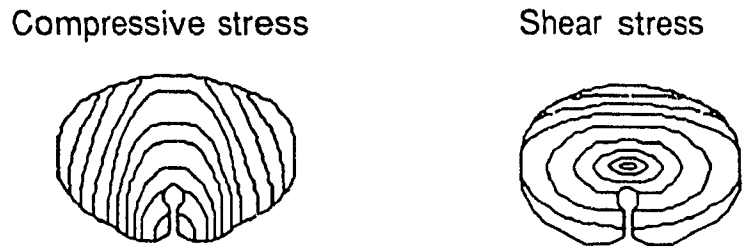

Fig A.2.6(a): Compressive stress decreases away from the contact point. Shear stress increases toward the center.

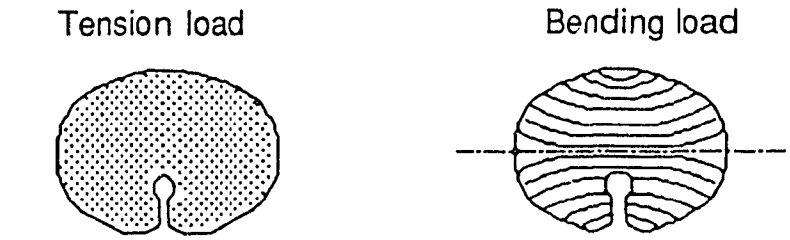

Fig A.2.6(b): Uniform stress from tensile load and tension/compression stresses from bending load.

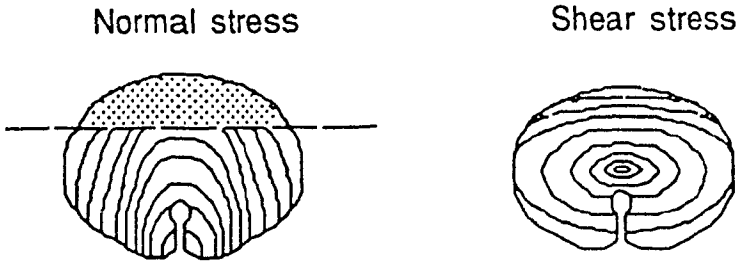

Fig A.2.6(c): Normal stress (perpendicular to the structure) and shear stress patterns for combined loads.

A.3 CERVICAL RANGE OF MOTION

A.3.1 More on How the Cervical Spine Moves

Fielding (1974) suggested that selective motion can occur at C0-C1 and C1-C2, but that movements of the lower segments are linked together.[31] However, Goel et al. (1988) found that axial rotation across C2-C3 occurred concurrently with the C0-C1 and C2-C3 joints.[72] The C0-C2 complex allows extensive motion, yet its vertebrae are interlocked to form a stable 3D structure. The complexity of this construct has led some investigators to suggest that it be tested as one unit.[72]

Contrary to early theories, Werne (1957) showed that flexion-extension occurs at C0-C1 as well as C1-C2.[106] Similarly, Jirout (1974) and Moroney et al. (1988) showed that rotation at C1-C2 accompanies lateral flexion.[107,11] Hence, lateral bending and axial rotation are coupled (fig A.3.1).[67] Each main translational motion is associated with five coupled motions.[10,11,72] We will consider coupled motion more carefully in chapter 3.

Axial translation of more than 1mm at C0-C1 is considered by some to be pathological. Surprisingly, instantaneous axis of rotation (IAR) calculations are still made on the basis of measurements made by Henke (1863).[111] Included among suggested IAR locations are the center of the vertebral body and the nucleus pulposa.[67] Rotation and translation in the cervical spine is illustrated in figure A.3.2.

Selecki (1969) found that after 30° of rotation there is kinking of the contralateral vertebral artery.[108] At 45° the ipsilateral artery also begins to kink. Indeed, some cases of stroke have even been reported following cervical manipulation. Hence, manipulation is contraindicated for patients with cervical spondylosis or vascular disease.[67]

Lysell (1969) observed that coupling of axial rotation and lateral flexion (ie. bending to the side) is stricter at C2-C3 than at C6-C7.[34] Penning (1988) related this to the guiding effect of the unciform processes, which are larger in the upper cervical area.[35]

According to Hall (1965), these are absent in quadrupeds and present only in bipeds.[105,109] He suggested that the former need lateral flexion in their necks for looking around and backwards. Bipeds, conversely, use rotation for the same purpose. Lysell also

reported no correlation between disc degeneration and loss of mobility. However, other investigators have disagreed with this finding.[35,67]

A.3.2 Comparison of Cervical and Lumbar Motion

The cervical articulations may be described as biconvex, or saddle joints.[35,67] This allows coupled rotation and lateral flexion, as well as flexion-extension (fig A.3.7). In contrast, rotation in the lumbar spine is almost entirely prevented by the crosswise arrangement of the annular fibers, as well as the orientation of the facets.[35]

Myklebust et al (1988) performed in-vitro experiments on the ligaments of the entire spine.[5] The ligaments showed greatest absolute distensibility in the cervical and lumbar regions. The anterior longitudinal ligament showed increasing values of failure deformation from the cervical to lumbar region.

The ligamentum flavum had the least variation. The supraspinal ligament had the largest deflection at failure. The ligaments on the convex side of the spinal curves were generally stronger. Increases in strength were also noted at the thoraco-lumbar and the cervico-thoracic junctions. Yoganandan et al. (1990) found similar results for the vertebral bodies at the latter junction.[6]

Much smaller loads appear to be required to produce similar principal motions in the cervical than in the lumbar area. This may be attributed to a difference in the size of motion segments and in the geometry of facets. Lateral translations coupled to lateral bending seem to be smaller for the cervical spine. However, accompanying axial rotations appear larger than, and in the opposite sense to, those in the lumbar region.[11] We will consider this topic further in chapter 2 (see section 2.3.4).

A.3.3 Radiographic Range of Motion Data

Mimura et al (1989) used bi-planar radiographs to determine in-vivo (ie. in living subjects) ranges of cervical rotational motion.[9] Average axial rotation between the occiput and C2 was found to be 75°. This was estimated to be 75% of total cervical rotation. Between C2 and C7 rotation averaged 4° to 8°.

Flexion occurred in association with rotation in the segments below C5-C6.

Conversely, extension occurred above C4-C5. According to Penning (1978), though, precise measurements in the plane of rotation from radiographs are very difficult.[72]

Patients participating in the passive measurements of Dvorak et al. (1988) received an analgesic prior to being examined.[60] Fixing bars were used to prevent motion of the thoracic spine (fig A.3.4). Only flexion-extension was considered.

Passive motion was assisted by an examiner clad in full gear to protect against radiation. Active motion was unassisted. The mean passive ranges of motion were 2° to 3° greater then the active at all levels of the cervical spine (see results in Appendix A.3.6).

A.3.4 Computer Tomography Range of Motion data

CT range of motion studies on normal patients were performed by Penning and Wilmink (1987) as well as Dvorak et al. (1987).[7,8] In the former, the role of the unciform processes in rotation was emphasized. Conversely, the latter was more concerned with the alar ligaments.

Penning and Wilmink (1987) found mean axial rotation to be 72.2°, with about 55% of this occurring at the C1-C2 level.[7] Rotation between the atlas and occiput was 1°. The range for atlanto-axial rotation was 29° to 46°. Such a large individual variation was consistent with Lysell's (1969) cadaver results.[34] However, he measured rotations only 75% as large as Penning and Wilmink.[7]

Conversely, Dvorak et al. (1987) found a mean rotation between the occiput and atlas of 4.5° on cadavers.[8] This increased to 9.5° after rupture of the alar ligament. This led them to suggest that this injury may occur upon rotation and flexion due to trauma, such as in rear end collisions. It should thus be detectable clinically by an increase in observed rotation.

Dvorak (1988) compared the data from the study by Dvorak et al. (1987) to that of Penning and Wilmink (1987).[7,8,33] He found that their results agreed, except at the atlanto-occipital joint. There Penning measured rotation of 1° and Dvorak 4°. This was attributed to the latter applying maximum force to assist in rotation. The combined results for the two studies are shown in section A.3.6.

A.3.5 In-Vitro Experimental Data

Few studies have reported the effects of rate of loading on the biomechanics of ligaments. According to Yoganandan et al. (1989), at that time no data was available to describe the dynamic properties of cervical ligaments.[4]

Hence, they evaluated the effects of rate of loading on the response of cervical spine ligaments. Failure was defined as the point on the tensile force-distraction curve where an increase in distraction resulted in a decrease in force (fig A.3.5).

In this study, midsubstance tears of the ligament structures were routinely observed at all rates of loading. An analogous load-deflection curve for a cervical vertebral body is shown in figure A.3.6.[6] Panjabi et al. (1986) found no significant variation in load deflection curves with vertebral level.[10]

In similar experiments Panjabi et al. (1988) found average axial rotation at C0-C1 of 7.2°.[71] This is much larger than the in-vivo values stated earlier (see section A.3.2). They emphasized that the special design of the articulations and ligaments together provide the specific movements of this region. See section A.3.6 for complete C0-C1 and C1-C2 motion data.

Motion of the markers attached to bones was recorded by two 35mm cameras. Digitization of the stereophotographs resulted in noncontacting (ie. natural) 3D motion measurement. The occiput and C1 were provided with special markers containing numerous steel balls distributed such that at least three were visible at any time by both cameras.

An analogous system using light emitting diodes (LEDs) was used by Goel et al. (1988) to track vertebral motion in the C0-C2 complex.[72] They found that a small load results in large motions across the C0-C2 complex. This supports the notion that the ligaments in this area are lax and that the head is therefore held firm primarily by muscle action.

A.3.6 Combined Cervical Range of Motion Results

The combined results for the range of motion studies discussed above are shown in tables A.3.1 to A.3.4 on the following pages.

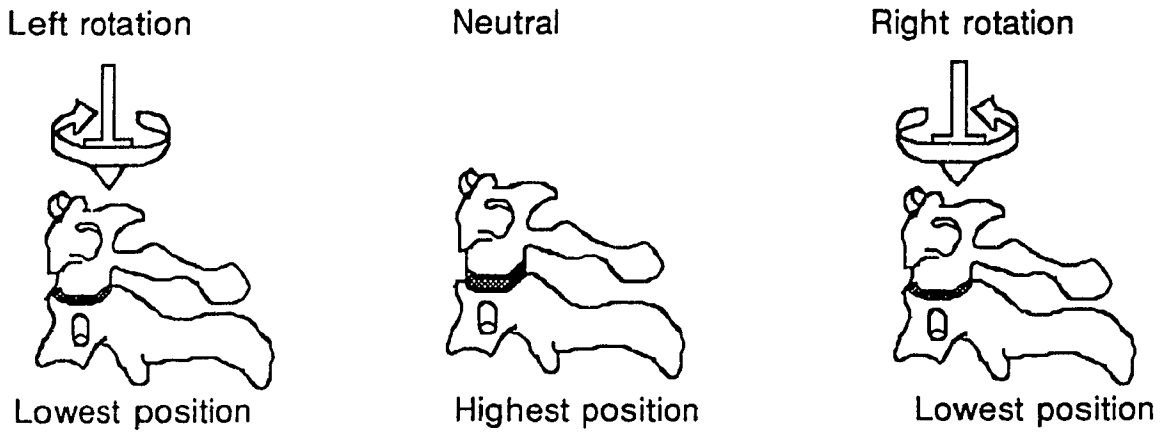

Fig A.3.1: Coupling of lateral bending and axial rotation, resulting in vertebral approximation. Adapted from Jofe et al. (1983).[67]

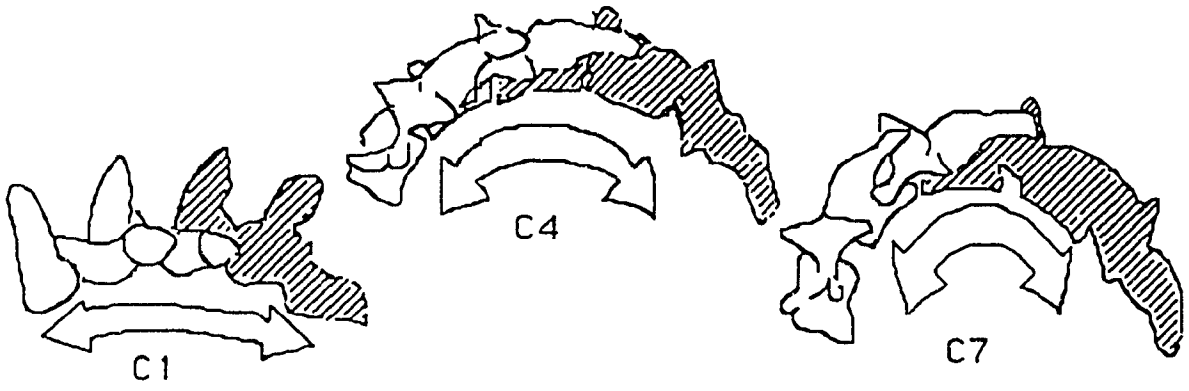

Fig A.3.2: Rotation and translation in the sagittal plane, depicting patterns of motion for C1, C4, and C7. The diagrams show the movement between full flexion and full extension. Adapted from Jofe et al. (1983).[67]

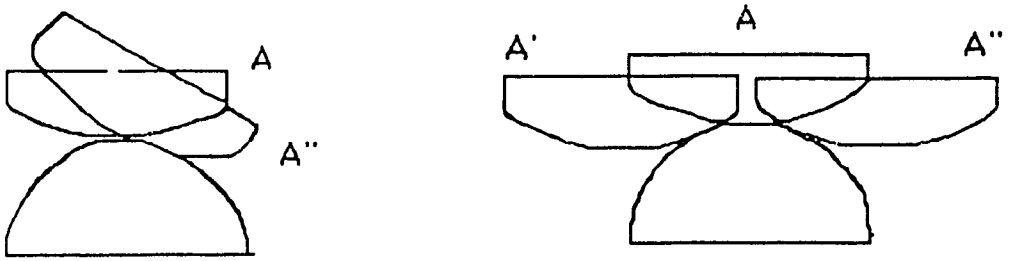

A = neutral position
A" = flexion position

A = neutral position
A' and A" = positions of rotation

Fig A.3.3: Atlanto-axial rocking and gliding motion. Adapted from Fielding (1974).[31]

Fig A.3.4: Passive vs active flexion and extension for functional radiographic diagnosis. Adapted from Dvorak et al. (1988). [60]

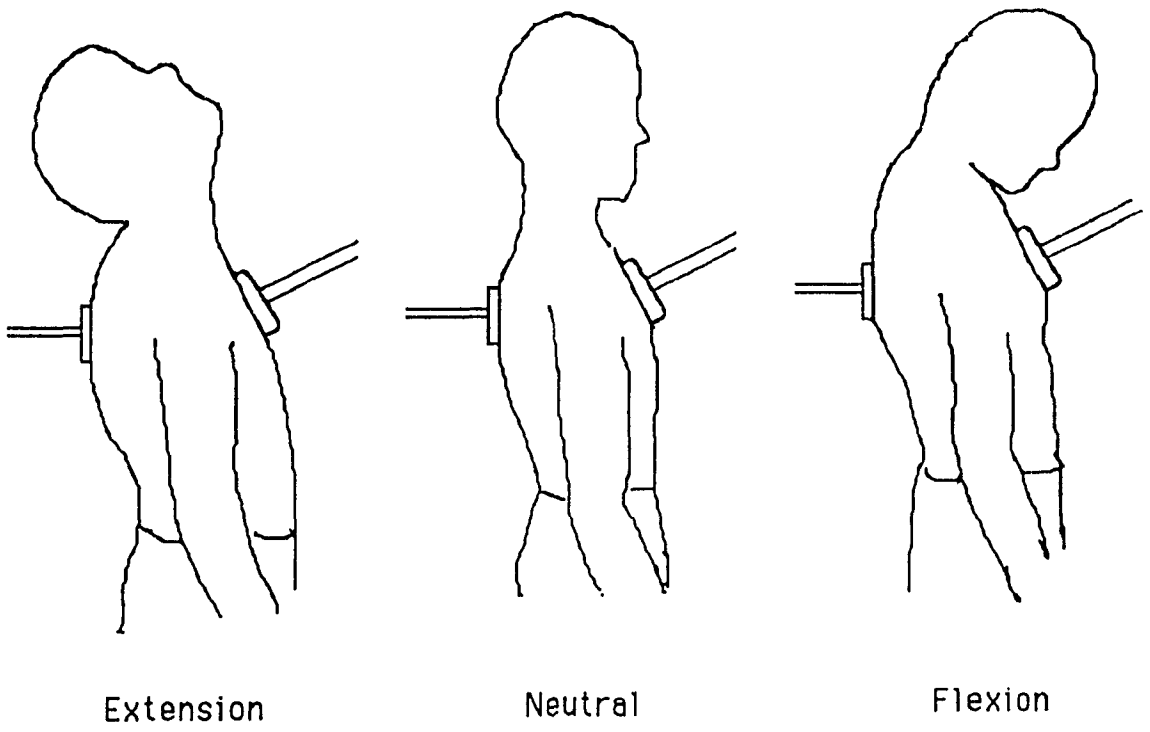

Fig A.3.4 (a): Active flexion and extension, showing ventral and dorsal pellots used to prevent thoracic motion.

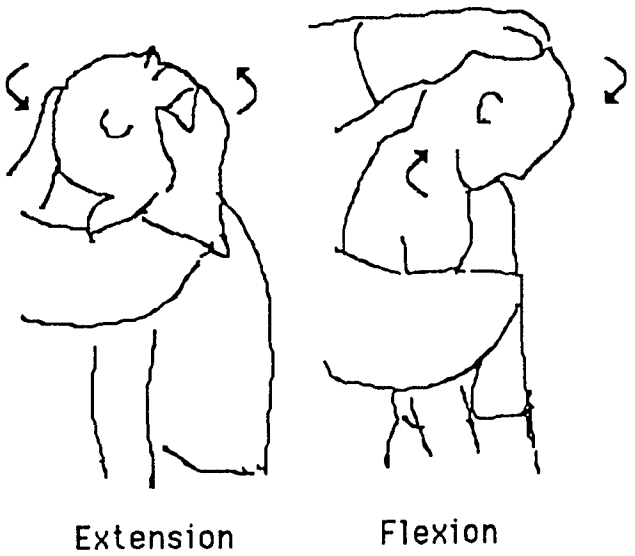

Fig A.3.4 (b): Passive flexion and extension, showing suited figure assisting subject in achieving maximum motion.

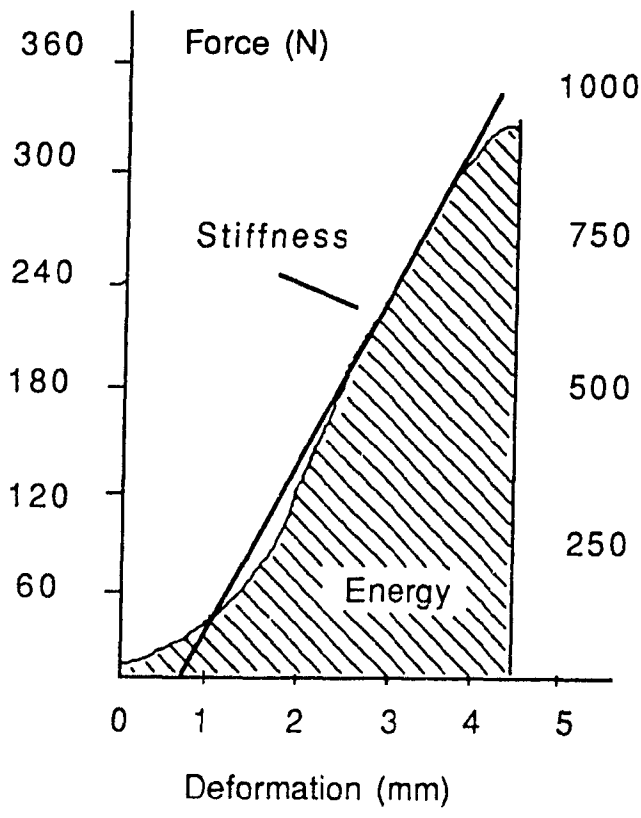

Fig A.3.5: (above left) Force distraction curve for cervical ligaments. Adapted from Yoganandan et al. (1989). [4]

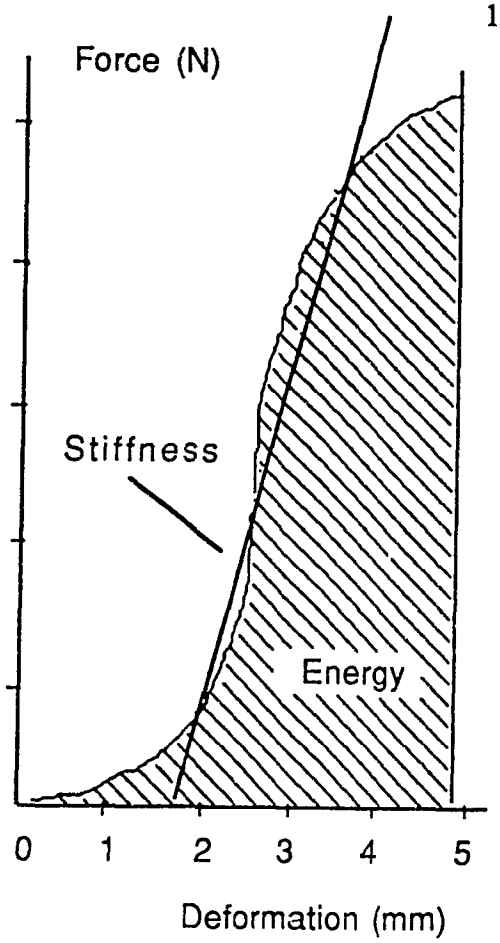

Fig A.3.6: (above right) Force distraction curve for cervical vertebra bodies. Adapted from Yoganandan et al. (1990). [6]

Fig A.3.7(a): (near right) Representation of two lumbar vertebrae. The main axes of motion cross at right angles at the center of disk. Adapted from Penning (1988). [35]

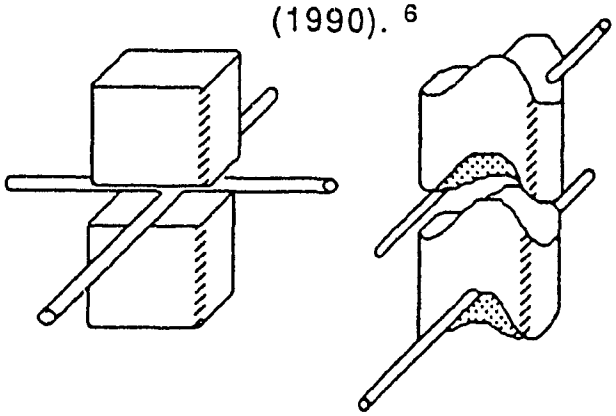

Fig A.3.7(b): (above far right) Representation of cervical bi-convex articulation. Intervertebral space is saddle shaped. Hence axes of motion are on opposite sides of the disk. Adapted from Penning (1988). [35]

Table A.3.1: Mean Value of Axial Rotation for C0-T1

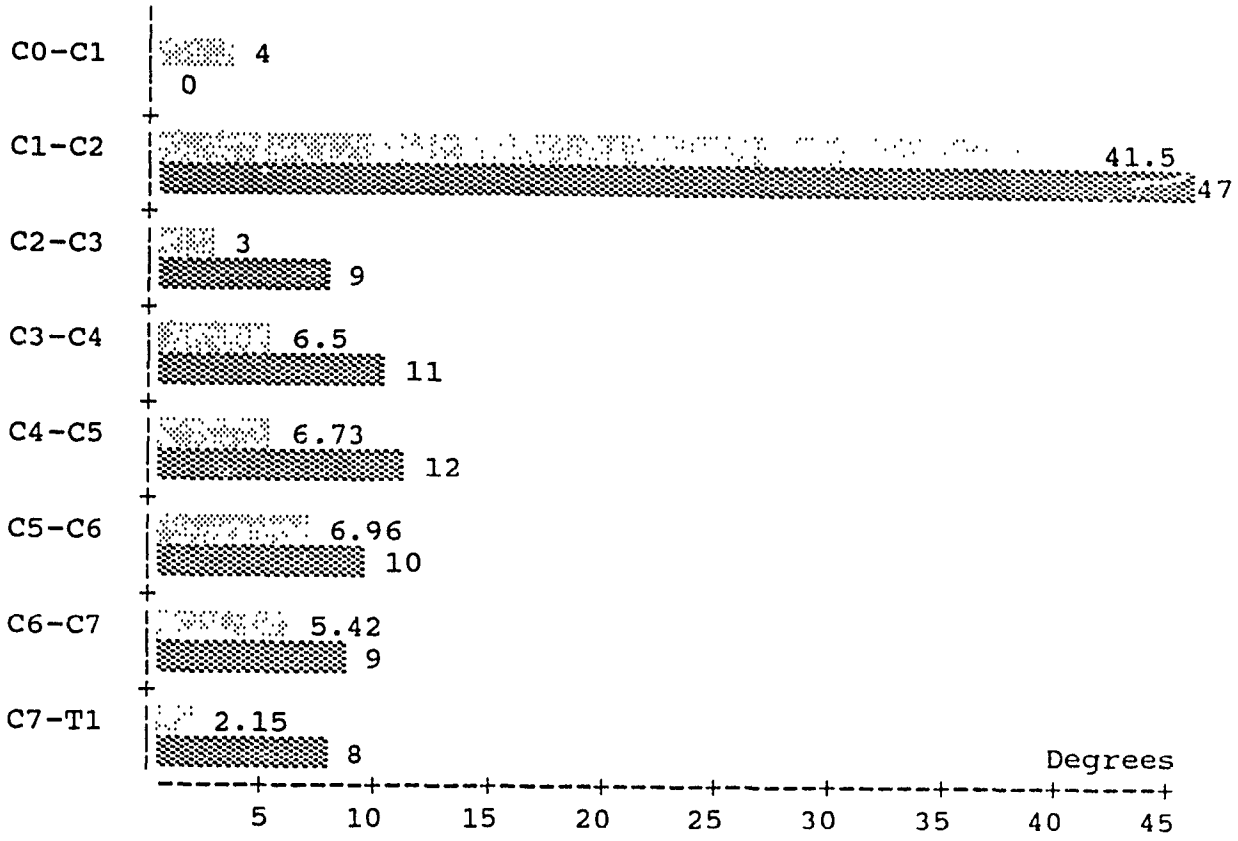

Combined CT in-vivo results of Penning and Wilmink (1987) with Dvorak et al. (1987), from Dvorak (1988a).[7,8,33]

In-vitro results from Jofe et al. (1983).[67]

Table A.3.2(a): Mean Value of Axial Rotation for C0-C1 *

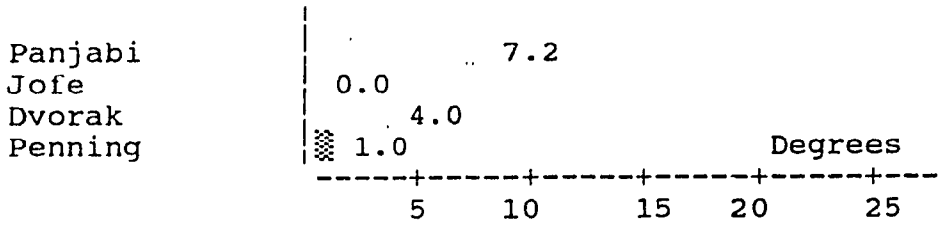

Table A.3.2(b): Mean Value of Axial Rotation for C1-C2 *

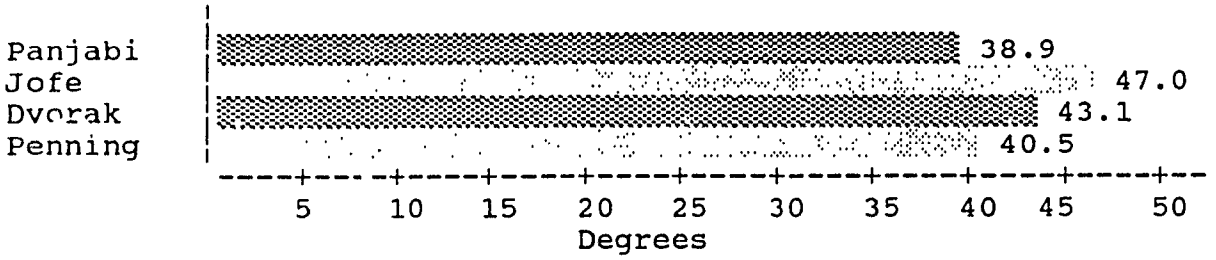

* Data from: Panjabi et al. (1988) [71]
Jofe et al. (1983) [67]
Dvorak et al. (1987) [8]
Penning and Wilmink (1987) [7]

Table A.3.2(c): Mean Value of Axial Rotation for C2-C7

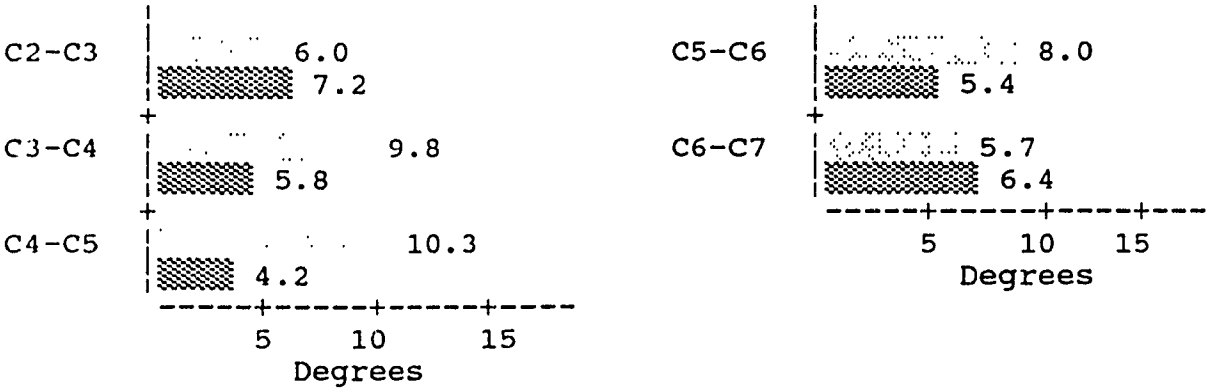

Lysell (1969), in-vivo [34]

Mimura et al. (1989), in-vivo bi-planar radiographs [9]

Table A.3.3(a): Principal Motions of C0-C1

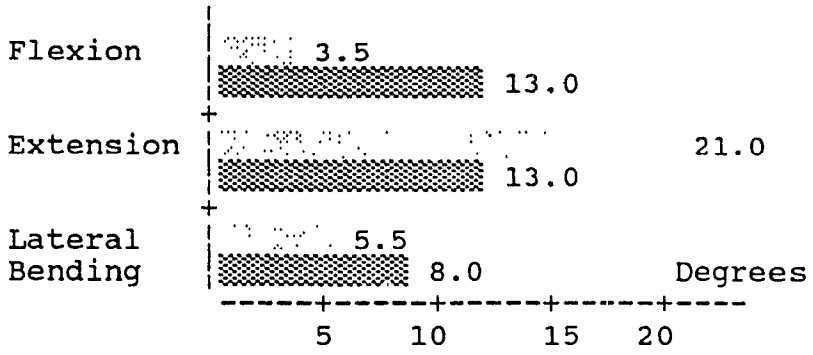

Table A.3.3(b): Principal Motions of C1-C2

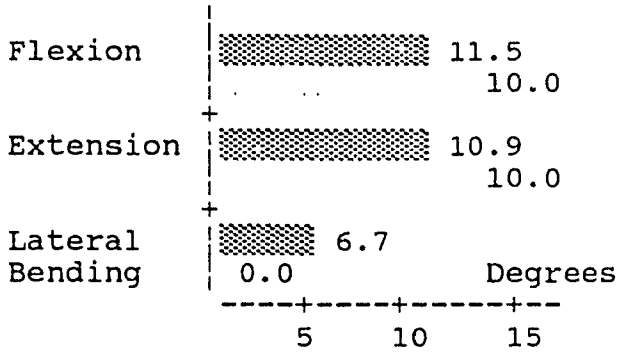

▒ In-vitro results from Panjabi et al. (1988) [71]

. In-vitro results from Jofe et al. (1983).[67]

Table A.3.3(c): Principle Motions of C2-T1 *

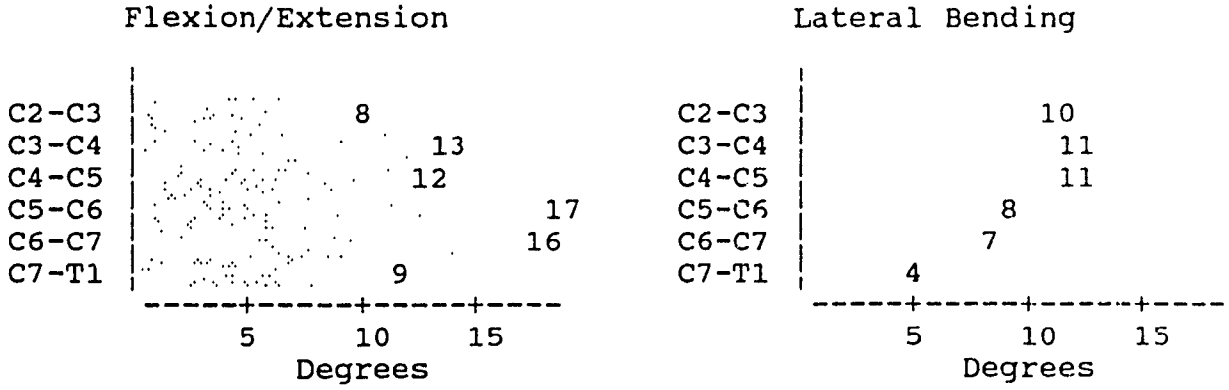

* From in-vitro data of Jofe et al. (1983).[67]

Table A.3.4(a): Active Flexion/Extension for C1-C7 *

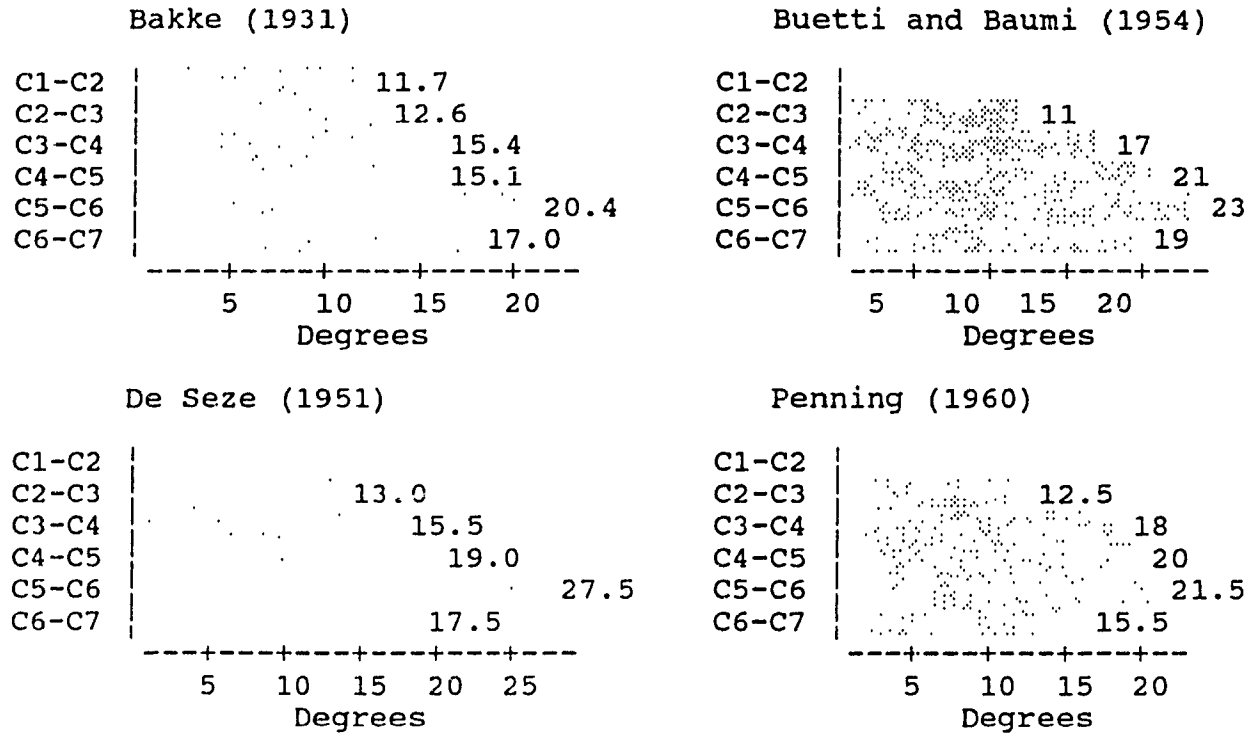

Table A.3.4(b): Active vs Passive Flexion/Extension *

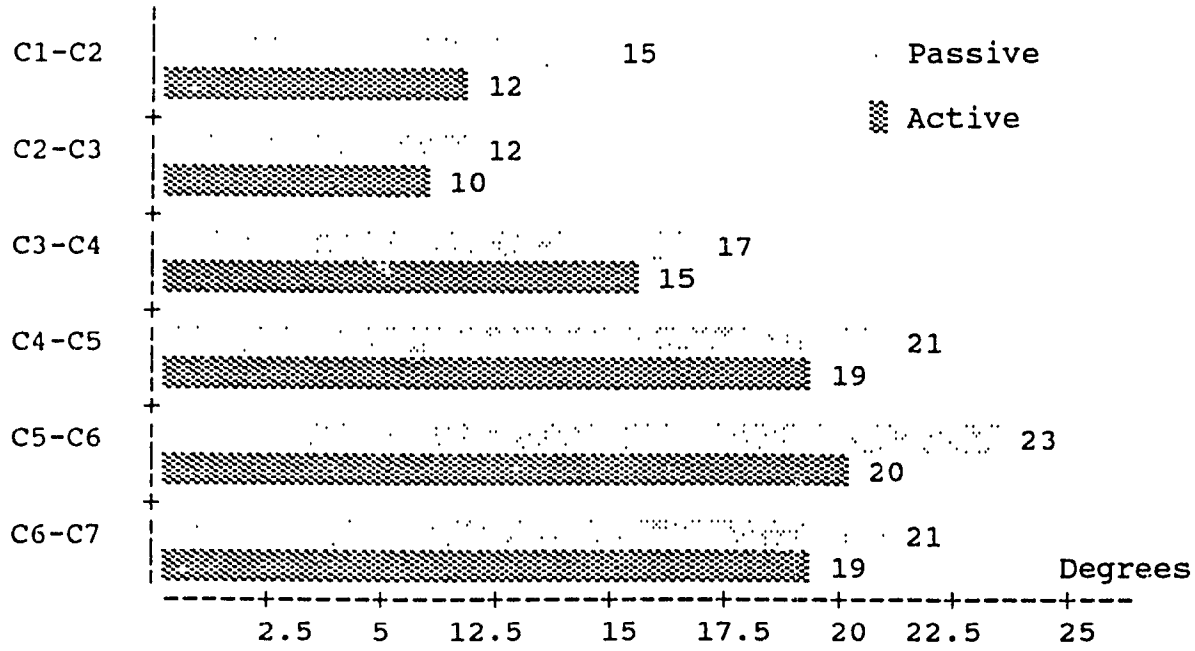

* From Dvorak et al. (1988b), in-vivo radiographic data [60]

A.4 INTERPRETATION OF DATA FROM RADIOGRAPHS AND FROM SKIN MARKERS

A.4.1 Functional Radiographic Examinations

Dvorak et al. (1988) compared different methods of measurement for cervical flexion-extension radiographs.[60] Measurements using the techniques of Penning (1960) and Buetti-Bauml (1954) were made by three observers independantly.[128,129] The Penning method was found to be more reliable.

Functional diagrams using the two methods are shown in f ,ure A.4.1. The Buetti-Baumi method shows one vertebra in a fixed position and the adjacent ones displaced relative to it. The angles of the lines drawn along the posterior border of each displaced vertebra represent its degree of flexion or extension.

The Penning method involves superimposing the extension film onto the flexion film, with the C7 position matching exactly. A line is then drawn along one of the edges of the flexion film onto the extension film. The procedure is repeated for each cervical vertebra. The angle between the two lines is the degree of flexion-extension between adjacent vertebrae.

In chapter 1 some data for segmental motion measured by the two methods was compared with that from other studies (see section A.3.6). A large variation in mobility occured for each segment.

However, functional radiographs in flexion and extension are widely used in Europe.[60] Hence, it would be desirable to produce comparable motion data with the Cerviscope. This would require a transformation function, as described earlier 4.1, in order to correlate radiographs with motion data from skin markers.

Reich and Dvorak (1986) performed an analogous study for functional radiographic evaluation in lateral bending.[75] They were primarily concerned with the extent of displacement in the atlanto-axial joint. It was concluded that defective ligaments in the upper cervical spine were apparent from lateral bending x-rays. They found that few methods exist for evaluating spinal lesions of ligaments in this portion of the spine.

The lateral displacement of the atlas with respect to the axis in sidebending was

considered useful in assessing C1/C2 stability. This is particularly relevant to the inflammatory reactions in the suboccipital ligaments of rheumatoid arthritis patients. Indeed, if left untreated, this condition may actually lead to cord compression and death. Hence, as in the case of flexion/extension, it would be desirable to establish a relationship between radiographs and the results for the Cerviscope in lateral bending.

A.4.2 Stretching of the Skin

One of the diagrams used to describe the experimental validation of the Spinoscope has been reproduced in figure A.4.2.[74] It illustrates the correlation between steel balls placed on the skin and the lumbar vertebrae underneath. In particular, a linear relationship was found between the true lumbosacral flexion angle and that measured for the steel balls. A similar correlation was found for lateral flexion. However, no attempt was made to draw conclusions regarding full sagittal extension.

The reason for this is that any type of skin markers would overlap in full extension. They would then become indistinguishable to the cameras. This is equally true for the lumbar and the cervical spine.

Hence, a partial sagittal flexion view is substituted for full extension in the cervical radiographs. This is consistent with the protocol used for lumbar radiographs, which called for a total of five views in forward flexion.[74]

The corresponding cervical radiographs will be taken with the subjects motionless. This is, of course equally true for the skin markers and the vertebrae. However, the Cerviscope will generally gather data while the subject moves. This is therefore a source of error in comparing the motion of markers and vertebrae.

This error may may be evaluated by establishing a Cerviscope data base for static positions. Then these may be compared to the dynamic data normally obtained. A similar procedure was suggested by Gracovetsky et al. (1990) for the Spinoscope.[29]

Note that both the Cerviscope and the Spinoscope software must be modified to display the data for the true vertebral motion. In their present form, they actually display the skin marker motion, which is not quite the same. Work is underway on such a transformation function and the resulting "virtual markers" are expected to be imple-

mented in the near future.

The protocol described in chapter 2, as well as in Appendix B, will be used to gather the cervical data. The angles of forward and lateral flexion will be measured from the radiographs. This will be done for the vertebrae as well as for the radio-opaque skin markers.

The relationship between the true flexion and that measured by the Cerviscope will thus be established. The procedure is analogous to that shown for the lower back in figure A.4.2. For the reasons outlined above, extension will not be measured.

Fig A.4.1 (a):

Penning method for determining flexion/extension. Extension film is suoerimposed on flexion, matching successive vertebrae. lines are drewn along an edge of the flexion film onto the extension film. The angles between succesive lines is the aangle of flexion extension for adjacent vertebrae. Adapted from Dvorak et al (1988). [60]

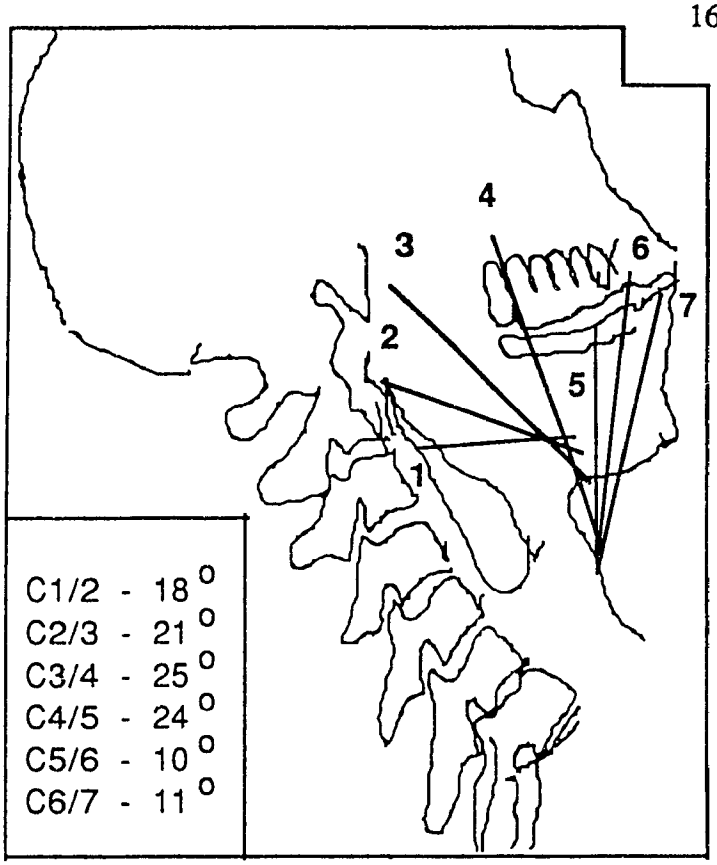

Fig A.4.1(b):

Buette-Bauml method. One vertebra is in fixed pos tion and adjacent vertebra in position of flexion/extension.The angle of lines drawn along the posterior border of the moving vertebra in its two end positions represents the degree of flexion extension motion. Adapted from Dvorak et al (1988). [60]

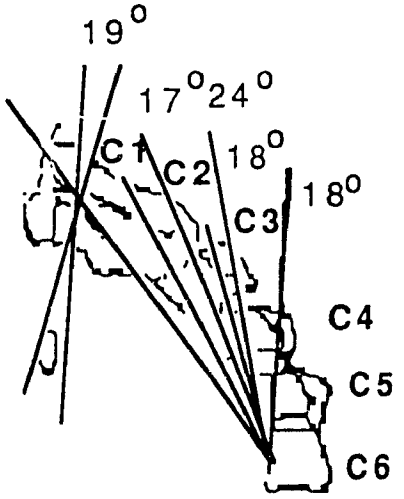

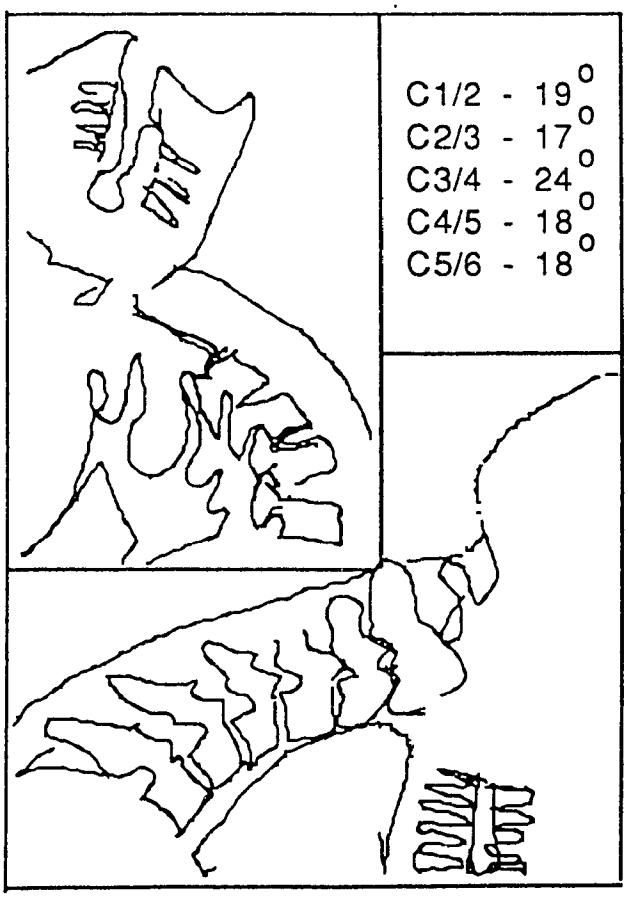

Fig A.4.2:

a) Definition of true lumbosacral angle Ψ and its approximation Ψ'. b) Correlation between Ψ and Ψ' for various radiographs in flexion/extension. c) Comparison of response for two different normal individuals. Adapted from Gracovetskty et al (1990).[74]

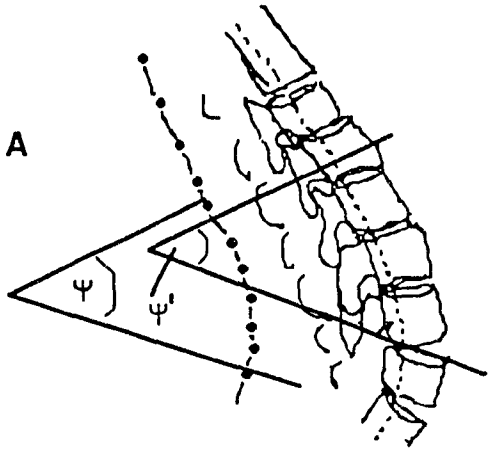

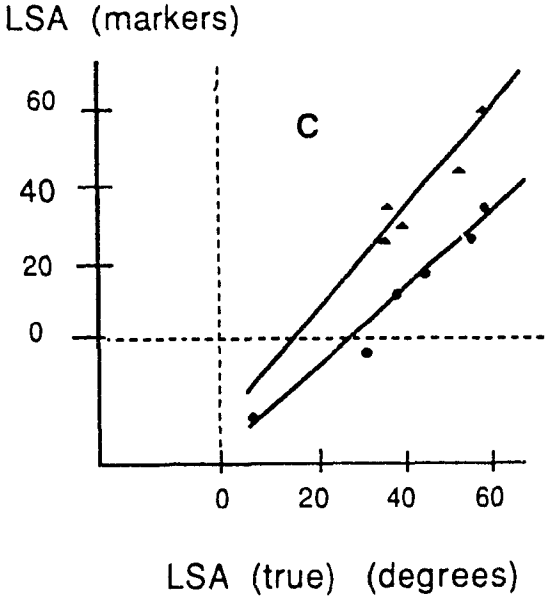

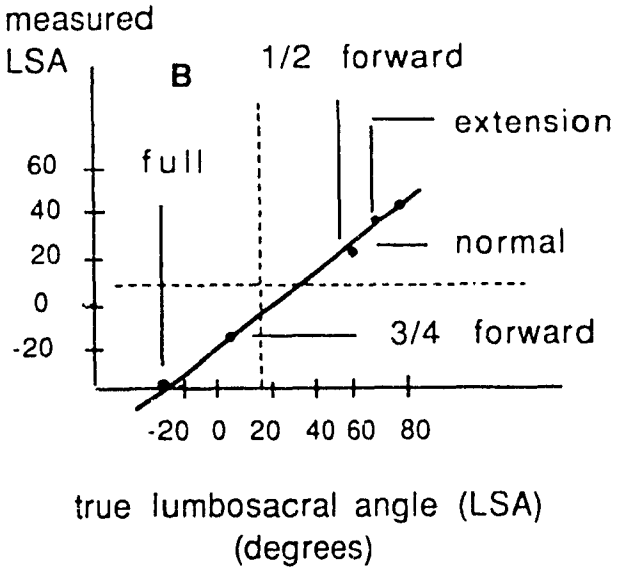

A.5 THREE DIMENSIONAL MOVEMENT: DESCRIBING COUPLED JOINT MOTION IN THE SPINE

A.5.1 The Need for Representing Coupled Motion

According to Stokes et al. (1987), the literature shows that as the spine is displaced away from its neutral position, axial rotation and lateral bending occur together.[86] However, the coupled motions occurring in the lumbar and cervical spine are known to be different.[7,10,11,35,67] The arrangement of cervical facets, ligaments and discs results in a unique type of coupled motion.[10]

Gracovetsky and Farfan (1986) considered axial rotation for the lumbar region.[81] The discs and facets were found to play distinct roles. The annulus appears to provide the means for storing energy in its fibers, while the facets may enhance coupling motion.

We can examine whether this argument applies to the cervical spine as well by comparing the facets for the lumbar and cervical vertebrae. Recall that we saw also from figure A.3.7 that in contrast to the lumbar joints, cervical articulations are biconvex.[35,67]

A.5.2 The Unique Nature of Coupled Motion in the Cervical Spine

We saw earlier (section 1.3.5) that the nature of coupled motion in the cervical spine may be attributed to the unique arrangement of facets, ligaments and discs in this region.[65,122] The geometry of the articulating surfaces and the elastic properties of the ligaments determine the relative motion of the vertebrae.

Hence, the kinematics of the lower and upper cervical spine appear to be quite different. In lateral bending to the left the spinous processes move to the right, and vice versa for bending to the right. This coupling decreases gradually between C2 and C7, due to the change in incline of the facet joints.[112] Reich and Dvorak (1986) found that a rotational component is always coupled with a segmental sidebending movement. [75]

Recall (section A.3.2) that the cervical articulations are described as biconvex, or saddle joints.[35,67] This allows coupling of rotation and lateral flexion, as well as flexion-extension. As the spine is displaced away from its neutral position, axial rotation and lateral bending occur together.[112] The major coupling patterns in the cervical spine are

illustrated in figure A.5.1.

A.5.3 Results of Previous Coupled Motion Studies

Hohl used cineradiography to illustrate cervical coupling as early as 1964.[31] Later, Panjabi and White (1971) helped to pioneer three dimensional mathematical techniques for analyzing biplanar radiography.[123]

They represented the displacement of vertebral bodies in terms of translation plus rotation. Euler's angles were introduced to represent the rotational aspect of transformations between moving reference frames. However, the error in using Euler's angles was considered by them to be unacceptable.[a]

In 1974, Suh also considered the distortion associated with radiographic images.[125] He adapted methods developed for surveying and map production to the analysis of X-rays of the cervical spine. This involved designing a radio-opaque reference frame that would appear on the radiograph along with the subject (fig A.5.2).

Brown et al (1976) constructed an analogous reference frame to appear in the X-rays, but this frame enclosed the entire torso.[126] They used anatomical landmarks to define the spatial orientation of the vertebrae. The orientation of each body was described by a translation vector and three Eulerian angles. Then the data was normalized to ensure a common basis for subsequent evaluation.

Several years later, Pearcy et al (1984), as well as Pearcy and Tibrewal (1984), were among many who elaborated upon these techniques.[121,127] They pointed out that the diagnosis of back pain "... requires a knowledge of the pattern of movement in normal individuals to establish what constitutes an abnormal movement and how it is related to pathology."

Mimura et al. (1989) used bi-planar radiographs to determine in-vivo ranges of cervical rotational motion.[9] They showed that the direction of lateral bending produced by coupling is dependant upon the level. Below C3-C4 lateral bending was in the same direction as rotation. Above C2-C3 it was in the opposite direction (fig A.5.3).

---

[a] Euler angles are defined in Appendix C.

Plamondon and Gagnon (1990) developed a method for controlling the experimental error involved in using Euler's angles.[41] They used the least squares method to correct for errors in determining anatomical landmarks, and concluded that this method can provide both accurate and precise results.

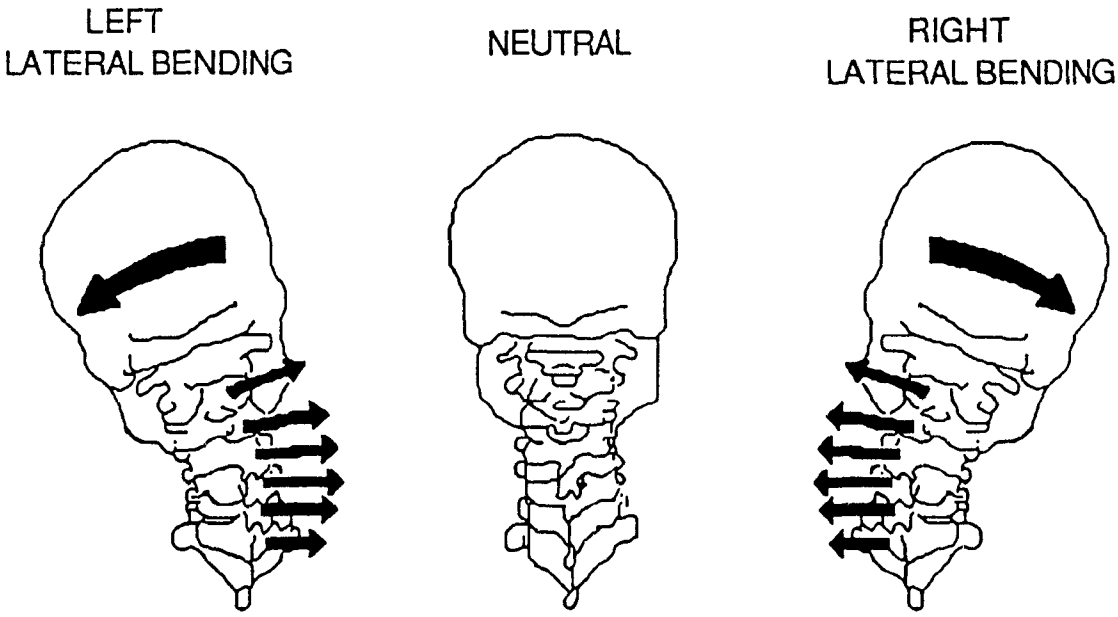

Fig A.5.1: Major cervical spine coupling pattern. When the head and neck are bent to the right, the spinous processes go to the left, and vice versa. Adapted from White and Panjabi (1978). [112]

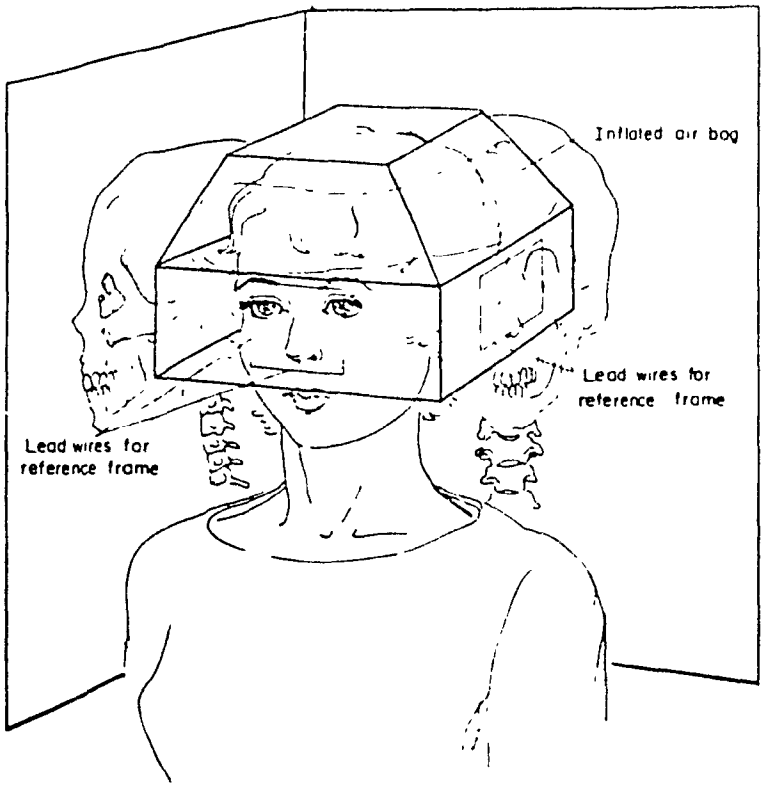

Fig A.5.2: Radio-opaque reference frame that appears on the bi-planar radiograph along with the subject. Adapted from Suh (1974). [125]

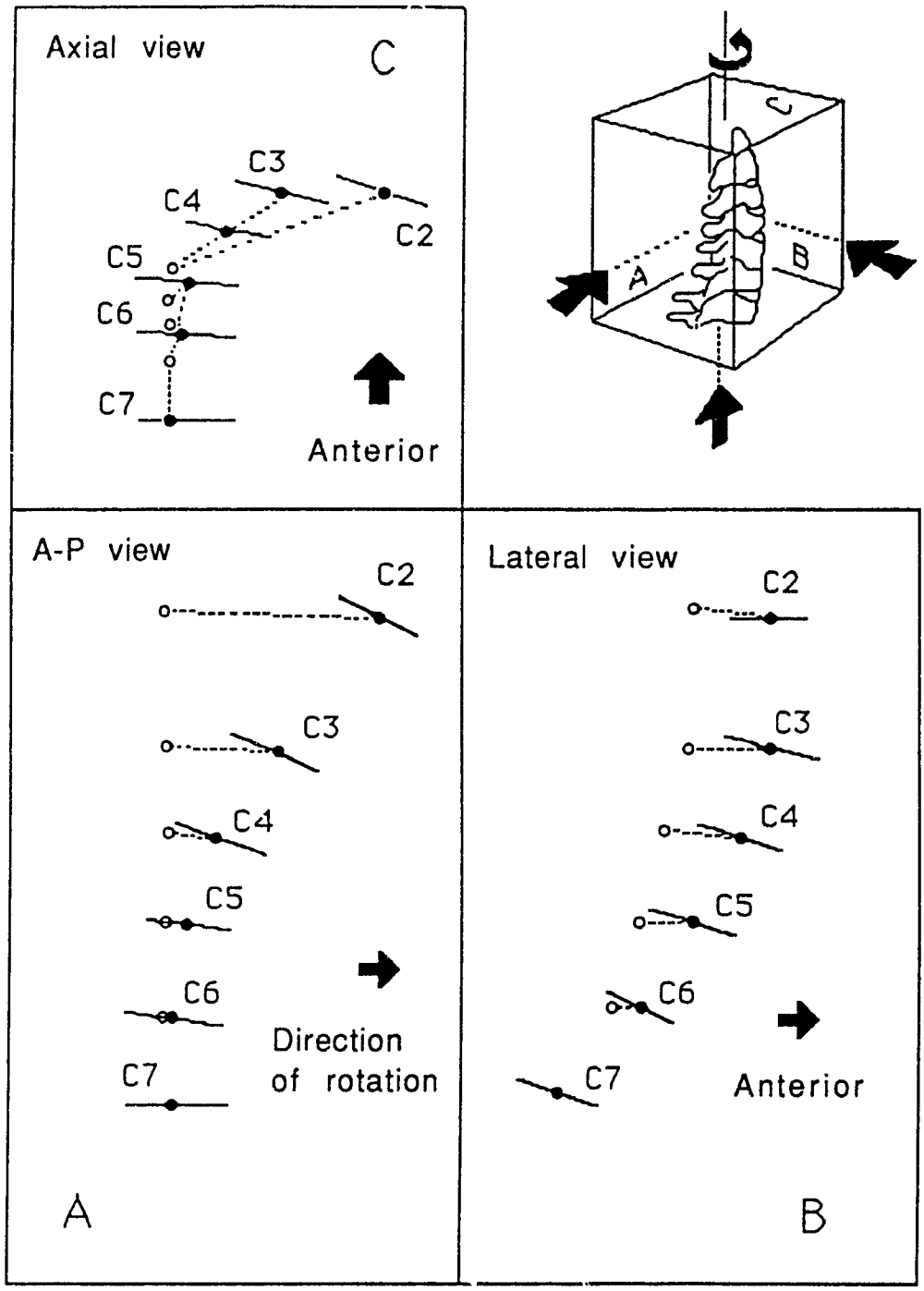

Fig A.5.3: The direction of coupling for lower and upper portions of the cervical spine. Adapted from Mimura et al. (1989). [9]

APPENDIX B: FURTHER INFORMATION RELATED TO THE EVALUATION OF THE INSTRUMENT

B.1 THE CERVISCOPE STANDARD REPORT

B.1.1 The Overview Page (page 1 of the standard report)

In addition to complete patient identification, this page contains neutral, forward flexion, and lateral bending views. The neutral position (labelled 'standing still') is presented from both the antero-posterior and lateral viewpoints. These may both be very useful in establishing a subject's condition. The A-P view will immediately indicate if the subject holds his/her head to one side, reflecting the possibility of lateral pathology - or incorrect positioning.

The lateral view of the neutral position, conversely, indicates the natural state of curvature in the subject's upper spine. An abnormal cervical lordosis or thoracic kyphosis may thus be identified. Recall from Appendix A.1 that straightening of the cervical lordosis is also thought to be anatalgic.[21] As we saw in Appendix A.1.5, Breig (1960) found that in normal motion the spinal cord folds and unfolds like an accordion.[100] However, it is possible that pathological subjects assume an anatalgic position in order to prevent pinching or clamping of the cord.[44]

Unfortunately, the lateral bending illustrated on the overview page of the standard report shows data only for either bending from left to right, or from right to left. The lateral view appearing on the screen when the report is printed will occur on the overview page by default. This requires caution when interpreting the data.

Nevertheless, this view indicates whether or not the subject is able to move his/her head laterally in a "normal" fashion. This should presumably result in a shape corresponding to half of a parabola. However, as we see in chapter 2 (section 2.3), the curve fitting by the software does not yet allow this.

The overview page also shows a view of sagittal flexion-extension. Full extension cannot be measured by the Cerviscope, since some of the IREDs become obscured at either end of this motion. However, a comparison of the measurable full flexion with the neutral position can still be useful.

In particular, the subject would be expected to exhibit exaggerated thoracic kyphosis and decreased cervical lordosis in forward flexion. If this does not occur, there

may be immediate cause for concern.

B.1.2 Sagittal Flexion Extension (movement 2)

The top of page 2 from the standard report illustrates forward flexion, showing gross motion, inter-segment mobility, and EMG data. This is referred to as movement 2 in the upper right corner of the page.

Below this appear various interpretations of the data performed by the Cerviscope software. This page thus combines and enhances the information from the corresponding screens of the Cerviscope report mode.

As described above, the forward flexion view indicates the change in lordosis and kyphosis in the upper spine. The display entitled 'inter-segment mobility' should thus show at a glance if intervertebral motion is impaired.

We saw in Appendix A.3 that compensatory hypermobility often occurs above and below fused or blocked vertebrae.[31] This should be evident from the curvature of the spine in forward bending.

Normal forward bending results in decreased lordosis in C2-C7 and increased kyphosis in T1-T6. The above should also be reflected in the areas designated "thoracic kyphosis" and "cervical lordosis" on the lower part of the page.

A reversed segmental curve in the neck is considered more significant than straightening of the lordosis. As we saw in Appendix A.1.4, this may indicate subluxation, ligament tear, or even disc herniation.[21]

B.1.3 Lateral Bending (movements 3 and 5)

The third and fourth pages of the standard report focus on lateral bending. The first considers bending from left to right, the second from right to left. Note that both pages are actually labelled 'Page 4' on the bottom right.

This is because the printout software still refers to the Spinoscope report, from which it was adapted. Page 3 of that report does not apply to the Cerviscope. The two versions of page 4 from the Cerviscope report are thus L-R and R-L lateral bending. These are referred to here as movements 3 and 5, respectively.

The tops of the pages for movements 3 and 5 include information on gross motion, intersegmental mobility, zoomed gross motion, and segmental orientation. The lower portion of these pages again illustrates various interpretations of the lateral bending data by the software.

A key factor to look for in lateral motion is symmetry between right and left bending. The gross motion for movements 3 and 5 should thus be compared. The relative rotation between vertebrae and subsequent contribution to overall motion should be determined from the intersegmental mobility display.

Another factor to consider is listing of the head when in the upright position. Listing can be seen from the gross motion and the segmental orientation displays. This may indicate induced derotation to compensate for an injury. Figure B.2.1 shows three examples of impaired lateral bending due to disc herniation.[79]

Interpretation of lateral bending for the Cerviscope is similar to that described in appendix E for the Spinoscope.[74] However, the curvature begins from the middle of the upper spine. For the lower spine the curvature starts near the bottom in lateral bending. According to Gracovetsky et al (1990), clinical diagnosis of more than one level of disc protrusion may not be possible from lateral bending studies.[29]

The Cerviscope display substitutes shoulder girdle movement for the pelvic motion of the Spinoscope. Since motion of the upper spine in relation to the shoulders is analogous to that of the lower spine with the pelvis, this appears to be a reasonable choice.

SPINEX MEDICAL TECHNOLOGIES INC.
1980 SHERBROOKE WEST, SUITE 1100
MONTREAL, QUEBEC
(514) 937 4751

TO:

RE: Spinoscope examination of [redacted] CERVICAL AST
SIN: [redacted] **W:** 135.0 lb **H:** 5 ft 7 **Sex:** F

Comment: PRIVEE
Visit comment: privee
Date: 18 JUN 1990 **Visit #:** 2 **Movement #:** 1 2 3

Date of injury:

Summary:

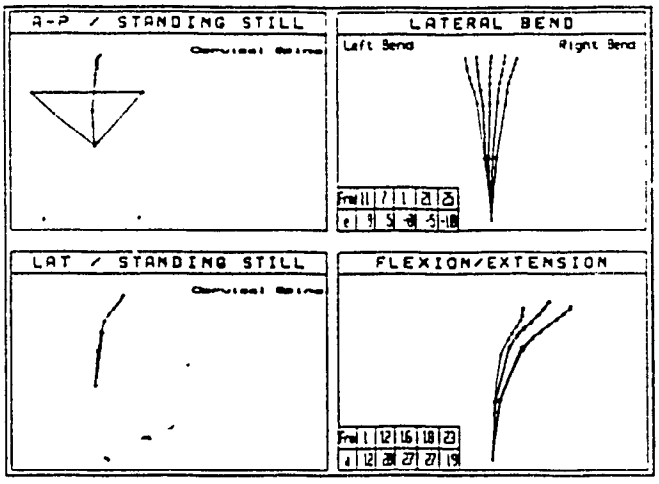

B. ROM Lateral Bending:

Left:	9 °	(20-30°)
Right:	10 °	(20-30°)

D. ROM Flexion / Extension:

Flex:	15 °	(80-90°)
Ext:	12 °	(20-30°)

FLEXION EXTENSION

Name: CERVICAL AST, [redacted] **SIN:** [redacted]
Date: 18 JUN 1990 **Visit #:** 2
Movement: Sagittal Flexion Extension **Movement #:** 2

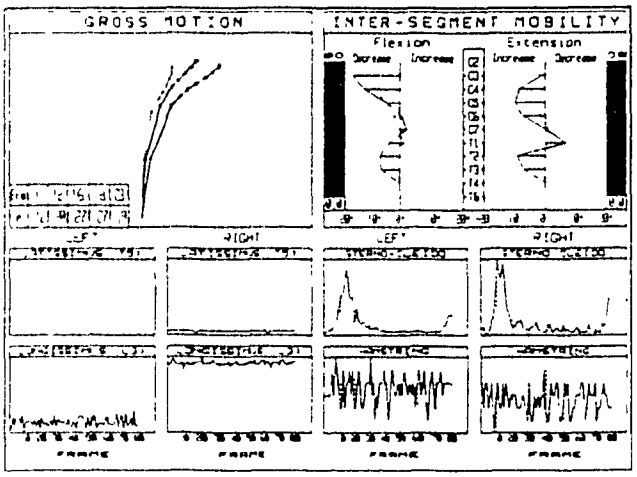

Intersegmental Mobility:
Normal
Abnormal
Restricted at
Excessive at

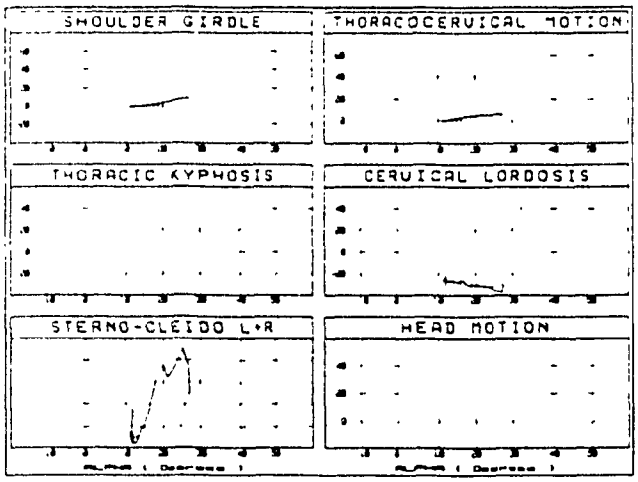

A. Shoulder Girdle: 57 % High

B. Thoracocervical Spine Motion: 43 % Normal

D. Cervical Lordosis Angle ROM: 16 • Low
ROM rate: 107 %

Tue Jul 24 1990 09:43

Ver. 5.00

LATERAL BEND

Name: CERVICAL AST, [redacted]
Date: 18 JUN 1990
Movement: Lateral Bend L-R

SIN: [redacted]
Visit #: 2
Movement #: 3

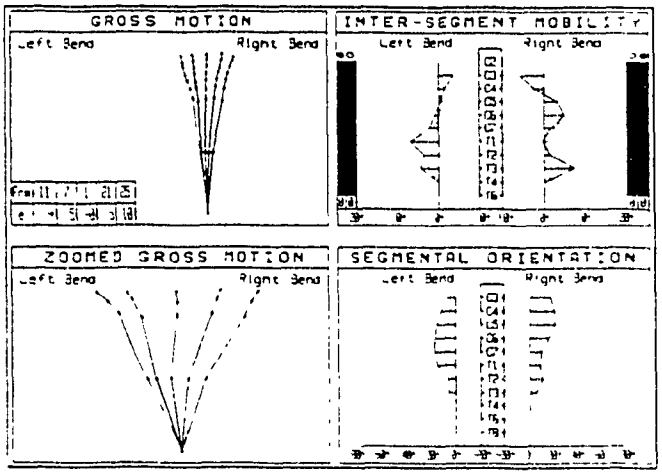

A. Gross Range of Motion:

Left:	9 °	(20-30°)
Right:	10 °	(20-30°)

B. Intersegmental Mobility:

	Left	Right
Normal		
Abnormal		
Restricted at		
Excessive at		

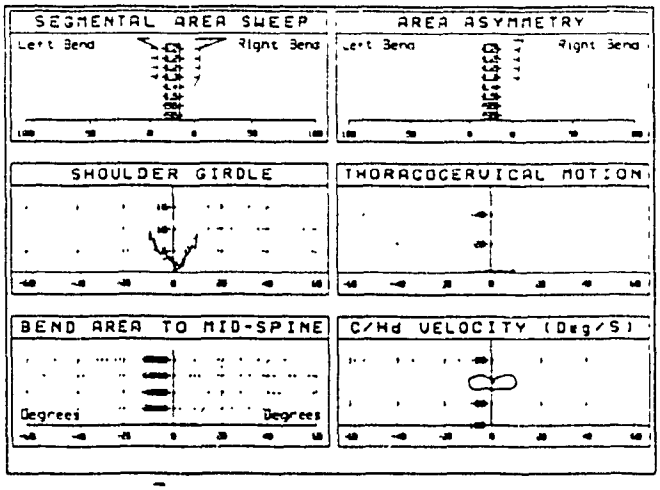

A. Segmental Area Sweep: Normal

Abnormal Motion: Left Right

Minor

C. Shoulder Girdle:

Left	79	%
Right	82	%

D. Thoracocervical Spine Motion:

Left	2	%
Right	4	%

F. Cervical / Head Velocity:

Normal Abnormal

LATERAL BEND

Name: CERVICAL AST, [redacted]
Date: 18 JUN 1990
Movement: Lateral Bend R-L

SIN: [redacted]
Visit #: 2
Movement #: 5

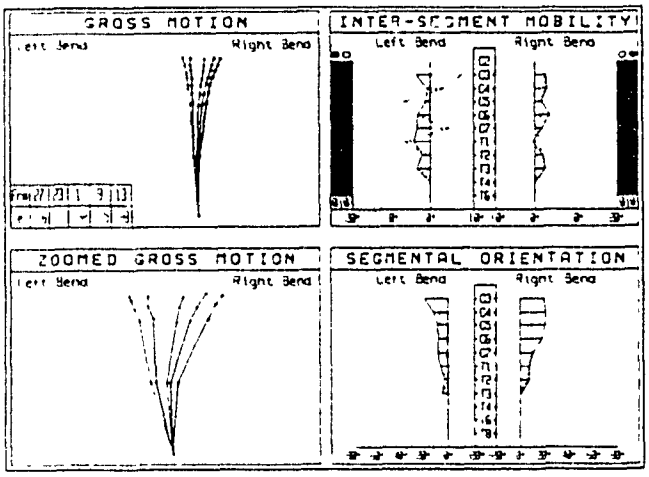

A. Gross Range of Motion:

Left:	8 °	(20-30°)
Right:	6 °	(20-30°)

B. Intersegmental Mobility:

	Left	Right
Normal		
Abnormal		
Restricted at		
Excessive at		

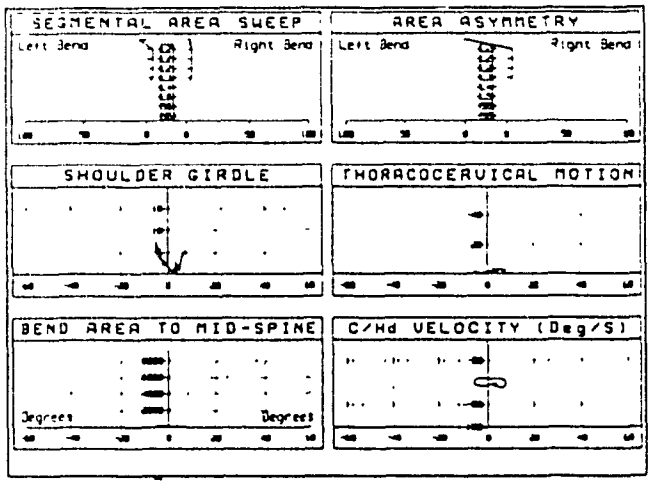

A. Segmental Area Sweep: Normal

Abnormal Motion: Left Right

Minor

C. Shoulder Girdle:

Left	79	%
Right	58	%

D. Thoracocervical Spine Motion:

Left	9	%
Right	13	%

F. Cervical / Head Velocity:

Normal Abnormal

Tue Jul 24 1990 10:11

Ver. 5.00

B.2 COMPARISON OF CERVICAL AND LUMBAR MOTION ANALYSIS

B.2.1 Characterizing the Functions of the Lower and Upper Spine

In studies of motion in the human spine, there are both differences and similarities between the various regions. The cervical and lumbar areas lend themselves particularly well to comparison, due to their respective physiological roles. While the lower back must support the weight of the entire torso, it must also provide a high degree of flexibility for normal locomotion.

The neck, conversely, supports only the weight of the head, but allows for an even greater range of motion. In contrast, movement in the thoracic spine is relatively constrained. The anatomy of these regions of the spine dictates how they each will move, but the interpretation of this motion remains controversial.

Our purpose here is to illustrate some of the similarities or differences in the analysis of motion in the cervical and lumbar spine. Recall that the overall analysis in the Spinoscope includes displays assessing cervical or lumbar lordosis, thoracic kyphosis, and inter-segmental mobility.

Characterization of coupled motion, to be described in chapter 3, involves a series of plots illustrating principal vs secondary motion. Principal movements include flexion-extension, lateral bending, and axial rotation These correspond to motion in the mid-sagittal, transverse, and coronal planes, respectively. We saw in figure 1.3.3 how these movements occur in the neck, as well as how flexion extension occurs for the entire spine.

We saw earlier in chapter 2 (section 2.2) that in the Cerviscope seven markers are affixed to the skin between C2 and T2, two more at T4 and T7, and three on the back of the head. Another IRED is placed above each of the iliac crests and the scapulae. EMG surface electrodes are placed above each of the sternocleidomastoid muscles. This configuration was illustrated in figure 2.2.2.

For the Spinoscope, twelve markers are placed above the spinous processes from S2 to C7. Two more are placed above the iliac crests, and the ankles. The two EMG electrodes are positioned bilaterally above multifidus at the level of L5. This configuration

is shown in figure 2.2.1, along with an overview of the entire Spinoscope system.

Here we will concentrate upon the comparison between the methodologies for motion analysis in the Spinoscope and Cerviscope. The Cerviscope testing protocol is analogous to that used for the Spinoscope. Yet the mechanisms of injury involved are generally different. For example, low back injuries often involve strains due to torsion combined with lifting. Neck injuries may also be due to torsion, but often in combination with sudden acceleration.

Smaller loads appear to be required to produce principal motion in the cervical spine.[11] Lateral translations coupled to lateral bending are smaller than for the lumbar area. Yet the accompanying rotations for the upper spine are larger than, and in the opposite direction to, those for the lower spine. Hence, neither the kinematics not the mechanics for these areas are quite the same.[67]

In the following sections we will attempt to identify some of the factors involved. The lumbar spine apperently distributes loads and transmits forces between various parts of the anatomy. Yet a heated controversy exists as to precisely how this is done (eg. the role of the thoracolumbar fascia, ligaments vs muscles, etc).[84,85,86]

The neck, conversely, needs only to support the head. However, this task includes stabilizing the head relative to the motion of the rest of the body. This involves complex responses to vestibular stimuli which are the subject of numerous investigations.[117,118]

A multitude of factors must be considered in understanding particular regions of the spine. The spinal cord, for example, is protected and distributed by the cervical and thoracic spinal columns - but not the lumbar. Conversely, the viscera of the abdomen are dependant upon the thoracolumbar spine to maintain their relative positions.

The vestibular system appears to interact with the neck to decouple the head from the motion of the body. However, the basic function of the neck may only be twofold:

i) to support, stabilize, and correctly orient the head, and

ii) to provide a venue for the passage of information, fluids, gases, and solids between the head and torso.

The forces involved are generally a fraction of those for the back. However, under high acceleration, the neck may support loads up to 50 g.[1] Optimization of some sort may

be performed by the central nervous system in order to stabilize head motion. For the lower back, an analogous optimization may occur to transmit heavy loads. Non-acute cervical dysfunction will often result in restricted head motion. Comparable lumbar pathology could lead to an inability to lift objects or walk without pain.

Dangerous loading to the lumbar spine may occur due to a large external moment. Another potential problem occurs when improper flexion occurs in the low back during a lift. A sudden, unexpected load may also result in soft tissue damage.[81] Yet, as we saw in Appendix A.1, these factors are comparable to situations which contribute to cervical spine injuries.

B.2.2 Analytical Techniques Used in Motion Analysis

Some techniques used to examine lumbar motion may be directly applied to the cervical spine. Gracovetsky and Farfan (1986) used computer generated drawings of the low back to characterize lumbar lordosis.[81] Their method may be equally applicable to the cervical spine.

The starting position was derived from the lateral upright standing radiographic view of a subject. Reference points on each disc were defined as the junction of the middle and posterior 1/3 of the discs.

The curve described by these points was then smoothly deformed to simulate lordotic changes in flexion-extension. The relative positions of all the muscles and ligaments were fully determined from this curve.

A similar approach was used by Helleur (1983) to model the soft tissues of the neck.[82] The result was a theory which described the reflexive muscle relaxation by pilots being ejected from aircraft. This sometimes fatal attempt to 'abort' the unacceptable load may be compared to a weightlifter purposely bailing out of a lift.[81]

Regarding the etiology of low back disorders, Gracovetsky and Farfan (1986) described two basic causes.[81] These are compression and torsional injuries. They involve damage to bone and ligamentous tissue, respectively. Both cases appear to result in similar symptoms.

Identifying the injury mode is not straightforward. However, a compression

fracture usually results in a painful response to forward or lateral flexion. Torsional failure, conversely, is characterized by pain following torsion of the spine in any direction.

These observations may be equally valid for the neck as for the lower back. It should be noted, though, that according to Adams (1987), the location of disc lesions does not support an etiology based on torsion.[84]

B.2.3 Determining Instability

Gracovetsky and Farfan (1986) related instability to the torque strength of the joint.[81] They found that as injuries diminish the ring of able layers of fibers in the annulus, torque strength decreases. Thus, instability occurs when this strength becomes less than the induced torque due to the load.

This is consistent with the definition of stability proposed by Pope and Panjabi (1985).[83] They perceived stability in the spine as being dependant upon restraints from ligaments, muscles and other soft tissues. The fibers of the annulus may conceivably be included in this group.

As we saw earlier, the nature of three-dimensional coupled motion in the spine depends upon the local anatomy. A spinal segment may nevertheless be stable in one direction while being unstable in another. Perhaps, then, stability should be treated as a mechanical entity, regardless of its origin. Instabilities in the cervical or the lumbar spine may thus be perceived as manifestations of the same condition.

Gracovetsky and Farfan (1986) identified some lower back control components to be the central nervous system, the sensory system, and muscular response.[81] This led them to suggest that a condition such as osteoarthritis may be attributable to a malfunction of the stress minimization strategy in the joints.

They also proposed that the posterior ligamentous structures could be involved in this control system. This hypothesis was supported by Yahia and Newman (1989), who found Pacinian and Ruffini receptors within these ligaments.[87] If these findings also apply to cervical ligaments, then the control hypothesis may be pertinent as well.

Some of the factors which may be involved in the control strategy for the cervical

spine are considered below (Appendix B.3). In order to help understand this material, a brief treatment of tensor algebra is also provided in Appendix C (together with the theory on linear transformations required as background for chapter 3).

B.2.4 Measuring EMG Activity

The Cerviscope report includes EMG data on only the sternocleidomastoid muscle in the neck, but this is meant to detect activity in underlying muscles as well.
The Spinoscope also reports on only one muscle.[74] There the firing of the multifidus is also considered indicative of the adjacent longissimus, illiocostalis, and gluteus muscles.

This is an important point, since the order of muscle firing may be crucial to the interpretation of motion data gathered by the Cerviscope.[77] In the case of the Spinoscope, ease of access to the multifidus muscle was used to help justify its selection for placement of EMG electrodes.[74] This may also be a reasonable argument for choosing the sternocleidomastoid in the neck.

One research group working with cervical EMG data, Schüldt and Harms-Ringdall (1988a,b), used electrodes on several neck muscles to examine neck pain in office workers.[12,13] They described the relationships between position and muscle activity during isometric extension. The configuration used by them was shown in fig A.2.1 of Appendix A.

They did not monitor the sternocleidomastoid directly, on the grounds that it is not activated during extension. They also pointed out that although subcutaneous muscles dominate, adjacent and deeper ones also contribute significantly to EMG activity.

Hence it is reasonable to assume that an electrode placed over the sternocleidomastoid will pick up splenius and levator scapulae activity. Schüldt and Harms-Ringdall (1988b) showed that only the activity of cervical erector spinae/trapezius and levator scapulae were influenced by neck position.[13] It is therefore conceivable that neck movement will cause the readings from the sternocleidomastoid electrode to change, through crosstalk from the levator scapulae.

This corresponds to findings during routine system testing prior to Cerviscope examinations (using the 'real time display' utility). In particular, the EMG from the

electrode over the sternocleidomastoid changes only if the subject presses a hand against his/her forehead (ie. isometric tension). Ordinarily, non-isometric movement does not result in EMG activity during such testing.

B.2.5 Physiological Significance of the Report

For the lumbar spine, the most comfortable lordosis chosen by a test subject was related to minimum EMG of multifidus by Gracovetsky (1987).[85] A single parameter, such as EMG, was thus never considered in isolation from others. This is reflected in the way the Spinoscope report screens display parameters in groups which are considered to be related. A similar approach was used to design the Cerviscope report displays.

For example, coordination between muscle firing and spinal motion is considered to be very specific in both the lumbar and cervical spine. Hence, the collection of EMG data is shown synchronously with spinal motion.

The ligamentous response is evaluated dynamically, due to the visco-elastic nature of the collagen fibers of which they are composed (ie. to avoid creep or hysteresis). Spinal function is generally emphasised over subjective symptoms, since the purpose of these instruments is to provide objective diagnoses. However, compensatory anomalies may indicate specific pathologies, which must also be recognized (eg. see Appendix A.3).[74]

One such instance occurs when facets remodel themselves to prevent pressure on a damaged disk.[76] Wolff's axioms of bone generation and absorption may be related to this phenomenon.[81] According to Gracovetsky (1988), how a given individual's spine responds to a specific task may be compared with some norm.[77] In the Spinoscope and Cerviscope, one criterion used for establishing this norm is the minimization or equalization of stress.

Another is the gradual unfolding of lordosis during the course of forward flexion. Failure of the lordosis to unfold is perceived as an attempt to avoid straining injured ligamentous tissue. Indeed, according to Herkowitz and Rothaman (1984), loss of cervical lordosis may also indicate instability.[78]

In lateral bending, protective scoliosis is interpreted as being indicative of injury

at a given level. Restriction in lateral movement or bending in the direction opposite to the gross motion are considered to be clues to this condition. Motion within individual segments is assumed to be impossible to control consciously. Hence, malingering can be identified by superposition of normal patterns with those of the supposedly injured patient.[77]

However, according to Gracovetsky et al (1990), localization to the correct intervertebral joint is not yet guaranteed.[29] It may therefore only be possible to detect general anomalies using skin markers (see Appendix A.4).

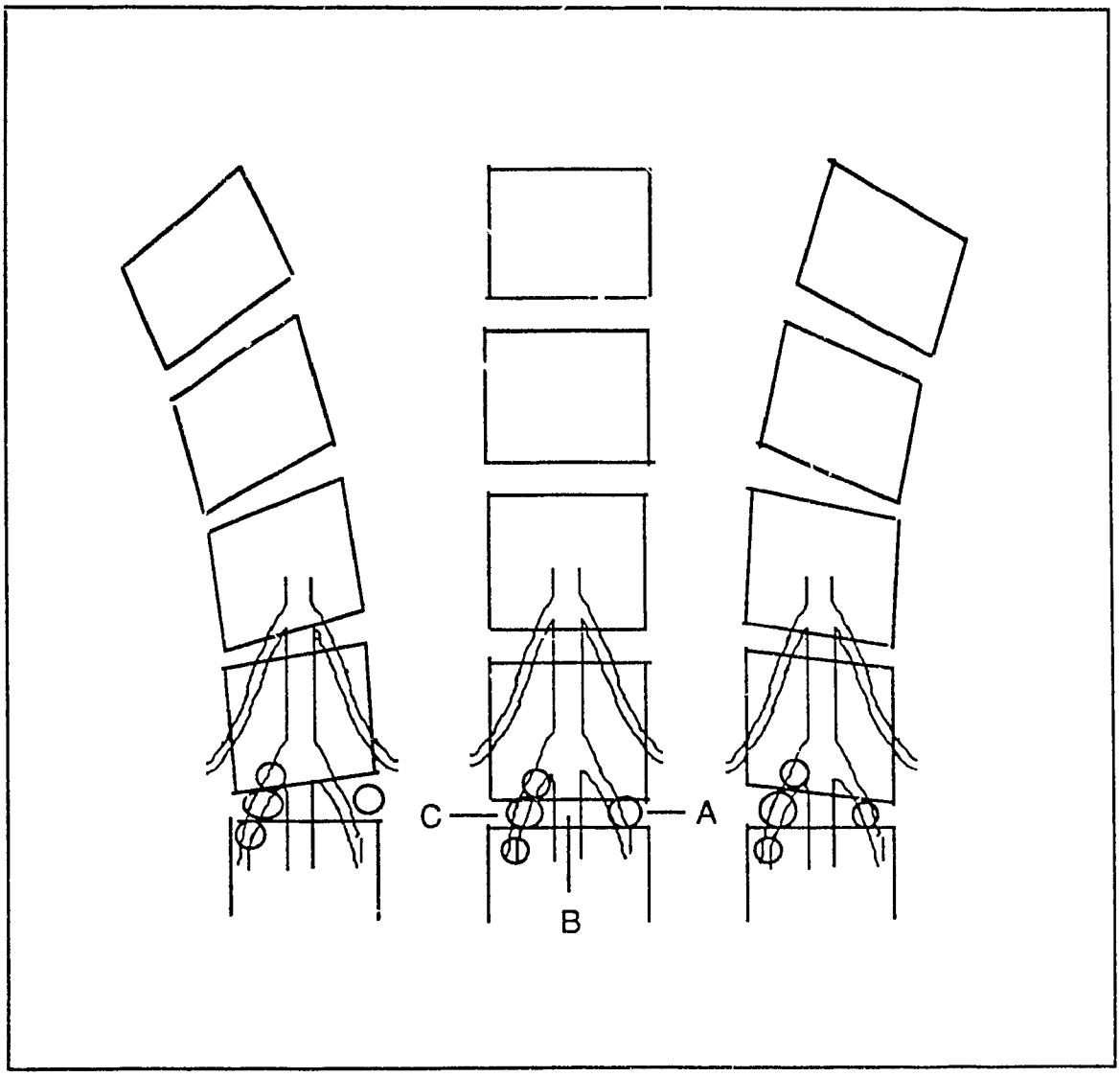

Fig B.2.1: Example of impaired (right) lateral bending due to herniated disc that is

a) lateral to the nerve root on the right,
b) medial to the nerve root on the left, or
c) entrapping the nerve root on the left.

Adapted from Weitz (1981). [79]

B.3 OPTIMAL CONTROL OF HEAD MOVEMENT

B.3.1 The Motor System of the Neck

More than 20 pairs of muscles link the skull, spinal column, and shoulder girdle in a variety of configurations.[124] The mechanical organization of both the muscular and skeletal structures would thus appear to influence the manner in which the nervous system will organize its neuronal output.

In man, head movements are usually categorized as flexion-extension, lateral bending, and rotation, according to the principle plane of motion along one of three orthogonal axes (see fig 1.3.3). In experimental animals, such as the cat, the corresponding vestibular terms are more commonly used. These are pitch, yaw, and roll, respectively.

However, when the animal is removed from a fixed reference frame, the movements required to elicit pitch, yaw, and roll will change. Hence, the descriptive terms of flexion-extension, lateral bending, and rotation may provide a more useful method of characterizing head movements. These terms do not depend on a particular relationship between posture and a gravity related reference frame.

The analysis of joint motion is closely related to the control of head movement. According to Richmond and Vidal (1988):[124]

" ... the articulations of the neck are deeply buried in soft tissue, and their motion can be difficult to monitor without highly specialized techniques. ... the maximal range of motion permitted at different cervical levels ... provides an important base of information for clinical assessments of musculoskeletal dysfunction."

This subject of cervical range of motion was considered in detail in chapter 1 (section 1.3.3) and Appendix A.3. We note here that there appears to be relatively little translatory motion between the C1 and C2 vertebrae of the upper cervical spine. The lower cervical column can undergo a more complicated, mixed movement that combines rotation with lateral flexion.

Richmond and Vidal (1988) continue:[124]

"Until recently, muscles crossing suboccipital joints have been considered to be

the prime movers of the head. However, muscles that operate across cervicothoracic joints must also play an important role in head movement by altering the position of the cervical column with respect to the rest of the body. ... Particular attention must (also) be paid to muscles that run between the scapula and the cervical vertebral column."

Neck muscles are characteristically arranged in layers. The muscles that link the skull to the vertebral column may be distinguished by the adjective "capitis" in their names.

The large size and ready accessibility of the long dorsal neck muscles have made these a common subject for experimental study. Each muscle is divided into serially linked compartments which are supplied by nerves from different segments of the spine.

The serial organization of compartments may have significance in the physiological control of long neck muscles. This is because effective shortening and development of external tension can only be achieved if the muscle components contract in a coordinated manner.

The long dorsal muscle may be specialized elements of a more extensive axial muscle system that runs the length of the spine. Hence, the "capitis" muscles are often matched by corresponding "cervicis" muscles that insert on cervical vertebrae rather than the skull.

The mechanical action of individual muscles has often been based on knowledge of muscle shape, attachment, and fiber architecture. However, these predictions may be quite arbitrary for neck muscles.

The long multiarticular muscles are usually assigned the role of turning, extending, or ventriflexing the head and neck. The shorter muscles close to the vertebral column are considered to "stabilize" the spine. More recent experiments have aimed at investigating the functional roles of neck muscles more systematically.

An unexpected result was found in comparing the EMG records from various neck muscles.[124] This was the extent to which EMG activity is synchronized from one muscle to another during some types of head motion. Such synchronization may suggest that the control mechanisms underlying motoneuron recruitment in neck muscles may be quite different from those in the lumbosacral spine.

B.3.2 Optimization Schemes from Traditional Biomechanics

As we saw in Appendix A.2, according to Schultz (1987) the choice of an objective function is a crucial factor in analytical models of spinal motion.[65] An indeterminate problem usually surfaces whenever analyses are undertaken to explain the forces and moments involved.

The number of unknowns often exceeds the number of equations of motion in dynamic problems (or equilibrium in static problems). Internal force estimates may be obtained by rendering the problem determinate through assumptions.

The models described in the biomechanics literature appear to fall into three categories: rigid-body models, lumped parameter deformable element models, and distributed-parameter deformable element models. Selection of the optimal solution from a number of possible solutions requires the choice of an appropriate cost function.[70] For example, one of the optimization schemes that is used minimizes the largest muscle contraction intensity needed to perform a task.[65]

A number of cost functions were investigated by Goel et al (1990).[70] Alternatives included minimization of anteroposterior disc force, the forces along the Y-axis, the work done by all components, and the work done by the posterior ligaments only. They selected minimization of anteroposterior shear in flexion/extension and of the work done by the posterior ligaments in lateral bending. According to them:

"In the absence of a direct experimental validation of the results predicted by the model, the appropriateness of the cost function chosen is not only hard to justify but assumes a very critical role."

They added that the formulation of an optimization based model requires the following data: lines of action, points of application, and physiological cross-section of muscles, as well as permissable stress intensities.

The above represent sampling of the optimization schemes that have been used in biomechanics applications. We now consider aspects of the alternative optimization schemes being considered in the neurophysiology literature.

B.3.3 Coordination Between Vestibular Input and Movement

Nashner et al (1988) considered head stabilization for subjects standing on a moving platform and adapting their posture to various perturbations.[118] They found that stabilization of the head is accomplished on a feedforwa.d basis by the simultaneous activation of hip and neck flexor muscles.

Their results suggested that control of head and body motions is coordinated during hip postural movement. They thus hypothesized that head and body motion may be controlled independently. The interaction of anticipatory and reactive control was also demonstrated when large perturbations forced subjects to use mixtures of ankle and hip responses.

The rotational orientation of the head was actively fixed with reference to gravity. This appeared to support the hypothesis that the vestibular system can be used as a 'reference sense'. Responses of patients with vestibular deficits further supported this hypothesis.

They concluded that there is significant interaction between mechanisms for organization of the senses and coordination of movements. Their results suggest that the pattern of postural movement selected depends on both the configuration of the support surface and the availability of sensory information.

Graf and Wilson (1989) considered afferent signals to the vestibular nuclei from receptors in the neck.30 They found that the best response vector orientation of neurons receiving vestibular input does not correspond to the semicircular canal geometry.

The response vector orientation of afferents from spindles in neck muscles were found to reflect the best pulling directions of the muscles in which they are located. Thus it was not considered surprising that they bear no relation to semicircular canal planes. However, they warned of the attempts by Pellionisz and Peterson (1988), which we will consider below, to model the sensorimotor transformations.[131]

According to Graf and Wilson (1989), our understanding of the spatial qualities of the afferents to the vestibular system and their relation to head-neck movement is still at an early stage.[130] Mechanical constraints limit the number of degrees of freedom of the head movement system. They thus suggested that a given motor control signal might

be economically distributed to multiple target sites which have the same functional context.

This calls for some kind of geometrical organization of the motor systems involved (see figure B.3.1). They suggested that the spatial organization of the semicircular canals in the head provides an optimal resolution for the detection of head movements in three dimensional space. Nevertheless, they concluded that how such information is utilized remains open to discussion.

B.3.4 A Tensorial Model for Control Optimization

Pellionisz (1984) described a controversial new model for the relationship between the central nervous and musculoskeletal systems.[132] Since the geometrical alignments of the vestibular receptors and the neck muscles have been measured experimentally, it may be possible to apply this model to the vestibulocollic reflex (VCR).[131]

This may allow us to predict the patterns of motor activation described earlier from the geometry of the receptors and effectors. It may also be possible to extend this model to voluntary neck movement.

According to the Pellionisz model, the central nervous system (CNS) must transform stimuli from the reference frame of the sensors into that of the motor system. As we saw earlier, tensors are mathematical operators expressing the relationships among vectorial representations in different frames of reference (see Appendix C for review of vector and tensor algebra).

The response of a sensor to a stimulus is independent of the responses of other sensors. It is proportional to the cosine of the angle between the sensor's axis of maximum sensitivity and the axis of the applied stimulus. The projection of a stimulus vector onto the sensor axis corresponds to the covariant representation, which we also defined earlier.

Conversely, the muscle activations that generate the response are not independent of one another. The forces or torques which they generate must be added in a parallelogram fashion to produce the desired movement. This corresponds to a contravarient representation.

The CNS may thus be perceived as a tensorial network. It converts covariant sensory input from one frame into a contravariant motor output in another frame. Pellionisz and Peterson (1988) described the tensorial model of the VCR as follows:[131]

"The VCR model has three transformation stages consisting of matrices that represent tensorial operations. Stage 1, a 3x3 matrix representing the vestibular metric tensor, converts vestibular sensory input from covariant to contravariant form. Stage 2, a 3x30 matrix representing the sensorimotor imbedding tensor, converts the signal from vestibular to neck motor coordinate frames. Stage 3, a 30x30 matrix,representing the neck motor metric tensor, converts the neck motor command from covariant to contravariant form."

The anterior, horizontal and posterior semicircular canals thus constitute a three dimensional reference frame.[133] Head movements are measured as the orthogonal projections of the movements on these axes. A compensatory head movement is then generated by the motor apparatus, using a 30-axis motor frame (see figure B.2.2).

However, the motor system is actually overcomplete.[131] There are thirty muscles generating head movements in three rotational degrees of freedom. Thus the number of independent muscles exceeds the number of degrees of freedom of the appendage which they control.

It follows that an infinite number of different muscle activation patterns can produce the same movement. An optimality criterion is required for choosing the particular pattern observed experimentally.

Pellionisz (1988) proposed a solution in the form of tensorial modelling.[133] This uses the difference between covariant and contravariant representations of the movement, expressed in the muscle frame of reference. The covariant representation can always be found uniquely by projecting the movement vector onto each of the muscle axes. The problem then, is to find a unique contravariant representation.

The central, covariant embedding tensor c_{ij} is considered to project the 3 sensory axes upon the 30 motor axes. This may be expressed as $c_{ij} = u_i \cdot v_j$, where **u** and **v** are the coordinates of the sensory and motor axes, respectively. Thus c_{ij} turns the physical contravariant input into the contravariant projection components.

However, two other conversions in the scheme are needed. The 3x3 sensory metric tensor g^{pr} converts covariant sensory reception into contravariant sensory perception. The 30x30 motor metric g^{ie} then converts the covariant motor intention into contravariant motor execution.

Mathematically, the required contravariant metric tensor g^{pr} can be expressed as the inverse of the covariant metric tensor g_{pr}. If g_{pr} is the scalar product of the vectors of coordinates in the sensory reference frame, then we have

$$g^{pr} = g_{pr}^{-1} = (u \cdot u)^{-1} .$$

Since the system is overcomplete, g_{pr} has an infinite number of inverses. The unique inverse g^{ie} that we seek can be obtained from the Moore-Penrose formula [134], given by the following sum of combined scalar and vector products:

$$g^{ie} = \Sigma_m \, 1/L_m \, (E_m \times E_m)$$

where E_m are the eigenvectors and L_m are the inverse eigenvalues of the system.

With the inverse thus calculated, the model predicts for each neck muscle a unique direction of head rotation for which that muscle should be maximally activated. According to Pellionisz (1988) , the model was found to correctly predict the VCR in decerebrate cats.[133]

Specific activation directions were consistently chosen by the cats from the infinite number of possible directions. This was considered to reflect an internal algorithm employed by the VCR to resolve the overcompleteness of the system.

In the vestibulocollic reflex, the muscles are maximally activated by rotations in planes other than the pulling ones. This may be due to the nonorthogonallity of the muscle axes. Again according to Pellionisz (1988), the tensorial model appears to correctly account for this as well.[133]

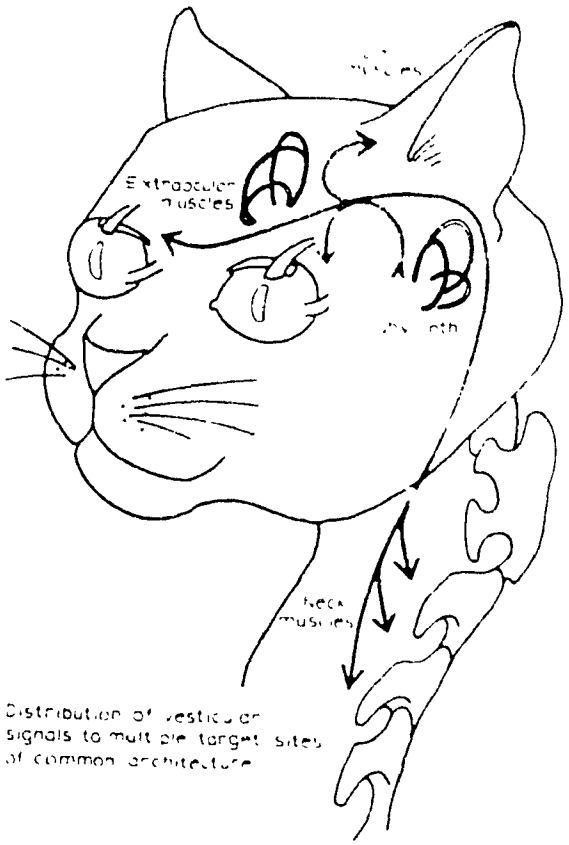

Fig B.3.1: Geometric organization of motor systems involved in the vestibular architecture. Adapted from Graf and Wilson (1989). [130]

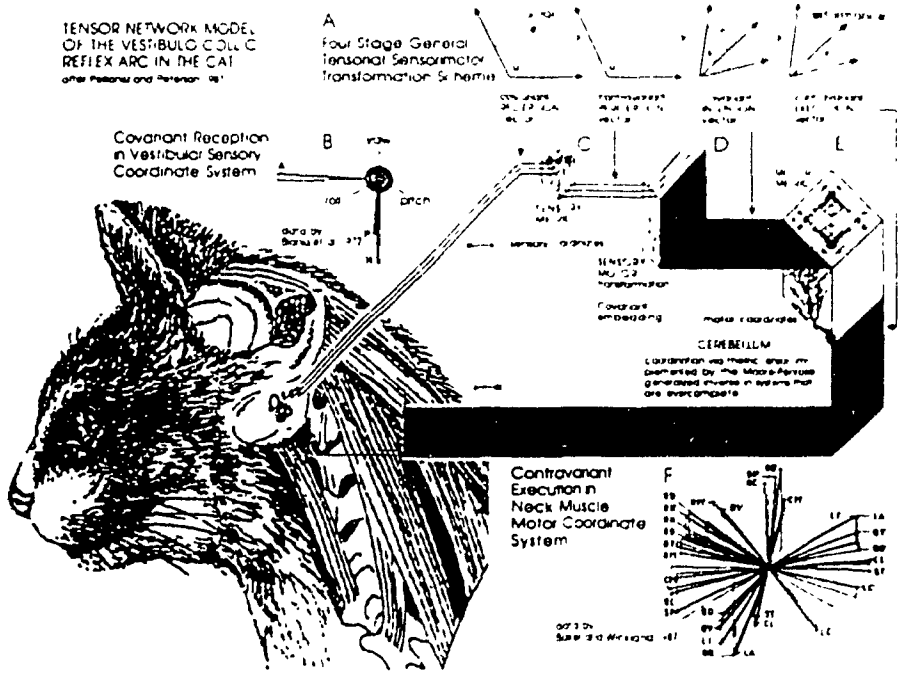

Fig B.3.2: Tensor network model of the vestibulocollic reflex arc in the cat. Adapted from Pellionisz and Peterson (1988). [134]

B.4 RESEARCH PROTOCOL AND INITIAL OBSERVATIONS

B.4.1 Initial Observations

A preliminary evaluation of the Cerviscope was performed using the data from twenty subjects. One group of subjects were randomly chosen volunteers examined at the Diagnospine Research lab [a]. The other group consisted of patients from an affiliated local clinic referred to here as AST.

The test procedures for examining these patients are described in research protocol below. This refers to the standard procedures now used for applying IREDs as precisely as possible on the subjects' neck and upper back. The protocol describes the research protocol designed for accumulating a database for the Cerviscope.

Figures B.4.1 and B.4.2 illustrate the standard report overview page for each of these subjects. There are several basic questions that can be posed immediately upon examination of this data. These are considered below.

Question: i) Are there clear differences between the representations of cervical motion among the various subjects ? If so, is there any noticeable pattern to these differences ? The answers to these questions will indicate if the Cerviscope is sensitive to variations among individuals.

Answer: The answer to the first part of this question appears to be 'yes'. Both flexion/extension and lateral bending views from figures B.4.1 and B.4.2 show distinct differences between subjects. The lateral 'standing still' view is similar for all subjects, but the question refers to dynamic views only. We will consider this further below.

The A-P 'standing still' view differs significantly between subjects. This is a reflection of the difficulty in placing the IREDs in a straight line on the patients. It also stems from the parallax effect due to their natural lordosis and kyphosis.

---

[a] Diagnospine is the research arm of Spinex, the manufacturer of the Cerviscope.

The answer to the second part of the question seems to be 'no'. There are no obvious patterns describing the differences between subjects. However, determination of these patterns would be equivalent to identifying specific pathologies. Hence, it is not surprising that this is not yet evident.

Question: ii) Is there a noticeable difference in the data for Diagnospine and AST subjects ? This is important in determining consistency of the Cerviscope from one installation to another.

Answer: Here it should be emphasised that all except the last three Diagnospine subjects were asymptomatic volunteers. The AST patients, conversely, were generally referred to that clinic for various neck problems.

Nevertheless, there are clear asymmetries in many of the Diagnospine subjects' views, particularly lateral bending. This may be due to adaptation to unsuspected abnormalities. Meanwhile, there are some apparently normal patients among the AST group.

Hence, there is not the pronounced difference expected among these two groups. Generally, the form of the curves for the various views is consistent for both groups. Thus the particular machine used to perform the examination does not appear to make an obvious difference.

Question: iii) Among the Diagnospine subjects, the first eight were examined by a single individual. The remaining examinations were performed by other personnel. Are there obvious differences between subjects 1-8 and 9-11 ? This, in turn, is important in determining consistency of the Cerviscope from one operator to another.

Answer: There appears to be no noticeable difference between the representations for the two groups. Recall that all three of subjects 9-11 were suspected of pathologies. However, as we shall see below, subjects 1-8 also appeared to exhibit some asymmetrical behaviour.

Question: iv) Are there any similarities between the various subjects ? There must be some consistency in order to identify normal patterns of motion.

Answer: The most obvious similarity among subjects is the lateral 'standing still' view. Hence, this may provide a standard by which other subjects may be judged. In other words, if this view is drastically different from the others, then that subject's entire set of data may be questionable.

The flexion/extension views exhibit similarities in general shape, but the changes in lordosis and kyphosis vary. This is encouraging, since these variations may provide an important diagnostic indicator (see section 2.2.3). The lateral bending views show very little similarity among subjects.

B.4.2 Research Protocol

The research protocol for the above preliminary study is described in the following pages [from Papagiannis, Asselin, and Roozmon (1990) [88]].

Cervical Spine Diagnosis: Research Protocol

Introduction

In recent years the cervical spine has become the subject of numerous biomechanical studies. Both in-vivo and in-vitro techniques have been employed to quantify the motion of the cervical spine segments.

It is also well established that diagnoses of non-acute injuries resulting from trauma are not evident and improperly diagnosed injuries may result in chronic long-term effects. Hyperextension and hyperflexion injuries were shown to be particularly conducive to this situation. Currently available systems (or instruments) for the purpose of cervical spine motion analysis do not lend themselves to routine evaluation of cervical soft tissue injuries. Hence, there appears to be a need for instrumentation that will permit objective clinical evaluation of patients.

The CERVISCOPE

The cervical spine diagnostic tool being evaluated is known as the CERVISCOPE. It is a modified version of the commercially available SPINOSCOPE which is used for thoracolumbar spine diagnoses; the CERVISCOPE functions and relies on the same principles (Refer to Spinoscope Documentation). The ability to objectively differentiate normal from pathological cervical segmental motion, Head-Cervical Spine-Shoulder coordination and muscular response should facilitate diagnosis.

Normative Data

A review of the literature related to cervical spine motion studies has shown that the available data is not readily usable with the CERVISCOPE. Hence, a complete set of normative data will be derived from CERVISCOPE examinations in conjuction with the current research. Normative data will provide a standard for comparison with subsequent evaluations of pathological subjects.

Research Protocol

The group of subjects to be examined with the CERVISCOPE may consist of people from the so called "normal" population (should conform with medically accepted standards of non-pathological spines) as well as people suffering from various non-acute cervical ailments.

Each subject should undergo a series of standard radiographs followed by a CERVISCOPE examination and independent clinical diagnosis (refer to the respective protocols below).

I. Para-Clinical Evaluation: Radiographs

Radiographs (X-rays) should be taken with all subjects wearing the CERVISCOPE harness as instructed by Diagnospine Research (refer to attached diagram). A small metallic chain acting as a plumb line should be hung in front of the exposure plane of all radiographs to insure proper identification of the vertical. The X-ray apparatus should be positioned so that the angle of incidence is 90 degrees.

The following protocol is suggested:

a) Three (3) A-P for lateral bending:
   - a.1 Full flexion to the left;
   - a.2 Standing Still (neutral position);
   - a.3 Full flexion to the right.

b) Three (3) lateral for flexion / extension:
   - c.1 Standing Still (neutral position);
   - c.2 Full Sagittal flexion;
   - c.3 Partial Sagittal flexion.

NOTE: To minimize iradiation exposure with "normal" subjects, either A-P or lateral radiographs (3) for each subject will suffice.

II. CERVISCOPE Standard Evaluation

Subjects should be sitting on a stool with the head and cervical spine complex moving inside the volume of the calibration frame (Refer to SPINOSCOPE Documentation on Calibration procedures). Subjects should be harnessed as instructed by Diagnospine personnel during installation of the CERVISCOPE (Refer also to the attached diagram). Please cut the round double-sided adhesive stickers as shown on the attached diagram to eliminate interaction between adjacent ones on the cervical spine.

The following movements should be performed:

1- Standing Still
2- Sagittal Flexion / Extension*
3- Lateral Bend L / R
4- Sagittal Flexion / Extension*
5- Lateral Bend R / L
6- O / M Rotation Neutral to Left
7- O / M Rotation Neutral to Right
8- Standing Still
9- **

* Full Extension movements cannot be recorded with the CERVISCOPE in its current implementation. Please, instruct the subject to return to the Neutral position after Flexion.

** Cerviscope data may also be recorded while the subject is walking on a treadmill. In some pathological cases this may be the only alternative measurement of neck function.

III. Clinical Evaluation

Independent clinical diagnoses should iclude a complete medical history of the subject and a detailed description of the clinical examination (Pain questionnaire, tests performed etc.) in order to establish possible normality criteria and help correlate clinical findings with Cerviscope evaluation. Clinical diagnoses may be based on any diagnostic tool other than the CERVISCOPE. One should note that MRI results will be beneficial in establishing pathological cases, particularly if

neurological dysfunction is suspected.

IV. Record Keeping

Good record keeping will allow for reliable data interpretation and help produce results in a reasonable time. Please retain the following for each patient examined:

i. Radiographs, clearly marked with the subject's name and the date of the exam. The vertical must be clearly visible.
ii. Data disk(s) from the CERVISCOPE (Archive Utility) (Printed reports are optional).
iii. Clinical evaluation, signed by attending physician.
iv. All other para-clinical evaluations received (i.e. MRI results) as fully documented as possible.
v. Personal records. Information required: Name, Age, Sex, Height and Weight.
vi. A photograph, if possible, of the IRED and EMG configuration on the subject.

Remarks

The present research proposal was prepared by Diagnospine Reasearch Inc. If you feel that certain omissions have been made, if you have any suggestions on improving the research protocol or if you would like any further clarifications or assistance from Diagnospine Research, please feel free to contact us. Any feedback received will be greatlly appreciated.

Fig B.4.1: Overview of Diagnospine subjects.

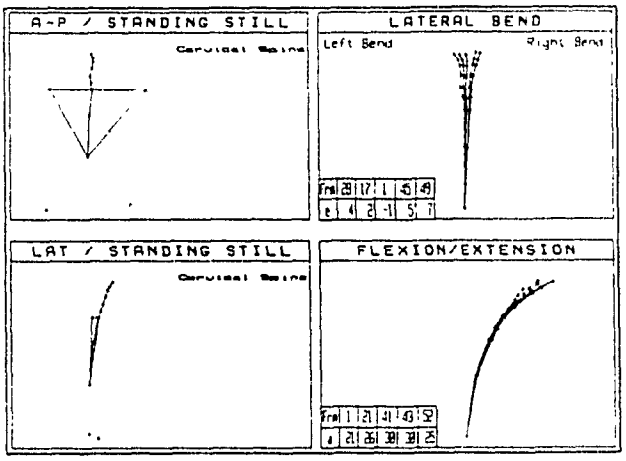

Subject ST.

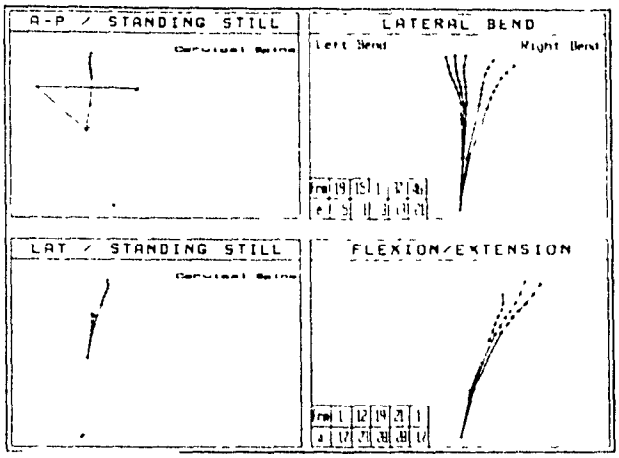

Subject RM.

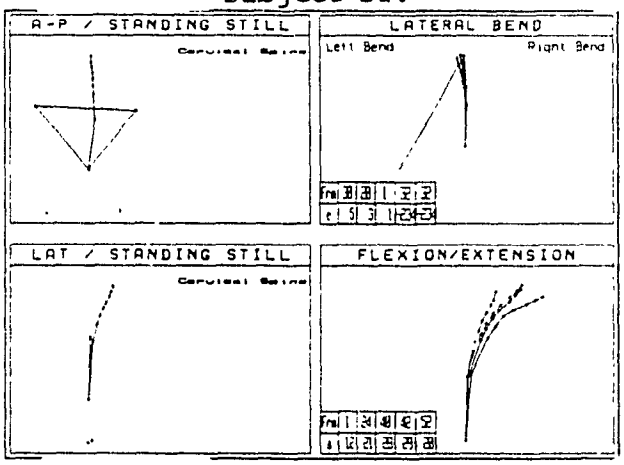

Subject HZ.

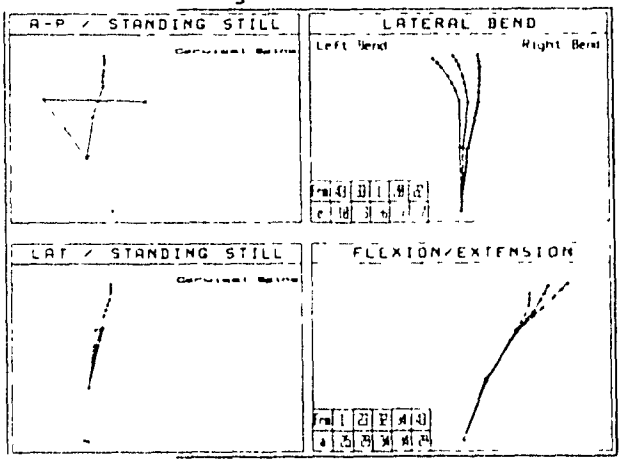

Subject BB.

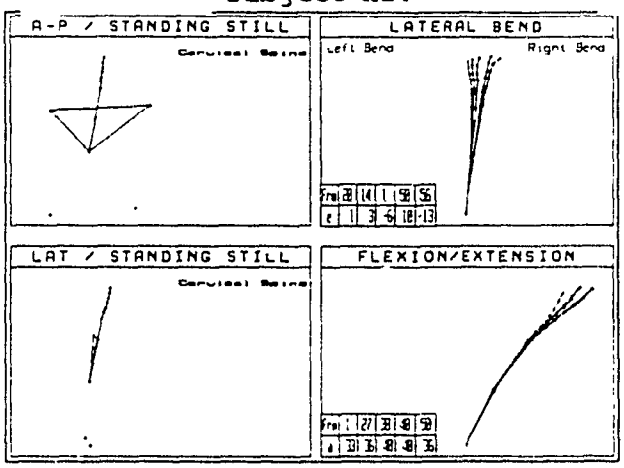

Subject MC.

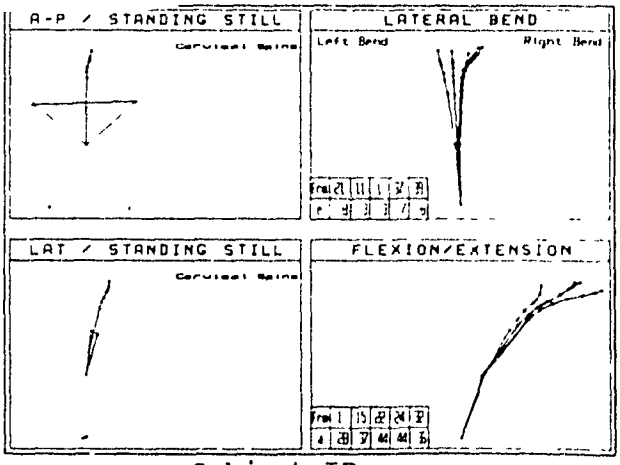

Subject ID.

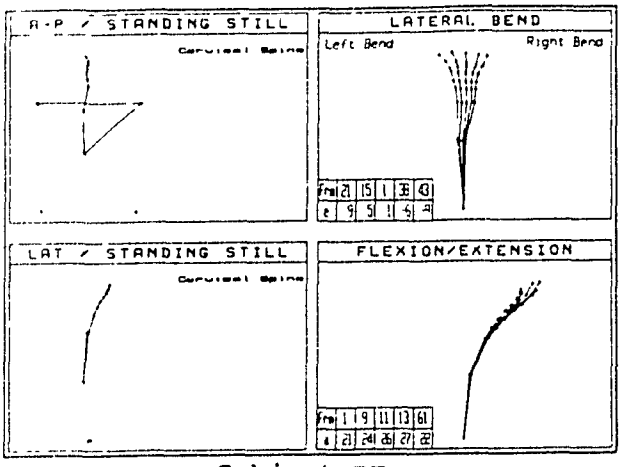

Subject RF.

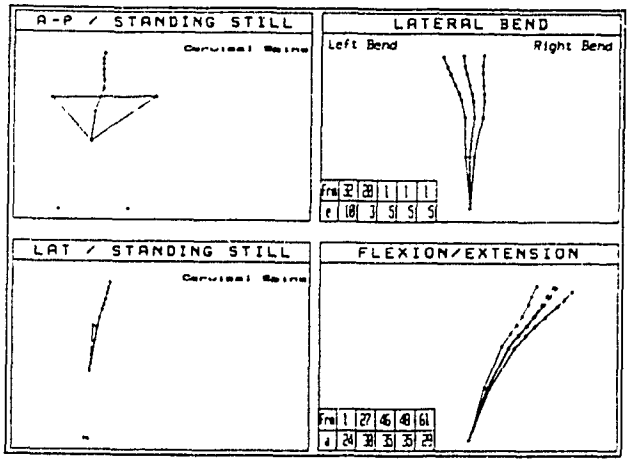

Subject RZ.

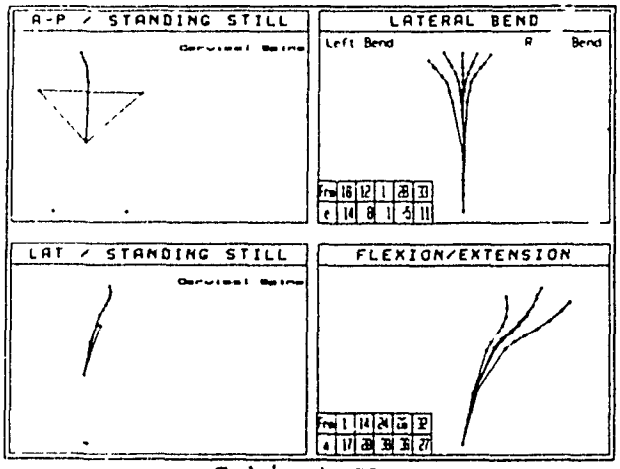

Subject SAG.

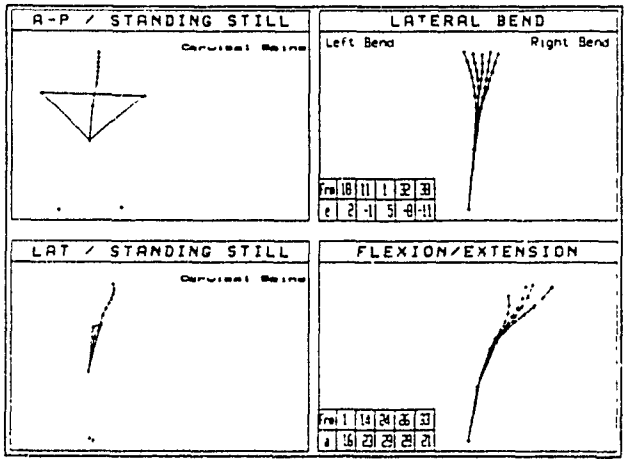

Subject SA.

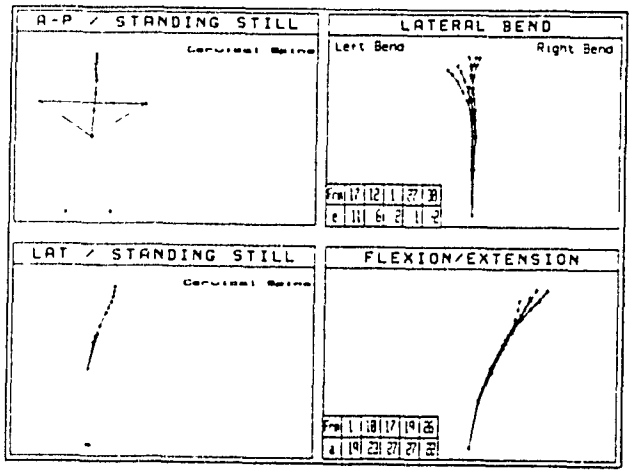

Subject AG.

Fig B.4.2: Overview of AST subjects.

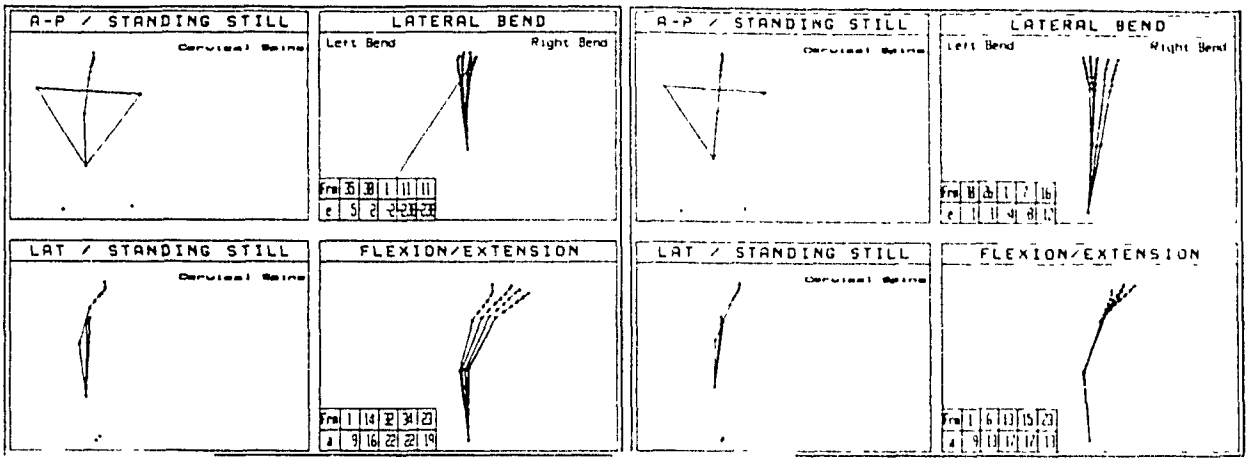

Subject CA.

Subject NB.

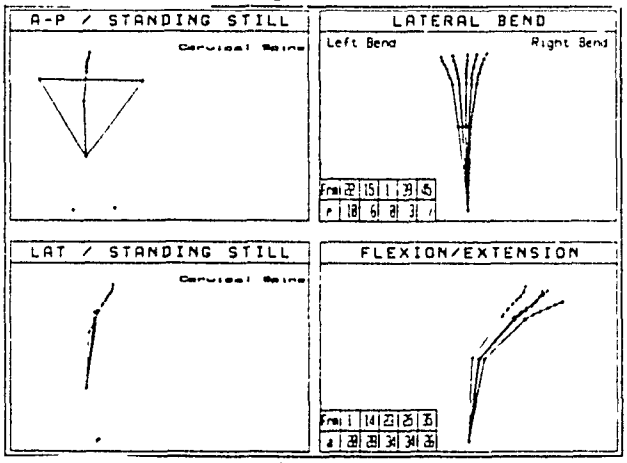

Subject LC.

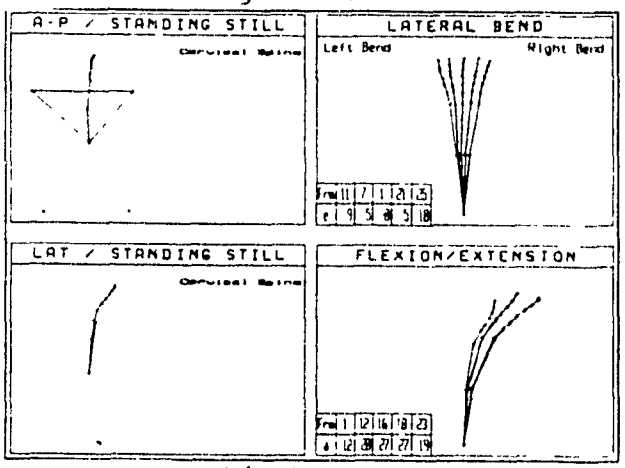

Subject MD.

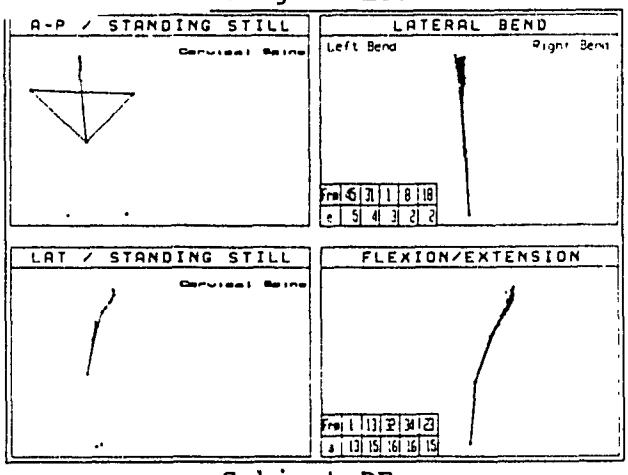

Subject DF.

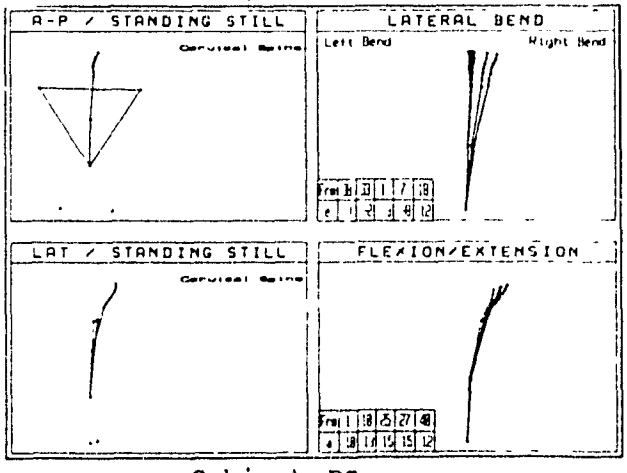

Subject PG.

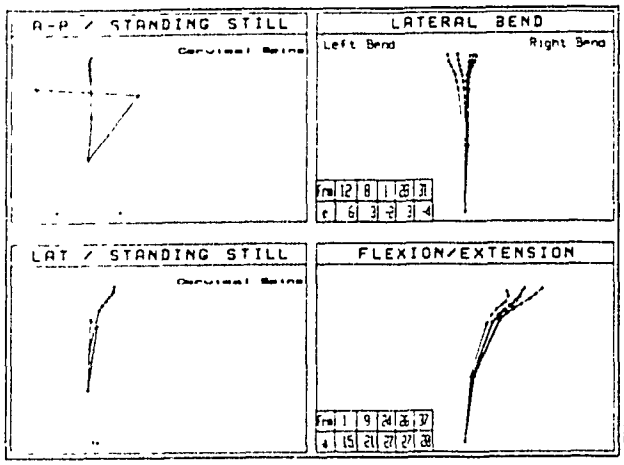

Subject PK.

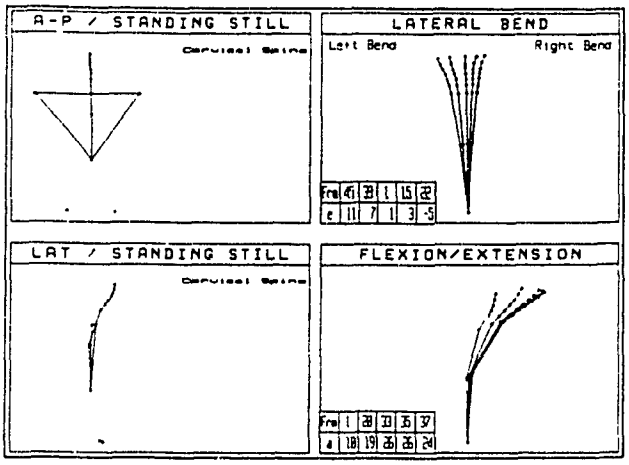

Subject ML.

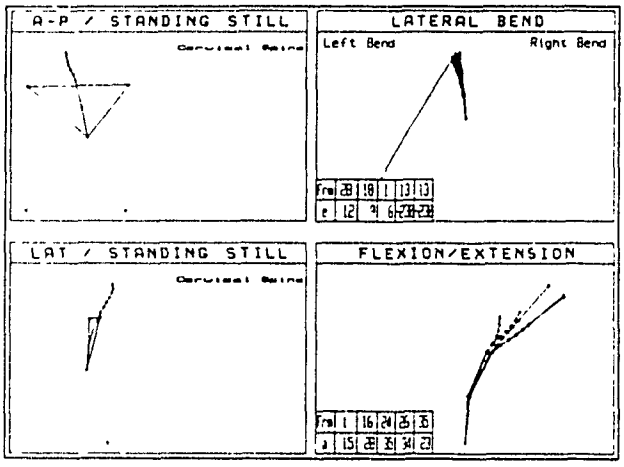

Subject RT.

APPENDIX C: VECTORS IN THREE DIMENSIONAL SPACE

C.1 Direction and Euler Angles

C.2 Transformation Matrices

C.3 Tensor Algebra

C.4 General Linear Transformations in 3D Space

C.5 Covariant and Contravariant Representations

C.1 DIRECTION AND EULER ANGLES

In order to describe the three dimensional orientation of a vector in space, we may refer to the angles made by the vector with the three principal axes. Figure C.1.1 (a) shows how these 'direction angles' α, β, and τ may be defined. Their cosines are referred to as 'direction cosines'.[137]

The three dimensional direction angles may easily be derived from the 2D projections of the 3D vector onto the three principal planes. This derivation was shown in figure 3.2.4 for the direction angles which were defined in chapter 3 for characterizing coupled joint motion. However, there they were called α, ϵ, and θ to be consistent with the nomenclature used for the Cerviscope and Spinoscope.

When these angles are used to describe the rotations of a reference frame, then they are referred to as 'Eulerian angles'. Figure C.1.1 (b) shows the relation of the Euler angles to the fixed and rotating reference frames.[138]

These are often described in terms of angles of nutation, precession, and proper rotation (ie. as in the motion of a gyroscope). The angle of nutation β is that between the positive directions of the z and z' axes. The angle α is the angle of precession, and τ is the angle of rotation. The transformation from one reference frame to another using Euler angles is described in detail below (see figure C.2.1).[139]

C.2 TRANSFORMATION MATRICES

In a plane, a second order transformation matrix may be used to describe a rotation between two orthonormal bases $(\mathbf{i},\mathbf{j})$ and $(\mathbf{i}',\mathbf{j}')$. If

$$\mathbf{i}' \cdot \mathbf{i} = \mathbf{j}' \cdot \mathbf{j} = \cos\alpha \quad \text{and} \quad \mathbf{i}' \cdot \mathbf{j} = -\mathbf{j}' \cdot \mathbf{i} = \sin\alpha$$

defines a rotation, then it follows that

$$\mathbf{i}' = \cos\alpha\mathbf{i} + \sin\alpha\mathbf{j} \text{ and } \mathbf{j}' = -\sin\alpha\mathbf{i} + \cos\alpha\mathbf{j}. \quad (1)$$

Hence, if the (**i**,**j**) frame is denoted by F, the component matrices of **i'** and **j'** in the frame F are the columns of the transformation matrix R, defined by:

$$\mathbf{R} = \begin{bmatrix} \cos\alpha & -\sin\alpha \\ \sin\alpha & \cos\alpha \end{bmatrix} \qquad (2)$$

This leads to the more general result representing the transformation of a vector **v** in (**i**,**j**) to **v'** in (**i'**,**j'**). We therefore have

$$\mathbf{v} = v_1\mathbf{i} + v_2\mathbf{j} \quad \text{and} \quad \mathbf{v} = v'_1\mathbf{i}' + v'_2\mathbf{j}'. \qquad (3)$$

Substituting from (1) into (3) gives

$$\mathbf{v} = (v'_1\cos\alpha - v'_2\sin\alpha)\mathbf{i} + (v'_1\sin\alpha + v'_2\cos\alpha)\mathbf{j} \qquad (4)$$

and using matrix notation leads to the result that

$$\begin{bmatrix} v_1 \\ v_2 \end{bmatrix} = \begin{bmatrix} v'_1\cos\alpha - v'_2\sin\alpha \\ v'_1\sin\alpha + v'_2\cos\alpha \end{bmatrix}$$

$$= \begin{bmatrix} \cos\alpha & -\sin\alpha \\ \sin\alpha & \cos\alpha \end{bmatrix} \begin{bmatrix} v'_1 \\ v'_2 \end{bmatrix}$$

or $V = \mathbf{R}\mathbf{V}'$, (5)

where **V** and **V'** are the column matrices shown above, and **R** is the transformation matrix defined earlier.

Similarly, the 3D transformation from

$\mathbf{v} = v_1\mathbf{i} + v_2\mathbf{j} + v_3\mathbf{k}$ to $\mathbf{v}' = v'_1\mathbf{i}' + v'_2\mathbf{j}' + v'_3\mathbf{k}'$ (6)

can be expressed by

$$\mathbf{v} = \left(\Sigma_q\ l_{1q}v'_q\right)\mathbf{i} + \left(\Sigma_q\ l_{2q}v'_q\right)\mathbf{j} + \left(\Sigma_q\ l_{3q}v'_q\right)\mathbf{k} \qquad (7)$$

where

$$L = \begin{bmatrix} l_{11} & l_{12} & l_{13} \\ l_{21} & l_{22} & l_{23} \\ l_{31} & l_{32} & l_{33} \end{bmatrix} \qquad (8)$$

is the 'orthogonal matrix', such that:

$$\begin{aligned} \mathbf{i}' &= l_{11}\mathbf{i} + l_{21}\mathbf{j} + l_{31}\mathbf{k}, \\ \mathbf{j}' &= l_{12}\mathbf{i} + l_{22}\mathbf{j} + l_{32}\mathbf{k}, \\ \mathbf{k}' &= l_{13}\mathbf{i} + l_{23}\mathbf{j} + l_{33}\mathbf{k}. \end{aligned} \qquad (9)$$

Now, since $(\mathbf{i},\mathbf{j},\mathbf{k})$ and $(\mathbf{i}',\mathbf{j}',\mathbf{k}')$ are unit vectors, it follows that

$$\Sigma_q\, l^2_{q1} = \Sigma_q\, l^2_{q2} = \Sigma_q\, l^2_{q3} = +1, \qquad (10)$$

where the summation is for q =1,2,3.

Furthermore, since $\mathbf{i}',\mathbf{j}',\mathbf{k}'$ are mutually orthogonal, their scalar products are zero.

Therefore :

$$\Sigma_q\, l_{q1}l_{q2} = \Sigma_q\, l_{q1}l_{q3} = \Sigma_q\, l_{q2}l_{q3} = 0, \qquad (11)$$

where the summation is again over q = 1,2,3.

Using the 'Kronecker delta' notation the six equations defined by (10) may be written as

$$\Sigma_q\, l_{qp}l_{qr} = \delta_{pr}\ , \qquad (p,r = 1,2,3). \quad (12)$$

where $\delta_{ks} = 1$ if k=s and 0 otherwise.

Hence, applying this notation to (7), we have the result that:

$$v_p = \Sigma_q\, l_{pq}v'_q\ , \ (p = 1,2,3) \text{ or } \mathbf{V} = \mathbf{LV}', \quad (13)$$

which describes the change of reference frame for the column vectors $\mathbf{v}$ and $\mathbf{v}'$.

From equation (9) it can be seen that the columns of L are the component matrices of $\mathbf{i}',\mathbf{j}',\mathbf{k}'$ relative to $\mathbf{i},\mathbf{j},\mathbf{k}$. We now define 'right hand' and 'left hand' reference frames by the conditions that the determinant $|L| = +1$ or $|L| = -1$, respectively. This is equivalent to saying that the vector product $\mathbf{k}' = \mathbf{i}' \times \mathbf{j}'$ or that $\mathbf{k}' = -\mathbf{i}' \times \mathbf{j}'$.

A three dimensional transformation from the frame $(\mathbf{i},\mathbf{j},\mathbf{k})$ to any other right handed frame $(\mathbf{i}',\mathbf{j}',\mathbf{k}')$ can be effected by three successive rotations through the Eulerian angles α,β, and γ.

In figure C.2.1, the transformation from $\mathbf{i},\mathbf{j},\mathbf{k}$ to

i',j',k' begins with a rotation through angle α about OZ. The transformation matrix representing the rotation is

$$\mathbf{R}_1 = \begin{bmatrix} \cos\alpha & -\sin\alpha & 0 \\ \sin\alpha & \cos\alpha & 0 \\ 0 & 0 & 1 \end{bmatrix}$$

The next rotation is through angle ß about the axis OA, and the third rotation by τ is about the axis OD. The matrices representing these two rotations are, respectively

$$\mathbf{R}_2 = \begin{bmatrix} 1 & 0 & 0 \\ 0 & \cos\beta & -\sin\beta \\ 0 & \sin\beta & \cos\beta \end{bmatrix} \quad \text{and} \quad \mathbf{R}_3 = \begin{bmatrix} \cos\tau & -\sin\tau & 0 \\ \sin\tau & \cos\tau & 0 \\ 0 & 0 & 1 \end{bmatrix}.$$

The three rotations may be considered to give a single transformation matrix $\mathbf{R} = \mathbf{R}_1\mathbf{R}_2\mathbf{R}_3$ which takes **i,j,k** into **i',j',k'**, where

$$\mathbf{R} = \begin{bmatrix} \cos\alpha\cos\tau-\sin\alpha\cos\beta\sin\tau & -\cos\alpha\sin\tau-\sin\alpha\cos\beta\cos\tau & \sin\alpha\sin\beta \\ \sin\alpha\cos\tau+\cos\alpha\cos\beta\sin\tau & -\sin\alpha\sin\tau+\cos\alpha\cos\beta\cos\tau & -\cos\alpha\sin\beta \\ \sin\beta\sin\tau & \sin\beta\cos\tau & \cos\beta \end{bmatrix}$$

This can be generalized to the rotation of a vector **v** in **i,j,k** to **w** in **i',j',k'**, where $\mathbf{w} = v_1\mathbf{i}' + v_2\mathbf{j}' + v_3\mathbf{k}'$. Substituting in equation (9), with **L** replaced by the rotation matrix $\mathbf{R} = (r_{pq})$ above, we have

$$\mathbf{w} = (\Sigma_q\, r_{1q}v_q)\mathbf{i} + (\Sigma_q\, r_{2q}v_q)\mathbf{j} + (\Sigma_q\, r_{3q}v_q)\mathbf{k} \quad (14)$$

so that the components of w in the **i,j,k** frame F are

$$w_p = \Sigma_q\, r_{pq}v_q\,. \quad (15a)$$

In matrix form, this equation is the same as (5) in 2D space. Hence, in 3D space we have

$$\mathbf{W} = \mathbf{RV}. \quad (15b)$$

Note that the effect of rotating the vector is the operation (15) above on **V**, while the effect of rotating the reference frame is the operation of $\mathbf{R}^{-1}$ on **V** (ie. since **R** is an orthogonal matrix then the inverse $\mathbf{R}^{-1}$ exists and is equal

to the transpose $\mathbf{R}^T$). Hence, it follows that

$$\mathbf{V} = \mathbf{R}^{-1}\mathbf{W} = \mathbf{R}^T\mathbf{W} \ . \qquad (16)$$

C.3 TENSOR ALGEBRA

We now consider the topic of tensors in 3D space. This follows from the vector analysis presented earlier and is useful in examining general transformations.

A second rank tensor **T** is a mathematical entity described by nine quantities t_{pq} (p,q = 1,2,3) relative to a given basis. Each suffix p,q of t_{pq} transforms like a vector suffix under rotation.

Tensors of rank n > 2 can be defined similarly. A tensor **T** of rank n has 3^n components $t_{pq\ldots r}$ (p,q,...,r = 1,2,3) where there are n suffixes p,q,...,r.

Recall that a vector **V** in 3D space is uniquely determined by its three components v_p relative to a basis **i,j,k**. These components obey the transformation laws (15) and (16) above.

Hence, if the nine components of **T** relative to a basis **i',j',k'** are t'_{rs} (r,s = 1,2,3), then the transformation law (13) is generalized to

$$t_{pq} = \Sigma_r \Sigma_s \, l_{pr} \, l_{qs} \, t'_{rs} \quad (p,q = 1,2,3) \qquad (17)$$

where **L** is the transformation matrix and summations are over values 1,2,3.

It may be convenient to regard (t_{pq}) as a 3x3 matrix **T** , with p labelling the rows and q the columns. Then

$$t_{pq} = \Sigma_r \Sigma_s \, l_{pr} \, t'_{rs} \, l_{sq}^T \qquad (18)$$

where $t'_{rs} = \Sigma_p \Sigma_q \, l_{rp}^T \, l_{sq}^T \, t_{pq}$

$$= \Sigma_p \Sigma_q \, t_{pq} \, l_{rp} \, l_{sq} \qquad (19)$$

is the inverse transformation involving the matrix $\mathbf{L}^{-1} = \mathbf{L}^T$.

We can now write the equations (18) and (19) as $\mathbf{T} = \mathbf{L}\mathbf{T}'\mathbf{L}^T$ and $\mathbf{T}' = \mathbf{L}^T\mathbf{T}\mathbf{L}$, respectively. This is a generalization of the equations for rotating vectors and reference frames given by equations (15b) and (16).[113]

C.4 GENERAL LINEAR TRANSFORMATIONS IN 3D SPACE

Let us now consider general linear transformations in 3D space. The operations of rotating a reference frame or a vector, considered earlier, were only a subset of all linear transformations. Each 3x3 matrix **A** defines a linear transformation of a 3 component vector **v** in 3D space.

The transformation analogous to equation (9) will define the three vectors $\mathbf{a}_1, \mathbf{a}_2, \mathbf{a}_3$ by

$$\begin{aligned} \mathbf{a}_1 &= a_{11}\mathbf{i} + a_{21}\mathbf{j} + a_{31}\mathbf{k}, \\ \mathbf{a}_2 &= a_{12}\mathbf{i} + a_{22}\mathbf{j} + a_{32}\mathbf{k}, \\ \mathbf{a}_3 &= a_{13}\mathbf{i} + a_{23}\mathbf{j} + a_{33}\mathbf{k}, \end{aligned} \quad \text{or} \quad (\mathbf{a}_1 \ \mathbf{a}_2 \ \mathbf{a}_3) = (\mathbf{i} \ \mathbf{j} \ \mathbf{k})\mathbf{A} \qquad (20)$$

where **A** is the matrix (a_{rs}), $(r,s = 1,2,3)$.

If we now add the constraint that the determinant $|\mathbf{A}|$ is nonzero, then the columns of **A** will be linearly independent. Hence the row vectors $\mathbf{a}_r$ $(r = 1,2,3)$ span the 3D space, and a unique inverse $\mathbf{A}^{-1}$ of **A** exists, where $(\mathbf{i} \ \mathbf{j} \ \mathbf{k}) = (\mathbf{a}_1 \ \mathbf{a}_2 \ \mathbf{a}_3)\mathbf{A}^{-1}$.

Note that $\mathbf{A}^{-1}$ is not necessarily equal to $\mathbf{A}^T$ in this case. Furthermore, the vectors $\mathbf{a}_r$ are not in general unit vectors, nor are they mutually orthogonal. A basis formed by such vectors is called an 'oblique frame of reference'.

Suppose now that a vector **v** is represented in terms of the two bases as

$$\mathbf{v} = v_1\mathbf{i} + v_2\mathbf{j} + v_3\mathbf{k} \qquad (21a)$$

and

$$\mathbf{v} = v_1'\mathbf{a}_1 + v_2'\mathbf{a}_2 + v_3'\mathbf{a}_3 \ . \qquad (22b)$$

Thus we can express the general transformation as

$$\mathbf{V} = \mathbf{AV}'. \qquad (23a)$$

If instead **v** is deformed by the transformation from **i,j,k** into a different vector **w** in $\mathbf{a}_1, \mathbf{a}_2, \mathbf{a}_3$ then we have

$$\mathbf{w} = v_1\mathbf{a}_1 + v_2\mathbf{a}_2 + v_3\mathbf{a}_3 \ . \qquad (24)$$

Hence

$$w_p = \Sigma_q \ a_{pq}v_q \quad \text{or} \quad \mathbf{W} = \mathbf{AV}, \qquad (25)$$

which is analogous to equations (15).

Now, if $(\mathbf{a}_1,\mathbf{a}_2,\mathbf{a}_3)$ and $(\mathbf{b}_1,\mathbf{b}_2,\mathbf{b}_3)$ are two oblique frames of reference, then they are related to $(\mathbf{i},\mathbf{j},\mathbf{k})$ by transformations of the form

$$(\mathbf{a}_1 \quad \mathbf{a}_2 \quad \mathbf{a}_3) = (\mathbf{i} \quad \mathbf{j} \quad \mathbf{k})\mathbf{A}_1 \quad \text{and} \qquad (26a)$$

$$(\mathbf{i} \quad \mathbf{j} \quad \mathbf{k}) = (\mathbf{b}_1 \quad \mathbf{b}_2 \quad \mathbf{b}_3)\mathbf{A}_2^{-1}, \qquad (26b)$$

for some 3x3 matrices $\mathbf{A}_1$ and $\mathbf{A}_2$, where the determinants $|\mathbf{A}_1|$ and $|\mathbf{A}_2|$ are nonzero.

Therefore, if we form the matrix product $\mathbf{M} = \mathbf{A}_2^{-1}\mathbf{A}$, with the determinant $|\mathbf{M}|$ nonzero, then it follows from equations (26) that the bases are related by the transformation

$$(\mathbf{a}_1,\mathbf{a}_2,\mathbf{a}_3) = (\mathbf{b}_1,\mathbf{b}_2,\mathbf{b}_3)\ \mathbf{M}. \qquad (27)$$

Hence the vector $\mathbf{v}$ considered above also has the representation

$$\mathbf{v} = v_1''\mathbf{b}_1 + v_2''\mathbf{b}_2 + v_3''\mathbf{b}_3\ , \qquad (21c)$$

and the component matrices in the two oblique frames are related by

$$\mathbf{V}'' = \mathbf{M}\mathbf{V}', \quad (23b)$$

which is analogous to equation (23a) above.

C.5 COVARIANT AND CONTRAVARIANT REPRESENTATIONS

The set of N vectors $\{\mathbf{e}^1,\mathbf{e}^2,\mathbf{e}^3,\ldots,\mathbf{e}^N,\}$ is said to be the 'reciprocal basis' relative to the basis $\{\mathbf{e}_1,\mathbf{e}_2,\mathbf{e}_3,\ldots,\mathbf{e}_N\}$ of an inner product space V if

$$\mathbf{e}^k \cdot \mathbf{e}_s = \delta_{k,s}\ , \qquad k,s = 1,2,\ldots, N$$

and as before, $\delta_{k,s}$ is the Kronecker delta defined by

$\delta_{k,s} = 1$ if k=s and 0 otherwise.

Thus a vector $\mathbf{v}$ has components v^k, k=1,2,...,N relative to the basis $\{\mathbf{e}^1,\mathbf{e}^2,\mathbf{e}^3,\ldots,\mathbf{e}^N,\}$ and components v_k, k=1,2,...,N relative to its reciprocal basis $\{\mathbf{e}_1,\mathbf{e}_2,\mathbf{e}_3,\ldots,\mathbf{e}_N\}$ (see figure C.5.1). Hence:

$$\mathbf{v} = \Sigma\ v_k\mathbf{e}_k \qquad \text{and} \qquad \mathbf{v} = \Sigma\ v^k\mathbf{e}^k\ .$$

The components $v^1,v^2,\ldots,v^N$ with respect to the basis

$\{\mathbf{e}_1, \mathbf{e}_2, \mathbf{e}_3, \ldots, \mathbf{e}_N\}$ are often called the 'contravariant components' of $\mathbf{v}$, while the components $v_1, v_2, \ldots, v_N$ with respect to the basis $\{\mathbf{e}^1, \mathbf{e}^2, \mathbf{e}^3, \ldots, \mathbf{e}^N,\}$ are called 'covariant components' (see figure C.5.2).

A substantial part of the usefulness of orthonormal bases is that each orthonormal basis is self-reciprocal. Hence contravariant and covariant components of vectors coincide. In orthonormal systems there is no need to distinguish between covariant and contravariant components. The indices may then be written simply as subscripts.[116]

Fig C.1.1: Direction and Euler angles.

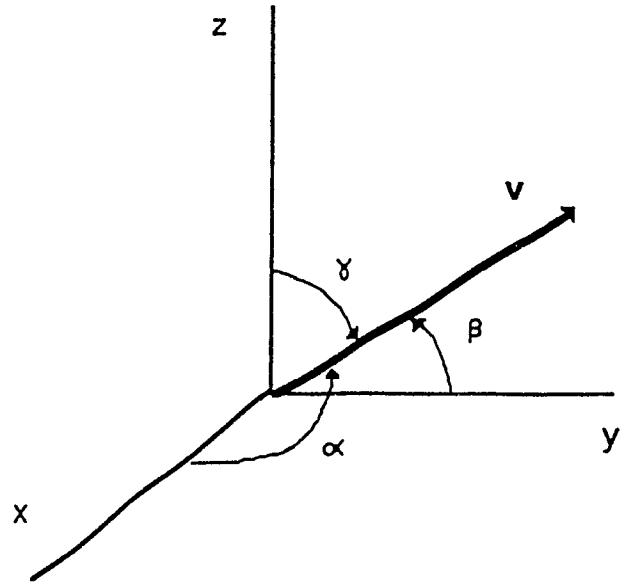

Fig C.1.1 (a): Direction angles between a 3D vector and the three principal coordinate axes. Adapted from Salas and Hille (1974).[137]

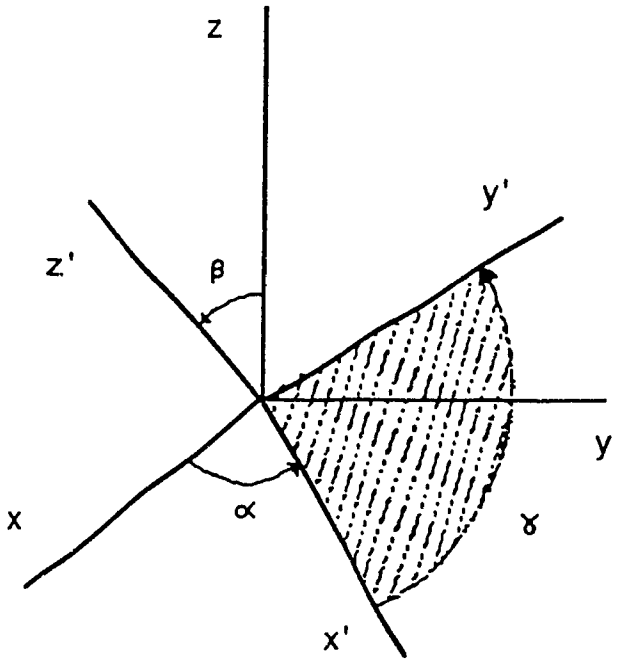

Fig C.1.1 (b): The relationship of the Eulerian angles of nutation, precession, and rotation to the fixed and rotating coordinate axes. Adapted from Fowles (1977).[138]

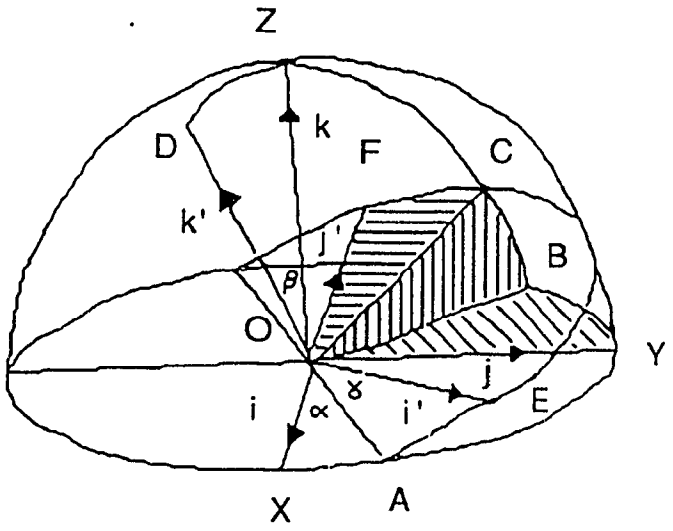

Fig C.2.1: Rotation between two reference frames in 3D space. Adapted from Chisholm (1978).[113]

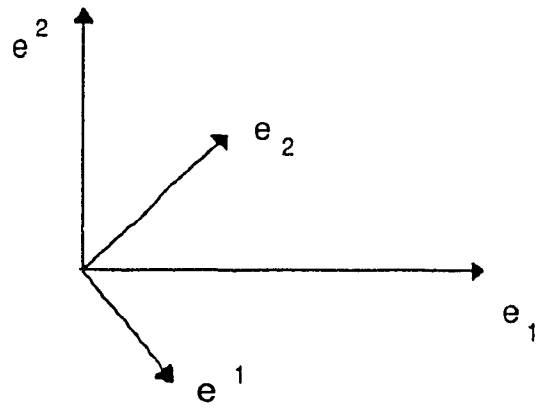

Fig C.5.1: A basis and reciprocal basis for R^2. Adapted from Bowen and Wang (1976).

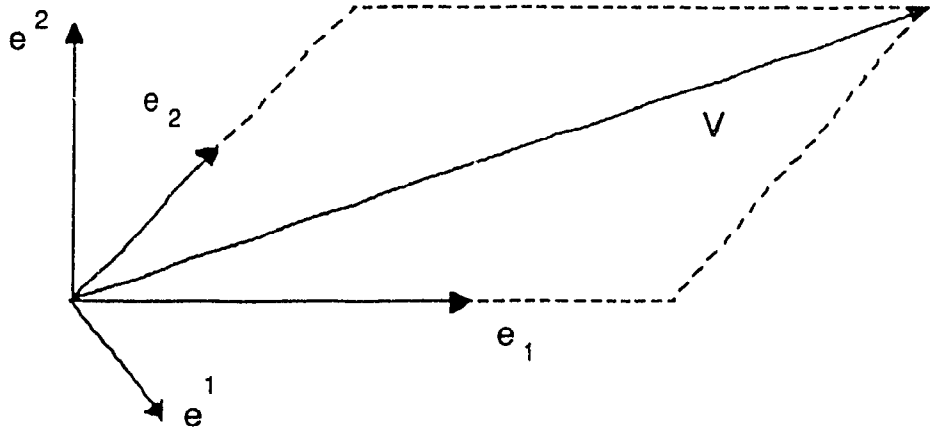

Fig C.5.2: The covariant and contravariant components of a vector in R^2. Adapted from Bowen and Wang (1976).

APPENDIX D: USER'S GUIDE TO THE ENHANCED CERVISCOPE DISPLAYS[a]

A. Getting Started

B. Cervical Report Menu

C. Definitions

D. Report Pages

E. Selecting New Parameters

F. Other Functions

---

[a] From Roozmon et al. (1991)[136]

New Cervical Report Software
Notes for the User

A. Getting Started

To get to the Cervical Report from the Spinoscope's main menu,
- choose "Report"
- a report selection menu will appear with the following choices:
  - Cervical Coupled Motion Display - the new cervical report
  - Regular Report Display - the original cervical report
  - Thoracic Report Display - the thoracic report
  - Spinobase Patient Selection - the database used to select a patient for viewing a cervical report
  - Gait Analysis Display - not available
  - Exit to Shell - to return to main menu
- click on "Spinobase Patient Selection" and select a patient
- exit the spinobase and select the "Cervical Coupled Motion Display" from the report menu.

B. Cervical Report Menu

By default, the software will display Page 1 of the report, which is labelled "3D Vector Motion". There are six pages in total. Look to the left of the screen and you will see the selection menu for the new cervical report with the following items:

Green Boxes (for selecting report pages):

3D Vector Motion	Page One
Absolute Angles vs. Time	Page Two
Relative Angles vs. Time	Page Three
Relative Angles vs Angles	Page Four
Normal Vector Position vs. Time	Page Five
Stick Figures	Page Six

Yellow Boxes (for changing the parameters):

Rotate Normal Vector
Select New Parameters Here

Red Boxes (functions):

Help
Print Page
Exit

Remarks Box

Please note that at the bottom of the screen there is a green "remarks" box. This box appears for every page and displays messages indicating the parameters that have been selected for display, the default values chosen by the computer, or instructions on using the mouse.

C. DEFINITIONS

The cervical report analyses and displays motion in terms of vectors and angles. The movements are

VECTORS

A vector is defined as a line that joins two points in space. In the Cervical Report, the points that are joined are LEDs. For Head Vectors, the default LEDs that are joined are numbers 1 and 2, and 1 and 3. For Neck Vectors, the default LEDs that are joined are numbers 4 and 17, and 4 and 18. For Thoracic Vectors, the default LEDs are numbers 12 and 17, and 12 and 18. Figure 1 shows how the LEDs on the back are arranged into vectors. Different sets of LEDs can be chosen to form the vectors. (For example, the Neck Vectors could be derived from LEDs 5, 17, and 18, or 6, 17, and 18, etc.) Chang-

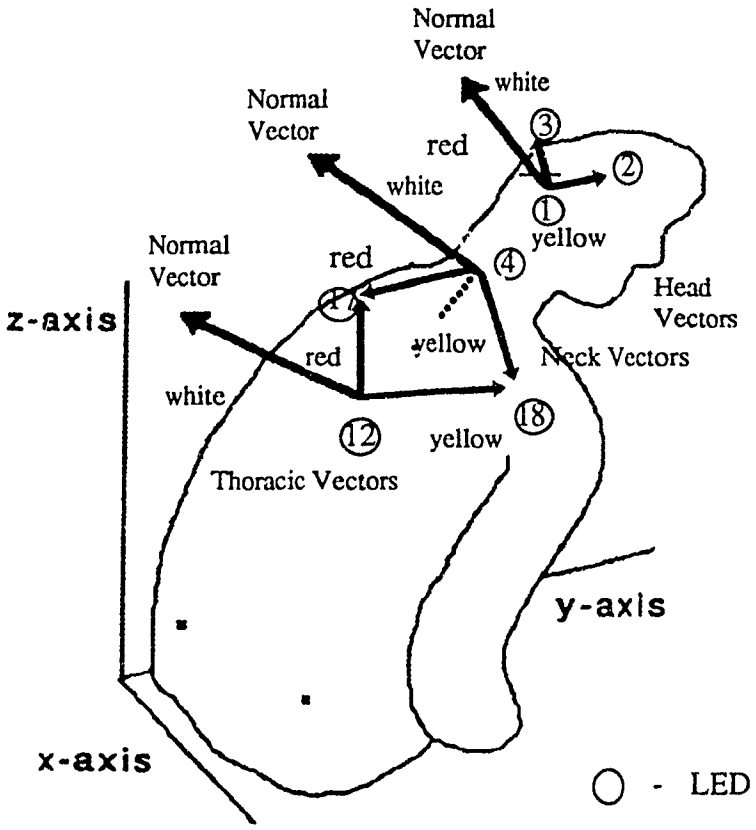

FIGURE 1: Vectors

All vectors are drawn from (originate from) a LED along the midline. To see the vectors on the screen, look on the first page "3D Vector Motion". The vectors are represented in several different configurations by red, yellow, and white lines. In figure 1 the vector extending to the left of the LED is represented on the page one screen by a red line. The vector to the right of the LED is represented by a yellow line.

See the vectors marked "Normal Vector in figure 1. A normal vector is represented on the page one screen by a white line. A normal vector is perpendicular to the plane formed by the left-extending (red on the screen) and right-extending (yellow on the

XZ = FRONTAL or EPSILON PLANE
XY = CORONAL or THETA PLANE
ZY = SAGITTAL or ALPHA PLANE

(please see next page for definitions of angles alpha, epsilon, and theta)

NORMAL VECTOR

A normal vector is a line that is at a ninety degree angle (perpendicular) to the plane formed by the other two vectors extending from the same LED. For instance, see figure 1. Vectors 4 - 17 and 4 - 18 form a plane. The normal vector is projected away from the plane at a ninety degree angle.

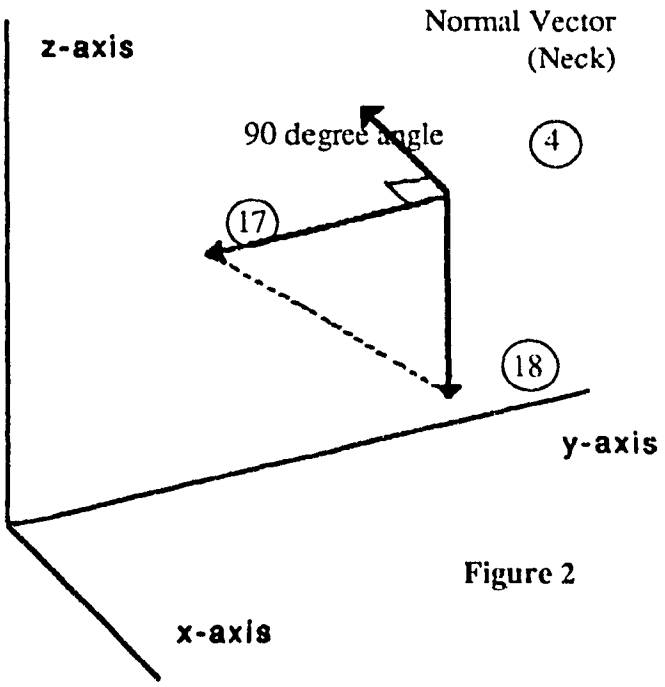

Figure 2

ANGLES

The Cervical report charts alpha, epsilon, and theta angles. These angles are calculated based on projections of the normal vectors onto the sagittal, frontal or coronal plane.

Figure 3 represents the epsilon angle of a normal vector during flexion/extension. The angle epsilon is derived from projecting the normal vector onto the frontal plane.

Note:
Vectors are displayed on pages one and five. Angles are displayed on pages two, three, and four.

Figure 3

In other words, as the examinee moves his/her neck forward within the sagittal plane the neck also moves slightly to the right in the frontal plane (ie. coupled motion). The angle epsilon describes this lateral motion.

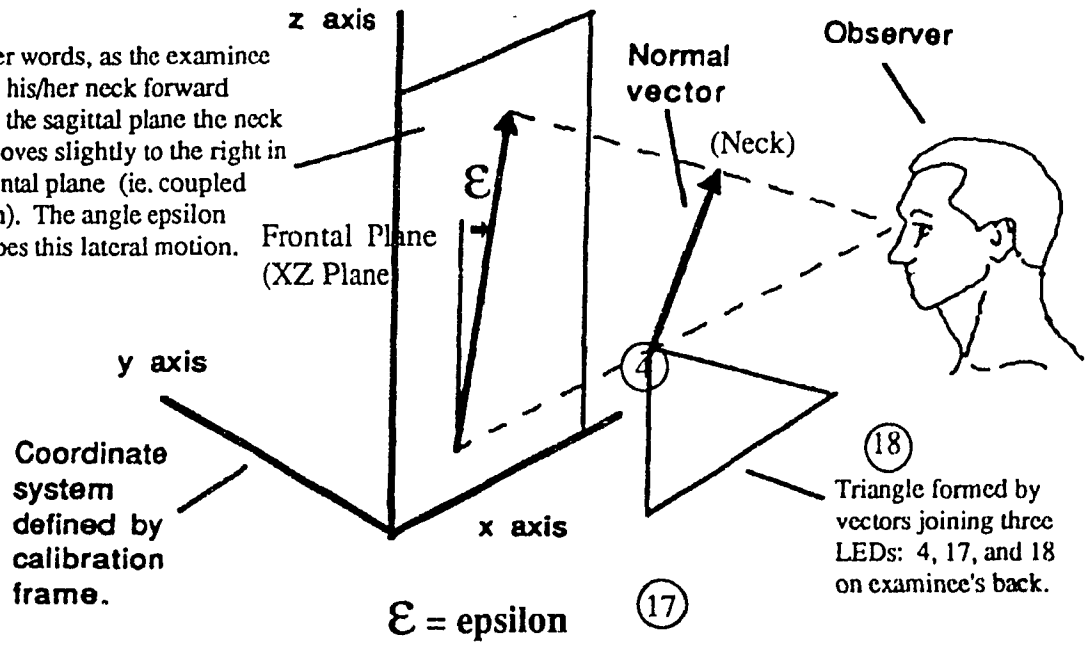

FRAMES

At the very bottom of the page one screen, there is a line indicating the default frame settings: "Displaying frames 0 to 70 in steps of 10 for FE." This means that the flexion/extension movement tracked by the computer has been broken down into frames. An analogy would be the way that film captures movement in a series of still photos, each one called a "frame". Zero is the starting frame, and shows the position of the vectors at the start of the movement, and 70 is the last frame. "In steps of 10" means that the computer is displaying the vectors as they were configured at frames 10, 20, 30, 40,. 50, 60, and 70. (To display other frames, use "Select New Parameters Here" .)

COUPLED MOTION

Looking at the angles of the vectors in different planes is a method of examining overall motion as well as coupled motion. An example of coupled motion is that when an examinee bends his/her head forward (flexion/extension) the neck will also exhibit motion laterally: concurrently bending to the side, if only slightly.

D. REPORT PAGES (see appendix for samples of report pages)

PAGE 1: 3D Vector Motion

On this page of the report, the motion of the cervical spine is represented by vectors: Head Vectors, Neck Vectors, and Thoracic Vectors. The vectors are shown for the default movement, which is flexion/extension. To choose another movement, you may use "Select New Parameters Here".

There are nine different sections to this page of the report. Three views of each group of vectors are displayed: Top, Back, and Side views (representing the coronal, frontal and sagittal planes) of the Head, Neck, and Thoracic vectors.

As described in the section on "VECTORS", red generally represents the vectors extending to the left out of the LED, yellow represents the vectors extending to the right, and white represents the normal vectors.

NOTE: For pages two and three the principal motion in each column is indicated by the boxes with red borders. The secondary, or coupled, motion is shown in the boxes with green borders.

PAGE 2: Absolute Angles vs Time

This page plots the angle of the normal vector versus time for three movements: Flexion/extension, Lateral bend, and Axial Rotation. The default normal vectors are the same as on page one, namely the vector extending from LED 1 (a Head Vector) and the vector extending from LED 12 (a Thoracic Vector). This is indicated in the box at the bottom of the screen: "Displaying angles for head vs thoracic (T6) LEDs. LED 1 and LED 12 are the normal vectors in the default configuration. To change vectors displayed, go to "Select New Parameters Here". One can even look at the motion of vectors of adjacent LEDs, which corresponds to intervertebral mobility (see section E to learn how this may be done).

Column 1: Principal Motion is Flexion/Extension

All three graphs in this column plot the angles of the Normal Head Vector (curve shown in red) and the Normal Thoracic vector (curve shown in yellow) over the course of the movement (frame 0 to 70). The three different graphs display the angles of these vectors in three different planes.

Alpha (YZ Plane/SAGITTAL PLANE)
- plots the angles of the vectors in the YZ plane versus time. In other words, this graph shows how the head moved forward within the sagittal plane and how the thoracic spine moved forward in this plane during the flexion/extension movement.

Epsilon (XZ Plane/FRONTAL PLANE)
- plots the angles of the vectors in the XZ plane. This graph shows how the head moved in the transverse plane (laterally) and how the thoracic spine moved in the transverse plane (laterally) during the flexion/extension movement.

Theta (XY Plane/CORONAL PLANE)
- plots the angles of the vectors in the XY plane. This graph shows how the head moved in the horizontal plane (axial rotation) and how the thoracic spine moved in the horizontal plane (axial rotation) during the flexion/extension movement.

Sample interpretation of graphs:

For the sample patient : The Alpha graph shows that he moved his head to a maximum of about 60 degrees forward at frame 40 and then brought his head about 10 degrees back at frame 70. He moved his thoracic spine to a maximum of about 5 degrees forward at frame 40. The Epsilon graph shows that he moved his head about 5 degrees laterally during the flexion/extension from frame 25 to 60.; and his thoracic spine movements laterally were insignificant. The Theta graph shows that the neck and thoracic had insignificant rotational movement during flexion/extension.

Column 2: Principal Motion is Lateral Bending

This column represents the angles Alpha (YZ Plane), Epsilon (XZ Plane), and Theta (XY Plane) for the lateral bend movement. For example, for the default parameters the Alpha (YZ Plane) box shows how the motion of the head (yellow curve) and the thoracic spine (red curve) in the sagittal plane during the lateral bend movement.

Sample interpretation of graphs:

For the sample patient: The Alpha box shows that he moved his head forward and backward as he performed the lateral bend motion (eg. at frame 65 he has bent his head 10 degrees forward). The Epsilon box shows that he laterally moved his head to a maximum of 10 degrees to the right (frame 30) and then 10 degrees to the left (frame 60). The Theta box shows that he rotated his head while he moved laterally to a maximum of 10 degrees at frame 30 and 10 degrees at frame 60.

Column 3: Principal Motion is Axial Rotation - not yet available

PAGE 3: Relative Angles vs Time

This page of the report shows the same type of information as page 2, except that you now observe the relationship between two normal vector angles. In other words, Alpha (YZ Plane) shows the relative motion of the thoracic and head vectors in the sagittal plane.

Again, looking at the box at the bottom of the screen, we can see that the default normal vectors are those for the head and the thoracic spine.

PAGE 4: Relative Angle vs Angle

This page combines the curves shown in separate boxes on PAGE THREE, thereby representing the coupled motion for two given directions in a single box.

FE vs LB for Flex/Ext shows the lateral coupled motion which occurs when bending in the sagittal plane. FE vs ROT for Flex/Ext shows the rotational coupled motion which occurs when bending in the sagittal plane. LB vs FE shows the coupled forward or backward motion that occurs when bending laterally. LB vs ROT shows the rotational coupled motion accompanying lateral bending. ROT vs FE and ROT vs LB show the coupled flexion/extension and lateral bending which accompanies axial rotation.

Again, the default normal vectors are LEDs 1 and 12.

PAGE 5: Normal Vector Position vs Time

This page shows the normal vector position with respect to the x, y, and z coordinates versus time for the Head, Neck, and Thoracic Vectors. For example, under the first column, in the first box, we see the position of the normal vector with respect to the x coordinate.

PAGE 6: Stick Figures

This page displays the motion of all the LEDs at different points in time in the movement from the side, top, and back. The default frames shown are multiples of 10. This may be changed by going to the section, "Select New Parameters Here." By adjusting the frames displayed, it is possible to view the orientation of the LEDs for any period of interest.

E. SELECTING NEW PARAMETERS

As indicated in the previous section, one can change the parameters that are displayed in the report. To access the menu for changing parameters, click on the box entitled "Select New Parameters Here". The following menu will appear: **(see appendix for sample of this report page)**

LED SETS
HIGH LED
LOW LED
FILT DATA
RESET ALL
FIRST FRAME
LAST FRAME
STEP SIZE
MOVEMENT
ALARM OFF

"LED SETS" box **- permits you to change which groups of LEDs are displayed (pages 2, 3, and 4)**

Go to page 2, 3, or 4, of the report. For these pages the report looks at the motion of the normal vectors of two groups of LEDs. As discussed earlier, the default groups are the head vectors and the thoracic vectors. To change these parameters in order to look at other groups, click on "LED SETS". At the bottom of the screen you will notice a green box displaying the message "Displaying angles for head vs. thoracic (T6) LEDs." If you click the left mouse button, it will change to head vs. neck. If you click the button again, it will change to neck vs. thoracic. Clicking one more time will bring it back to the default head vs. thoracic. Use the mouse as described to choose the two groups you would like to see. Now regenerate the screen to display the graphs for these new parameters by clicking on the box for the desired page. For example, to view page two after changing the parameters, click on the box "Absolute Angles vs Time" and the new screen will appear.

"HIGH LED" and "LOW LED" boxes **- permit you to change the LEDs from which the normal vector originates (pages 2, 3, and 4)**

NOTE: You can view the motion between two vertebrae (ie. intervertebral mobility) by choosing any two adjacent LEDs !

Go to page 2, 3, or 4. First use the above described method for choosing two groups of LEDs. It is straightforward if you wish to choose two LEDs which are from different groups. Example: You wish to see the LED at C3 versus the LED at T1. Choose "Neck vs Thoracic". The default for neck versus thoracic is C2 versus T6. To change this, click on LOW LED (which corresponds to the LED that is lower on the examinee's back), and T6 will change to T4, click again and T1 will appear. Click on HIGH LED, and C2 will change to C3. Regenerate the screen for the new parameters by clicking on the name of the page, for example, "Absolute Angles vs Time". The re-generated screen will map the motion of the newly selected LEDs.

DETERMINING INTERVERTEBRAL MOBILITY

If you wish to compare the motion of any two LEDs along the cervical or thoracic spine, first use the LED SETS function to choose "Neck vs Thoracic". For example, suppose that you wish to see the intervertebral motion between C4 and C5. Use LED SETS to choose "Neck vs Thoracic". You will see that the default for these groups assigns the LEDs at C2 and T6 as the selected LEDs. Click on "LOW LED" and the T6 changes to T4. Click this again and it changes to T1, continue clicking until you see C5. Now click on "HIGH LED" and the C2 changes to C3. Click again and C4 appears. Re-generate the screen by selecting the page name again.

"FILT DATA" box **- permits you to display unfiltered or filtered curves (pages 2 to 5)**

The default displays show filtered (ie. smoothed) curves. This function allows you to see the curves as they would appear using raw, or unfiltered, data. You can change the display on pages 2 to 5 in order to display unfiltered data. This has little effect for pages displaying angles, since the angles are always calculated from the smoothed position curves for the LED data. Clicking on "FILT DATA" will result in the remarks box at the bottom of the page stating "Displaying filtered data only". Click the mouse button again , and the message will change to "Displaying unfiltered data only". A third click will show the message "Displaying both filtered and unfiltered curves".

"RESET ALL" box **- permits you to change all the pages back to the default settings**

After you have made changes to some of the parameters, you may wish to return to the default values. Simply click on "RESET ALL" and then select the page you want to view. The display will have returned to the default parameters. Clicking on "Select new parameters here" will re-enable the parameter changes as before.

"FIRST FRAME", "LAST FRAME", and "STEP SIZE" boxes **- permit you to change which part of the movement you view: (ie. the beginning, the middle, the end, etc.) and how it is displayed (ie. every 5 frames, every 10 frames, etc.**

NOTE: These functions allow you to view the standing still position corresponding to frame 0 !

Go to the first page, "3D Vector Motion". The remarks box at the bottom of the screen will indicate the default settings: "Displaying frames 0 to 70 in steps of 10.". Suppose now that you want to display only part of the flexion phase of the movement. By looking at the angles on page 2 of the report, you determine that flexion motion goes from , say, frame 0 to frame 25. Now suppose that the part of flexion that you want to view includes frames 10 to 25. Click on LAST FRAME. Clicking on the right mouse button will decrease the value of the last frame in increments of 10 frames. Click on the

VIEWING THE STANDING STILL POSITION

To view the "standing still position", click on LAST FRAME, and use the mouse buttons to change this value to 1. Then click on FIRST FRAME and use the mouse buttons to change this value to 0. The step size need only be greater than or equal to one. Then re-generate the screen by selecting page 1 and you will see the configuration of the vectors for the standing still position.

"MOVEMENT" box **- permits you to change the principal motion that the report is displaying (all pages)**

Go to "MOVEMENT". The green remarks box at the bottom of the screen indicates the default movement, which is FE (i.e.. flexion/extension). To choose Lateral Bend, click the mouse bottom and the movement changes to LB. Select any page to display an analysis of the lateral bend movement.

Note: the axial rotation movement will later be added to the above principal motions.

"ALARM OFF" box **- permits you to remove the warning that is displayed at the top of the page**

If any LEDs were obscured during the recording session, a message will appear in red at the top of the screen. It is necessary to interpret with caution any report which has such an error message. If you do wish to proceed with an interpretation, you can switch the message off, so that you can view the full screen again. Click on "ALARM OFF" and the message will disappear.

F. OTHER FUNCTIONS

At the bottom of the menu, there are three other boxes, labelled "HELP", "PRINT SCREEN", and "EXIT".

While you are viewing a particular page, you may have a question about what is being displayed, etc. You can click on "HELP" and a brief tutorial will appear for that page.

If you want to print a report, go to the first page that you wish printed, and click on "PRINT SCREEN". The computer will print whatever currently appears on that screen. To print a full report, for the time being you must go to each screen individually and click on "PRINT SCREEN".

Finally, **to exit the new cervical report,** click on the "EXIT" box. This will return you to the report selection menu, from where you may select another form of the report, or return to the original Spinoscope menu.

Note: in the future, an "overlay" function and an "overview" page (ie. occupying the single red and green menu boxes which are currently empty) are expected to be among the features added to the new cervical report .

APPENDIX E: GLOSSARY OF CLINICAL TERMS[a]

Term	Definition
active movement:	without assistance
alar ligaments:	one of two strong bands which extend from the odontoid process to attach to the occiput
analgesic:	an agent which reduces pain
analtagic position:	position which reduces pain
annulus fibrosis:	peripheral part of an intervertebral disc
anterior:	pertaining to the front of a body
anthropo-dynamic model:	analytical model which takes into account known physiological quantities
anthropomorphic tables:	comparative measurements of the human body and its parts
atlas:	the first cervical vertebra
atlanto/axial/ occipital:	pertaining to the joint between the head and neck
avulsion:	forcible separation of two parts
axis:	second cervical vertebra
bi-planar radiographs:	radiographs which combine information from projections onto two orthogonal planes
caudad:	in a direction towards the tail
cephalad:	in a direction towards the head
cervical (cervico):	relating to the neck (vertebrae 1 to 7)
cervical plexus:	related to the first four cervical nerves

[a] See also Appendix A for illustrations of the major cervical anatomy and muscles, as well as figure 1.3.1 for an overview of the spine and the planes of physiological motion.

cineradiography:	consecutive radiographs viewed as moving pictures
collagen:	class of scleroproteins occurring in bone and cartilage, forming ground substance or fibers of connective tissue
compression:	being pressed together into a narrower space
contralateral:	relating to the opposite side
coronal:	frontal
distensibility:	ability to stretch or enlarge
dorsal:	pertaining to the back
dura (mater):	tough, fibrous membrane forming outer envelope of the brain and spinal cord
dysphagia:	difficulty in swallowing
edema:	accumulation of fluid in tissue
erector spinae:	erector muscle which runs along the back of the entire spine
etiology:	study of cause of disease and mode of operation
extrafusal fibers:	external to muscle spindle fibers
extension:	straightening out of a joint or set of joints
facets:	indentation in vertebral body for attaching cartilage
flexion:	the act of bending
gluteus:	the buttock
grey matter:	connections between ganglion and trunks of spinal nerves
hemorrhage (haemorrhage):	bleeding
hypermobility:	excessive mobility of an abnormal kind
hypomobility:	state in which the mobility is reduced
iliocostalis:	lateral column of sacrospinalis muscle
intersegmental mobility:	relative movement between center points of two adjacent vertebrae
intramedullary fissure:	furrow within the spinal cord
intervertebral disc:	connective bond between adjacent vertebrae

intrafusal:	relating to muscle spindle
in-vitro:	pertaining to non-living tissue
in-vivo:	related to tissue within a living organism
ipsilateral:	occurring or located on the same side
ischemia(ischaemia):	local anemia due to mechanical obstruction of the blood supply
isometric tension:	maintained muscle tension not resulting in movement
kyphosis:	forward curvature of the spine
lateral bending:	flexion to either side
levator scapulae muscle:	arises from upper four cervical transverse processes and inserts into the scapula
ligamentum flavum:	yellow elastic ligaments which bind the vertebral laminae together
longissimus:	forms the medial column of the sacrospinalis muscle
longitudinal ligaments:	broad bands of fibers which extend along the anterior and posterior surfaces of the vertebral bodies
lordosis:	backward curvature of the spine
lumbar:	lower back (lowest 5 movable vertebrae of the spine)
luxation:	dislocation
medial:	pertaining to the middle
motion segment:	any two adjacent vertebrae and the disk or ligamentous tissue joining them together
myelopathy:	disturbance or disease of the spinal cord
myelography:	injection of contrast material to show the spinal cord in radiographs or CT scans
muscle fibril:	fine muscle fiber
necrosis:	death of a portion of tissue
neutral position:	neither in flexion or extension
occipital (occipetal):	relating to the back part of the skull or head

odontoid process (dens):	tooth shaped protrusion of the axis running through the center of the atlas and up to the occiput (see fig 1.3.7)
osteoarthritis:	chronic arthritis of a degenerative type
osteoporosis:	rarefaction of bone due to loss of calcium associated with aging
osteophyte:	bone spurs resulting from increased contact between adjacent surfaces following disk degeneration
Pacinian receptors:	laminated corpuscles involved in sensing pressure
paresis:	temporary or permanent paralysis
passive movement:	not produced by the active effort of the individual
periarticular:	about a joint
posterior:	pertaining to the rear
radicular branches of pia dura (mater):	the root of the membrane of connective tissue which sheaths blood vessels entering the nervous system
rotation:	the act of turning about an axis
Ruffini receptors:	nerve endings in the skin associated with sensing heat
sacrospinalis muscle:	extensor of the vertebral column
sagittal:	from the side
spinal canal:	conduit within the spinal column for the spinal cord and fluid
spinalis:	medial part of sacrospinalis muscle
spinous processes:	bony protrusions occurring posterior to the vertebrae
splenius muscle:	see figure 1.4.2
spondylitic myelopathy:	spurs in the midline over the posterior aspect of intervertebral space, resulting in encroachment on contents of spinal canal and cord compression
spondylosis:	inflammation of the spine
spondylolisthesis:	forward displacement of one vertebrae upon the one below
spondylolysis:	breaking down of a vertebra

spondylitic radiculopathy:	laterally or posterolaterally directed osteophytes, causing irritation of nerve root in invertebral foramen
stereophotographs:	combining 2D pictures in an optical device to simulate a 3D effect
sternocleidomastoid:	see figures 1.4.1 and 1.4.2
subluxation:	incomplete dislocation
sulcal vertebral artery:	superior aspect of posterior arch of atlas that transmits vertebral artery medially toward foramen magnum
supraspinal ligament:	series of fibrous bands connecting the tips of the spinous processes
sympathetic nervous system:	autonomic system associated with involuntary muscle activity
terminal vessels:	relating to the extremity of the artery
thoracic (thoraco):	referring to the chest or middle portion of the spine
tinnitus:	ringing in the ears
translation:	displacement in any direction without rotation
transverse ligament:	strong band passing behind the odontoid process and attached on each side to the atlas
trapezius:	large flat muscle of the back inserting into upper border of scapula
transverse processes:	bony protrusion extending from the sides of the vertebrae
unciform processes:	smooth surface of bone which articulate with adjacent vertebrae
ventral:	pertaining to the front
vertebral end plate avulsion:	tearing away or forcible separation of vertebral end plate
vertebra prominens:	the easily locatable spinous process of the seventh cervical vertebra
vestibulocollic reflex:	reflex relating head movement with the vestibular senses
whiplash:	a sudden backward snapping of the head and neck followed by forward recoil
zygapophyseal:	relating to articular process of vertebra

First cervical vertebra (atlas) from the top.

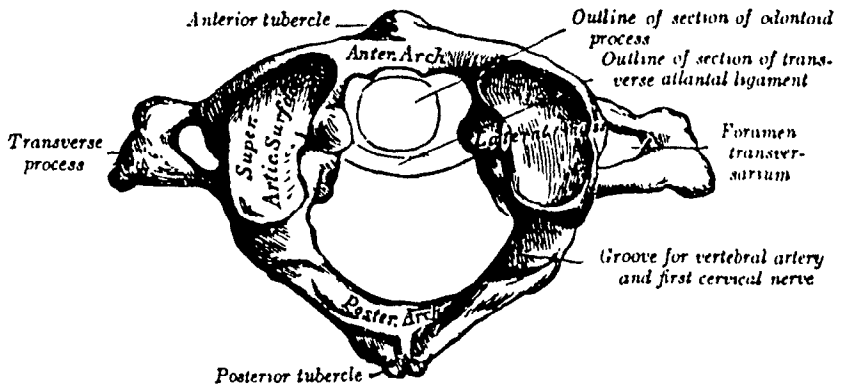

Second cervical vertebra (axis) from the side.

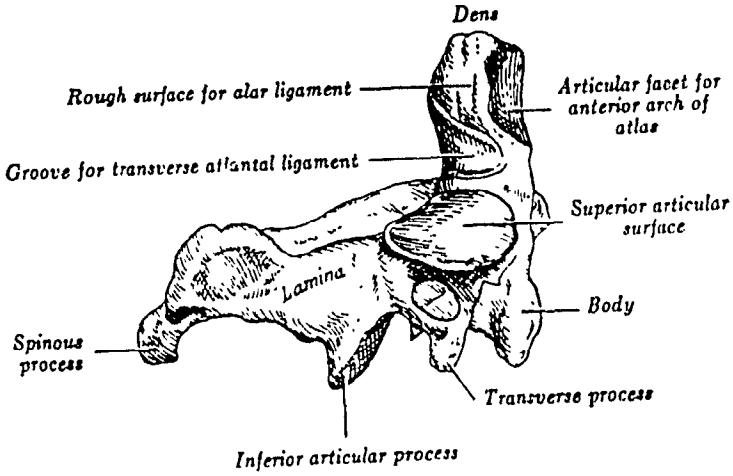

Typical cervical vertebra from the top.

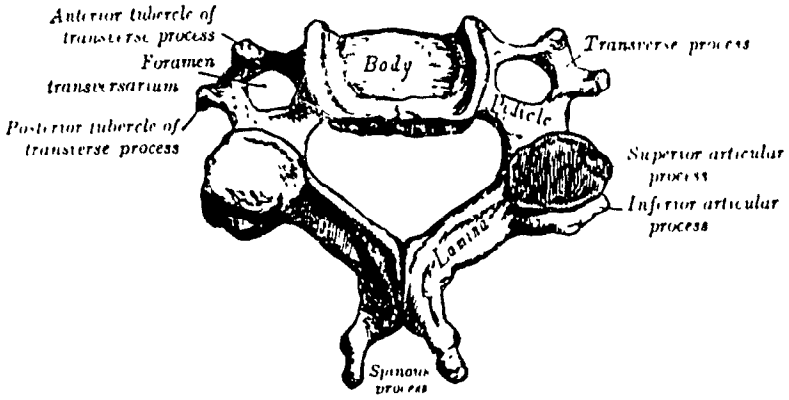

Typical cervical vertebra from the side.

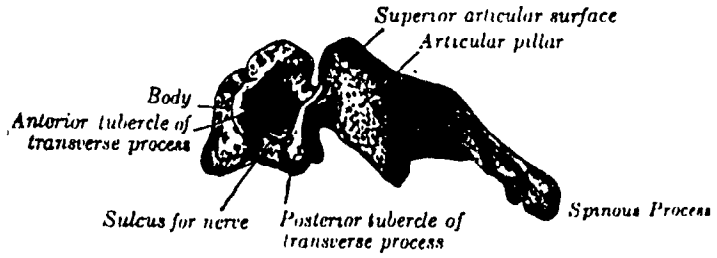

Fig E.1: The cervical vertebrae. Adapted from Van Dyke Carter (1973).135